Cardiff University

School of Chemistry

AMPHIPHILIC LIGAND ARCHITECTURES FOR S-, D- AND F-BLOCK METALLOSURFACTANTS TOWARDS MICELLAR SYSTEMS AND MICROEMULSIONS

Thesis submitted for the degree of Doctor of Philosophy by

Emily Claire Stokes

July 2017

DECLARATION

This work has not been submitted in substance for any other degree or award at this or any other university or place of learning, nor is being submitted concurrently in candidature for any degree or other award.

Signed …… (candidate) Date ……

STATEMENT 1

This thesis is being submitted in partial fulfillment of the requirements for the degree of PhD

Signed …… (candidate) Date ……

STATEMENT 2

This thesis is the result of my own independent work/investigation, except where otherwise stated, and the thesis has not been edited by a third party beyond what is permitted by Cardiff University's Policy on the Use of Third Party Editors by Research Degree Students. Other sources are acknowledged by explicit references. The views expressed are my own.

Signed …… (candidate) Date ……

STATEMENT 3

I hereby give consent for my thesis, if accepted, to be available online in the University's Open Access repository and for inter-library loan, and for the title and summary to be made available to outside organisations.

Signed …… (candidate) Date ……

STATEMENT 4: PREVIOUSLY APPROVED BAR ON ACCESS

I hereby give consent for my thesis, if accepted, to be available online in the University's Open Access repository and for inter-library loans **after expiry of a bar on access previously approved by the Academic Standards & Quality Committee.**

Signed …… (candidate) Date ……

Cardiff University

School of Chemistry

Abstract

Doctor of Philosophy

AMPHIPHILIC LIGAND ARCHITECTURES FOR S-, D- AND F-BLOCK METALLOSURFACTANTS TOWARDS MICELLAR SYSTEMS AND MICROEMULSIONS

By Emily Claire Stokes

The design, synthesis and characterisation of a range of surfactant-based ligand architectures is presented. The amphiphilic ligands have been shown to form metallosurfactants with a wide range of s-, d- and f-block metals as well as being able to form stable micellar systems either through self-assembly or *via* doping into a carrier microemulsion. The overall aim of this work was to produce surfactant ligands capable of sequestering metal ions and localising them on the surface of micellar droplets within an oil-in-water microemulsion.

Chapter Two investigates the formulation and characterisation of a 1-alkyl-3-methyl imidazolium based micellar system capable of forming stable microemulsions with extremely high oil loadings as well as acting as a carrier for more complex surfactants. This chapter also describes the synthesis and characterisation two novel macrocyclic ligand architectures designed to coordinate a range of s-, d- and f-block metals to form a series of metallosurfactants capable of aggregation in aqueous media.

Chapter Three explores an array of acyclic surfactant ligands synthesised from ethylene diamine and diethylene triamine precursors and functionalised with poly-alcohol arms. These amphiphilic ligands were coordinated to Ni(II) and Cu(II) in order to gain insight into their coordination geometries via photophysical studies. Tensiometric investigations of the free ligands and their Sr(II) and Y(III) metallosurfactants assessed their microemulsion compatibility as alternatives to macrocyclic architectures.

Chapter Four presents a series of cationic bis-cyclometallated Ir(IIII) complexes where the diimine ligand is a bipyridine species functionalised with a lipophilic alkyl chain and the cyclometallating ligands contain ethyl ester moieties which, upon deprotection, afford water soluble complexes. Combined tensiometric and photophysical studies found these species to be dual emissive as free complexes in solution, with emission arising from both ligand-centred and metal-to-ligand charge transfer mechanisms. Upon aggregation into micelles however, either a quenching of the ligand-centred emission or an enhancement of the metal-to-ligand charge transfer rendered the complexes mono-emissive.

Chapter Five reports the synthesis and characterisation of three novel DO3A-based surfactant ligands incorporating pendent chromophores as antennae for near-IR sensitised emission from a range of Ln(II) ions. Luminescent lifetime studies determined that the ligands form 8-coordinate complexes with hydration states suggesting the presence of 0-1 inner sphere water molecules. Combined tensiometric and photophysical studies proved the metallosurfactants to be capable of self-assembly into micelles in aqueous media and found aggregation to have a notable effect on the local environment of the Ln(III) ions.

Acknowledgments

As many people will understand, a PhD is not the work of a single person but rather the collection and application of other people's knowledge, skills, advice and support gathered over many years. From those who shared their wisdom over a cup of tea to those who shouted opinions across the lab and others whose equipment was borrowed and not necessarily returned, there are many people who have contributed to this thesis and deserve my deepest thanks.

First and foremost I would like to thank my supervisors, Simon and Ian, for giving me the opportunity to do this PhD in the first place and for trusting me with their research, but also for their unfaltering enthusiasm and support over the years. Thank you for pushing me to learn new things and for teaching me many others, I hope I did a good job!

Thank you also to the NDA and NNL for their funding and support, especially to my industrial supervisor Colin Harvey and to Dr Simon Woodbury. Dr Jeremy Andrew at Dounreay is also thanked for his constant support and interest as well as his collaboration in testing the new LSC cocktails.

Thank you to the people who gave their time to help me obtain data: Dr Jenn Jones at Manchester for recording many Eu(III) complex lifetimes, Drs Simon Coles and Neil Horton at Southampton for the crystal structures and Dr Alison Paul for allowing me exclusive access to the tensiometer and for helping me to understand the theory behind it. A special thanks go to the students whose work contributed towards this thesis: Jenny Sharpe and Alice Gillman, who produced some great results despite my supervision!

I am extremely grateful to all of the technical staff who have kept my work afloat in various ways: Dr Rob Jenkins, Robin Hicks, Simon Waller, Tom Williams, Rob Ashton, Louise Pritchard, Gaz Coleman, Jamie Cross, Sham Ali, Evelyn Blake, Simon James and Andy Ough-Jones.

I owe a huge debt of gratitude to my fantastic lab sisters Emily and Lara for looking after me, making the lab a fun place to work and generally being gorgeous human beings! I am also deeply grateful to Gez, who has been by my side through all of this from day one and Nadine, for always being there with a smile and a hug when I needed it!

Thank you also to everyone else with whom it has been a pleasure to share a lab: Hallett, Mark, Mauro, Adam, Kaitlin, Sam and, though it pains me to say it, Ollie. You have all taught me things about chemistry, life and learning not to freak out when the lab is a mess. We've been together through the days so cold you could see your breath, the days so hot we were sweating just standing still, some very bad radio station choices and some fantastic pub sessions, I wouldn't have missed it for the world!

To all the other members of the department past and present: Alex, Ali, Alice M., Andy W., Angelo, Axel, Ben Ward, Ben Woods, Brendan, Corey, Dayna, Jimmy, Lenali, Lewis, Mohammed B., Mohammed H., Nuha, Owen, Seni, Siôn, Tom, Yashar and Woody, it's been a pleasure to work with you, drink with you and argue with you, thank you for putting up with me! I also have to add a special mention to the two little girls who were born during my time here, Anwen and Millicent, thank you simply for being adorable!

My greatest thanks, however, go to Simon; not only for all the chemistry-related support but for helping me with life in general. You reached out to me when I really needed it and understood things no one else could. You believed in me when I had no belief in myself and you put up with my moods, inherent pessimism and illogical arguments. You always managed to brighten up the darkest days and never gave up on me, even when I was being difficult. It is safe to say that without you I never would have made it this far. Thank you not only for being a fantastic supervisor but for also being the most wonderful friend.

Contents

List of Figures

List of Tables

List of abbreviations

Solvents, Reagents, Compounds and Chemicals	
bis-MSB	1,4-bis(2-methylstyryl)benzene
BOC	*tert*-butyloxycarbonyl
butyl-PBD	2-(4-biphenylyl)-5-(4-tert-butylphenyl)-1,3,4-oxadiazole
CTAB	cetyltrimethylammonium bromide
cyclen	1,4,7,10-tetraazacyclododecane
DCE	1,2-dichloroethane
DCM	dichloromethane
DIEA	*N,N*-diisopropylethylamine
dien	diethylene triamine
DHN	1,5-dihydroxynaphthalene
dimethyl-POPOP	1,4-bis(4-methyl-5-phenyl-2-oxazolyl)benzene
DIN	di-isopropyl naphthalene
DMA	*N,N*-dimethylacetamide
DMF	*N,N*-dimethylformamide
DOTA	1,4,7,10-tetraazacyclododecane-1,4,7,10-triaceticacid
DO3A	1,4,7,10-tetraazacyclododecane-1,4,7-triacetic acid
DTPA	diethylenetriamine pentaaceticacid
EDTA	ethylenediaminetetraacetic acid
en	ethylene diamine
LAB	linear alkyl benzene
$MeImC_n$	1-alkyl-3-methyl imidazolium
MTAB	myristyltrimethylammonium bromide
NOTA	1,4,7-triazacyclononande-1,4,7-tiaceticacid
NPE	nonylphenol ethoxylate
N2O4	1,4,10,13-tetraoxa-7,16-diazacyclooctadecane
PBD	2-phenyl-5-(4-biphenylyl)-1,3,4-oxadiazole
PNPD	*p*-nitrophenyl dodecanoate
PNPO	*p*-nitrophenyl octanoate
PNPP	*p*-nitrophenyl picolinate
POPOP	1,4-bis(5-phenyl-2-oxazolyl)benzene
PPO	2,5-diphenyloxazole
PXE	phenylxylylethane
SDS	sodium dodecyl sulphate
SHIDA	sodium hexadecyliminodiacetate
TACN	1,4,7-triazacyclanonane
TFA	trifluoroacetic acid
Triton X-100	octylphenol ethoxylate
Me	methyl
Et	ethyl
OEt	ethoxy
EO	ethoxylate
Et_2O	diethyl ether
EtOAc	ethyl acetate
O^tBu	*tert*-butoxy
^tBu	*tert*-butyl
AcOH	acetic acid
EtOH	ethanol
MeOH	methanol
BuOH	1-butanol

MeCN	acetonitrile
NBu_4	tetrabutylammonium
NEt_3	trimethylamine
bpy	2,2'-bipyridine
ppy	2-phenylpyridine
thpy	2-(thiophen-2-yl)pyridine
OTf/Triflate	trifluoromethanesulfonate
fac	facial
Ln	lanthanide
N^N	polyaromatic diimine ligand
C^N	cyclometallating ligand

Spectroscopy and Techniques	
LSC	liquid scintillation counting
NMR	nuclear magnetic resonance
FT	fourier transformation
IR	infra-red
TLC	thin layer chromatography
HR	high resolution
LR	low resolution
MS	mass spectrometry
ES	electrospray ionisation
EI	electron ionisation
AP	atmospheric pressure ionisation
MRI	magnetic resonance imaging
CA	contrast agent
TEM	transmission electron micrograph
OLED	organic light emitting diode
DFT	density functional theory
s	singlet
t	triplet
d	doublet
q	quartet
quin.	quintet
dd	doublet of doublets
dt	doublet of triplets
td	triplet of doublets
m	multiplet
app.	apparent
$\{^1H\}$	proton decoupled
δ	chemical shift
ppm	parts per million
br.	broad
MALDI	matrix assisted laser desorption ionisation
TOF	time of flight
m/z	mass to charge ratio

Photophysics	
UV-Vis	ultra-violet visible
ISC	intersystem crossing
IC	internal conversion
NIR	near infra-red
NR	non-radiative
S	singlet state
T	triplet state
$h\nu_A$	absorption energy
$h\nu_{F/P}$	fluorescence/phosphorescence emission energy
^{1}MLCT/^{3}MLCT	singlet/triplet metal-to-ligand charge transfer
CT	charge transfer
HOMO	highest occupied molecular orbital
LUMO	lowest unoccupied molecular orbital
ET	energy transfer
BET	back energy transfer
λ	wavelength
em	emission
abs	absorption
ν	frequency
Φ/QY	quantum yield
τ	lifetime
sh.	shoulder

Micellar Parameters	
o/w	oil-in-water microemulsion
w/o	water-in-oil microemulsion
CMC	critical micelle concentration
DVT	drop volume tensiometry
APM	area per molecule
IL	ionic liquid
SAIL	surface active ionic liquid
UPW	ultra-pure water
MicroE	microemulsion
AIE	aggregation induced emission
ACQ	aggregation caused quenching
σ	surface tension
V	volume
g	acceleration due to gravity
ρ	density
r	radius
F	correction factor

Other	
RT	room temperature
LT	low temperature
N_A	the Avagadro constant
xs	excess

Chapter One

Introduction

1.1 Introduction

Surfactants are one of the most extensively studied types of molecules in chemistry. Their unique solution and interfacial properties mean that they have wide reaching applications. Most surfactant molecules comprise organic compounds, however in recent years there has been increasing interest in metal-binding surfactants capable of forming micellar droplets in which the metal is localised on the interface.

1.2 Surfactants

Surfactants – a portmanteau of 'surface active agents' – are amphiphilic molecules comprising a hydrophilic (polar) head group and a hydrophobic (non-polar) tail group. They are typically categorised according to the overall charge of the molecule and therefore fall into one of four classes: anionic, cationic, non-ionic and zwitterionic.

While the nature of surfactant head groups is seen to vary a great deal, there is less diversity seen in the nature of the hydrophobic tail group. Most reported surfactants contain a long, straight hydrocarbon chain typically of 8 to 20 carbon atoms. However, other examples of hydrophobic moieties include branched hydrocarbons, long perfluoroalkyl chains and polysiloxane derivatives.[1]

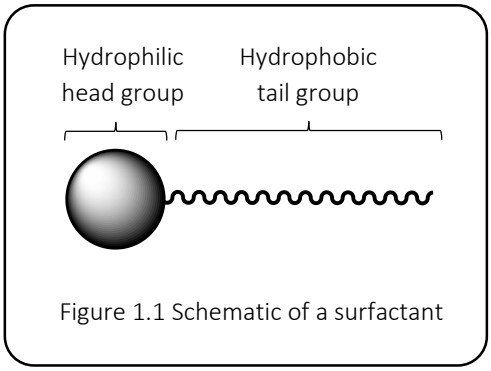

Figure 1.1 Schematic of a surfactant

When surfactants are present at low concentrations in aqueous media there is a thermodynamic drive to satisfy the requirements of both parts of the amphiphile. The hydrophilic head group is strongly attracted to the water molecules whilst the hydrophobic tail group is not. In order to resolve this the surfactant molecules arrange themselves at the air/water interface (also referred to as the gas/liquid interface) with the hydrophobe orientated away from the water. This concentration of surfactant molecules at the surface is termed **adsorption** and has a profound effect on the surface tension of the solution, as discussed below. Although there is a strong desire for surfactant molecules to lie at the air/water interface, thermal energy of the liquid and

Brownian motion mean that there is an equilibrium between those at the surface and those present in the bulk, even at low concentrations.

The length of the hydrophobic tail group is known to have a direct effect on a number of physical properties of the surfactants. For example, increasing the length of the tail group decreases the solubility of the surfactant in water, whilst increasing solubility in organic solvents. Longer-chained surfactants have an increased tendency to adsorb at the interface and, head-group size permitting, pack more closely at the interface than their shorter-chained analogues.[1]

Although all of the systems considered here involve a gas/liquid interface, surfactant adsorption can occur at other types of interfaces such as solid/gas, solid/liquid and between two immiscible liquids such as oil and water.

1.3 Micelles

As the concentration of surfactant increases, the surface becomes crowded to the point where no more surfactant molecules can be adsorbed at the interface and must therefore be accommodated in the bulk of the water. However, both of the amphiphilic parts of the surfactant need to be satisfied and only a very small portion of individual surfactant molecules can exist in the aqueous phase. At this point the surfactant molecules spontaneously self-assemble to create a microphase in which the hydrophobic tail groups aggregate in the centre, shielded from the aqueous phase and the hydrophilic head groups face outward; these aggregates are termed micelles.

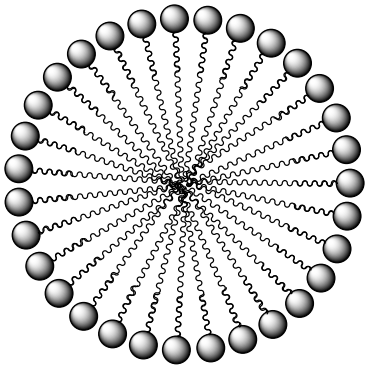

Figure 1.2 Schematic of a micellar arrangement in an aqueous environment

There are three main parameters which contribute to the free energy of aggregation and therefore determine the size and shape of the micelle. Firstly, transfer of the hydrophobic moieties out of the aqueous phase and into the arranged interior of the aggregate leads to a favourable **hydrophobic contribution**. This takes into account the conformational free energy of the tail groups inside the micelle with regard to the constraints caused by alignment of the head groups on the aggregate surface. Secondly, there is a **surface term** which represents the antagonistic interactions of the surfactant head groups as they pack closely together. This may consist of electrostatic repulsion caused by like charges on the head groups, steric hindrance arising from the structural conformation or the presence of water molecules within the aggregate shell. Finally, there is a **packing term** which relates to the favourable, entropy-driven process by which the hydrophobic tail groups expel the head groups and water from the core of the aggregate.[2]

The simplest form that micelles can take is to arrange into a spherical aggregate where the radius is dictated by the all-*trans* length of the hydrocarbon tail, this in turn influences the arrangement of the head groups at the micellar interface. For more complex, non-spherical aggregates (*e.g.* rods, ellipsoids) the possible structures are limited by the need to keep the hydrophobic tail away from the aqueous phase and the hydrophilic head on the aggregate interface. However, the smallest dimension of these structures is still limited by the length of the hydrophobic tail. The nature of variables such as the head-group and the area it occupies, the surfactant ionic strength, the hydrophobic volume and the temperature also contribute to predictions about the size and shape of an aggregate.[3]

As the concentration of surfactant is increased it generally leads to the formation of more micelles of the same size and shape, which are approximately monodispersed in the solution, rather than creating larger micelles. This also means that there is a very narrow size distribution of micelles and therefore the system can be characterised by a single critical micelle concentration (see section **1.5**, below). However, when the surfactant concentration is high enough some spherical micelles can become larger aggregates such as rods or tubes. Further increasing concentration can lead to the formation of liquid crystals, however this is limited by the solubility of the surfactant.[4]

Surfactant molecules in a micelle are associated physically, not chemically, meaning that micellisation is a reversible process and that the properties of the micelles can vary in response to solution conditions such as temperature, pH or presence of salt.

The descriptions above relate to surfactant molecules in aqueous media. Micellisation can also occur in organic media, however in order to accommodate the amphiphilic nature of the surfactant, micelles form with the hydrophilic head groups at the centre and the hydrophobic tail groups facing outward. These aggregates are termed **reverse micelles**.

1.4 Surface Tension

In the bulk of the continuous aqueous phase each water molecule experiences short-range attractive forces of equal magnitude in all directions from its neighbouring molecules. Those at the surface (air/liquid interface) of the water, however, have no 'upward' forces acting on them but still experience the same amount of attraction in other directions. These unbalanced forces manifest in a net inward pull where as many water molecules as possible will move away from the surface towards the bulk of the liquid. This gives rise to a spontaneous contraction of the liquid known as the **surface tension**.

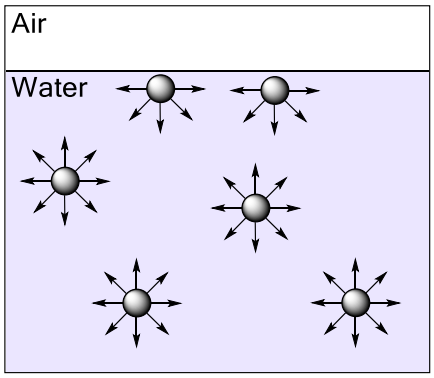

Figure 1.3 Attractive forces acting on water molecules in the interior of the liquid *vs*. the surface

Adsorption of surfactants at the air/liquid interface causes a decrease in the surface tension of the water. When a full monolayer is formed and the surface is packed the surface tension is at a minimum, after this point there is no further (significant) reduction. When a monolayer of surfactants forms at the interface it changes the surface from being aqueous in nature, which has an inherently high surface tension, to being a hydrocarbon surface, which has an inherently low surface tension.

Reducing the surface tension of water is a useful process as it allows water to mix with immiscible liquids such as oil. Often, only a small proportion of surfactant is required to sufficiently lower the surface tension, for many surfactants as little as 0.1% can reduce the surface tension of water from 72 mN m^{-1} (surface tension of pure water at 298 K) to around 32 mN m^{-1}.[5]

1.5 The Critical Micelle Concentration

The point at which the air/liquid interface becomes fully populated and surfactants start to aggregate into micelles is known as the **critical micelle concentration** (**CMC**). This parameter is characteristic of the components and conditions of a surfactant solution as micelle formation depends both on factors intrinsic to the surfactant molecule such as structure, size or charge and external factors such as pH, temperature or the presence of other compounds in solution.[1]

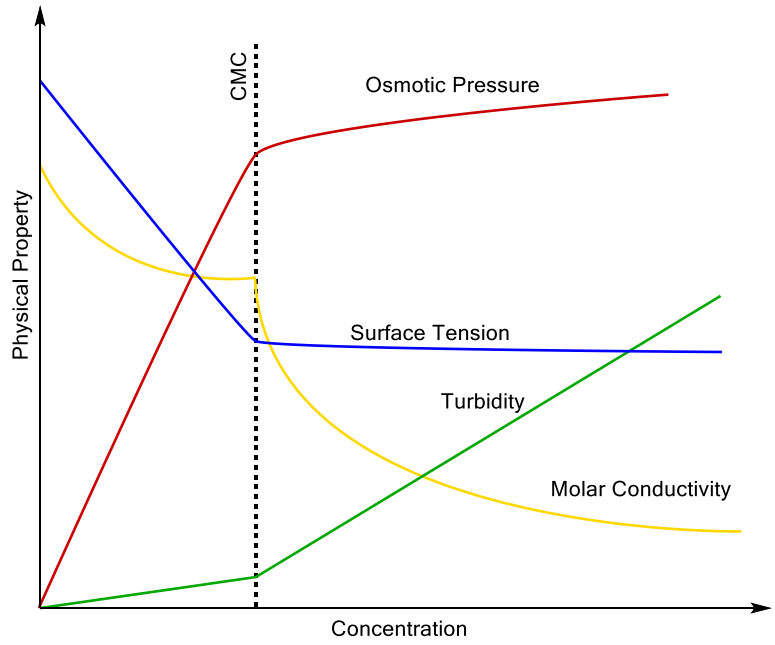

Figure 1.4 Changes in selected physical properties of typical surfactants in aqueous media in relation to the CMC[6]

When the CMC is reached there is a sudden change in many of the physical properties of a micellar system such as the surface tension, electrical conductivity, osmotic pressure and turbidity, as illustrated in Figure 1.4. Measurement of these changes with increasing concentration of surfactant not only allows for determination of the CMC, but also provides information about surfactant purity.

The surface tension of a solution can be measured using techniques such as drop volume tensiometry (DVT) as discussed below. Figure 1.5 shows an example of the profile obtained from plotting the ln[surfactant/M] *vs.* surface tension (in mN m^{-1}). The diagram can be divided into four distinct regions, as illustrated, corresponding to (a) pure water, which has a surface tension of 72 mN m^{-1} at 298 K; (b) as the concentration of surfactant increases molecules adsorb at the air/water interface reducing the surface tension; (c) when the interface is fully saturated the surface tension reaches a minimum, at this point aggregates begin to form, therefore this concentration corresponds to the CMC; (d) as the concentration continues to increase more micelles are formed, as they are not surface active any changes in the surface tension observed after this point are due to adsorption or desorption of surfactant molecules at the air/water interface. This method of characterisation can also provide information on the purity of the surfactant as any deviation from this profile can indicate the presence of surface active impurities in the solution. [7] Determination of the CMC for a particular surfactant is important as it defines the limiting concentration for use in processes that require the presence of micelles.[6]

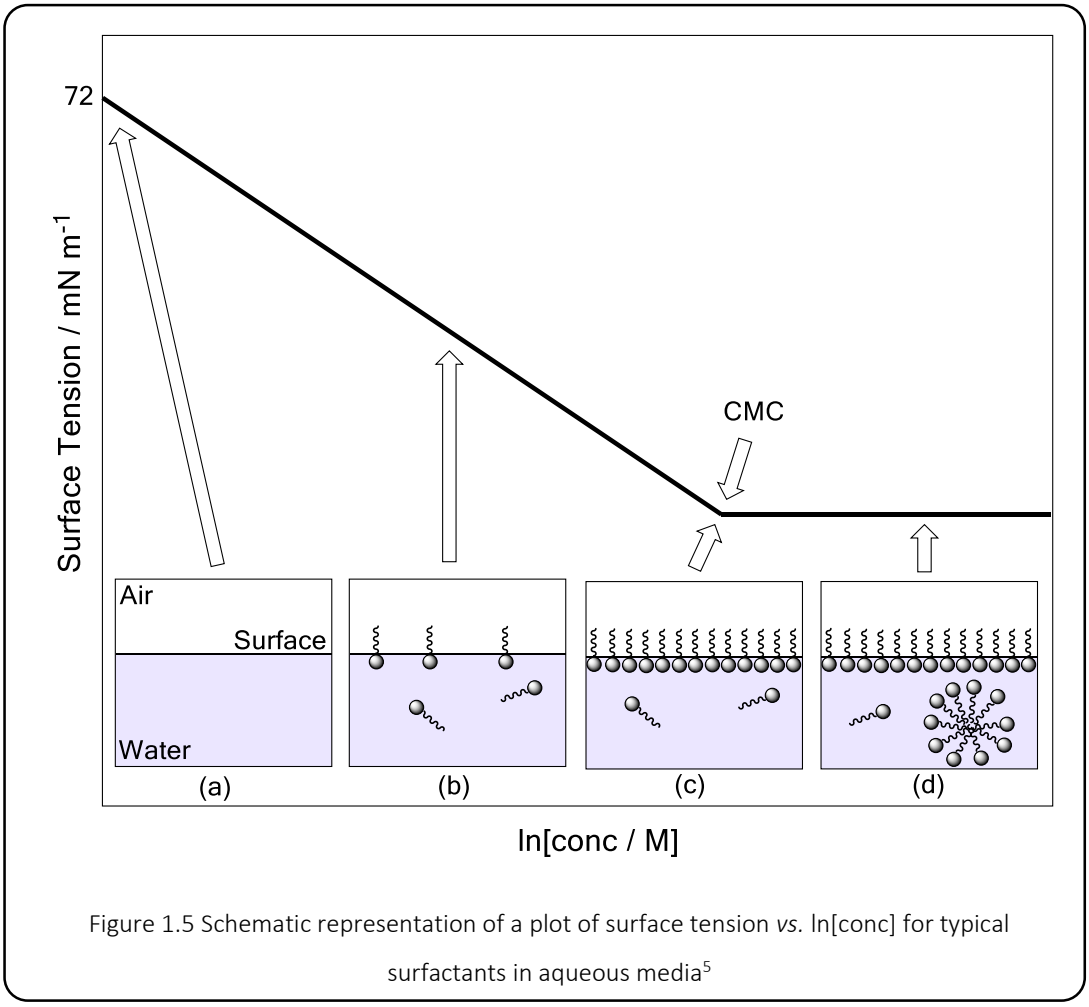

Figure 1.5 Schematic representation of a plot of surface tension *vs.* ln[conc] for typical surfactants in aqueous media[5]

As well as providing a value for the CMC the surface tension plot can be used to calculate the surface area of a micelle occupied by a single surfactant head group, or area per molecule (APM).

In the low concentration region of the surface tension plot (Figure 1.5 (b)) the relationship between surface tension and ln[surfactant] is a secondary polynomial relationship. In the region where surfactant concentration is high (Figure 1.5 (d)) the relationship is linear. The point where these two lines intersect is the CMC (Figure 1.5 (c)).

The APM is defined in Equation 1.1, where N_A is the Avogadro constant and Γ is the surface excess concentration (in mol m^{-2}) which is the area-related concentration of the surfactant at the interface.

——— …….Equation 1.1

——— ———…….Equation 1.2

The value of the surface excess (Γ) is calculated by Equation 1.2 where R is the gas constant (J K^{-1} mol^{-1}), T is the temperature (K) and $(dy/dlnc)$ is the differential of the equation for the polynomial section ($ax^2 + bx + c$) of the surface tension plot where x = ln[CMC/M]. The value n relates to the number of species formed in solution by the surfactant. For non-ionic surfactants n = 1 whereas for ionic surfactants n = 2 as both the surfactant and its counter ion have to be taken into consideration. However, in reality for ionic surfactants the degree of dissociation between the surfactant and its counter ion influences this value, therefore in most cases the true value lies somewhere between n = 1 and n = 2.[7]

1.6 Drop Volume Tensiometry

In this thesis all the surface tension data were obtained *via* drop volume tensiometry (DVT) as it is a versatile method which can be applied to all types of surfactants. DVT measures the dynamic surface tension of a liquid in the bulk air phase and therefore allows for determination of a surfactant's CMC, as described above.

During a DVT measurement a sample of known concentration is loaded into a syringe mounted above a quartz cuvette. A motorised driver pushes down on the syringe plunger at a predetermined rate (flow rate), creating a drop at the tip of the syringe capillary. The drop slowly

grows in size until it detaches, as it falls it cuts a light barrier which registers as a measurement. As the flow rate and the time required for the drop to detach are accurately measured the precise volume of the drop at the point of detachment can be determined. This is repeated over a wide range of concentrations and the surface tension measurements plotted against ln[surfactant/M] to give a plot similar to that shown in Figure 1.5, above.

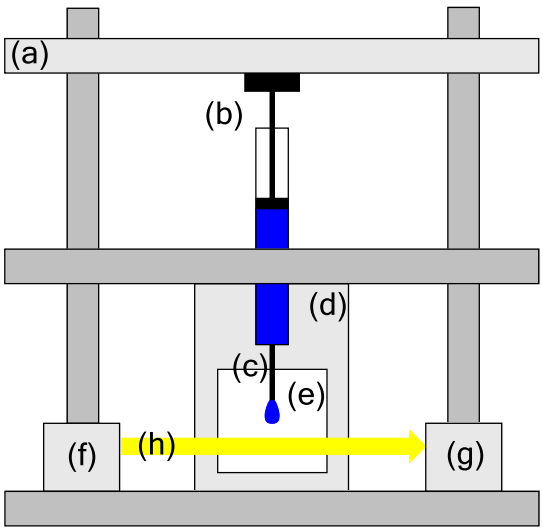

Figure 1.6 Schematic of DV tensiometer (a) syringe motor (b) syringe (c) metal capillary (d) measurement cell (e) quartz cuvette (f) light source (g) detector (h) light beam

The shape of the drop which forms at the end of the capillary is a result of the antagonistic forces of surface tension and acceleration due to gravity. The inward pull of surface tension means that the ideal form of the droplet is spherical, but acceleration due to gravity distorts it from the ideal. Detachment of the drop requires the formation of a new interface, in order for the drop to detach from the capillary the force created by the weight of the drop must be greater than the force created by the surface tension on the circumference of the capillary. The flow of the tensiometer steadily increases the volume of the drop until it reaches a value at which it cannot be counterbalanced by the surface tension and so the drop detaches.

Equation 1.3 describes the existing force balance between the surface tension and the acceleration due to gravity:

.....Equation 1.3

Where σ is the surface tension (mN m^{-1}); V is the drop volume (µL); g is the acceleration due to gravity (ms^{-2}); $\Delta\rho$ is the difference of the densities of the two adjacent phases (g mL^{-1}); r_{cap} is the radius of capillary (mm) and F is a correction factor (determined experimentally and theoretically).

The correction factor (F) is required because the drop detaches from the neck of the syringe capillary rather than from the direct tip. The term $2.\pi.r_{cap}$ represents the circumference of the capillary which is the edge along which the surface tension (σ) acts to counterbalance the force represented by $V.\Delta\rho.g.$[4,5]

1.7 Microemulsions

One of the key properties of aqueous micellar systems at concentrations above the CMC is their ability to solubilise liquids which would otherwise be immiscible with water, such as organic solvents and oils. Without the presence of surfactants the combination of oil and water results in the formation of unstable, cloudy emulsions or in the formation of two discrete phases.

When an immiscible organic phase is added to an aqueous micellar system it is sequestered at the centre of the micelles. The hydrophobic tail groups interact with the oil phase inside the micelle while the hydrophilic head groups lie at the micellar interface, creating a stable oil droplet. Section 1.3 described how in micelles the smallest size parameter is determined by the length of the hydrophobic tail group, however, they are capable of expansion as oil is added and dissolved within the micelle. The oil-containing droplets are typically monodisperse and within the range of 0.01 to 0.1 µm and therefore, unlike emulsion droplets, are too small to scatter light. This creates thermodynamically stable, transparent solutions known as microemulsions.

Microemulsions comprising oil droplets dispersed in a continuous aqueous phase are termed oil-in-water (o/w) microemulsions. The reverse situation is also possible, water can be added to an oil phase containing surfactants in reverse-micelle arrangements to give a water-in-oil microemulsion (w/o).

Microemulsions represent an intermediate state between the micellar system and a traditional emulsion. The oil-solubilising ability of a particular microemulsion is dictated by a number of parameters such as the amount and type of surfactant present, the type of oil, the pH and the temperature of the overall system. For example, non-ionic surfactants are typically capable of solubilising more oil than ionic surfactants and systems that form larger micelles are generally better at solubilisation.[8]

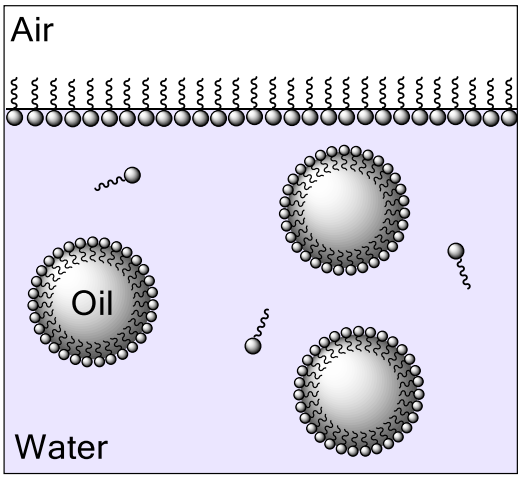

Figure 1.7 Schematic of an o/w microemulsion

Microemulsions are a valuable medium for a wide variety of applications as they allow immiscible solvents to come into close contact with one another. They are also highly tuneable as many of their components can be varied in order to tailor the microemulsion to the requirements of the applications.

1.8 Mixed Surfactant Systems

For most industrial and commercial needs it is not possible to create a microemulsion with the desired properties using only a single surfactant. Therefore mixed-surfactant systems are employed, comprising two or more types of surfactant in varying ratios. The additional surfactants are often termed **co-surfactants** or **hydrotropes** and can greatly alter the properties of the microemulsions they comprise and extend the ranges at which they are useful.

Co-surfactants tend to have large head groups and short tail groups, compared to the main surfactants, which often gives them a 'wedge-like' shape. This allows them to be incorporated into the outer region of the micelle, in between the main surfactants, which can reduce electrostatic repulsion between surfactant head groups, thus altering the curvature and stability of the micelle. In many cases a co-surfactant is added to prevent large micelles from forming by stabilising the spherical micelles and preventing sphere to rod transitions. This in turn reduces the viscosity of the microemulsions even at high concentrations and in the presence of dissolved salts.

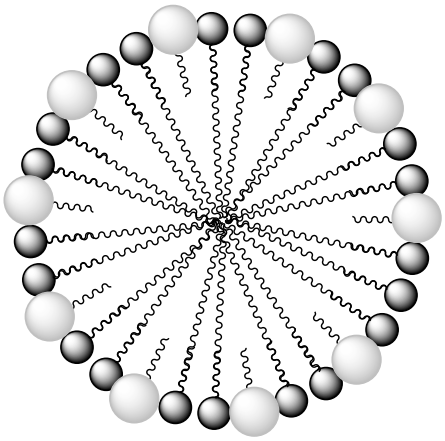

Figure 1.8 Schematic of a 2-component mixed-surfactant micellar system (dark grey = surfactant; pale grey = co-surfactant)

Most mixed-surfactant solutions are formulated in order to reduce the CMC of the overall system. Those in which the CMC of the mixed system is lower than those of the individual surfactants exhibit **synergism**. However, it is possible that the CMC of the mixed system will be higher than those of the constituent surfactants, this is classed as **negative synergism**. It is also possible that the CMC will be an intermediate value.[1,3,4]

Like the main surfactants in a micellar system, co-surfactants may be ionic, non-ionic or zwitterionic. Figure 1.9, below, shows some example species that have been used as co-surfactants with sodium dodecyl sulphate (SDS) which is the most widely-used surfactant to date.

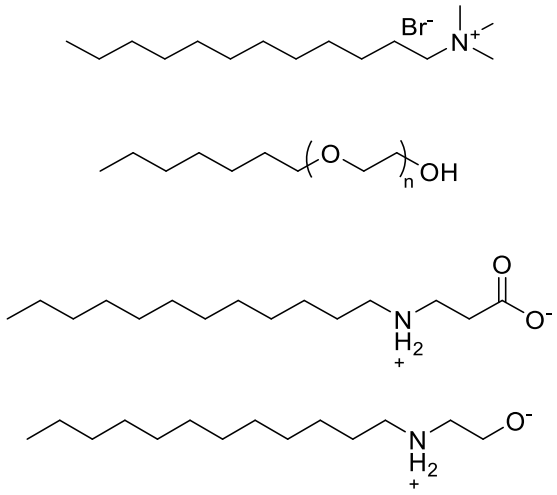

Figure 1.9 Examples of various cosurfactants reported for SDS (top to bottom [9,10,11,12])

1.9 Metallosurfactants

All of the surfactants considered so far have been organic molecules, however, interest in recent years has increased with regard to metal-containing surfactants, or **metallosurfactants**. These are amphiphilic molecules where the hydrophobic tail group is usually a long chain hydrocarbon and the hydrophilic head group comprises a metal complex, typically a d- or f-block metal. Metallosurfactants offer the ability to localise the physicochemical properties of metal ions at oil/water or air/water interfaces.[13]

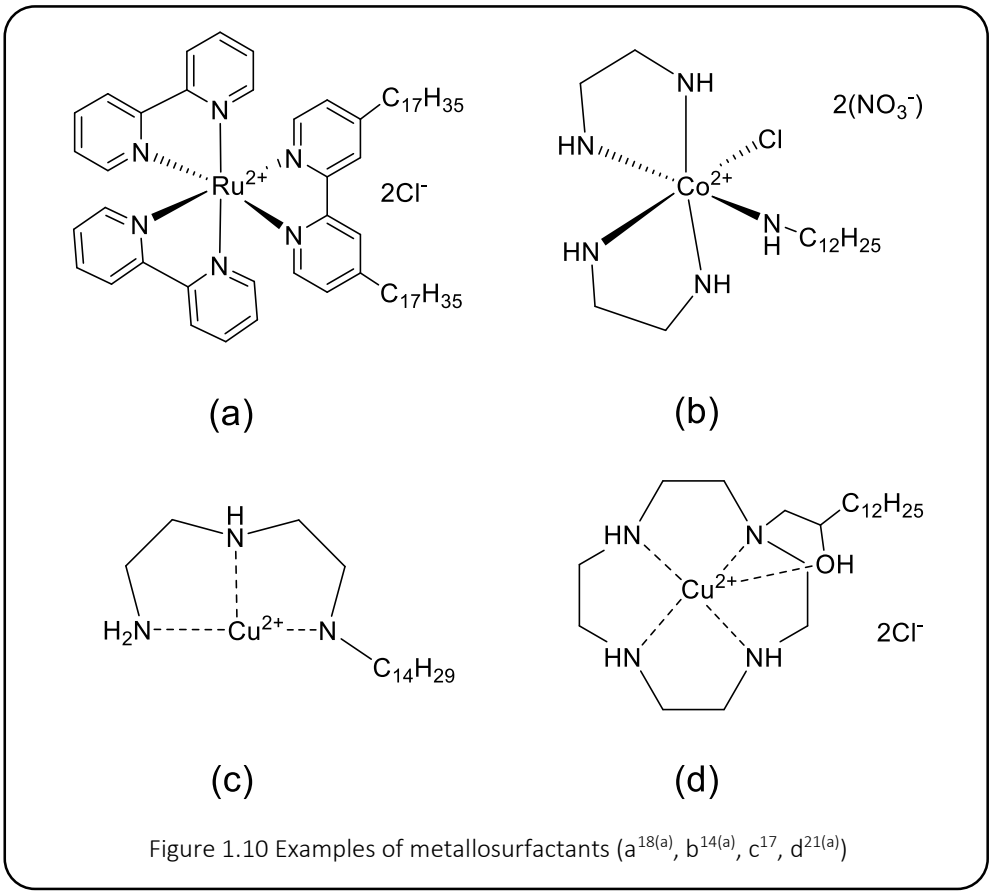

Figure 1.10 Examples of metallosurfactants (a[18(a)], b[14(a)], c[17], d[21(a)])

There is a great deal of diversity in the structures of reported metallosurfactants. Most examples comprise metal complexes in which the ligand architecture provides the amphiphilic moiety. This may be as a monodentate ligand,[14,15,16] an acyclic multidentate ligand[17,18,19] or a macrocyclic multidentate ligand.[20,21,22] Multidentate ligands are generally more favourable due to the chelate effect meaning they provide a greater degree of stability which prevents the metal ions being free within a micellar system, leading to unwanted interactions. The other form of metallosurfactants reported are those in which the metal ion is present as a cationic counter ion to the anionic surfactant.[23,24,25]

Metals used in metallosurfactants include Ag(I),[26] Co(III),[14,20,21(c,d),23(a,b),27] Cu(II),[17,21,23(b,c),27] Fe(II/III),[15,23(a,b),25] Gd(III),[22] Ir(III),[18] Ni(II),[21(a,b),23(b),27] Pd(II),[16,24] Ru(II),[18(a),19] and Zn(II).[23(a)] These metallosurfactants have been reported in a wide range of applications as magnetic resonance imaging contrast agents,[22] molecular sensors,[20] precursors for thin-film optoelectronics,[18] antimicrobial agents,[26] templating species for mesoporous materials,[18(b),19(d),21(d),25] catalysts[17,19(c)] and anti-cancer agents.[26]

1.10 Microemulsions in Liquid Scintillation Counting Methods

Despite the plethora of applications described for microemulsions in the literature, the focus of this thesis is the design of systems with potential as liquid scintillation counting (LSC) cocktails.

The technique of LSC is employed by the nuclear industry to detect analytes of interest such as ^{90}Sr, ^{137}Cs, ^{55}Fe, ^{63}Ni, ^{3}H, ^{151}Sm, ^{155}Eu and ^{121m}Sn which are typically low-level β or βγ emitters. Many commercial LSC cocktails comprise microemulsions as they provide the ideal conditions for efficient LSC and can accommodate all of the components required.

1.10.1 Principles of LSC

The method of LSC relies on the radioactive decay process of the analyte which releases energy which is absorbed by a non-emissive solvent, typically an aromatic species with high π electron density which can efficiently transfer energy between molecules until it comes into contact with a scintillant. Scintillants are highly conjugated emissive molecules which can absorb energy from solvent molecules and emit it as light as they relax back to the ground state. In some cases only one scintillant is required if it emits light in the correct range for the detector, however in most cases two scintillants are required. The primary scintillant absorbs energy from the solvent and emits it at a wavelength compatible with excitation of the secondary scintillant, which then emits light at a wavelength in the optimum detection range of the photomultiplier tube detector.

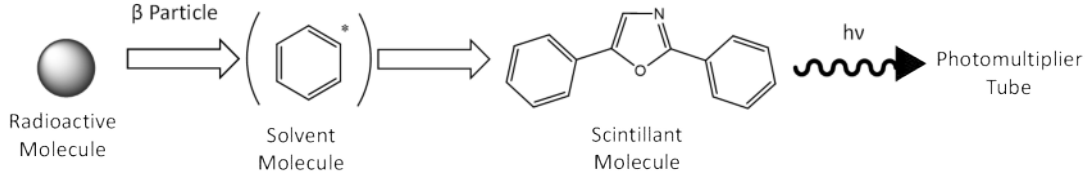

Figure 1.11 Representation of the LSC process
(2,5-diphenyloxazole shown here as an example scintillant)

Commercial solutions, known as cocktails, provide all of the required components for LSC and are tailored to the nature of the analyte under investigation. Section 1.10.5 tabulates a number of commercial cocktails and their components.

Most commercial cocktails are w/o microemulsions as the analytes are water soluble whereas the scintillants required for detection are only soluble in organic media. Therefore a microemulsion is the ideal medium for LSC cocktails as it enables the water and oil phases to come into very close contact, thus allowing energy from the decay to be efficiently transferred to the scintillants whilst reducing the amount of energy lost through interaction with water molecules. Surfactants are required to create a microemulsion stable enough to withstand the required counting time.

1.10.2 Solvents

Most LSC cocktails are w/o microemulsions and therefore the properties of the solvent (oil) will generally dictate the properties of the overall system. Original commercial cocktails used benzene and substituted benzenes (such as toluene, xylene and pseudocumene (1,2,4-trimethylbenzene)) but these solvents are generally highly toxic, irritant and highly flammable.

"Opti-Fluor" was developed in 1984 and uses a linear alkyl benzene (LAB) which has a much higher flash point than the other solvents at ~137 °C, making it a safer alternative. It is also much less harmful to the environment as it is a precursor to dodecyl benzene (soap powder) and is biodegradable when combined with detergents. Di-isopropyl naphthalene (DIN) is a similarly useful LSC solvent due to its high aromaticity, high flash point (~145 °C) and biodegradability when combined with detergents. Phenylxylylethane (PXE) has similar properties to DIN, but is more viscous. LAB, DIN and PXE are in use in current LSC cocktails but despite being less hazardous than earlier solvents they are still regarded as irritants.[28,31,32,33,34]

1.10.3 Scintillants

Scintillant molecules are typically highly conjugated polyaromatics. Some solutions use only primary scintillants whilst others use both primary and secondary. A secondary scintillant is required when the emission wavelength of the primary scintillant does not match the energy range of the detector. In these cases, emission from the primary scintillant excites a secondary scintillant due to an overlap in their emission and absorption wavelengths, respectively.

Relaxation of the secondary scintillant results in emission at a wavelength compatible with the detector.

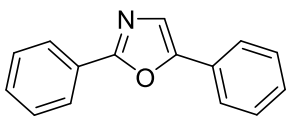

2,5-diphenyloxazole (PPO)

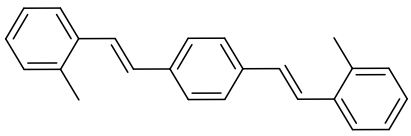

1,4-bis(2-methylstyryl)benzene (bis-MSB)

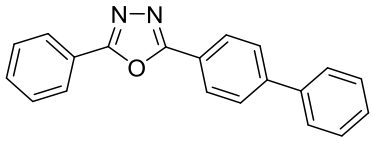

2-phenyl-5-(4-biphenylyl)-1,3,4-oxadiazole (PBD)

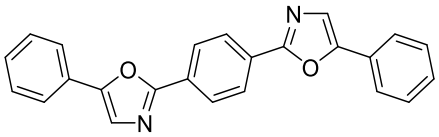

1,4-bis(5-phenyl-2-oxazolyl)benzene (POPOP)

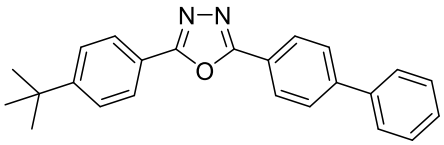

2-(4-biphenylyl)-5-(4-tert-butylphenyl)-1,3,4-oxadiazole (butyl-PBD)

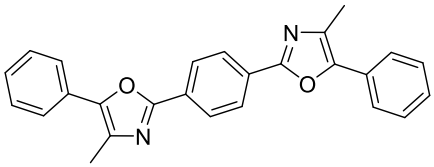

1,4-bis(4-methyl-5-phenyl-2-oxazolyl)benzene (dimethyl-POPOP)

Figure 1.12 Examples of primary and secondary scintillants

A large number of scintillants have been developed over the years. In the 1950s-60s Hayes and Ott published a definitive paper of oxazole scintillants exploring the UV absorption and fluorescence spectra of a series of fluorophores as well as providing the synthesis and evaluation of their scintillation efficiency.[29] Figure 1.12, above, shows the most common primary and secondary scintillants that have been in use since the Hayes and Ott study.

1.10.4 Surfactants

The first microemulsion cocktails developed used Triton X-100 (octylphenol ethoxylate) surfactants.[30] However, the majority of LSC cocktails use NPEs (nonylphenol ethoxylates) to form the basis of a microemulsion, the performance of which can then be enhanced by addition of other detergent additives. NPEs are available in various ethoxylate chain lengths (EO = 5 to 10) but few are used in cocktails. The longer the chain the better the cocktails' performance at or above 20 °C, whereas shorter chain lengths perform better at lower temperatures. The major

disadvantage for NPEs is that at loadings of >20% gels and semi-gels form, leading to the requirement of additives to extend the working range of the cocktails.

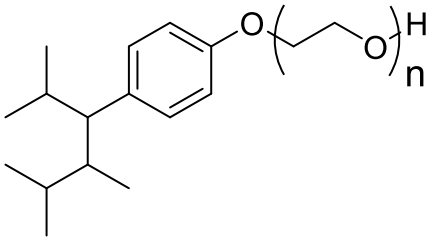

Figure 1.13 NPE (nonylphenol ethoxylate) n = 5-10

The problem of gel formation can be overcome by addition of co-solvents, typically long-chain alcohols such as diglycols. Sulphosuccinate additives also extend the capacity for water and dilute aqueous samples, therefore a common component of LSC cocktails is dioctyl sulphosuccinate.

There is a stability problem with samples at 0.5 M or greater as the microemulsion can break down to give a "milky" solution. Use of free-acid or neutralised phosphate esters can be used to circumvent this issue as they increase microemulsion stability in more concentrated samples. These species can be derived from NPEs or alcohols.

1.10.5 Commercial LSC Cocktails

Table 1.1, below, compiles various examples of commercially available LSC cocktails. From these examples it can be seen that there are a number of components common to many cocktails, such as linear alkyl ethoxylates, DIN isomer solvents and scintillants such as PPO and bis-MSB.

Commercial Name	Composition
Econscint Ultra[a]	bis(1-methyethyl)naphthalene 60-80%
	butyl dioxitol 5-10%
	linear alkyl phenyl ethoxylates 20-40%
Ecoscint[a]	N-alkylene 70-85%
	linear alkyl phenyl ethoxylates 15-30%
	1-methoxy-2-(2-methoxyethoxy)ethane 1-3%
Ecoscint A[a]	PXE 55-70%
	linear alkyl phenyl ethoxylates 30-40%
	MeOH 1-3%

Scint Logic U[b]	PXE 50-70%
	primary alcohol ethoxylate 5-10%
	butoxyethanol 5-10%
	linear alkyl phenyl ethoxylates 20-30%
Scint Logic LB[b]	bis(1-methyethyl)naphthalene 60-80%
	butyl dioxitol 5-10%
	linear alkyl phenyl ethoxylates 20-40%
Flow Logic MC[b]	1,2,4-trimethylbenzene 50-70%
	butanol-2-methyl-propan-1-ol 10-15%
	ethoxylated nonylphenol 10-20%
Ultima Gold[c]	DIN isomers 60-80%
	alkylphenolpolyglycolether 10-20%
	2-ethylhexylphosphatediethanolamine salt 10-20%
	sodium dioctyl sulphosuccinate $\leq$ 2.5%
	triethyl phosphate $\leq$ 2.5%
	PPO $\leq$ 2.5%
	bis-MSB $\leq$ 2.5%
	water
Insta-gel[c]	1,2,4-trimethylbenzene 40-60%
	alkylphenolpolyglycolether 40-69%
	nonylphenolethoxylatephosphatediethanolamine salt $\leq$ 2.5%
	PPO $\leq$ 2.5%
	bis-MSB $\leq$ 2.5%
	water
Optiphase[c]	DIN isomers 40-60%
	alkylphenolpolyglycolethanol 20-40%
	2-(2-butoxyethoxy)ethanol 10-20%
	phenolethoxylatedphosphateddiethanolamine salt 10-20%
	sodium dihexyl sulphosuccinate 2.5-10%
	sodium dioctyl sulphosuccinate $\leq$ 2.5%
	PPO $\leq$ 2.5%
	bis-MSB $\leq$ 2.5%
	water

ProFlowP+[d]	DIN isomers 40-60%
	alcohol ethoxylate 20-40%
	2-(2-methoxyethoxy)ethanol 2-10%
	2-(2-ethoxyethoxy)ethanol 2-10%
	alcohol ether phosphate ester 2-10%
	polyoxyethylene C_8-C_{10} ether phosphate 1-5%
	PPO 0.1-1%
	bis-MSB 0.1-1%

Table 1.1 Commercial LSCs: a[31] b[32] c[33] d[34] (components named as they are listed in sources)

1.11 Project Aims

The aim of the work presented in the thesis was to develop a range of surfactant ligand architectures capable of binding various s-, d- and f-block metals and localising them on the surface of a micellar droplet. A diverse array of ligand architectures were developed in order to produce a breadth of metallosurfactant compounds with various properties. Tensiometry was used to assess the purity of surfactants and their ability to form micelles in both single- and mixed-surfactant systems. For the single-surfactant systems the CMC was calculated, allowing for direct comparisons to be made between different micellar systems. Complexes with chromophoric ligands were investigated via combined tensiometry and photophysical studies to provide insight into the effect of aggregation upon the properties of the metal complexes. Finally, the stability and oil-solubilising ability of subsequent microemulsions were established.

The foundation the work presented herein was the development microemulsions which have the potential to act as LSC cocktails for a wide range of analytes. For example, radioactive Sr(II) and Y(III) are common by-products of nuclear fission and are often found in ground water which also contains other ions, such as Ca(II). Various lanthanides were studied as they allow for photophysical characterisation of the micellar systems as well as being other radioanalytes of interest. Ni(II) and Cu(II) were also studied as they provide useful insight into the structural properties of the ligand complexes. Although design of the micellar systems was based applications as LSC cocktails, systems such as those described here may also have potential applications as imaging agents, drug delivery systems or as precursors to materials such as OLEDs.

1.12 References

1. M. J Rosen, *Surfactants and Interfacial Phenomena*, Wiley, USA, 2nd edn., 1989.

2. (a) R. Nagarajan and E. Ruckenstein, *J. Colloid Interface Sci.*, 1977, **60**, 221. (b) R. Nagarajan and E. Ruckenstein, *J. Colloid Interface Sci.*, 1979, **71**, 580. (c) J. N. Israelachvili, D. J. Mitchell and B. W. Ninham, *J. Chem. Soc., Faraday Trans. 2*, 1976, **72**, 1525–1568. (d) J. N. Israelachvili, S. Marčelja and R. G. Horn, *Q. Rev. Biophys.*, 1980, **13**, 121–200. (e) C. Tanford, *J. Phys. Chem*., 1974, 78, 2469-2479.

3. T. Hargreaves, *Chemical Formulation: An Overview of Surfactant-based Preparations Used in Everyday Life*, RSC, Cambridge, 2003

4. D. J. Shaw, *Introduction to Colloid and Surface Chemistry*, Butterworth-Heinemann Ltd., Oxford, 4th edn., 1992

5. Krüss educational resources, www.kruss.de/services/education-theory/glossary/drop-volume-tensiometer/ and www.kruss.de/services/education-theory/glossary/cmc/ (accessed March 2017)

6. W.C. Preston, *J. Phys. Colloid Chem.*, 1948, **52**, 84

7. Mukerjee et al. Journal of Colloid and Interface Science, 2013, **394**, 329-336

8. R. Nagarajan and E. Ruckenstein, *Langmuir*, 1991, **7**, 2934–2969.

9. Lucassen-Reynders, E.H., J. Lucassen and D. Giles *J. Colloid Interface Sci.*, 1981, **81** 150.

10. Holland P., and D.N. Rubingh, *J. Phys. Chem.,* 1983, **87**, 1984-1990.

11. Lange H. and Beck K.H. *Kolloid Z.Z. Polym.*, 1973, **251**, 424.

12. Tajima K., Nakamura, A. and Tsutsui T., *Am. Oil Chem. Soc.*, 1986, **63**, 566.

13. (a) J. Le Moigne, J. Simon, *J. Phys. Chem*., 1980, **84**, 170. (b) M. Cinquini, F. Montanari, P. Tundo, *J. Chem. Soc. Chem. Commun*., 1975, 393.

14. (a) T. A. Wagay, J. Dey, S. Kumar, V. K. Aswal and K. Ismail, *Colloid. Surf. A.*, 2016, **503**, 61–69. (b) S. C. N. Chandar, D. Sangeetha and M. N. Arumugham, *J. Solution Chem.*, 2011, **40**, 608–620. (c) A. Riyasdeen, R. Senthilkumar, V. S. Periasamy, P. Preethy, S. Srinag, M. Zeeshan, H. Krishnamurthy, S. Arunachalam and M. A. Akbarsha, *RSC Adv.*, 2014, **4**, 49953–49959. (d) T. A. Wagay, J. Dey, S. Kumar, V. K. Aswal and K. Ismail, *RSC Adv.*, 2016, **6**, 66900–66910. (e) R. S. Kumar, H. van den Bergh and G. Wagnières, *J. Solution Chem.*, 2012, **41**, 294–306.

15. R. Dong and J. Hao, *Chem. Phys. Chem.*, 2012, **13**, 3794–3797.

16. G. R. Chaudhary, P. Singh, G. Kaur, S. K. Mehta, S. Kumar and N. Dilbaghi, *Inorg. Chem.*, 2015, **54**, 9002–9012.

17. A. Polyzos, A. B. Hughes and J. R. Christie, *Langmuir*, 2007, **23**, 1872–1879.

18. (a) A. Guerrero-Martínez, Y. Vida, D. Domínguez-Gutiérrez, R. Q. Albuquerque and L. De Cola, *Inorg. Chem.*, 2008, **47**, 9131–9133. (b) M. de B. e S. Botelho, J. M. Fernandez-Hernandez, T. B. de Queiroz, H. Eckert, L. D. Cola and A. S. S. de Camargo, *J. Mater. Chem.*, 2011, **21**, 8829–8834. (c) J. M. Fernández-Hernández, L. De Cola, H. J. Bolink, M. Clemente-León, E. Coronado, A. Forment-Aliaga, A. López-Muñoz and D. Repetto, *Langmuir*, 2014, **30**, 14021–14029.

19. (a) D. Domínguez-Gutiérrez, M. Surtchev, E. Eiser and C. J. Elsevier, *Nano. Lett.*, 2006, **6**, 145–147. (b) J. A. Lebrón, F. J. Ostos, M. L. Moyá, M. López-López, C. J. Carrasco and P. López-Cornejo, *Colloid. Surf. B.*, 2015, **135**, 817–824. (c) M. J. Danks, H. B. Jervis, M. Nowotny, W. Zhou, T. A. Maschmeyer and D. W. Bruce, *Catal. Lett.*, 2002, **82**, 95–98. (d) K. E. Amos, N. J. Brooks, N. C. King, S. Xie, J. Canales-Vázquez, M. J. Danks, H. B. Jervis, W. Zhou, J. M. Seddon and D. W. Bruce, *J. Mater. Chem.*, 2008, **18**, 5282–5292.

20. (a) G. E. Jaggernauth and R. A. Fairman, *Inorg. Chem. Commun.*, 2011, **14**, 79–82. (b) G. E. Jaggernauth and R. A. Fairman *Inorg. Chem. Commun.*, 2014, **43**, 15–18.

21. (a) P. C. Griffiths, I. A. Fallis, D. J. Willock, A. Paul, C. L. Barrie, P. M. Griffiths, G. M. Williams, S. M. King, R. K. Heenan and R. Görgl, *Chem. Eur. J.*, 2004, **10**, 2022–2028. (b) P. C. Griffiths, I. A. Fallis, C. James, I. R. Morgan, G. Brett, R. K. Heenan, R. Schweins, I. Grillo and A. Paul, *Soft Matter*, 2010, **6**, 1981–1989. (c) N. Hondow, J. Harowfield, G. Koutsantonis, G. Nealon and M. Saunders, *Micropor. Mesopor. Mat.*, 2012, **151**, 264–270. (d) G. A. Koutsantonis, G. L. Nealon, C. E. Buckley, M. Paskevicius, L. Douce, J. M. Harrowfield and A. W. McDowall, *Langmuir*, 2007, **23**, 11986–11990.

22. (a) Y. Chen, Q. Zhu, X. Cui, W. Tang, H. Yang, Y. Yuan and A. Hu, *Chem. Eur. J.*, 2014, **20**, 12477–12482. (b) Q. Zhu, F. Pan, Y. Tian, W. Tang, Y. Yuan and A. Hu, *RSC Adv.*, 2016, **6**, 29441–29447. (c) Y. Chen, H. Yang, W. Tang, X. Cui, W. Wang, X. Chen, Y. Yuan and A. Hu, *J. Mater. Chem. B*, 2013, **1**, 5443–5449.

23. (a) S. K. Mehta and R. Kaur, *J. Colloid Interface Sci.*, 2013, **393**, 219–227. (b) P. Garg, G. Kaur and G. R. Chaudhary, *RSC Adv.*, 2016, **6**, 108573–108582. (c) R. Kaur, S. Gupta, S. K. Mehta, Y. Imai, T. Takiue, H. Matsubara and M. Aratono, *New J. Chem.*, 2014, **38**, 3925–3932.

24. G. Kaur, G. Karir and S. K. Mehta, *Colloids Surf. A,* 2013, **434**, 25–34.

25. S. Kim, P. Durand, T. Roques-Carmes, J. Eastoe and A. Pasc, *Langmuir*, 2015, **31**, 1842–1849.

26. G. Kaur, S. Kumar, R. Kant, G. Bhanjana, N. Dilbaghi, S. K. Guru, S. Bhushan and S. Jaglan, *RSC Adv.*, 2016, **6**, 57084–57097.

27. G. Kaur, P. Singh, S. K. Mehta, S. Kumar, N. Dilbaghi and G. R. Chaudhary, *Appl. Surf. Sci.*, 2017, **404**, 254–262.

28. R. Edler, *Perkin Elmer Application Note: Cocktails for Liquid Scintillation Counting*, Perkin Elmer Inc., Germany, 2015 (http://www.perkinelmer.com/lab-solutions/resources/docs/APP_Cocktails-for-Liquid-Scintillation-Counting-011940_01.pdf accessed June 2017)

29. D. G. Ott, F. N. Hayes, E. Hansbury and V. N. Kerr, *J. Am. Chem. Soc.*, 1957, **79**, 5448–5454.

30. M. S. Patterson and R. C. Greene, *Anal. Chem.*, 1965, **37**, 854-857

31. MSDS from https://www.nationaldiagnostics.com/liquid-scintillation/msds (accessed June 2017)

32.ScintLogicLB: http://ehsrms.uaa.alaska.edu/CMS/Laboratory/MSDS/MSDS%20by%20Vendor/LabLogic/ScintLogicLB.pdf; ScintLogic U: http://ehsrms.uaa.alaska.edu/CMS/Laboratory/MSDS/MSDS%20by%20Vendor/LabLogic/ScintLogicU.pdf; FlowLogicMC: http://ehsrms.uaa.alaska.edu/CMS/Laboratory/MSDS/MSDS%20by%20Vendor/LabLogic/FlowLogicMC.pdf (all accessed June 2017)

33. MSDS from http://www.perkinelmer.com/category/scintillation-cocktails (accessed June 2017)

34. MSDS from http://www.meridian-biotech.com/prosafe-cocktails/ (accessed June 2017)

Chapter Two

Macrocyclic Ligand Architectures towards Metallosurfactants and Metallomicelles

2.1 Introduction

2.1.1 Surface Active Ionic Liquids

Ionic Liquids (ILs) are a class of compound described as molten salts, with melting points below 100 °C. They have received substantial attention in the last decade due to their unique properties such as negligible vapour pressure, high ionic conductivity, non-flammability and wide liquid temperature range. They have been found to have a range of applications such as catalysis,[1] preparation of mesoporous materials[2,3] and as greener alternatives to traditional organic solvents.[4]

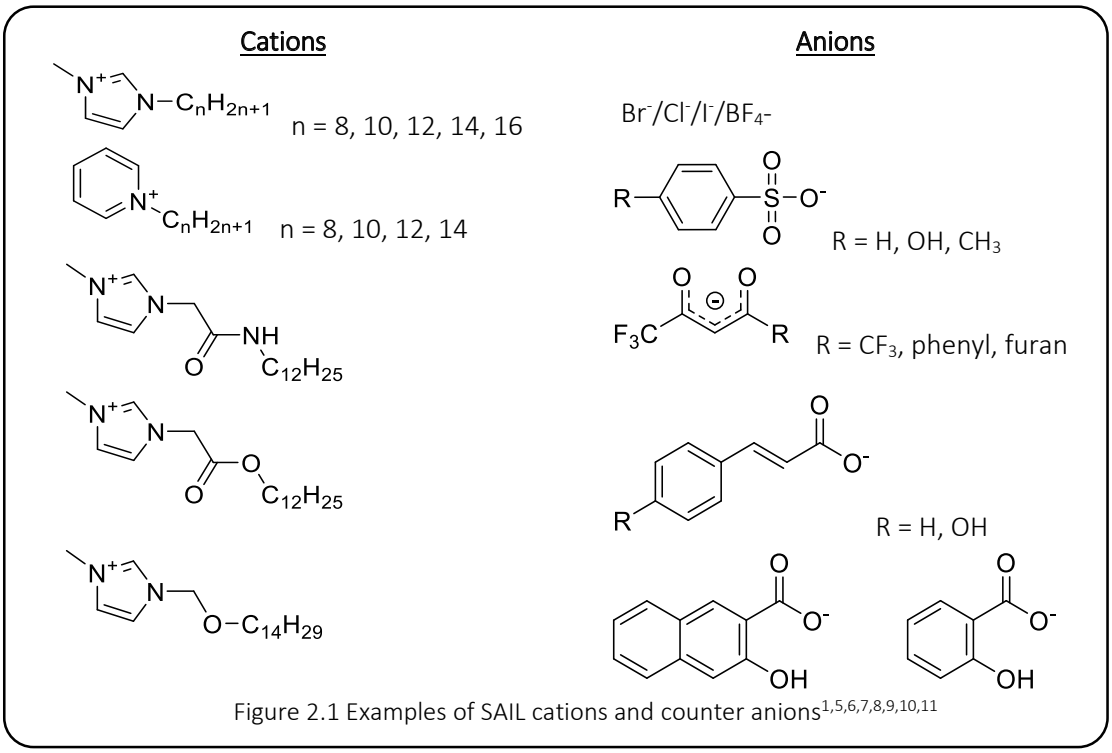

Figure 2.1 Examples of SAIL cations and counter anions[1,5,6,7,8,9,10,11]

Surface active ILs (SAILs), such as those shown in Figure 2.1, are ILs of amphiphilic nature, typically cationic compounds with long alkyl chains, usually of 8-16 carbon atoms. They have been found to have great efficiency at forming micelles in aqueous media where hydrophobic interactions between alkyl chains are the driving force behind micellisation.[12] One of the key properties of SAILs is their highly tuneable physicochemical properties such as melting point, lipophilicity, conductivity and viscosity. They are miscible with water and many organic solvents making them ideal candidates for microemulsion formulation[13,14] and have been described as having higher surface activity and lower CMC values than their traditional analogues.[6,15,16,17] The properties of these compounds can be easily tuned *via* variation in the nature of the cationic head group and

the counter anion.[2] The nature of the anion has been found to have a significant influence on the micellisation ability and the properties of the subsequent aggregates.[3,7,8,18,19]

One of the most well-known SAIL cations is 1-alkyl-3-methyl imidazolium ($MeImC_n^+$) which has been studied with a range of alkyl chain lengths and various anions. There are many literature examples of these cations and similar derivatives in a number of applications. For example, a range of such surfactants have been described which show promise as chemical demulsification agents for enhanced oil recovery.[20] A 2009 investigation by Trewyn *et al*. describes [$MeImC_n$]X SAILs (n = 12, 14, 16; X = Cl^-/Br^-) as templates in the synthesis of controlled drug delivery in nanodevices.[5] It is also among a number of studies to report the antibacterial properties of such SAILs, an effect which was found to increase with hydrophobicity.[12]

A small number of studies describe the incorporation of these SAILs into mixed-surfactant systems. The synergistic interactions between mixed surfactants have been found to produce systems with very different properties to their individual systems. For example, lower CMC values were reported for the mixed systems compared to the individual ones, this was attributed to synergistic interactions due to non-ideal mixing of aggregates.[14] Studies report the incorporation of [$MeImC_n$]X into solutions of SDS (sodium dodecyl sulphate)[9] and CTAB (cetyltrimethylammonium bromide)[21] where they have been found to influence the size and shape of micelles as well as altering the overall CMC of the system.

2.1.2 Macrocyclic Amphiphiles

Macrocyclic surfactants are amphiphilic molecules in which the head group is a multidentate cyclic species, typically capable of metal-binding. For most literature examples of such ligands the hydrophobic moiety is often a long alkyl chain, typically comprising 8-16 carbon atoms.[22] More variation is seen in the nature of the head group as different environments are required for the binding of different metals. The most common macrocyclic head groups reported are based on 1,4,7,10-tetraazacyclododecane (cyclen), 1,4,7-triazacyclanonane (TACN) or crown ether moieties.[23] Amphiphilic metallosurfactants are desirable species as they offer the opportunity to organise surface active species into a controlled volume and to concentrate metal ions on the interface of a micellar system.[24] Design of such systems requires a head group capable of binding the metal ion strongly in order to reduce the number of components which simplifies the system and allows for accurate determination of CMC values.

Extensive work has been carried out by Griffiths & Fallis *et al*. regarding TACN and cyclen based amphiphiles and the aggregation properties of their metallosurfactants. Micelles formed from aggregation of these ligands were found to be of the conventional structure in aqueous media, *i.e.* the hydrophobic alkyl chains aggregate in the core of the micelle, arranging the macrocyclic groups at the micellar interface. These micellar systems were found to conform to classical behaviour as the CMC was reduced by a factor of 2 for each methylene unit added to the hydrophobic chain. However, non-classical behaviour was observed in terms of head group structure as the CMC was found to increase by a factor of 3 for the inclusion of 3 additional methylene units into the head group.[24]

Exchanging the protonated alkyl chain for its fluorinated analogue was found to have a negligible effect on the interfacial structure. This was attributed to the bulky head groups being the dominating factor for packing arrangements at the interface. This was supported by the observation of a constant difference in the order of magnitude of the CMC values between the cyclen and TACN ligands, which also indicates that a small change in the nature of the head group has a large effect on the CMC of the resulting system.

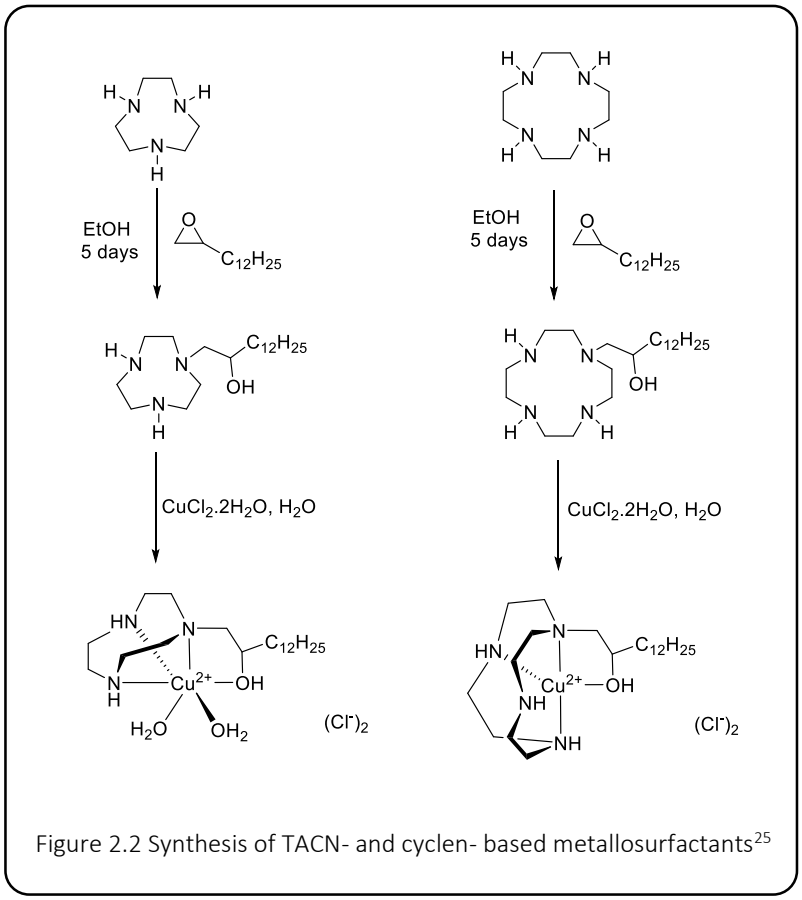

Figure 2.2 Synthesis of TACN- and cyclen- based metallosurfactants[25]

Cu(II) complexes of the TACN- and cyclen-derived ligands were found to form ellipsoid-shaped micelles. However, presence of s- or d-block metal cations in the macrocyclic head group was found to have very little effect on micellisation and therefore the micelle morphology. This may be attributed to the micellar system being of pH 5 meaning that the amine component of the head group will already be protonated prior to coordination of Cu(II) resulting in no significant change in the overall charge of the head group.[22,24,25]

1,4,10,13-Tetraoxa-7,16-diazacyclooctadecane (N2O4) and analogous crown ether amphiphiles are most commonly reported as ion-channels or transporters able to span cellular bilayers.[26,27,28] The most commonly reported ion-channels involve Na^+ and Cl^- transport.[29,30,31,32,33] However, similar amphiphiles have also been reported in the synthesis of Langmuir films.[34,35]

De Wall *et al*. described the synthesis and characterisation of a number of mono-, bis- and tris-alkylated crown ether derivatives. The mono-alkylated amphiphiles formed small aggregates of micellar or vesicular structure. As in other investigations the head group was found to be the dominant feature in determining micelle shape and size whereas the driving force behind micellisation was that of the interaction between hydrophobic tail-groups.[36,37]

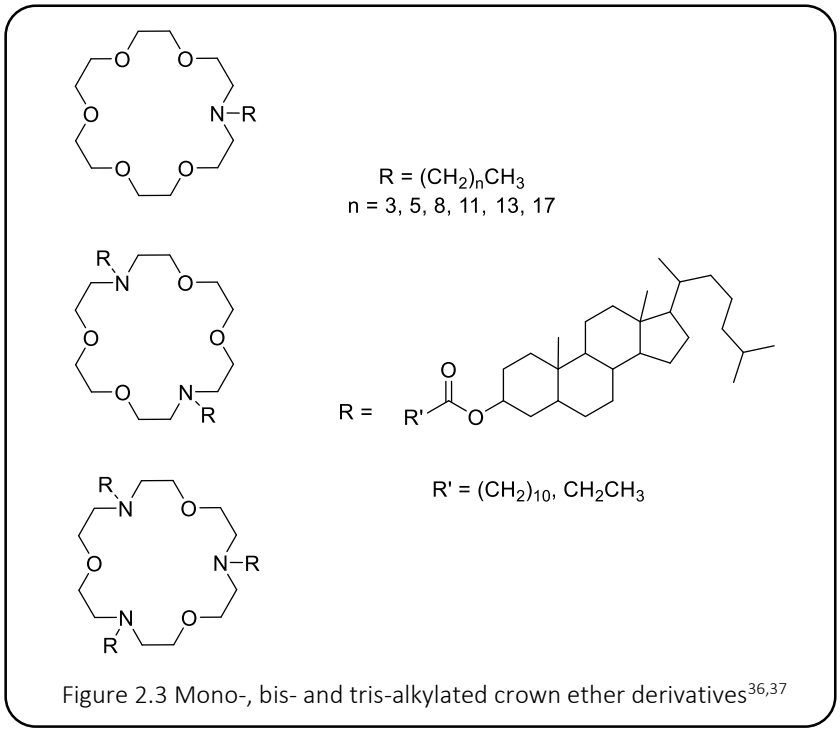

Figure 2.3 Mono-, bis- and tris-alkylated crown ether derivatives[36,37]

The majority of studies concerning 1,4,7,10-tetraazacyclododecane-1,4,7-triacetic acid (DO3A) based amphiphiles predominantly report Gd(III) complexes in large aggregated structures or

dendrimers.[38,39,40,41,42] It is generally noted that self-assembly or incorporation into such macromolecules significantly reduces the rotational motion of the Gd(III) complex increasing the relaxivity (compared to the free complex) and thus enhancing the contrast effect for molecular resonance imaging (MRI).[41,43] This is demonstrated in the study by Li *et al*. who report a self-assembled Gd(III) micellar aggregate which can control contrast abilities. An aggregation-based "switching-off" of contrast is afforded by shielding of the Gd(III) centre, a process which is reversed by disruption of the aggregate by a superior guest molecule, freeing the Gd(III) complex.[40]

Many studies focus on the incorporation of amphiphilic Gd(III) complexes into liposome arrangements. [44,45] Othman *et al.* reported squalenoyl-based species which self-assemble into micelles or liposomes and were found to be capable of forming mixed micelles with human serum albumin towards the development of anti-cancer drugs.[46] Other reports describe them as self-assembling precursors to formation of nanoparticles capable of combining anti-cancer medicines with MRI contrast agents such as those described by Arias *et al.*[47]and Liang *et al*.[48]

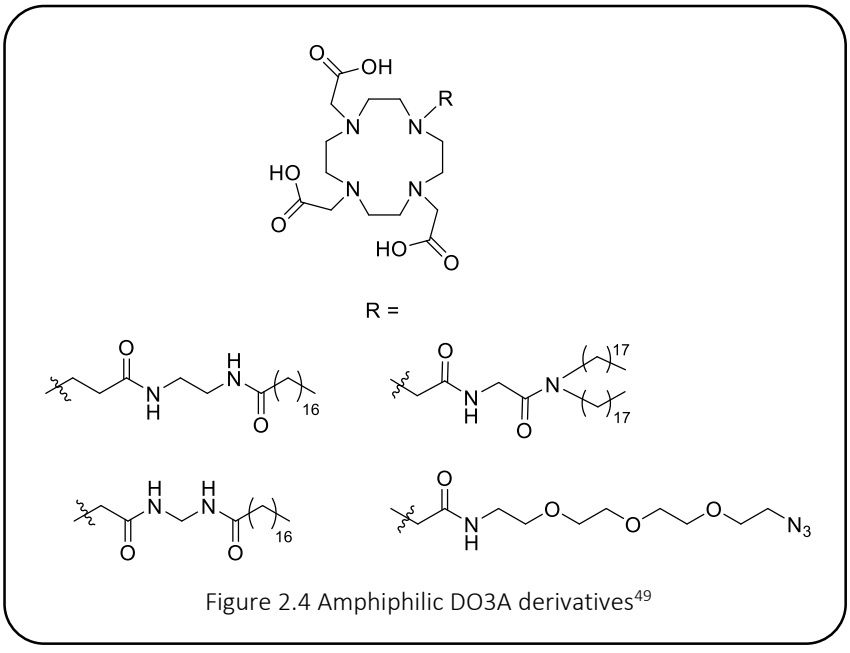

Figure 2.4 Amphiphilic DO3A derivatives[49]

Most other reports of macrocyclic amphiphiles incorporate supramolecular structures such as calixarenes or variations thereof. They have been reported as media for the enhancement of chemical reaction rates as well as for regio- and stereo-selectivity. Although fairly common in the literature, the supramolecular structures of these surfactants vary greatly from the macrocyclic species described herein.[50,51,52,53]

2.2 Aims

The aim of this chapter was to synthesise macrocyclic surfactant architectures capable of metal binding with the overall aim of creating micellar systems where the metal ion is bound at the surface of the micellar droplet. This approach aimed to concentrate the metal species on the surface of the micelle and thus investigate the effect of aggregation on the properties of the complexes.

Two ligands were synthesised, both incorporating a macrocyclic head group (**DO3A** or **N2O4**) and a dodecyl tail, capable of binding various metals. Complexes were made by addition of metal salts ($SrCl_2$, YCl_3, $NiCl_2$, $CaCl_2$, $MgCl_2$, $BaCl_2$, NaCl, $Eu(OTf)_3$, $Gd(OTf)_3$) to aqueous solutions of the ligands.

^{1}H NMR spectroscopy and MS were used to provide structural characterisation. Drop volume tensiometry provided insight into the micellar systems of the ligands and complexes, probing their ability to self-aggregate in aqueous solution and investigating the effects of metal salt addition.

This chapter also describes a series of imidazolium-based surfactants which are known to form stable micellar systems at room temperature. Investigations were carried out to establish the effect of surfactant chain-length on oil-solubilising ability.

A mixed-surfactant micellar system was formulated by doping the **N2O4** amphiphile into the imidazolium/BuOH system. The aim of this was to create a compromise between metal binding ability and oil-loading capacity. As before, tensiometric studies were used to establish the microemulsion compatibility of these systems.

2.3 Results and Discussion

2.3.1 Methylimidazolium SAILs

2.3.1.1 Synthesis and Characterisation

A series of 1-alkyl-3-methylimidazolium (**MeImC$_n^+$**) species were synthesised with varying alkyl chain lengths (n = 8, 10, 12, 14, 16) and either bromide or chloride counter ions. These species form a series of cationic surfactants used to investigate how the varying parameters affect the properties of the resulting microemulsions.

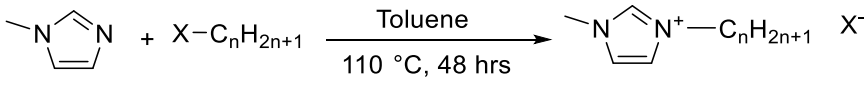

Figure 2.5 [MeImC$_n$]X Synthesis; X = Cl^-, Br^-; n = 8, 10, 12, 14, 16

Ionic liquids such as **[MeImC$_n$]X** have been reported as efficient co-surfactants in mixed surfactant systems.[5,12,20] Their relatively cheap and easy synthesis means they can be effectively used as the bulk surfactant in a system doped with a more expensive or harder to synthesise surfactant, or one which cannot form micelles alone (*e.g.* if the Krafft point is below room temperature or solubility is poor). This also creates greener microemulsions due to the ILs being non-toxic and more easily disposed of than other traditional surfactants.

[MeImC$_n$]X surfactants were synthesised in good yields (80-98%) *via* reaction of 1-methyl imidazole with the corresponding 1-bromo or 1-chloro alkane in refluxing toluene over 48 hours (as shown in Figure 2.5). The IL nature of the products meant that some products were solid at room temperature and so could be isolated *via* filtration of the reaction mixture, whereas some products were viscous oils at room temperature and were isolated *via* extraction into DCM.

All of the **[MeImC$_n$]X** compounds were characterised via ^{1}H NMR spectroscopy. Each compound exhibited a characteristic singlet resonance at ~9.75 ppm corresponding to the NC***H***N proton as well as two singlets at ~7.5 ppm arising from the other two aromatic protons. For each compound there was a clear singlet resonance visible at ~4.0 ppm corresponding to the imidazolium methyl group. The other resonances observed relate to the alkyl chain. As chain length was the only variation between the cations the only difference observed between species was the integration

of the peak representing the bulk of the chain protons at ~1.2 ppm. Successful synthesis was also confirmed by mass spectrometry which consistently showed peaks for $[M\text{-}X]^+$ for all of the compounds (X = Br^-/Cl^-).

2.3.1.2 Microemulsion Compatibility

The **[MeImC$_n$]X** salts were used to formulate a range of micellar systems with 1-BuOH of the form **[MeImC$_n$]X**/BuOH/H_2O (where n = 8-16 and X = Cl^-/Br^-), which had been previously developed within the group. The microemulsion compatibility of these micellar systems was assessed by testing their oil-solubilising ability in order to compare the effects of chain length and counter ion identity.

1 g samples of the micellar systems were formulated by weight in a 1:1:7 ratio of **[MeImC$_n$]X**:BuOH:H_2O. The solutions were kept at 25 °C using a water bath on a thermostated hotplate and 2 µL aliquots of oil were added periodically. The solutions typically required shaking and standing to form clear microemulsions. The aliquots were added until the solutions no longer became clear after vigorous shaking and long standing times. This point was established as the limit of the oil-solubilising ability.

Surfactant	Capacity / wt% (at 25 °C)			
	Toluene	Styrene	1-Octene	1-Octyne
[MeImC$_8$]Br	9.3	3.8	5.3	3.8
[MeImC$_{10}$]Br	9.9	4.8	5.7	5.6
[MeImC$_{12}$]Br	24.1	7.4	10.1	12.3
[MeImC$_{12}$]Cl	19.3	9.1	7.6	9.5
[MeImC$_{14}$]Br	7.4	5.6	11.9	14.4
[MeImC$_{16}$]Cl	8.2	4.7	16.2	19.4

Table 2.1 Effect of chain length and counter ion identity on oil-loading capacity

Table 2.1, above, shows the approximate oil loading capacities of the various micellar systems. All of the loading capacities are relatively high, particularly for the C_{12} systems which showed consistently high loading for all of the oils tested, whereas those with longer or shorter chains showed greater variation in loading with different oils. For the oils tested the C_{12} system showed the greatest oil-solubilising ability, with the bromide counter ion generally giving a higher loading capacity than the chloride analogue. Thus, the **[MeImC$_{12}$]Br** system was chosen for use in further investigations, particularly due to the extremely high toluene loading capacity.

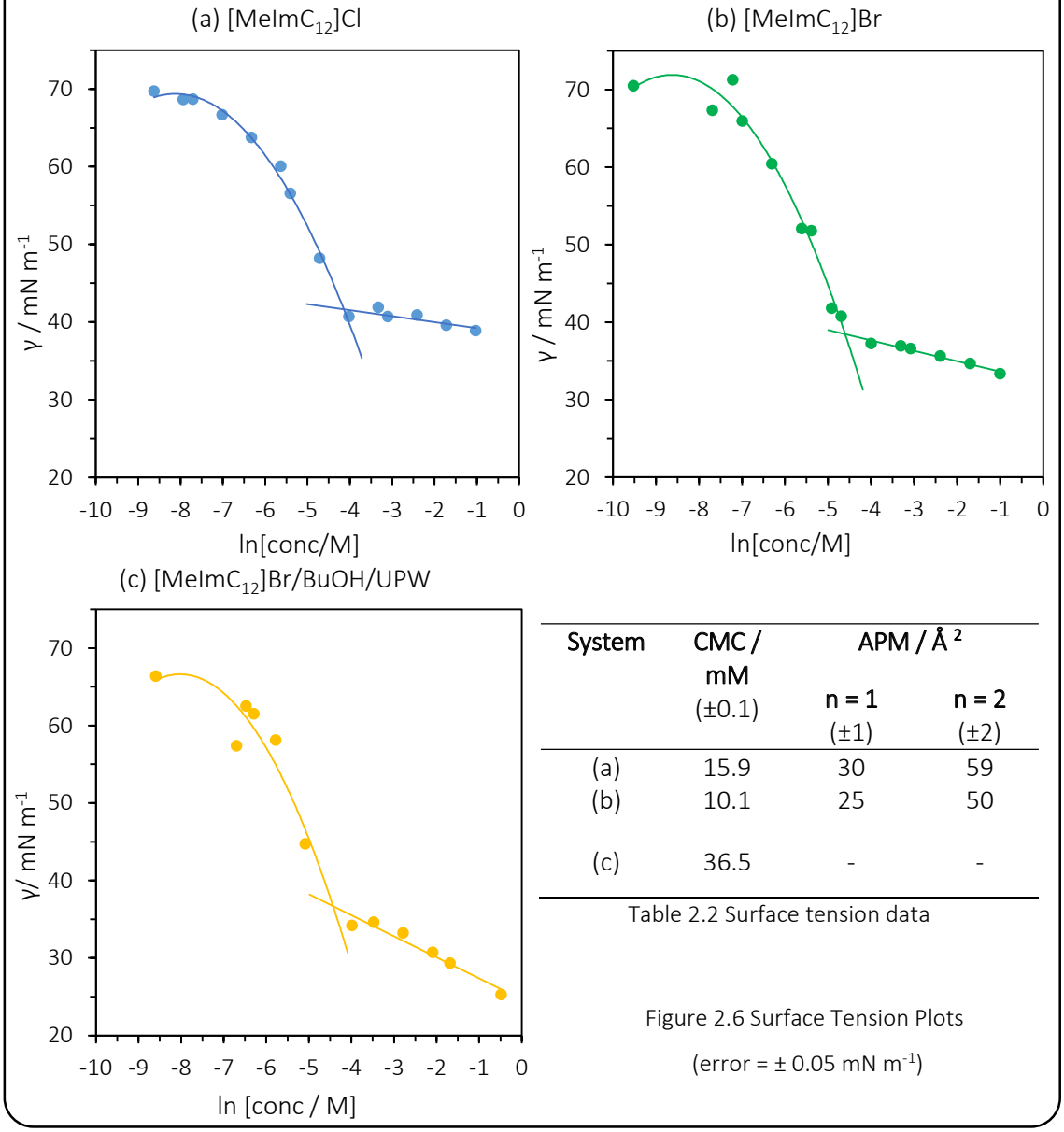

System	CMC / mM (±0.1)	APM / Å ² n = 1 (±1)	APM / Å ² n = 2 (±2)
(a)	15.9	30	59
(b)	10.1	25	50
(c)	36.5	-	-

Table 2.2 Surface tension data

Figure 2.6 Surface Tension Plots

(error = ± 0.05 mN m^{-1})

Drop volume tensiometry (DVT) was used to determine the CMC for the chloride and bromide salts of **MeImC$_{12}$$^{+}$** and the mixed surfactant system of **[MeImC$_{12}$]Br** with BuOH (1:1 wt/wt). Figure 2.6, above, shows the change in surface tension against ln[surfactant concentration] for each of the three solutions. Each system shows a polynomial decrease in surface tension with increasing concentration up until the CMC, after which the decrease is linear and much more subtle.

One of the problems posed by mixed surfactant systems is the possibility of the two different surfactants forming discrete micelles instead of micelles incorporating both types of surfactant.

If this were the case it may be expected that the surface tension data would show a CMC point relating to one of the surfactants while the other would act as a surface active impurity. This would be seen as a deviation from linearity in the data post-CMC. As the mixed surfactant system seen in Figure 2.6(c) shows a linear relationship between surface tension and ln[concentration] post-CMC it indicates that mixed micelles are forming, as desired.

Table 2.2 shows the CMC for each system and the area per molecule (APM) values calculated subsequently. An important consideration in the calculation of APM is the Gibb's pre-factor (n) which varies from n = 1 to n = 2 according to the level of dissociation occurring between the surfactant and its counter ion (see section **1.5**). For non-ionic surfactants there are no counter ions present therefore n = 1. Ionic surfactants require consideration of the orientation and conformation of both the surfactant molecules and their counter ions, hence n = 2. As these systems are ionic it would be expected that n = 2 would be the most appropriate value, however the real APM value is most likely to lie somewhere between these two values.

It is not possible to accurately determine the APM for a mixed surfactant system. Even though the system studied here has two surfactants present in a 1:1 weight ratio the average APM is not simply a sum of the individual APM values of the two surfactants. This may be due to a number of reasons, for example, the presence of a co-surfactant may alter the electrostatic repulsion of the main surfactants allowing them to pack more closely than in the single-surfactant micelle. For the **[MeImC$_n$]X**/BuOH system studied here it may also be possible that the shorter-chained BuOH co-surfactant is not located at the surface of the micelle (which would directly contribute to the average APM) but is instead located deeper within the micellar shell and thus affects the micelle curvature whilst not directly contributing to the average APM.

The nature of the micellar system described here means that it can be doped with a wide range of surfactants to form stable mixed-surfactant systems. This is particularly useful when the added surfactant is not capable of forming micelles alone, is expensive, or is difficult to synthesise. The low cost and ease of synthesis of the **[MeImC$_n$]X** surfactants mean that it can be easily produced in large quantities from commercially available materials.

2.3.2 N2O4 Surfactant Ligands and Complexes

2.3.2.1 Design, Synthesis and Characterisation

Amphiphilic ligand architectures were designed which incorporated a macrocyclic head group capable of metal-binding and a lipophilic alkyl chain in order for these species to self-assemble into micelles in aqueous media. The aim of this was to produce surfactant molecules capable of binding metals and localising them on the surface of a micellar droplet to create a system which could be adapted into a novel LSC cocktail.

A 1,4,10,13-tetraoxa-7,16-diazacyclooctadecane (**N2O4**) head group was chosen as it is known to bind Sr(II) with good affinity.[54] **N2O4** combines both the macrocyclic and chelate effects making it suitable for strong metal binding which is a key characteristic in micellar systems as impurities such as labile metal ions can cause erroneous CMC measurements.

A dodecyl chain was chosen for the lipophilic moiety of the ligand as it is one of the most commonly used in the literature where it is often the optimum choice for formation of self-assembled micelles. It is also consistent with the lipophilic moieties of the **[MeImC$_n$]X** surfactants outlined above as well as other metallosurfactants discussed throughout this thesis.

Figure 2.7 outlines the synthesis of the well-known **N2O4** macrocycle and its functionalisation into an amphiphilic ligand. The bis-benzyl protected macrocycle was synthesised in accordance with the procedure outlined by Parker[55] from the commercial starting material 1,2-bis(2-chloroethoxy)ethane. Two separate reactions were required to convert this starting material into precursors capable of forming the macrocycle. Firstly, reaction with NaI in acetone yielded the bis-iodo analogue as a pale yellow oil.[56] Secondly, 1,2-bis(2-chloroethoxy)ethane was heated to reflux in an excess of benzylamine to afford the bis-benzyl protected species. The protected macrocycle was then formed by the reaction of these two precursors with NaI and Na_2CO_3 in MeCN.

Each step of the synthesis was confirmed by ^{1}H NMR spectroscopy as shown in Figure 2.8, below. Firstly, the conversion of 1,2-bis(2-chloroethoxy)ethane to 1,2-bis(2-iodoethoxy)ethane was confirmed by a shift of -0.32 ppm in the X-C***H***$_2$ proton resonances (Figure 2.8a&b). The bis-benzyl species was easily identifiable due to the aromatic signals appearing around 7.2-7.3 ppm which integrated with the resonances of the aliphatic region (Figure 2.8c).

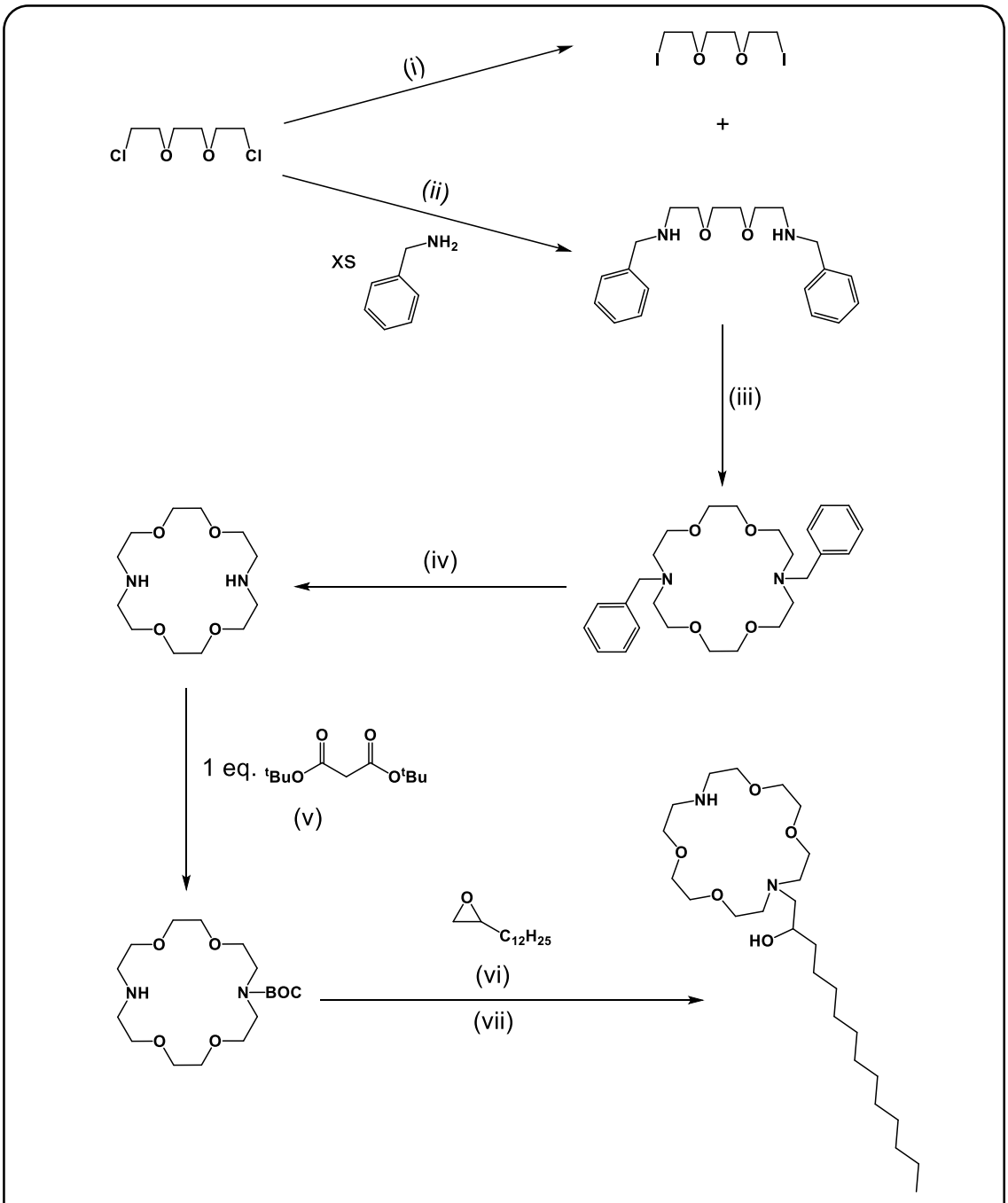

Figure 2.7 $N2O4mC_{12}$ Synthesis (i) NaI, acetone, 56 °C, 24 hrs; (ii) 120 °C, 24 hrs; (iii) NaI, Na_2CO_3, MeCN, 86 °C, 48 hrs; (iv)[55] $H_{2\,(g)}$, $Pd(OH)_2$/C 20 wt%, EtOH, ~5 days, RT; (v) 1,4-dioxane, 30 mins at 40 °C then 24 hrs at RT; (vi) EtOH, 78 °C, 3-5 days; (vii) DCM, TFA, RT, 24 hrs.[32]

The bis-benzyl macrocycle (Figure 2.8d) was deprotected by stirring in EtOH with catalytic amounts of $Pd(OH)_2$ on carbon (20 wt%) under a H_2 atmosphere for 3-5 days. It was found that any trace impurities in the bis-benzyl macrocycle would hinder deprotection, therefore bulb-to-bulb distillation (kugelrohr apparatus, 111-114 °C) of the precursor was required in order to

obtain complete conversion. As the reaction mixture was too dilute to study progression *via* TLC the reaction was followed *via* ^{1}H NMR spectroscopy. As the reaction progressed the aromatic signals arising from the benzyl groups diminished until they were no longer present (Figure 2.8e) yielding pure **N2O4** macrocycle.

Functionalisation of the deprotected macrocycle was originally attempted using stoichiometric control, *i.e.* adding only one equivalent of epoxide in order to functionalise just one of the amine sites. This technique, however, led only to the formation of bis-substituted species and unreacted macrocycle. The same result was observed when 10 equivalents of macrocycle were added to the epoxide in the expectation that this large excess would favour mono-functionalised products after removal of unreacted macrocycle.

Selective protection was therefore required in order to produce the mono-substituted macrocycle. This was achieved using *tert*-butyloxycarbonyl (BOC) protection.[32] The pure macrocycle was reacted with one equivalent of di-*tert*-butyl dicarbonate which yielded a mixture of unreacted macrocycle (**N2O4**), mono-substituted species (**N2O4mBOC**) and bis-substituted species (**N2O4bBOC**). The unreacted macrocycle was simply removed *via* precipitation with Et_2O however the substituted species could only be separated by column chromatography (neutral alumina, DCM). The **N2O4bBOC** was eluted as the first fraction as a colourless oil using DCM. The desired **N2O4mBOC** product was eluted as the second fraction as a pale yellow oil using DCM/MeOH (9:1). These species were characterised *via* ^{1}H NMR spectroscopy where the integration ratio between the *tert*-butyl moiety of the BOC protecting group and the aliphatic protons of the macrocyclic framework distinguished between the bisBOC and the monoBOC species (Figure 2.8f).

Functionalisation was then achieved *via* the reaction of **N2O4mBOC** with 1,2-epoxytetradecane by stirring both reagents for 5 days in refluxing EtOH. Deprotection of the product using standard techniques (dichloromethane/trifluoroacetic acid (DCM/TFA) 1:1) and repeated sonication in hexane to remove unreacted epoxide gave the desired **N2O4mC$_{12}$** species. Figure 2.8 below shows how the synthesis of the ligand was followed *via* ^{1}H NMR spectroscopy.

Although the racemic 1,2-tetradecane diol used to form the corresponding epoxide was obtained from commercial sources, repeated recrystallisation from EtOAc was required to remove any branched material. The diol was stirred in $CHCl_3$ with HBr/AcOH (45% w/v) for over night under

inert conditions. The reaction was quenched with water and the product extracted into DCM and dried *in vacuo* to give a white residue. This was then dissolved in dry MeOH and stirred for 2 hours in the presence of K_2CO_3. Again, the reaction was quenched with water, the product extracted into DCM and dried *in vacuo* to give a white residue. The crude product was purified using bulb-to-bulb distillation (kugelrohr apparatus, 95-96 °C) to give the desired racemic epoxide as a clear, colourless oil.[25] Methods are available for either separating the racemic mixture or for synthesising a single enantiomer, however, for these requirements the use of chiral epoxide was not deemed important so the material was simply used in its racemic form.

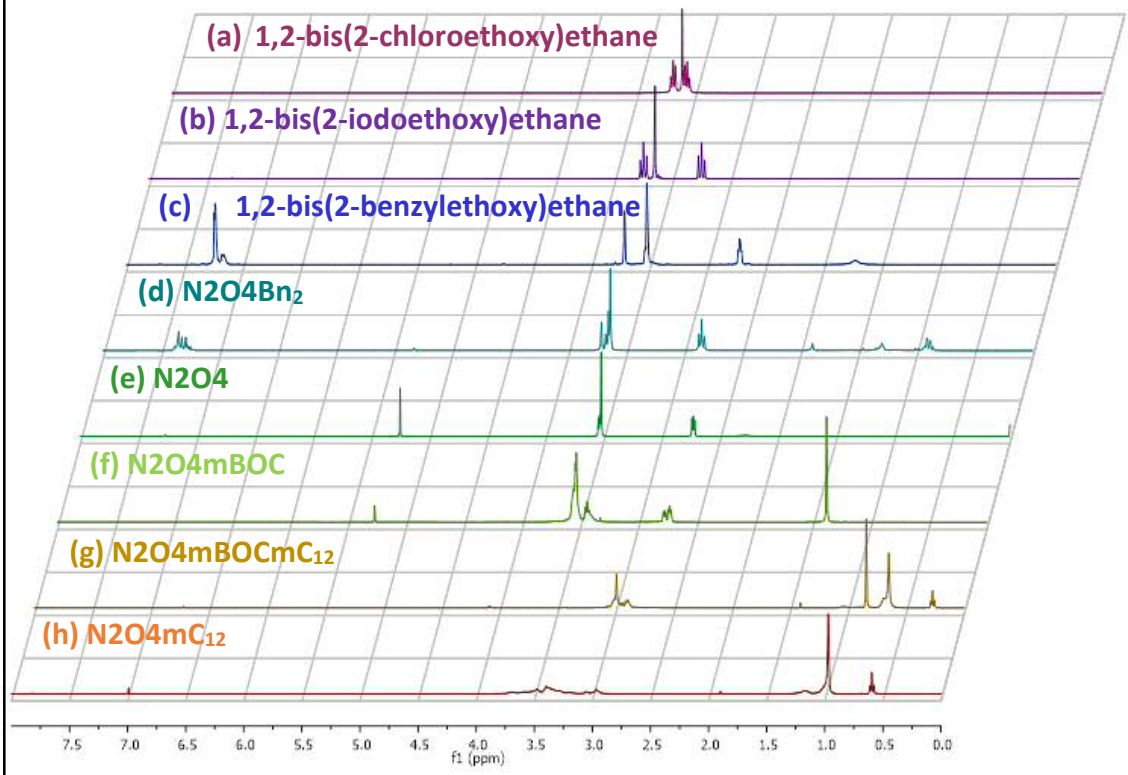

Figure 2.8 ^{1}H NMR spectra for N2O4mC$_{12}$ synthesis (all measured in $CDCl_3$)

The **N2O4** macrocycle and its precursors have been previously reported, therefore successful synthesis was confirmed by comparison of recorded ^{1}H and $^{13}C\{^1H\}$ NMR spectra with those reported. The BOC-protected and C_{12} functionalised ligands were characterised *via* ^{1}H and $^{13}C\{^1H\}$ NMR spectroscopy but successful synthesis was also confirmed *via* MS. This was especially important in cases such as **N2O4mC$_{12}$** (Figure 2.8h) where the macrocyclic resonances in the ^{1}H NMR spectrum are broad and structureless, making them difficult to assign.

Complexes were formed by the addition of 1.1 equivalents of the metal chloride or triflate salts to an aqueous solution of the ligand ($SrCl_2$, YCl_3, $NiCl_2$, $CaCl_2$, $MgCl_2$, $BaCl_2$, NaCl, $Eu(OTf)_3$, $Gd(OTf)_3$). For the case of $SrCl_2$, the ^1H NMR spectra showed no shift in resonances between the free ligand and the metal salt solution, suggesting a lack of coordination. However, MS yielded a peak corresponding to $[M\text{-}Cl]^+$ which, along with the change in the CMC observed (detailed in section 2.3.2.2 below) suggests that the Sr(II) complex may have been successfully formed.

The ^1H NMR spectra of the other metal ions tested were similarly unaffected and the IR spectra of the **N2O4mC$_{12}$** ligand and its complexes showed little to no variation in the stretching and bending frequencies upon addition of the metal ions. However, mass spectrometry gave peaks for Ca(II), Na(I) and Eu(III) complexes although those of Y(III), Ni(II), Mg(II) and Ba(II) only showed peaks for the uncomplexed free ligand. For those species which showed peaks corresponding to complexes in the LR mass spectra the HR spectra were recorded. The HR spectra for the Na(I) and Eu(III) complexes showed parent cation peaks however the spectra for the Ca(II) and Sr(II) complexes did not show peaks in the same ranges as their LR mass spectra which may be due to either complex degradation or fragmentation during measurement.

Despite the inconsistency of the MS results the change in CMC observed on addition of YCl_3 (section 2.3.2.2) suggests that coordination was successful. Likewise, the absorption spectrum detailed below suggests the same for Ni(II). Since tensiometry is a time- and material-consuming technique only a selection of systems were chosen for further evaluation (see section 2.3.2.2).

The Ni(II) complex of **N2O4mC$_{12}$** was formed *via* the addition of 1.0 equivalents of $NiCl_2.6H_2O$ to an aqueous solution of the ligand. Coordination was confirmed by ^1H NMR spectroscopy which showed a slight shift in proton resonances in line with metal coordination as well as a broadening of the peaks related to the paramagnetism of the metal ion, however only the free ligand was observed *via* mass spectrometry suggesting fragmentation upon ionisation.

The similarity in the absorption profile of **$[Ni(N2O4mC_{12})]^+$** (Figure 2.9) and octahedral **$[Ni(H_20)_6]^{2+}$** (Figure 2.10) suggest the complex has an octahedral (or near-octahedral) geometry. The absorption maxima for the $^3A_{2g} \rightarrow {}^3T_{1g}(F)$ (13986 cm^{-1}) and $^3A_{2g} \rightarrow {}^3T_{1g}(P)$ (25284 cm^{-1}), which correspond to ν_2 and ν_3 respectively, can be easily assigned from the spectrum however the absorption maximum for the $^3A_{2g} \rightarrow {}^3T_{2g}$ (ν_1) transition is not visible. Nevertheless, the value for this transition can be determined from the ratio between ν_2 and ν_3 as outlined by Lever[57] which

predicts the absorption maximum for the ν_1 transition to lie at 8428 cm^{-1}. This transition corresponds to the octahedral crystal field splitting parameter ($\Delta_{Oct} = \nu_1$) the value of which is very similar to that of **$[Ni(H_2O)_6]^{2+}$** at 8500 cm^{-1}.[58]

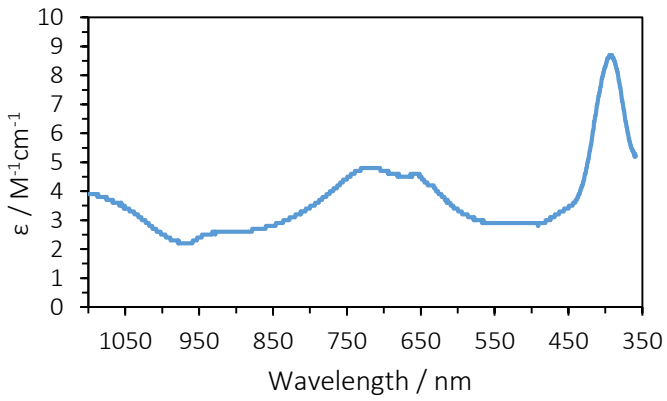

Figure 2.9 Absorption Spectrum of $[Ni(N2O4mC_{12})]^+$ measured in UPW ($5x10^{-5}$ M)

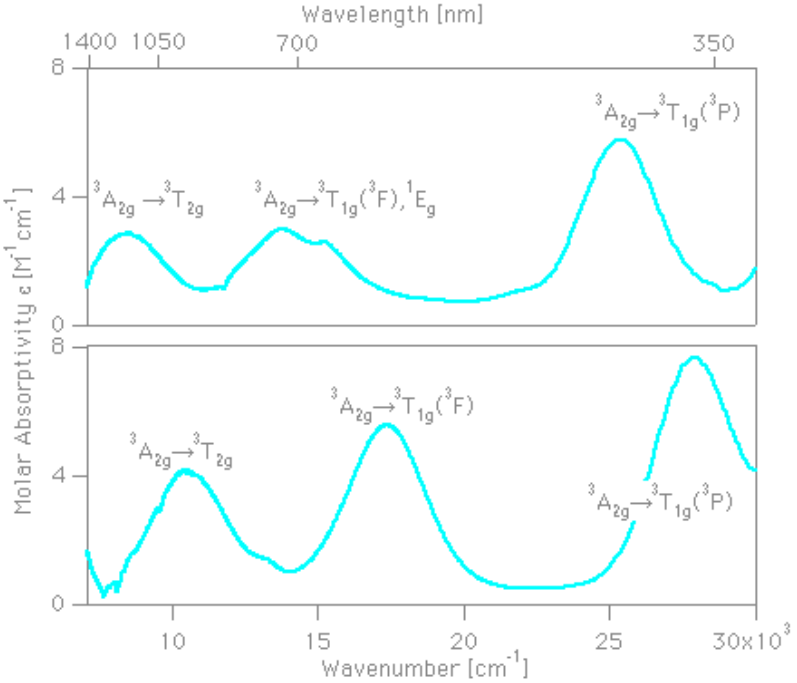

Figure 2.10 Absorption spectra for $[Ni(H_2O)_6]^{2+}$ (top 0.101 M in aqueous solution) and $[Ni(NH_3)_6]^{2+}$ (bottom, 0.315 M in aqueous NH_3 solution)[59]

As is common with octahedral Ni(II) complexes, there is another peak visible close to the $^3T_{1g}(F)$ peak which corresponds to the spin-forbidden $^3A_{2g} \rightarrow {}^1E_g$ (at 15326 cm^{-1}) transition. These transitions lie so close in energy that spin-orbit coupling allows the spin-forbidden transition to gain intensity from the spin-allowed transition leading to the observation of two close peaks in the absorption spectrum. Although these two transitions have been discretely assigned here, this

is not strictly accurate as the two states are technically mixed and therefore cannot be separated.[60]

The Racah B parameter was calculated to be 932 cm^{-1} based on the equation:

——————……. Equation 2.1

From this the nephelauxetic effect (β) of the ligand is found to be 0.86 based on the equation:

————……..Equation 2.2

Where the Racah B parameter for the free ion of Ni(II) is 1080 cm^{-1}.[24]

Although there are no literature examples of Ni(II) coordinated to a mono-substituted **N2O4** macrocycle such as **N2O4mC$_{12}$**, Selmeczi *et al.* reported detailed characterisation of a symmetrical **N2O4** species functionalised with two 1-benzyl-1H-1,2,3-triazol-4-yl arms. Absorption studies of the complex suggested an octahedral-type geometry as three transitions were seen at 12422, 16667 and 26667 cm^{-1} corresponding to ν_1, ν_2 and ν_3, respectively. X-ray crystallography studies confirmed a slightly distorted octahedral geometry in which the axial sites were occupied by two O atoms of the crown moiety and the equatorial positions comprised the two N atoms of the crown and two N atoms from the side arms.[23]

A number of other studies report octahedral-type coordination of first row transition metals which occupy the crown ring cavity of an **N2O4**-based ligand. However, they all concern symmetric bis-substituted species in which the side arms contribute to the coordination sphere.[54,61]

Based on these studies it may be assumed that **N2O4mC$_{12}$** coordinates to Ni(II) *via* two O atoms and two N atoms from the crown moiety. The hydroxy group of the lipophilic chain is available to coordinate to the metal but the lack of a second side arm leaves one coordination site unassigned. It may be possible for the crown moiety to arrange itself so that another O atom of the ring may occupy this site or it may be the case that a water or chloride ligand coordinates to the metal. However, this cannot be definitively assigned without crystallographic data.

2.3.2.2 Microemulsion Compatibility

Drop Volume Tensiometry (DVT) was used to investigate the micellar properties of the **N2O4mC$_{12}$** ligand and its complexes both alone and when doped into the **[MeImC$_{12}$]Br**/BuOH/H_2O micellar system. The tensiometry curves for each system are shown in Figure 2.11 along with their CMC values.

Firstly, the **N2O4mC$_{12}$** ligand was found to form micelles in an aqueous environment with a relatively low CMC of 0.75 mM (Figure 2.11a). The oil-solubilising ability of this system, however, was found to be extremely poor with a toluene-solubilising ability of <1 wt% at room temperature. Another micellar solution was formulated by doping 2 wt% **N2O4mC$_{12}$** into the **[MeImC$_{12}$]Br**/BuOH/H_2O micellar system discussed in section **2.3.1.** Figure 2.11c shows the tensiometry data for this system which was found to have a much higher toluene loading capacity of ~10 wt%.

When 1.1 equivalents of $SrCl_2.6H_2O$ were added to the doped system the CMC altered significantly from 2.24 mM (Figure 2.11c) to 15.9 mM (Figure 2.11d) which is suggestive of metal binding. Similarly a CMC of 20.2 mM was recorded when $YCl_3.6H_2O$ was added to the doped system (Figure 2.11e). When both metals were added simultaneously at 1.1 equivalents each a CMC of 14.7 mM was observed (Figure 2.11f). Although this would seem to point toward the preferential binding of Sr(II) as the CMC value is closer to that of the Sr(II)-doped system than the Y(III)-doped one it is not possible to definitively conclude this as the atomic radii of the two metals are too similar. A technique such as proximity scintillation using radioactive and non-radioactive samples in competition may be able to confirm which metal is bound preferentially.

Although tensiometry cannot prove the localisation of the metal on the surface of this micelle the results suggest that this may be the case. For example, as the surfactants of the carrier microemulsion are amphiphilic it can be assumed that in aqueous media they assemble with the hydrophobic tail groups on the inside of the micelle and the head groups on the micellar interface. The change in micelle morphology afforded by doping suggests that the **N2O4mC$_{12}$** species is efficiently incorporated into the carrier micellar system so it may be concluded that this surfactant arranges itself likewise. The Sr(II) and Y(III) doping tests show a change in micelle morphology on addition of the metal salts which suggests the occurrence of metal binding. Ultimately, all of the results point towards the formation of a micellar system incorporating a

ligand capable of metal-binding and aligning with its co-surfactants therefore suggesting the localisation of the metal on the micellar interface.

Based on results described elsewhere in this thesis (Chapter 3), the doped microemulsions were formulated *via* a one-step method whereby all of the non-aqueous components were combined prior to the addition of water. This method was found to produce a system containing a single type of micelle (indicated by a clear CMC point) whereas addition of the doped ligand to a pre-formed solution of **[MeImC$_{12}$]Br**/BuOH/H_2O seemed to create a mixture where the doped ligand was simply dissolved in the aqueous phase.

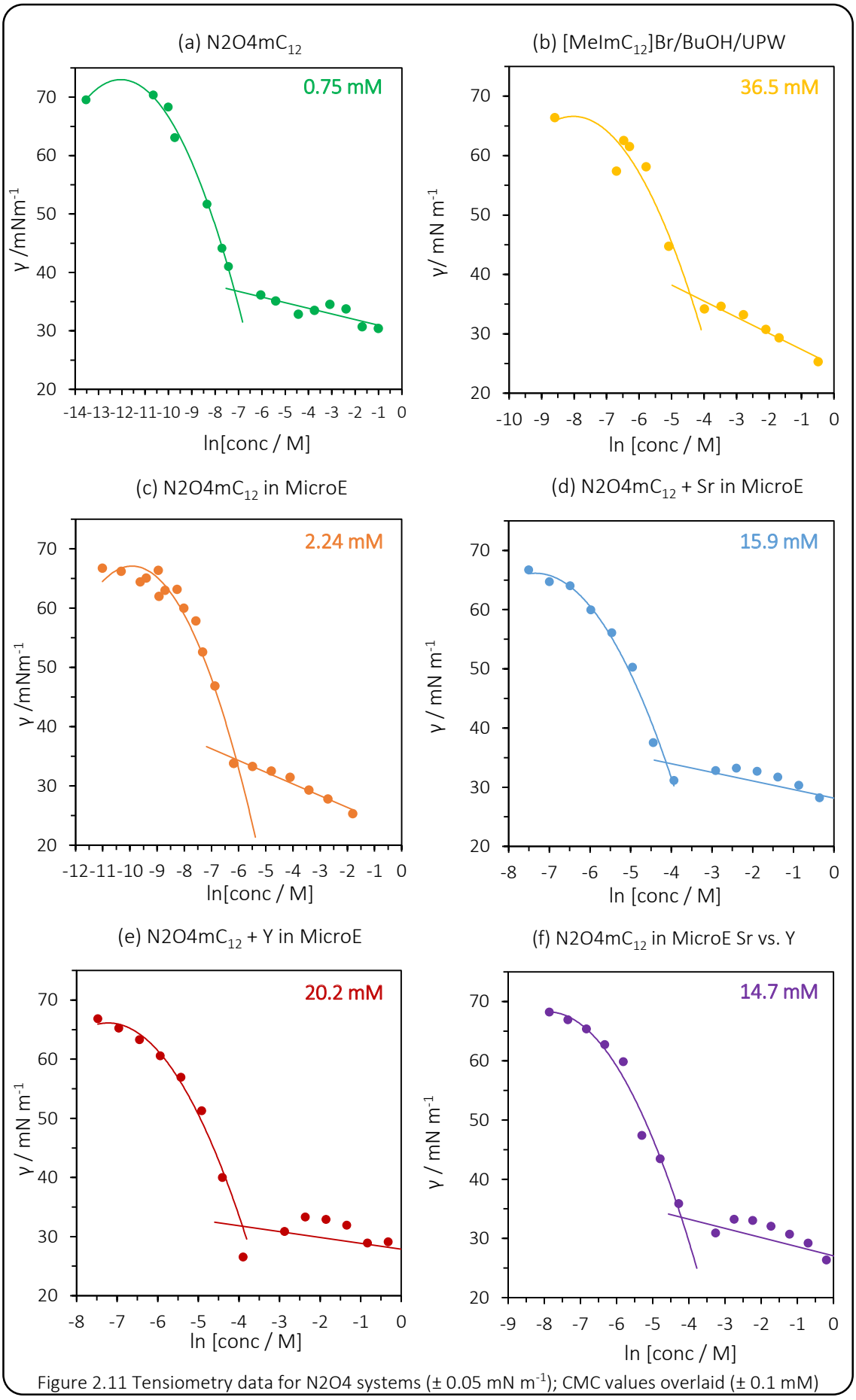

Figure 2.11 Tensiometry data for N2O4 systems (± 0.05 mN m^{-1}); CMC values overlaid (± 0.1 mM)

2.3.3 DO3AC$_{12}$ Surfactant Ligand and Complexes

2.3.3.1 Design, Synthesis and Characterisation

1,4,7,10-Tetraazacyclododecane-1,4,7-triacetic acid (**DO3A**) is a well-known macrocyclic architecture which is capable of binding a number of different metals due to its four macrocyclic N-donors and three carboxylic acid O-donors.[62] The free amine site on the macrocycle allows for further functionalisation to incorporate different characteristics into the molecule. In the case discussed here the remaining site is functionalised with a dodecyl chain attached *via* an amide linker. This creates an amphiphilic ligand architecture containing a metal-binding head group and a lipophilic tail allowing for self-assembly in aqueous media, ideally localising the metal on the micellar interface.

The **DO3AC$_{12}$** ligand was synthesised from commercial cyclen (1,4,7,10-tetraazacyclododecane) which was converted to the *tert*-butyl triester form in accordance with the literature procedure.[63] 2-Chloro-*N*-dodecylacetamide was synthesised *via* the addition of chloroacetyl chloride to 1-dodecylamine. The cyclen triester was stirred in MeCN at 50 °C in the presence of Cs_2CO_3 for 30 minutes prior to the addition of 2-chloro-*N*-dodecylacetamide in MeCN, after which the reaction was heated to reflux for 72 hours under inert conditions. Removal of the caesium salts *via* filtration and recrystallisation from boiling toluene to remove any unreacted triester yielded the ligand in its protected form. Deprotection was achieved using standard *tert*-butyl cleavage conditions (1:1 TFA:DCM) to give the free ligand as a hygroscopic TFA adduct.

Each step of the ligand synthesis was followed via ^{1}H NMR spectroscopy. Although the spectrum of the **DO3AC$_{12}$** ligand gave only broad, featureless peaks in the region of 4.0-2.8 ppm corresponding to the macrocyclic protons, they integrated with the more defined peaks around 1.27 and 0.87 ppm corresponding to the bulk alkyl chain and the terminal methyl group, respectively. Successful synthesis was confirmed by HRMS which gave a peak at *m/z* 570.3868 corresponding to $[M-H]^-$.

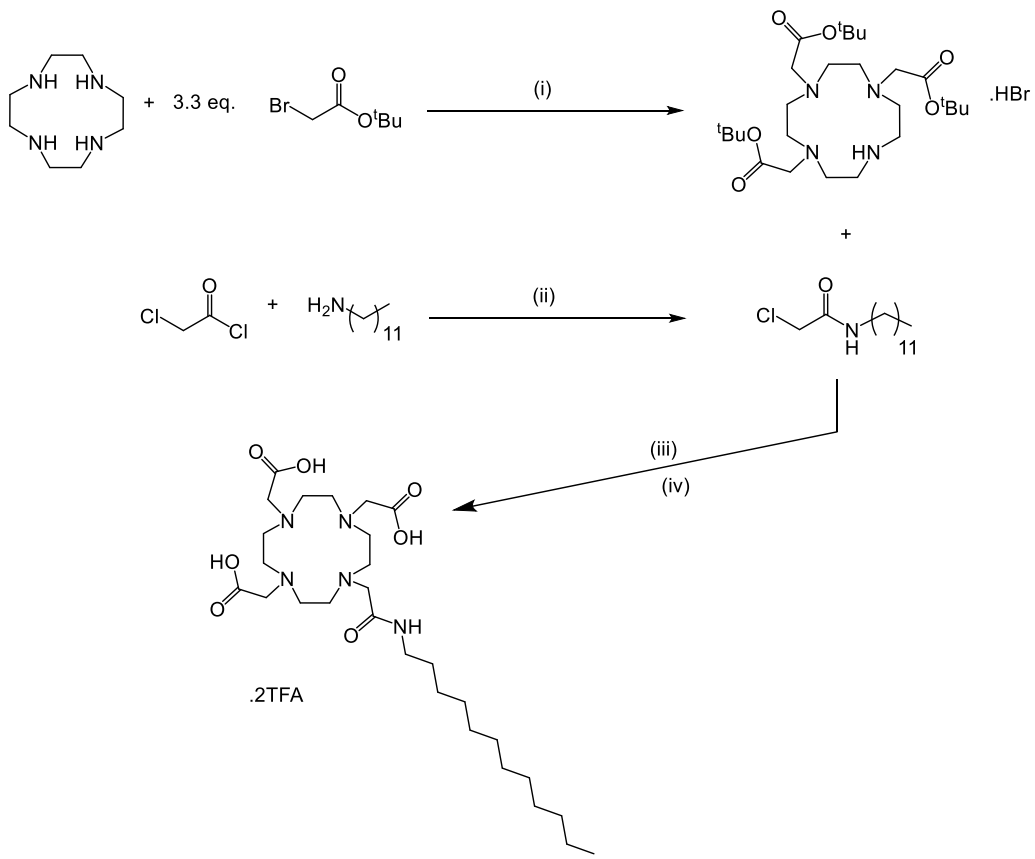

Figure 2.12 $DO3AC_{12}$ Synthesis (i) $NaHCO_3$, MeCN, 86 °C, 48 hrs; (ii) MeCN, NEt_3, RT, 48 hrs; (iii) Cs_2CO_3, MeCN, 30 mins at 50 °C then 48 hrs at RT; (iv) DCM, TFA, RT, 24 hrs [63]

Complexes of the ligand were formulated by the addition of 1.1 equivalents of the corresponding metal chloride or lanthanide triflate salts to an aqueous solution the **$DO3AC_{12}$** ligand ($SrCl_2$, YCl_3, $NiCl_2$, $CaCl_2$, $MgCl_2$, $BaCl_2$, NaCl, $Eu(OTf)_3$, $Gd(OTf)_3$). As for the **$N2O4mC_{12}$** analogues described in section **2.3.2.1** the ^1H NMR spectra for the free ligand and complexes showed no significant shift in the resonances upon addition of metal which would suggest a lack of coordination. Comparison of the IR spectra for the free **$DO3AC_{12}$** ligand and its complexes showed no change in the stretching and bending frequencies of the C=O and C-O bonds. However, a slight decrease was observed in the value of the N-H frequency from 1663 cm^{-1} for the free ligand to around 1574-1660 cm^{-1} for the complexes. Despite the inconclusive IR and ^1H NMR spectroscopy results, MS showed peaks corresponding to either $[M+H]^+$, $[M]^+$ or $[M-H]^-$ for each product. This, along with the change in CMC observed upon addition of $SrCl_2$ (section **2.3.3.2**) suggests that metal coordination was generally successful.

Similarly to the **[Ni(N2O4mC$_{12}$)]** complex, the absorption spectrum of the **[Ni(DO3AC$_{12}$)]** complex was recorded in water (Figure 2.13). While the three transitions are still visible for this complex ($^3A_{2g}$ → $^3T_{2g}$ (9639 cm^{-1}), $^3A_{2g}$ → $^3T_{1g}$(F) (14025 cm^{-1}), and $^3A_{2g}$ → $^3T_{1g}$(P) (19139 cm^{-1})) the ratio of peak intensities is very different, most notably for v_1 which has a much stronger peak than that observed for **[Ni(H$_2$O)$_6$]$^{2+}$** (Figure 2.10, above) suggesting that the coordination geometry is square planar rather than octahedral. This may be due to the size of the macrocycle; for **N2O4mC$_{12}$** the cavity is relatively large which may allow the Ni(II) ion to fit inside, whereas the **DO3AC$_{12}$** macrocycle is much smaller and therefore cannot surround the metal ion in the same way. The coordination geometry may also be influenced by the lability of the carboxylic acid arms of the **DO3AC$_{12}$** ligand.

The suggested square planar geometry of the **[Ni(DO3AC$_{12}$)]** complex is similar to those reported for other Ni(II) species with a cyclen-based ligands.[64] There is an additional feature present in the absorption spectrum of **[Ni(DO3AC$_{12}$)]** at 656 nm which is reminiscent of that obtained in Lifschitz salts in which an octahedral/square planar mixture or equilibrium exists.[65]

The marked change between the absorption profiles of **[Ni(H$_2$O)$_6$]$^{2+}$** and **[Ni(DO3AC$_{12}$)]** suggests that the metal has been successfully coordinated to the ligand. This was supported by the ^{1}H NMR spectrum of the solution which showed a slight shift in the proton resonances along with a broadening of peaks arising from the paramagnetism of Ni(II), both of which indicate successful metal coordination.

The octahedral crystal field splitting parameters (Δ_{Oct}) for each of the complexes are similar at 9339 cm^{-1} and 8500 cm^{-1} for **[Ni(DO3AC$_{12}$)]** and **[Ni(H$_2$O)$_6$]$^{2+}$**, respectively.[58] This value is derived from the position of the v_1 transition and is not related to the intensity of the peaks, therefore it does not reflect the difference in the absorption spectra of the two species.

Racah B parameter for this complex was found to be 283 cm^{-1} and thus the nephelauxetic parameter (β) = 0.26 (Equation 2.2, above). This value is much smaller than that of **N2O4mC$_{12}$** indicating that **DO3AC$_{12}$** is the softer of the two ligands having a greater degree of d-electron delocalisation over the ligand therefore giving a complex of greater covalent character. However, these calculations are only approximations as they assume octahedral geometry.[65]

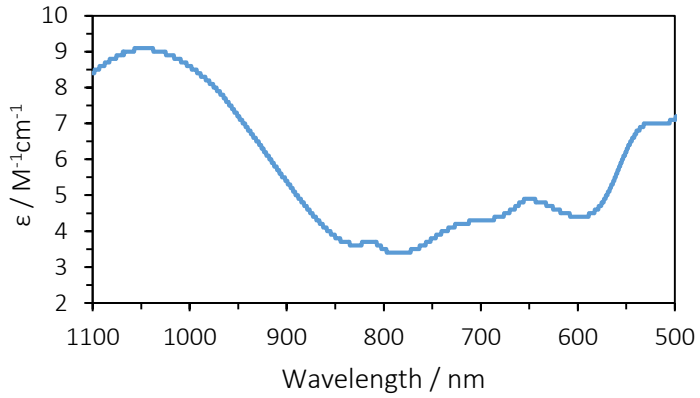

Figure 2.13 Absorption Spectrum of [Ni(DO3AC$_{12}$)] measured in water (5x10^{-5} M)

2.3.3.2 Microemulsion Compatibility

The microemulsion compatibility of the **DO3AC$_{12}$** ligand was assessed using DVT. Figure 2.14, below, shows the surface tension data for both the free ligand and the Sr(II) complex. The ^{1}H NMR spectrum of the complex showed insufficient perturbation to confirm metal binding. For other studies in this thesis, changes in the surface tension profile were able to confirm metal binding when ^{1}H NMR spectroscopy studies were inconclusive. However, for the **DO3AC$_{12}$** system described here the change in CMC profile upon addition of $SrCl_2$ is not of sufficient magnitude to provide conclusive evidence of metal binding. In this case, the Sr(II) may be bound to the metal as intended, or it may simply be dissolved in the aqueous medium – a process which would have no effect on the surface tension profile as $SrCl_2$ is not surface active and would therefore not be seen as an impurity.

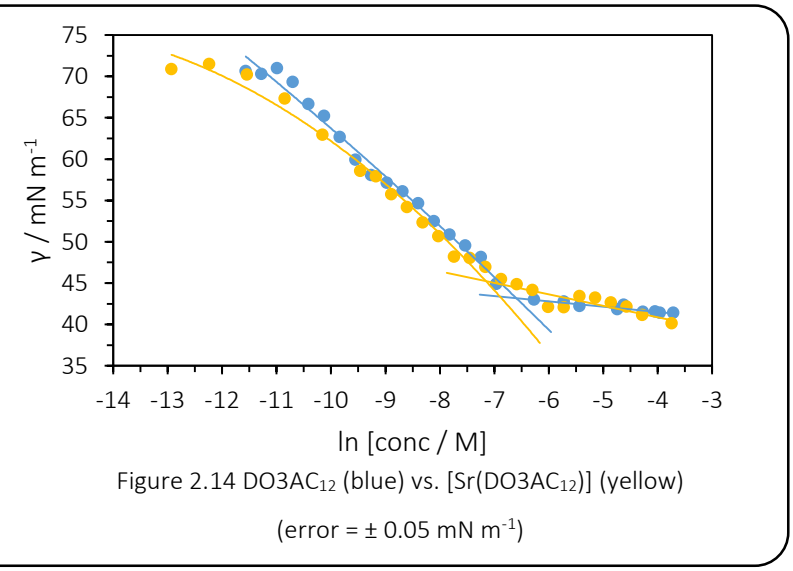

Figure 2.14 DO3AC$_{12}$ (blue) vs. [Sr(DO3AC$_{12}$)] (yellow)

(error = ± 0.05 mN m^{-1})

System	CMC / mM (±0.1)	APM / Å ^{2}	
		n = 1 (±1)	n = 2 (±2)
$DO3AC_{12}$	1.36	65	129
$[Sr(DO3AC_{12})]$	0.78	58	115

Table 2.3 CMC and APM data

The CMC was obtained for each system and thus the APM calculated (Table 2.3). It can be seen that the CMC and APM values are slightly lower for **$[Sr(DO3AC_{12})]$** than for the free ligand. This is suggestive that micelles form more readily for the complex than for the free ligand, an effect that can be attributed to a decrease in electrostatic repulsion which would be observed upon metal complexation which would allow the surfactants to pack more closely, hence the lower APM value. However, when taking the error associated with these measurements into account, the difference in CMC and APM values are not significantly different to confirm metal binding.

Although the data here cannot confirm metal binding or localisation of the metal on the micellar surface it can be predicted with reasonable certainty. As the **$DO3AC_{12}$** ligand is amphiphilic and is shown to self-assemble in water, therefore it may be assumed that it exhibits classical behaviour, *i.e.* the hydrophobic tail groups form the core of the aggregate and the macrocyclic head groups are therefore aligned at the micellar interface. Therefore it can be considered likely that if a metal is bound by the macrocyclic head groups it would therefore be aligned at the interface of the micellar droplet. However, further investigation is needed in order to test this hypothesis.

2.4 Conclusions

This chapter reports the design, synthesis and characterisation of two novel macrocyclic amphiphiles, **DO3AC$_{12}$** and **N2O4mC$_{12}$**. Tensiometric studies proved these ligands to be capable of self-aggregation in water to give stable micellar systems with CMC values of 1.36 mM and 0.75 mM, respectively. The amphiphilic nature of these ligands led to the assumption that they exhibited classical aggregation behaviour, arranging into micelles with the hydrophobic tail groups orientated toward the centre of the aggregate away from the water, aligning the macrocyclic head groups at the micellar interface.

Addition of various metal salts ($SrCl_2$, YCl_3, $NiCl_2$, $CaCl_2$, $MgCl_2$, $BaCl_2$, NaCl, $Eu(OTf)_3$, $Gd(OTf)_3$) to aqueous solutions of the ligands led to changes in the CMC and APM values for the micellar systems indicating a change in micelle morphology. Although NMR and IR spectroscopy could not conclusively confirm metal coordination, the majority of MS results along with tensiometric and absorption studies suggested coordination was generally successful.

A series of imidazolium-based surfactants were synthesised which were capable of self-assembly and exhibited very high oil-loading capacities in the presence of a BuOH co-surfactant. The optimised mixed-surfactant system was used as a carrier microemulsion for the **N2O4mC$_{12}$** ligand in order to create a micellar system capable of both metal-binding and high oil-loading.

2.5 Experimental

2.5.1 General Experimental for all Chapters

All reagents used were commercial grade and used without further purification unless otherwise stated. ^{1}H and $^{13}C\{^{1}H\}$ NMR spectra were recorded on an NMR-FT Bruker 500, 400, 300 or 250 MHz spectrometer in $CDCl_3$, CD_3OD, CD_3CN or D_2O solutions. ^{1}H and $^{13}C\{^{1}H\}$ NMR chemical shifts (δ) are reported in ppm and are referenced to the residual solvent signal. Spin-spin coupling constants *J* are given in Hz. Low resolution mass spectra (LRMS) were obtained by Cardiff University staff. High resolution mass spectra were either obtained by Cardiff University staff (on a Waters MALDI-TOF mx) or by the EPSRC National Mass Spectrometry Service at Swansea University, UK (on a Thermo Scientific LTQ Orbitrap XL). UV-Vis studies were performed on a Shimadzu UV-1800 spectrophotometer in MeCN or H_2O solutions at room temperature. Photophysical studies were performed on a JobinYvon–Horiba Fluorolog spectrometer fitted with a JY TBX picoseconds photodetection module in MeCN, EtOH, MeOH, D_2O or H_2O solutions. Emission spectra were uncorrected and excitation spectra were instrument corrected. The pulsed source was a Nano-LED configured for 295, 372 or 459 nm output operating at 1 MHz. Luminescence lifetime profiles were obtained using the JobinYvon–Horiba FluoroHub single photon counting module and the data fits yielded the lifetime values using the provided DAS6 deconvolution software. Quantum yield measurements were obtained on aerated MeCN solutions of the complexes using $[Ru(bpy)_3][(PF_6)_2]$ in aerated MeCN as a standard (Φ = 0.016). Electrochemical studies were carried out using a Parstat 2273 potentiostat in conjunction with a three-electrode cell. The auxiliary electrode was a platinum wire and the working electrode a platinum (1.0 mm diameter) disc. The reference was a silver wire separated from the test solution by a fine porosity frit and an agar bridge saturated with KCl. Solutions (10 ml DCM) were 1.0×10^{-3} mol dm^{-3} in the test compound and 0.1 mol dm^{-3} in $[NBu_4][PF_6]$ as the supporting electrolyte. Under these conditions, E0, for the one-electron oxidation of $[Fe(\eta\text{-}C_5H_5)_2]$ added to the test solutions as an internal calibrant, is +0.46 V in DCM.[66] Unless specified, all electrochemical values are at ν = 200 mV s^{-1}. Drop volume tensiometry was undertaken using a Lauda TVT1 tensiometer. Calibration was carried out using miliQ ultra-pure water (72 mN m^{-1} at 298 K) and ethanol (22 mN m^{-1} at 298 K). Samples were measured at room temperature in miliQ ultra-pure water. Infra-red spectra were obtained from a Shimadzu IR-Affinity-1S FTIR.

2.5.2 [MeImC$_n$]X Experimental

General synthesis: 1-methyl imidazole and the corresponding 1-bromo or 1-chloro alkane (1 eq.) were stirred in refluxing toluene for 48 hrs under inert conditions (N_2 atmosphere). Products which precipitated from the reaction mixture upon cooling were isolated *via* filtration. Those which did not precipitate were extracted into DCM, washed with water, dried over $MgSO_4$ and dried *in vacuo*. The products were obtained as white solids or colourless semi-solids in yields of 80-98%

Synthesis of [MeImC$_8$]Br

Yield: 97.58 g, 355 mmol, 94%. ^{1}H NMR (250 MHz, $CDCl_3$): δ_H = 10.11 (1H, s, NC***H***N), 7.59 (1H, t, $^3J_{HH}$ = 1.7 Hz, CH_3NC***H***CHN), 7.41 (1H, t, $^3J_{HH}$ = 1.8 Hz CH_3NCHC***H***N), 4.23 (2H, t, $^3J_{HH}$ = 7.4 Hz, NC***H***$_2$$CH_2$-), 4.03 (3H, s, NC***H***$_3$), 1.81 (2H, app. quin., J_{HH} = 7.1 Hz, NCH_2C***H***$_2$), 1.22 (4H, app. d, J_{HH} = 3.7 Hz, -(C***H***$_2$)$_2$-), 1.15 (6H, s, -(C***H***$_2$)$_3$-), 0.77 (3H, t, $^3J_{HH}$ = 6.5 Hz, CH_2C***H***$_3$) ppm. ^{13}C{^{1}H} NMR (75 MHz, $CDCl_3$) δ_C = 135.8, 124.3, 121.3, 49.0, 35.8, 30.7, 29.3, 28.1, 28.0, 25.2, 21.6, 13.1 ppm. HRMS (ES$^+$) found *m/z* 195.1851, calculated 195.1856 for $[C_{12}H_{23}N_2]^+$. IR (solid/cm^{-1}): *v* 3389 br. (C-H), 3055 (H-C=), 1568 (C=C), 1456 (C-H), 1169 (C-N).

Synthesis of [MeImC$_{10}$]Br

Yield: 68.02 g, 224 mmol, 89%. ^{1}H NMR (400 MHz, $CDCl_3$): δ_H = 9.87 (1H, s, NC***H***N), 7.56 (1H, t, $^3J_{HH}$ = 1.7 Hz, CH_3NC***H***CHN), 7.37 (1H, t, $^3J_{HH}$ = 1.7 Hz CH_3NCHC***H***N), 4.17 (2H, t, $^3J_{HH}$ = 7.4 Hz, NC***H***$_2$$CH_2$-), 3.97 (3H, s, NC***H***$_3$), 1.75 (2H, app. quin., J_{HH} = 7.3 Hz, NCH_2C***H***$_2$), 1.17 (4H, app. d, J_{HH} = 4.0 Hz, -(C***H***$_2$)$_2$-), 1.09 (10H, s, -(C***H***$_2$)$_9$-), 0.72 (3H, t, $^3J_{HH}$ =6.9 Hz, CH_2C***H***$_3$) ppm. ^{13}C{^{1}H} NMR (75 MHz, $CDCl_3$) δ_C = 136.9, 123.8, 121.9, 50.0, 36.7, 31.7, 30.2, 29.3, 29.2, 29.1, 28.9, 26.1, 22.5, 14.0 ppm. HRMS (ES$^+$) found *m/z* 223.2162, calculated 223.2168 for $[C_{14}H_{27}N_2]^+$. IR (solid/cm^{-1}): *v* 3393 br. (C-H), 2920, 2851 (C-H), 1634, 1570 (C=C), 1456 (C-H), 1167 (C-N).

Synthesis of [MeImC$_{12}$]Br

Yield: 80.80 g, 244 mmol, 97%. ^{1}H NMR (300 MHz, $CDCl_3$): δ_H = 10.00 (1H, s, NC***H***N), 7.57 (1H, t, $^3J_{HH}$ = 1.7 Hz, CH_3NC***H***CHN), 7.39 (1H, t, $^3J_{HH}$ = 1.7 Hz CH_3NCHC***H***N), 4.23 (2H, t, $^3J_{HH}$ = 7.4 Hz, NC***H***$_2$$CH_2$-), 4.03 (3H, s, NC***H***$_3$), 1.81 (2H, app. quin., J_{HH} = 6.9 Hz, NCH_2C***H***$_2$), 1.22 (4H, app. d, J_{HH} = 4.0 Hz, -(C***H***$_2$)$_2$-), 1.15 (14H, s, -(C***H***$_2$)$_9$-), 0.78 (3H, t, $^3J_{HH}$ = 6.6 Hz, CH_2C***H***$_3$) ppm. ^{13}C{^{1}H} NMR (75 MHz, $CDCl_3$) δ_C = 136.1, 123.4, 121.6, 49.4, 36.2, 31.2, 29.7, 28.9, 28.8, 28.7, 28.4, 25.6, 22.0, 13.5 ppm. HRMS (ES$^+$) found *m/z* 251.2474, calculated 251.2482 for $[C_{16}H_{31}N_2]^+$. IR (solid/cm^{-1}): *v* 3476,

3428 (C-H), 3065, 3061 (H-C=), 2914, 2851 (C-H), 1630 (C=C/C=N), 1572 (C=C), 1474 (C-H), 1177 (C-N), 862 (C-H).

Synthesis of [MeImC$_{12}$]Cl

Yield: 57.59 g, 201 mmol, 80%. ^{1}H NMR (250 MHz, $CDCl_3$): δ_H = 10.22 (1H, s, NC***H***N), 7.58 (1H, t, $^{3}J_{HH}$ = 1.7 Hz, CH_3NC***H***CHN), 7.36 (1H, t, $^{3}J_{HH}$ = 1.8 Hz CH_3NCHC***H***N), 4.21 (2H, t, $^{3}J_{HH}$ = 7.4 Hz, NC***H***$_2CH_2$-), 4.02 (3H, s, NC***H***$_3$), 1.80 (2H, app. quin., J_{HH} = 6.5 Hz, NCH_2C***H***$_2$), 1.21 (4H, app. d, J_{HH} = 4.1 Hz, -(C***H***$_2)_2$-), 1.15 (14H, s, -(C***H***$_2)_9$-), 0.78 (3H, t, $^{3}J_{HH}$ = 6.9 Hz, CH_2C***H***$_3$) ppm. ^{13}C{^{1}H} NMR (75 MHz, $CDCl_3$) δ_C = 137.0, 123.7, 121.7, 49.7, 36.3, 31.6, 30.1, 29.3, 29.1, 29.0, 28.8, 26.0, 22.4, 13.9 ppm. HRMS (ES$^+$) found *m/z* 251.2487, calculated 251.2482 for $[C_{16}H_{31}N_2]^+$. IR (solid/cm^{-1}): *v* 3458, 3410 (C-H), 3084, 3051 (H-C=), 2916, 2851 (C-H), 1636 (C=C/C=N), 1572 (C=C), 1474 (C-H), 1179 (C-N), 860 (C-H).

Synthesis of [MeImC$_{14}$]Cl

Yield: 88.75 g, 247 mmol, 98%. ^{1}H NMR (400 MHz, $CDCl_3$): δ_H = 10.12 (1H, s, NC***H***N), 7.55 (1H, t, $^{3}J_{HH}$ = 1.7 Hz, CH_3NC***H***CHN), 7.37 (1H, t, $^{3}J_{HH}$ = 1.8 Hz CH_3NCHC***H***N), 4.26 (2H, t, $^{3}J_{HH}$ = 7.4 Hz, NC***H***$_2CH_2$-), 4.07 (3H, s, NC***H***$_3$), 1.85 (2H, app. quin., J_{HH} = 7.3 Hz, NCH_2C***H***$_2$), 1.27 (4H, app. d, J_{HH} = 4.2 Hz, -(C***H***$_2)_2$-), 1.19 (18H, s, -(C***H***$_2)_9$-), 0.82 (3H, t, $^{3}J_{HH}$ =6.9 Hz, CH_2C***H***$_3$) ppm. ^{13}C{^{1}H} NMR (75 MHz, $CDCl_3$) δ_C = 136.2, 123.5, 121.6, 49.4, 36.3, 31.3, 29.1, 29.0, 28.9, 28.8, 28.5, 22.1, 13.6 ppm. HRMS (ES$^+$) found *m/z* 279.2802, calculated 279.2795 for $[C_{18}H_{35}N_2]^+$. IR (solid/cm^{-1}): *v* 3476, 3428 (C-H), 3065, 3061 (H-C=), 2914, 2849 (C-H), 1630 (C=C/C=N), 1574 (C=C), 1474 (C-H), 1176 (C-N), 862 (C-H).

Synthesis of [MeImC$_{16}$]Cl

Yield: 60.68 g, 157 mmol, 87%. ^{1}H NMR (250 MHz, $CDCl_3$): 10.00 (1H, s, NC***H***N), 7.57 (1H, t, $^{3}J_{HH}$ = 1.7 Hz, CH_3NC***H***CHN), 7.38 (1H, t, $^{3}J_{HH}$ = 1.8 Hz CH_3NCHC***H***N), 4.23 (2H, t, $^{3}J_{HH}$ = 7.4 Hz, NC***H***$_2CH_2$-), 4.03 (3H, s, NC***H***$_3$), 1.81 (2H, app. quin., J_{HH} = 6.9 Hz, NCH_2C***H***$_2$), 1.22 (4H, app. d, J_{HH} = 4.5 Hz, -(C***H***$_2)_2$-), 1.16 (22H, s, -(C***H***$_2)_{11}$-), 0.78 (3H, t, $^{3}J_{HH}$ =6.6 Hz, CH_2C***H***$_3$) ppm. ^{13}C{^{1}H} NMR (75 MHz, $CDCl_3$) δ_C = 136.8, 123.8, 121.9, 49.9, 36.7, 31.7, 30.2, 29.5, 29.4, 29.2, 28.9, 26.1, 22.5, 14.0 ppm. HRMS (ES$^+$) found *m/z* 307.3104, calculated 307.3108 for $[C_{20}H_{39}N_2]^+$. IR (solid/cm^{-1}): *v* 3474, 3425 (C-H), 3065, 3061 (H-C=), 2914, 2849 (C-H), 1630 (C=C/C=N), 1574 (C=C), 1474 (C-H), 1175 (C-N), 862 (C-H).

2.5.3 N2O4 Experimental

Precursors:

Synthesis of 1,2-bis(2-iodoethoxy)ethane[55]

1,2-bis(2-chloroethoxy)ethane (8.40 mL, 53.8 mmol) and NaI (17.5 g, 117 mmol) were stirred in acetone (30 mL) at 56 °C for 24 hrs under a N_2 atmosphere. The reaction was cooled to RT, filtered to remove NaCl and the solvent removed *in vacuo* to give an orange residue. The crude product was dissolved in Et_2O (~100 mL), washed with 10% sodium thiosulphate (2 x ~25 mL) to remove iodine and dried over $MgSO_4$. The solvent was removed *in vacuo* to give the title compound as a pale yellow oil. Yield: 14.77 g, 39.9 mmol, 74%. ^{1}H NMR (400 MHz, $CDCl_3$): δ_H = 3.71 (4H, t, $^3J_{HH}$ = 5.5 Hz, OC***H***$_2$C***H***$_2$O), 3.61 (4H, s, OC***H***$_2$CH$_2$I), 3.21 (4H, t, $^3J_{HH}$ = 5.7 Hz, OCH$_2$C***H***$_2$I) ppm.

Synthesis of *NN*'-dibenzyl-4,7-dioxa-1,10-diazadecane[55]

Benzylamine (196 mL, 1.80 mol) and 1,2-bis(2-cholorethoxy)ethane (19.0 mL, 0.12 mol) were stirred at 120 °C for 48 hrs under a N_2 atmosphere. The reaction was cooled to RT and NaOH (8.10 g, 0.20 mol) was added before the reaction was returned to 120 °C for 1 hour. Vacuum distillation of unreacted benzyl amine afforded a cloudy white residue which was dissolved in $CHCl_3$ (~200 mL), washed with water and dried over $MgSO_4$. Solvent was removed *in vacuo* to give the title compound as a pale yellow oil. Yield: 34.37 g, 0.12 mol, 86%. ^{1}H NMR (400 MHz, $CDCl_3$): δ_H = 7.34-7.21 (10H, m, arom.), 3.68 (4H, s, C***H***$_2$-arom.), 3.63-3.61 (16H, m, OC***H***$_2$), 2.82 (8H, t, $^3J_{HH}$ = 5.9 Hz, OCH$_2$C***H***$_2$N) ppm.

Synthesis of 1,2-epoxytetradecane[25]

1,2-tetradecane diol (8.00 g, 34.7 mol) was added to HBr/AcOH (45% w/v) in $CHCl_3$ (375 mL, 1:7 v/v) and stirred overnight under a N_2 atmosphere. Water was added, the product extracted into DCM and dried *in vacuo* to give a yellow oil (5.46 g, 16.3 mol). The oil was dissolved in dry MeOH (60 mL) and K_2CO_3 (8 g, 57.9 mmol) added, the solution was stirred overnight under a N_2 atmosphere. The reaction was quenched with water, extracted into DCM and dried *in vacuo*. Bulb-to-bulb distillation of the crude product (kugelrohr apparatus 95-96 °C) isolated the product as a colourless oil. Yield: 1.79 g, 8.43 mol, 24%. ^{1}H NMR (400 MHz, $CDCl_3$): δ_H = 3.74-3.59 (2H, br. s, OC***H***$_2$), 3.46-3.37 (1H, br. s, OC***H***(CH$_2$)), 2.87-2.66 (2H, br. s, CHC***H***$_2$), 1.46-1.36 (2H, br. s, CHCH$_2$C***H***$_2$), 1.24 (18H, s, -(C***H***$_2$)$_9$-), 0.87 (3H, app. s, C***H***$_3$) ppm.

Macrocycles:

Synthesis of 7,16-bisbenzyl-1,4,10,13-tetraoxa-7,16-diazacyclooctadecane[55]

NN'-dibenzyl-4,7-dioxa-1,10-diazadecane (6.03 g, 18.4 mmol) and 1,2-bis(2-iodoethoxy)ethane (8.16 g, 22.1 mmol) were added to MeCN (250 mL) with Na_2CO_3 (9.32 g, 88.0 mmol) and NaI (1.45 g, 9.68 mmol) and the resulting solution stirred at 82 °C for 48 hrs under a N_2 atmosphere. The mixture was cooled and filtered to remove inorganic solids. The residue was washed with hot MeCN (2 x ~50 mL) and the combined organic fractions dried *in vacuo* to yield a semi-solid mass. This residue was dissolved in 1,4-dioxane and warm acetone (~40 mL, 1:1 v/v) and the solution left to crystallise overnight at -15 °C. The pale yellow solid was filtered, dissolved in $CHCl_3$ and washed with water (2 x ~100 mL). The organic layer was separated and the aqueous layer washed with further $CHCl_3$ (2 x ~50 mL). The combined organic layers were dried over $MgSO_4$ and the solvent removed *in vacuo* to give a dark yellow residue. Repeated recrystallisation from boiling hexane afforded the crude product as a pale yellow crystalline solid. Bulb-to-bulb distillation (kugelrohr apparatus 80-83 °C) gave the title compound as colourless oil which solidified on standing. Yield: 2.32 g, 5.24 mmol, 29%. ^{1}H NMR (400 MHz, $CDCl_3$): δ_H = 7.31 (10H, m, arom.), 3.71 (4H, s, arom.-C***H***$_2$), 3.65 (16H, m, OC***H***$_2$), 2.85 (8H, t, $^3J_{HH}$ = 5.9 Hz, $OCH_2C\boldsymbol{H}_2N$) ppm.

Synthesis of 1,4,10,13-tetraoxa-7,16-diazacyclooctadecane[55] (N2O4)

7,16-Bisbenzyl-1,4,10,13-tetraoxa-7,16-diazacyclooctadecane (2.30 g, 5.19 mmol) was stirred in EtOH with $Pd(OH)_2$ (20wt%) on carbon (~ 0.30 g) under a H_2 atmosphere for 3-5 days. The reaction was flushed with N_2 for approx. 1 hr and the catalyst removed by filtration through celite. The solvent was removed *in vacuo* to isolate the product as a white solid. Yield: 1.17 g, 4.46 mmol, 85%. ^{1}H NMR (250 MHz, $CDCl_3$): δ_H = 3.61-3.57 (16H, m, OC***H***$_2$), 2.78 (8H, t, $^3J_{HH}$ = 4.7 Hz, NC***H***$_2$), 2.35 (2H, br. s, N***H***) ppm.

Synthesis of *tert*-butyl-1,4,10,13-tetraoxa-7,16-diazacyclooctadecane-7-carboxylate (N2O4mBOC)[32]

N2O4 (2.00 g, 7.62 mmol) was added to 1,4-dioxane (40 mL) and stirred at 40 °C to aid dissolution. Di-*tert*-butyl dicarbonate (1.66 g, 7.61 mmol) in 1,4-dioxane (20 mL) was added dropwise over a period of 10 mins. The reaction was stirred at 40 °C for a further 30 mins then at RT overnight under a N_2 atmosphere. The volume was reduced *in vacuo* and ether added to precipitate unreacted N2O4 which was isolated as a white solid. The filtrate was dried *in vacuo* to give a yellow oil. The crude product was purified by column chromatography (alumina, Brochmann I,

neutral, 50-200 µm, DCM). After elution of the *bis*-BOC protected species with DCM/MeOH (99:1) as a colourless fraction the product was eluted as a pale yellow fraction with DCM/MeOH (9:1). The solvent was removed *in vacuo* to give a pale yellow oil. Yield: 0.69 g, 1.91 mmol, 25%. ^{1}H NMR (400 MHz, $CDCl_3$): δ_H = 3.59-3.55 (16H, m, OC***H***$_2$), 3.47 (4H, app. t, J_{HH} = 5.5 Hz, OC(O)NC***H***$_2$), 3.14 (1H, br. s, N***H***), 2.75 (4H, app. t, J_{HH} = 4.6 Hz, NC***H***$_2$CH$_2$O), 1.41 (9H, s, OC(C***H***$_3$)$_3$) ppm. ^{13}C{^{1}H} NMR (75 MHz, $CDCl_3$) δ_C = 155.3 (***C***O), 79.4 (***C***O), 69.9, 69.7, 53.4, 49.1, 47.0, 28.3 ppm. LRMS (ES$^+$) found *m/z* 363.25, calculated 363.25 for [M+H]$^+$. IR (solid/cm^{-1}): *v* 2924, 2854 (C-H), 1719, 1665 (C=O), 1182, 1126 (C-O), 1087 (C-N).

Synthesis of 16-*tert*-butyl-7-(2-hydroxytetradecyl)-1,4,10,13-tetraoxa-7,16-diazacyclooctadecane (N2O4mBOCmC$_{12}$)

1,2-Epoxytetradecane (0.37 g, 1.74 mmol) was added to **N2O4mBOC** (0.38 g, 1.04 mmol) in EtOH (20 mL). The reaction was refluxed for at least 5 days under a N_2 atmosphere. The reaction was cooled to RT and solvent removed *in vacuo* to give the crude product as a pale brown oil. Yield: 0.16 g, 0.28 mmol, 27%. ^{1}H NMR (400 MHz, $CDCl_3$): δ_H = 4.20 (1H, br. s, OH), 3.58-3.28 (18H, m, C***H***$_2$ (macrocycle)), 2.77 (6H, t, $^{3}J_{HH}$ = 4.5 Hz C***H***$_2$ (macrocycle)), 1.35-1.31 (9H, m, C(C***H***$_3$)$_3$), 1.16-1.10 (25H, m, NC***H***$_2$C***H***(OH) & -(C***H***$_2$)$_{11}$-), 0.78 (3H, t, $^{3}J_{HH}$ = 6.8 Hz, CH$_2$C***H***$_3$) ppm. ^{13}C{^{1}H} NMR (125 MHz, $CDCl_3$) δ_C = 163.5 (***C***O), 69.5 (***C***O), 66.0, 49.6, 32.1, 29.8, 29.5, 29.6, 22.8, 14.3 ppm. LRMS (ES$^+$) found *m/z* 575.47, calculated 575.46 for [M+H]$^+$. IR (solid/cm^{-1}): *v* 3314 br. (O-H), 2967, 2924 (C-H), 1659 (C=O), 1379 (C-H), 1138, 1128, 1107 (C-O), 953, 818, 669 (C-H).

Synthesis of 7-(2-hydroxytetradecyl)-1,4,10,13-tetraoxa-7,16-diazacyclooctadecane (N2O4mC$_{12}$)

Removal of the BOC protecting group was achieved via addition of TFA (approx. 1 mL) to the crude product dissolved in minimum DCM, the solution was stirred overnight at RT under a N_2 atmosphere. The solvent was removed *in vacuo* and the crude product washed successively with methanol (3 x ~20 mL) and dried *in vacuo*. The crude product was stirred in hexane for 16 hrs to remove unreacted epoxide. The solvent was decanted and the product dried *in vacuo* to give the title compound as a brown oil. Yield: 0.29 g, 0.60 mmol, 47%. ^{1}H NMR (400 MHz, $CDCl_3$): δ_H = 7.42-7.17 (1H, br. s, N***H***), 3.94-3.20 (24H, m, C***H***$_2$(macrocycle)), 1.47-1.41 (3H, m, NC***H***$_2$C***H***(OH)), 1.25-1.21 (22H, br. s, -(C***H***$_2$)$_{11}$-), 0.84 (3H, t, $^{3}J_{HH}$ = 6.7 Hz, C***H***$_3$) ppm. ^{13}C{^{1}H} NMR (125 MHz, $CDCl_3$) δ_C = 72.4, 70.3, 69.7, 69.1, 66.6, 65.8, 65.5, 65.3, 65.1, 64.2, 59.8, 48.7, 47.8, 31.9, 29.7, 29.6, 29.5, 29.4, 25.7, 25.3, 22.7, 14.1 ppm. LRMS (AP$^+$) found *m/z* 475.41, calculated 475.41 for

$[M+H]^+$. HRMS (ES^+) found *m/z* 475.4097, calculated 475.4097 for $[C_{26}H_{55}N_2O_5]^+$. IR (solid/cm^{-1}): *v* 2914, 2849 (C-H), 1682 (N-H), 1458 (C-O), 1202 (C-N), 1109 (C-O), 1060 (C-N), 831, 795, 719 (C-H).

General Complex Synthesis:

1.1 eq. metal chloride or lanthanide triflate salt was added to an aqueous solution of the ligand. IR spectroscopy was carried out using dried aliquots of the complex solutions. ^1H NMR spectroscopy was attempted for the Eu(III) complexes but yielded only poor quality spectra which are not included here. As the complexes were not isolated, no yields were obtained for these compounds.

Synthesis of [Sr(N2O4mC$_{12}$)]Cl

^1H NMR (400 MHz, D_2O): δ_H = 3.85-3.80 (8H, m, OC***H***$_2$C***H***$_2$O), 3.74 (10H, s, NC***H***$_2$), 3.38-3.32 (8H, m, OC***H***$_2$CH$_2$N), 1.53 (3H, s, NC***H***$_2$C***H***(OH)), 1.30 (20H, s, -(C***H***$_2$)$_{10}$-), 0.90-0.87 (3H, m, C***H***$_3$) ppm. $^{13}C\{^1H\}$ NMR (125 MHz, D_2O) δ_C = 69.8, 69.5, 65.4, 65.3, 65.1, 47.3, 46.7, 31.5, 29.2, 28.9, 22.3, 13.7 ppm. LRMS (ES^+) found *m/z* 561.26, calculated 561.30 for $[M-Cl]^+$. IR (solid/cm^{-1}): *v* 3435 br., 3234 br. (O-H), 2980, 2922, 2852 (C-H), 1672 (N-H), 1452 (C-H), 1381 (C-O), 1201 (C-N), 1126 (C-O), 952, 799, 719 (C-H).

Synthesis of [Y(N2O4mC$_{12}$)]2Cl

^1H NMR (400 MHz, D_2O): δ_H = 3.83-3.80 (8H, m, OC***H***$_2$C***H***$_2$O), 3.74 (10H, s, NC***H***$_2$), 3.35-3.33 (8H, m, OC***H***$_2$CH$_2$N), 1.51 (3H, s, NC***H***$_2$C***H***(OH)), 1.30 (20H, s, -(C***H***$_2$)$_{10}$-), 0.89 (3H, t, $^3J_{HH}$ = 6.6 Hz, C***H***$_3$) ppm. $^{13}C\{^1H\}$ NMR (125 MHz, D_2O) δ_C = 70.1, 69.7, 69.5, 65.3, 63.9, 58.8, 47.3, 46.7, 34.4, 32.0, 31.7, 30.0, 29.7, 29.5, 29.3, 29.2, 29.1, 24.9, 22.7, 22.4, 13.8 ppm. LRMS (ES^+) found *m/z* 475.41, calculated 475.41 for $[M-Y-2Cl+H]^+$. IR (solid/cm^{-1}): *v* 3333 br., 3227 br. (O-H), 2980, 2924 (C-H), 1678, 1641 (N-H), 1462 (C-H), 1391 (C-O), 1198 (C-N), 1138 (C-O) 953, 797, 719 (C-H).

Synthesis of [Ni(N2O4mC$_{12}$)]Cl

^1H NMR (300 MHz, D_2O): δ_H = 3.38-3.30 (8H, m, OC***H***$_2$C***H***$_2$O), 3.72 (10H, s, NC***H***$_2$), 3.83-3.77 (8H, m, OC***H***$_2$CH$_2$N), 1.57-1.46 (3H, s, NC***H***$_2$C***H***(OH)), 1.38-1.22 (20H, s, -(C***H***$_2$)$_{10}$-), 0.87 (3H, t, $^3J_{HH}$ = 5.8 Hz, C***H***$_3$) ppm. $^{13}C\{^1H\}$ NMR (125 MHz, D_2O) δ_C = 69.4, 68.9, 65.2, 47.2, 46.6, 33.9, 31.3, 28.9, 28.6, 22.1, 13.8 ppm. LRMS (ES^+) found *m/z* 475.41, calculated 475.41 for $[M-Ni-Cl+H]^+$. UV/Vis (H_2O): λ_{max}/nm (ε/$M^{-1}cm^{-1}$) = 1100 (4), 732 (5), 662 (5), 396 (9). IR (solid/cm^{-1}): *v* 3325 br. (O-H), 2980, 2926 (C-H), 1672 (N-H), 1454, 1381 (C-H), 1200 (C-N), 1132 (C-O), 957, 795, 721 (C-H).

Synthesis of [Ca(N2O4mC$_{12}$)]Cl

^{1}H NMR (400 MHz, D_2O): δ_H = 3.82-3.81 (8H, m, OC***H***$_2$C***H***$_2$O), 3.74 (10H, s, NC***H***$_2$), 3.35-3.33 (8H, m, OC***H***$_2$CH$_2$N), 1.52 (3H, s, NC***H***$_2$C***H***(OH)), 1.30 (20H, s, -(C***H***$_2$)$_{10}$-), 0.89 (3H, t, $^{3}J_{HH}$ = 6.7 Hz, C***H***$_3$) ppm. ^{13}C{^{1}H} NMR (125 MHz, D_2O) δ_C = 69.8, 69.5, 65.4, 65.3, 65.1, 58.7, 47.3, 46.7, 32.1, 31.5, 30.2, 29.7, 29.2, 29.0, 28.9, 22.7, 22.3, 13.7 ppm. LRMS (ES$^+$) found *m/z* 513.36, calculated 513.36 for [M-Cl]$^+$. IR (solid/cm^{-1}): *v* 3356 br. (O-H), 2980, 2970, 2887 (C-H), 1678 (N-H), 1462, 1381 (C-H), 1250 (C-N), 1161, 1132 (C-O), 951, 799, 721 (C-H).

Synthesis of [Mg(N2O4mC$_{12}$)]Cl

^{1}H NMR (400 MHz, D_2O): δ_H = 3.81 (8H, app. s, OC***H***$_2$C***H***$_2$O), 3.74 (10H, s, NC***H***$_2$), 3.34 (8H, app. s, OC***H***$_2$CH$_2$N), 1.50 (3H, s, NC***H***$_2$C***H***(OH)), 1.30 (20H, s, -(C***H***$_2$)$_{10}$-), 0.89 (3H, app. s, C***H***$_3$) ppm. ^{13}C{^{1}H} NMR (125 MHz, D_2O) δ_C = 69.7, 69.5, 65.3, 65.1, 47.3, 46.7, 34.6, 32.0, 31.9, 30.1, 30.0, 29.8, 29.7, 29.4, 25.0, 22.7, 22.6, 13.8 ppm. HRMS (ES$^+$) found *m/z* 497.3976, calculated 497.3930 for [$C_{26}H_{54}N_2O_5Na$]$^+$ ([M-Mg-Cl+Na]$^+$). IR (solid/cm^{-1}): *v* 3314 br. (O-H), 2970, 2889 (C-H), 1678 (N-H), 1462, 1381 (C-H), 1202 (C-N), 1130 (C-O), 951, 818, 721 (C-H).

Synthesis of [Ba(N2O4mC$_{12}$)]

^{1}H NMR (400 MHz, D_2O): δ_H = 3.83-3.81 (8H, m, OC***H***$_2$C***H***$_2$O), 3.75-3.74 (10H, s, NC***H***$_2$), 3.38-3.34 (8H, m, OC***H***$_2$CH$_2$N), 1.52 (3H, s, NC***H***$_2$C***H***(OH)), 1.31 (20H, s, -(C***H***$_2$)$_{10}$-), 0.90 (3H, t, $^{3}J_{HH}$ = 7.1 Hz, C***H***$_3$) ppm. ^{13}C{^{1}H} NMR (125 MHz, D_2O) δ_C = 70.1, 69.8, 69.5, 65.3, 65.1, 47.3, 46.7, 31.8, 29.6, 22.5, 13.8 ppm. LRMS (ES$^+$) found *m/z* 497.40, calculated 497.38 for [M-Ba+Na+H]$^+$. IR (solid/cm^{-1}): *v* 3387 br. (O-H), 2980, 2970, 2924 (C-H), 1674, 1608 (N-H), 1462, 1381 (C-H), 1202 (C-N), 1128 (C-O), 951, 831, 799, 719 (C-H).

Synthesis of [Na(N2O4mC$_{12}$)]

^{1}H NMR (400 MHz, D_2O): δ_H = 3.83-3.82 (8H, m, OC***H***$_2$C***H***$_2$O), 3.75-3.74 (10H, s, NC***H***$_2$), 3.35-3.34 (8H, m, OC***H***$_2$CH$_2$N), 1.52 (3H, s, NC***H***$_2$C***H***(OH)), 1.31 (20H, s, -(C***H***$_2$)$_{10}$-), 0.90 (3H, t, $^{3}J_{HH}$ = 6.8 Hz, C***H***$_3$) ppm. ^{13}C{^{1}H} NMR (125 MHz, D_2O) δ_C = 69.8, 69.5, 65.3, 47.3, 46.7, 31.7, 29.4, 29.2, 22.4, 13.8, 13.7 ppm. LRMS (AP$^+$) found *m/z* 497.40, calculated 497.39 for [M+H]$^+$. HRMS (AP$^+$) found *m/z* 497.3918, calculated 497.3930 for [$C_{26}H_{54}N_2O_5Na$]$^+$. IR (solid/cm^{-1}): *v* 3431 br. (O-H), 2980, 2924 (C-H), 1680 (N-H), 1460, 1391, 1384 (C-H), 1200 (C-N), 1115 (C-O), 966, 831, 797, 719 (C-H).

Synthesis of [Eu(N2O4mC$_{12}$)]2OTf

^{1}H NMR (300 MHz, D_2O): δ_H = 3.73 (8H, app. t, J_{HH} = 4.7 Hz, OC***H***$_2$C***H***$_2$O), 3.65 (10H, s, NC***H***$_2$), 3.25 (8H, app. t, J_{HH} = 4.5 Hz, OC***H***$_2$CH_2N), 1.51-1.38 (3H, br. s, NC***H***$_2$C***H***(OH)), 1.33-1.16 (20H, s, -(C***H***$_2$)$_{10}$-), 0.85-0.79 (3H, m , C***H***$_3$) ppm. ^{13}C{^{1}H} NMR (125 MHz, D_2O) δ_C = 69.7, 69.4, 65.2, 47.2, 31.9, 30.0, 29.8, 29.4, 22.6, 13.7 ppm. HRMS (ES$^+$) found *m/z* 625.3690, calculated 625.3689 for [$C_{26}H_{52}N_2O_5Eu$]$^+$. IR (solid/cm^{-1}): *v* 3358 br. (O-H), 2980, 2970, 2889 (C-H), 1659 (N-H), 1462, 1381 (C-H), 1250 (C-N), 1152, 1032 (C-O), 949, 816, 644 (C-H).

Synthesis of [Gd(N2O4mC$_{12}$)]2OTf

LRMS (ES$^+$) found *m/z* 475.41, calculated 475.41 for [M-Gd-2OTf +H]$^+$. IR (solid/cm^{-1}): *v* 3345 br. (O-H), 2980, 2970 (C-H), 1666 (N-H), 1462, 1381 (C-H), 1249 (C-N), 1161, 1032 (C-O), 951, 816, 644 (C-H).

2.5.4 DO3A Experimental

Synthesis of 1,4,7-tris(tert-butoxycarbonyl methyl) 1,4,7,10-tetrazacyclododecane[63]

Sodium acetate (1.57 g, 19.1 mmol) was added to 1,4,7,10-tetrazacyclododecane (1.00 g, 5.80 mmol) in DMA (10 mL) and cooled to -20 °C. *tert*-Butyl bromoacetate (3.73 g, 19.1 mmol) in DMA (10 mL) was added dropwise over approx. 30 minutes. The reaction was allowed to reach RT and stirred overnight under a N_2 atmosphere. The mixture was poured over water (~60 mL) and additional water (~70 mL) was added until the formation of a clear solution. $KHCO_3$ (3.00 g, 30.0 mmol) was added portion-wise until the formation of the title compound as a white precipitate (HBr salt). Yield: 2.87 g, 4.82 mmol, 83%. ^{1}H NMR (400 MHz, $CDCl_3$): δ_H = 10.19-9.86 (1H, br. s, N***H***), 3.36 (4H, s, 1,7-NC***H***$_2$C$O_2{}^t$Bu), 3.27 (2H, s, 4-NC***H***$_2$C$O_2{}^t$Bu), 3.14-3.05 (4H, br. m, 9,11-NC***H***$_2$), 2.96-2.83 (12H, br. m, 2,3,5,6,8,12-C***H***$_2$), 1.45-1.44 (27H, m, C(C***H***$_3$)$_3$) ppm.

Synthesis of 2-chloro-*N*-dodecylacetamide

NEt_3 (0.41 mL, 2.94 mmol) was added to 1-dodecylamine (0.50 g, 2.70 mmol) in MeCN (5 mL). The mixture was cooled to 0 °C, chloroacetylchloride (0.37 mL, 4.65 mmol) in MeCN (5 mL) was added dropwise and the reaction stirred at RT for 48 hours under inert conditions. The solvent was removed *in vacuo*, the crude product dissolved in DCM and washed with water. Solvent was removed *in vacuo* to give the title compound as a dark brown oil which solidified on standing. Yield: 0.45 g, 1.72 mmol, 63%. ^{1}H NMR (400 MHz, $CDCl_3$): δ_H = 6.69 (1H, br. s, N***H***), 4.00 (2H, s,

ClC***H***$_2$), 3.24 (2H, q, $^3J_{HH}$ = 6.8 Hz, C***H***$_2$CH$_3$), 1.52-1.46 (2H, m, NHC***H***$_2$), 1.25-1.21 (18H, m, -(C***H***$_2$)$_9$-), 0.83 (3H, t, $^3J_{HH}$ = 6.8 Hz, C***H***$_3$) ppm.

Synthesis of 1-dodecylamido-4,7,10-tris(tert-butoxycarbonylmethyl)-1,4,7,10-tetraazacyclododecane (Protected DO3AC$_{12}$)

Cs_2CO_3 (0.55 g, 1.69 mmol) was added to 1,4,7-tris(tert-butoxycarbonylmethyl)-1,4,7,10-tetrazacyclododecane (0.50 g, 0.84 mmol) in MeCN (15 mL) and stirred at 50 °C for approx. 30 minutes. 2-Chloro-*N*-dodecylacetamide (0.26 g, 0.95 mmol) in MeCN (10 mL) was added and the mixture stirred at 82 °C for 72 hours under a N_2 atmosphere. The reaction was cooled to RT and filtered to remove caesium salts. The solvent was removed *in vacuo* to give a brown residue. Unreacted macrocycle was removed via recrystallisation from toluene to isolate the title compound as a brown oil. Yield: 0.49 g, 0.66 mmol, 68%. ^{1}H NMR (300 MHz, $CDCl_3$): δ_H = 3.26-3.11 (6H, m, NC***H***$_2$C***H***$_2$N), 2.81-2.65 (10H, m, NC***H***$_2$C***H***$_2$N), 2.43 (8H, s, 1,4,7-NC***H***$_2$C(O)), 1.54 (s, C(C***H***$_3$)$_3$), 1.53 (s, C(C***H***$_3$)$_3$), 1.38-1.31 (22H, m, -(C***H***$_2$)$_{11}$-), 0.96 (3H, t, $^3J_{HH}$ = 6.4 Hz, C***H***$_3$) ppm. ^{13}C{^{1}H} NMR (125 MHz, CD_3CN) δ_C = 171.6, 118.3, 81.2, 81.1, 57.6, 57.0, 55.6, 54.1, 53.2, 52.8, 30.4, 30.3, 28.4, 28.3, 23.4, 14.4, 1.8, 1.6, 1.5, 1.3, 1.1, 1.0 ppm. HRMS (ES$^+$) found *m/z* 762.5701, calculated 762.5715 for $[C_{50}H_{77}N_5O_7Na]^+$. IR (solid/cm^{-1}): *v* 2924, 2853 (C-H), 1728 (C=O), 1665, 1533 (N-H), 1456 (C-H), 1366 (C-O), 1256, 1215 (C-N), 1150, 1123 (C-O), 849, 743 (C-H).

Synthesis of 1-dodecylamido-1,4,7,10-tetraazacyclododecane-4,7,10-triacetic acid (DO3AC$_{12}$)

Deprotection was achieved by adding TFA (~6 mL) to **Protected DO3AC$_{12}$** (0.52 g, 0.70 mmol) in DCM (7 mL). The solvent was removed *in vacuo* and the residue washed with MeOH (3 x ~20 mL) and dried *in vacuo*. The crude product was dissolved in MeCN, precipitated with Et_2O and filtered *in vacuo* to give the title compound as a pale brown solid. Yield: 0.33 g, 0.58 mmol, 82%. ^{1}H NMR (500 MHz, D_2O): δ_H = 3.98-3.62 (8H, m, NC***H***$_2$C(O)), 3.56-2.97 (18H, m, NC***H***$_2$), 1.51 (2H, s, NHCH$_2$C***H***$_2$), 1.28 (18H, s, -(C***H***$_2$)$_9$-), 0.87 (3H, t, $^3J_{HH}$ = 5.9 Hz, C***H***$_3$) ppm. ^{13}C{^{1}H} NMR (125 MHz, $CDCl_3$) δ_C = 172.0 (***C***O), 170.8 (***C***O), 58.3, 56.7, 56.2, 54.9, 53.5, 52.6, 52.0, 39.5, 32.0, 29.8, 29.6, 29.5, 28.3, 22.8, 14.2 ppm. HRMS (ES$^-$) found *m/z* 570.3868, calculated 570.3872 for $[C_{28}H_{52}N_5O_7]^-$. IR (solid/cm^{-1}): *v* 3271 br. (O-H), 2926, 2855 (C-H), 1719 (C=O), 1663 (N-H), 1458 (C-H), 1352, 1180, 1128, 1088 (C-O), 795, 719, 679 (C-H).

General Complex Synthesis:

1.1 eq. metal chloride or lanthanide triflate salt was added to an aqueous solution of the ligand. IR spectroscopy was carried out using dried aliquots of the complex solutions. ^{1}H NMR spectroscopy was attempted for the Eu(III) complexes but yielded only poor quality spectra which are not included here. As the complexes were not isolated, no yields were obtained for these compounds.

Synthesis of [Sr(DO3AC$_{12}$)]

^{1}H NMR (500 MHz, D_2O): δ_H = 4.00-3.69 (8H, m, NC***H***$_2$C(O)), 3.58-3.00 (18H, m, NC***H***$_2$), 1.51 (2H, s, NCH$_2$C***H***$_2$), 1.28 (18H, s, -(C***H***$_2$)$_9$-), 0.87 (3H, t, $^{3}J_{HH}$ = 6.3 Hz, C***H***$_3$) ppm. ^{13}C{^{1}H} NMR (125 MHz, D_2O) δ_C = 176.6 (***C***O), 174.3 (***C***O), 172.7 (***C***O), 169.4 (***C***O), 55.5, 55.0, 53.1, 51.8, 49.1, 47.7, 42.2, 39.6, 31.9, 29.8, 29.7, 29.4, 29.3 ppm. LRMS (ES$^+$) found *m/z* 658.28, calculated 658.29 for [M+H]$^+$. HRMS (ES$^+$) found *m/z* 658.2905, calculated 658.2923 for [$C_{28}H_{52}N_5O_7Sr$]$^+$. IR (solid/cm^{-1}): *v* 3381 br. (O-H), 2924, 2855 (C-H), 1659 (C=O), 1574 (N-H), 1456 (C-H), 1356 (C-O), 1206, 1155 (C-N), 1088 (C-O), 916, 827, 727, 691 (C-H).

Synthesis of [Y(DO3AC$_{12}$)]

^{1}H NMR (500 MHz, D_2O): δ_H = 4.02-3.60 (8H, m, NC***H***$_2$C(O)), 3.58-2.95 (18H, m, NC***H***$_2$), 1.50 (2H, s, NCH$_2$C***H***$_2$), 1.27 (18H, s, -(C***H***$_2$)$_9$-), 0.89-0.83 (3H, m, C***H***$_3$) ppm. ^{13}C{^{1}H} NMR (125 MHz, D_2O) δ_C = 175.6 (***C***O), 174.4 (***C***O), 169.3 (***C***O), 55.4, 55.1, 53.1, 51.8, 49.1, 47.7, 42.2, 39.6, 31.9, 29.8, 29.7, 29.4, 28.8, 26.9, 22.6, 18.0, 13.8 ppm. LRMS (ES$^+$) found *m/z* 658.28, calculated 658.28 for [M+H]$^+$. HRMS (ES$^+$) found *m/z* 658.2822, calculated 658.2847 for [$C_{28}H_{51}N_5O_7Y$]$^+$. IR (solid/cm^{-1}): *v* 3348 br. (O-H), 2982, 2972, 2924 (C-H), 1728 (C=O), 1581 (N-H), 1460 (C-H), 1383 (C-O), 1242, 1236 (C-N), 1161, 1082, 1029 (C-O), 947, 636 (C-H).

Synthesis of [Ni(DO3AC$_{12}$)]

^{1}H NMR (500 MHz, D_2O): δ_H = 4.00-3.62 (8H, m, NC***H***$_2$C(O)), 3.51-3.04 (18H, m, NC***H***$_2$), 1.55-1.43 (2H, br. s, NCH$_2$C***H***$_2$), 1.34-1.19 (18H, br. s, -(C***H***$_2$)$_9$-), 0.86 (3H, t, $^{3}J_{HH}$ = 4.1 Hz, C***H***$_3$) ppm. ^{13}C{^{1}H} NMR (125 MHz, D_2O) δ_C = 49.0, 47.6, 42.1, 39.5, 31.8, 29.7, 29.3, 28.8, 26.9, 22.5, 13.9 ppm. LRMS (ES$^+$) found *m/z* 628.31, calculated 628.32 for [M+H]$^+$. HRMS (ES$^+$) found 628.3209, calculated 628.3220 for [$C_{28}H_{52}N_5O_7Ni$]$^+$. UV/Vis (H_2O): λ_{max}/nm (ε/M^{-1}cm^{-1}) = 1051 (9), 728 (4), 656 (5), 537 (7). IR (solid/cm^{-1}): *v* 3310 br. (O-H), 2926, 2855 (C-H), 1724 (C=O), 1632, 1580 (N-H), 1464, 1408 (C-H), 1240, 1225 (C-N), 1165, 1096, 1028 (C-O), 920, 721, 636 (C-H).

Synthesis of [Ca(DO3AC$_{12}$)]

^{1}H NMR (500 MHz, D_2O): δ_H = 4.02-3.61 (8H, m, NC***H***$_2$C(O)), 3.58-3.00 (18H, m, NC***H***$_2$), 1.51 (2H, s, NCH$_2$C***H***$_2$), 1.28 (18H, s, -(C***H***$_2$)$_9$-), 0.90-0.84 (3H, m, C***H***$_3$) ppm. ^{13}C{^{1}H} NMR (125 MHz, D_2O) δ_C = 174.4 (***C***O), 162.9 (***C***O), 162.6 (***C***O), 53.0, 51.8, 49.1, 47.7, 42.2, 39.6, 31.9, 29.8, 29.7, 29.4, 28.8, 26.9, 22.6, 13.8 ppm. LRMS (ES$^-$) found *m/z* 608.34, calculated 608.33 for [M-H]$^-$. HRMS (ES$^-$) found *m/z* 608.3358, calculated 608.3337 for [$C_{28}H_{50}N_2O_7Ca$]$^-$. IR (solid/cm^{-1}): *v* 3356 br. (O-H), 2982, 2922, 2855 (C-H), 1632 (N-H), 1423 (C-H), 1383 (C-O), 1184 (C-N), 1150, 1088 (C-O), 953, 799, 719, 567 (C-H).

Synthesis of [Mg(DO3AC$_{12}$)]

^{1}H NMR (500 MHz, D_2O): δ_H = 3.99-3.80 (8H, m, NC***H***$_2$C(O)), 3.57-2.96 (18H, m, NC***H***$_2$), 1.50 (2H, s, NCH$_2$C***H***$_2$), 1.27 (18H, s, -(C***H***$_2$)$_9$-), 0.86 (3H, t, $^{3}J_{HH}$ = 6.5 Hz, C***H***$_3$) ppm. ^{13}C{^{1}H} NMR (125 MHz, D_2O) δ_C = 174.4 (***C***O), 163.1 (***C***O), 162.8 (***C***O), 53.1, 51.8, 49.1, 47.7, 42.3, 39.6, 31.9, 29.8, 29.4, 28.9, 27.0, 22.6, 13.8 ppm. LRMS (ES$^+$) found *m/z* 594.38, calculated 594.37 for [M+H]$^+$. HRMS (ES$^+$) found *m/z* 594.3741, calculated 594.3717 for [$C_{28}H_{52}N_5O_7Mg$]$^+$. IR(solid/cm^{-1}): *v* 3310 br. (O-H), 2980, 2970, 2926, 2856 (C-H), 1726 (C=O), 1584 (N-H), 1445 (C-H), 1381 (C-O), 1245 (C-N), 1159, 1082, 1030 (C-O), 949, 638 (C-H).

Synthesis of [Ba(DO3AC$_{12}$)]

^{1}H NMR (500 MHz, D_2O): δ_H = 4.00-3.62 (8H, m, NC***H***$_2$C(O)), 3.56-2.99 (18H, m, NC***H***$_2$), 1.52 (2H, s, NCH$_2$C***H***$_2$), 1.29 (18H, s, -(C***H***$_2$)$_9$-), 0.88 (3H, t, $^{3}J_{HH}$ = 6.0 Hz, C***H***$_3$) ppm. ^{13}C{^{1}H} NMR (125 MHz, D_2O) δ_C = 174.4 (***C***O), 163.0 (***C***O), 162.7 (***C***O), 53.1, 51.8, 49.1, 47.7, 42.3, 31.9, 29.8, 29.7, 29.4, 28.8, 27.0, 22.6, 13.8 ppm. HRMS (ES$^+$) found *m/z* 708.2970, calculated 708.2923 for [$C_{28}H_{52}N_2O_7Ba$]$^+$. IR (solid/cm^{-1}): *v* 3389 br. (O-H), 2926, 2855 (C-H), 1651 (C=O), 1612 (N-H), 1460 (C-H), 1356, 1313 (C-O), 1248, 1200 (C-N), 1161, 1087 (C-O), 916, 827, 770, 694, 689 (C-H).

Synthesis of [Na(DO3AC$_{12}$)]

^{1}H NMR (500 MHz, D_2O): δ_H = 4.02-3.60 (8H, m, NC***H***$_2$C(O)), 3.58-2.97 (18H, m, NC***H***$_2$), 1.52 (2H, s, NCH$_2$C***H***$_2$), 1.29 (18H, s, -(C***H***$_2$)$_9$-), 0.91-0.85 (3H, m, C***H***$_3$) ppm. ^{13}C{^{1}H} NMR (125 MHz, D_2O) δ_C = 174.4 (***C***O), 163.0 (***C***O), 162.7 (***C***O), 53.1, 51.8, 49.1, 42.3, 31.9, 30.2, 29.8, 29.4, 28.8, 26.9, 22.6, 13.8 ppm. HRMS (ES$^+$) found *m/z* 594.3851, calculated 594.3843 for [$C_{28}H_{53}N_5O_7Na$]$^+$. IR (solid/cm^{-1}): *v* 3408 br., 3090 br. (O-H), 2980, 2926, 2854 (C-H), 1666 (N-H), 1462, 1381 (C-H), 1352 (C-O), 1176 (C-N), 1128, 1113 (C-O), 910, 826, 799, 719, 689 (C-H).

Synthesis of [Eu(DO3AC$_{12}$)]

^{1}H NMR (500 MHz, D_2O): δ_H = 4.15-2.68 (26H, br. m, NC***H***$_2$C(O)), 1.43-1.32 (2H, br. s, NCH$_2$C***H***$_2$), 1.25-1.13 (18H, br. s, -(C***H***$_2$)$_9$-), 0.79 (3H, t, $^{3}J_{HH}$ = 5.8 Hz, CH_3) ppm. ^{13}C{^{1}H} NMR (125 MHz, D_2O) δ_C = 163.1 (***C***O), 162.8 (***C***O), 64.9, 63.0, 60.5, 59.6, 56.2, 31.8, 29.6, 29.3, 22.5, 13.7 ppm. LRMS (ES$^+$) found *m/z* 722.21, calculated 722.30 for [M+H]$^+$. HRMS (ES$^+$) found *m/z* 722.3033, calculated 722.3001 for [$C_{28}H_{51}N_5O_7Eu$]$^+$. IR (solid/cm^{-1}): *v* 3346 br. (O-H), 2980, 2926, 2857 (C-H), 1730 (C=O), 1632 (N-H), 1582, 1462 (C-H), 1393 (C-O), 1223 (C-N), 1159, 1084, 1026 (C-O), 945, 634 (C-H).

Synthesis of [Gd(DO3AC$_{12}$)]

LRMS (ES$^+$) found *m/z* 727.23, calculated 727.30 for [M+H]$^+$. HRMS (ES$^-$) found *m/z* 725.2879, calculated 725.2874 for [$C_{28}H_{49}N_5O_7Gd$]$^-$. IR (solid/cm^{-1}): *v* 3445 br., 3316 br. (O-H), 2926, 2857 (C-H), 1728 (C=O), 1585, 1568 (N-H), 1462, 1408 (C-H), 1238, 1223 (C-N), 1163, 1082, 1026 (C-O), 947, 635 (C-H).

2.6. References

1. P. Zhang, Y. Gong, Y. Lv, Y. Guo, Y. Wang, C. Wang and H. Li, *Chem. Commun.*, 2012, **48**, 2334–2336.

2. M. Yang, B. Mallick and A.-V. Mudring, *Cryst. Growth Des.*, 2014, **14**, 1561–1571.

3. A. Cognigni, P. Gaertner, R. Zirbs, H. Peterlik, K. Prochazka, C. Schröder and K. Bica, *Phys. Chem. Chem. Phys.*, 2016, **18**, 13375–13384.

4. T. Hargreaves, *Chemical Formulation*, Royal Society of Chemistry, Cambridge, 2003

5. B. G. Trewyn, C. M. Whitman and V. S.-Y. Lin, *Nano Lett.*, 2004, **4**, 2139–2143.

6. G. Singh, G. Singh and T. S. Kang, *Phys. Chem. Chem. Phys.*, 2016, **18**, 25993–26009.

7. Y. Bi, L. Zhao, Q. Hu, Y. Gao and L. Yu, *Langmuir*, 2015, **31**, 12597–12608.

8. W. Xu, T. Wang, N. Cheng, Q. Hu, Y. Bi, Y. Gong and L. Yu, *Langmuir*, 2015, **31**, 1272–1282.

9. A. Beyaz, W. S. Oh and V. P. Reddy, *Colloid. Surf. B*, 2004, **35**, 119–124.

10. H. Wang, L. Zhang, J. Wang, Z. Li and S. Zhang, *Chem. Commun.*, 2013, **49**, 5222–5224.

11. G. Singh, G. Singh and T. S. Kang, *J. Phys. Chem. B*, 2016, **120**, 1092–1105.

12. A. Cornellas, L. Perez, F. Comelles, I. Ribosa, A. Manresa and M. T. Garcia, *J. Colloid Interface Sci.*, 2011, **355**, 164–171.

13. A. H. Rageh and U. Pyell, *J. Chromatogr. A*, 2013, **1316**, 135–146.

14. X. Qi, X. Zhang, G. Luo, C. Han, C. Liu and S. Zhang, *J. Disper. Sci. Technol.*, 2013, **34**, 125–133.

15. B. Dong, N. Li, L. Zheng, L. Yu and T. Inoue, *Langmuir*, 2007, **23**, 4178–4182.

16. T. J. Trivedi, K. S. Rao, T. Singh, S. K. Mandal, N. Sutradhar, A. B. Panda and A. Kumar, *ChemSusChem*, 2011, **4**, 604–608.

17. K. Srinivasa Rao, T. Singh, T. J. Trivedi and A. Kumar, *J. Phys. Chem. B*, 2011, **115**, 13847–13853.

18. K. Tanaka, T. Hiraoka, F. Ishiguro, J.-H. Jeon and Y. Chujo, *RSC Adv.*, 2014, **4**, 28107–28110.

19. S. Kanjilal, S. Sunitha, P. S. Reddy, K. P. Kumar, U. S. N. Murty and R. B. N. Prasad, *Eur. J. Lipid Sci. Technol.*, 2009, **111**, 941–948.

20. X. Li, S. R. A. Kersten and B. Schuur, *Energy Fuels*, 2016, **30**, 7622–7628.

21. C. Chadha, G. Singh, G. Singh, H. Kumar and T. S. Kang, *RSC Adv.*, 2016, **6**, 38238–38251.

22. P. C. Griffiths, I. A. Fallis, T. Chuenpratoom and R. Watanesk, *Adv. Colloid Interface Sci.*, 2006, **122**, 107–117.

23. K. Selmeczi, J.-P. Joly, M. Allali, V. Yeguas, B. Henry and M. Ruiz-Lopez, *Eur. J. Inorg. Chem.*, 2014, **2014**, 4934–4945.

24. P. C. Griffiths, I. A. Fallis, C. James, I. R. Morgan, G. Brett, R. K. Heenan, R. Schweins, I. Grillo and A. Paul, *Soft Matter*, 2010, **6**, 1981–1989.

25. P. C. Griffiths, I. A. Fallis, D. J. Willock, A. Paul, C. L. Barrie, P. M. Griffiths, G. M. Williams, S. M. King, R. K. Heenan and R. Görgl, *Chem. Eur. J.*, 2004, **10**, 2022–2028.

26. W. M. Leevy, M. E. Weber, M. R. Gokel, G. B. Hughes-Strange, D. D. Daranciang, R. Ferdani and G. W. Gokel, *Org. Biomol. Chem.*, 2005, **3**, 1647–1652.

27. W. M. Leevy, J. E. Huettner, R. Pajewski, P. H. Schlesinger and G. W. Gokel, *J. Am. Chem. Soc.*, 2004, **126**, 15747–15753.

28. L. J. Lalgee, L. Grierson, R. A. Fairman, G. E. Jaggernauth, A. Schulte, R. Benz and M. Winterhalter, *Biochim. Biophys. Acta*, 2014, **1838**, 1247–1254.

29. O. Murillo, I. Suzuki, E. Abel, C. L. Murray, E. S. Meadows, T. Jin and G. W. Gokel, *J. Am. Chem. Soc.*, 1997, **119**, 5540–5549.

30. H. Shabany, R. Pajewski, E. Abel, A. Mukhopadhyay and G. W. Gokel, *J. Heterocyclic Chem.*, 2001, **38**, 1393–1400.

31. M. E. Weber, W. Wang, S. E. Steinhardt, M. R. Gokel, W. M. Leevy and G. W. Gokel, *New J. Chem.*, 2006, **30**, 177–184.

32. A. C. Hall, C. Suarez, A. Hom-Choudhury, A. N. A. Manu, C. D. Hall, G. J. Kirkovits and I. Ghiriviga, *Org. Biomol. Chem.*, 2003, **1**, 2973–2982.

33. N. K. Djedovič, R. Ferdani, P. H. Schlesinger and G. W. Gokel, *Tetrahedron*, 2002, **58**, 10263–10268.

34. T. Miyazawa, M. Suzuki and K. Fujio, *Colloid Surf. A*, 2015, **482**, 447–453.

35. P. A. Heiney, M. R. Stetzer, O. Y. Mindyuk, E. DiMasi, A. R. McGhie, H. Liu and A. B. Smith, *J. Phys. Chem. B*, 1999, **103**, 6206–6214.

36. S. L. De Wall, K. Wang, D. R. Berger, S. Watanabe, J. C. Hernandez and G. W. Gokel, *J. Org. Chem.*, 1997, **62**, 6784–6791.

37. A. H. M. Elwahy and A. A. Abbas, *J. Heterocyclic Chem.*, 2008, **45**, 1–65.

38. M. Grogna, R. Cloots, A. Luxen, C. Jérôme, J.-F. Desreux and C. Detrembleur, *J. Mater. Chem.*, 2011, **21**, 12917–12926.

39. M. Lee, M. S. Tremblay, S. Jockusch, N. J. Turro and D. Sames, *Org. Lett.*, 2011, **13**, 2802–2805.

40. V. Li, Y.-J. Ghang, R. J. Hooley and T. J. Williams, *Chem. Commun.*, 2014, **50**, 1375–1377.

41. A. Morisco, A. Accardo, D. Tesauro, R. Palumbo, E. Benedetti and G. Morelli, *Biopolymers*, 2011, **96**, 88–96.

42. M. Othman, D. Desmaële, P. Couvreur, L. V. Elst, S. Laurent, R. N. Muller, C. Bourgaux, E. Morvan, T. Pouget, S. Lepêtre-Mouelhi, P. Durand and R. Gref, *Org. Biomol. Chem.*, 2011, **9**, 4367–4386.

43. F. Fernández-Trillo, J. Pacheco-Torres, J. Correa, P. Ballesteros, P. Lopez-Larrubia, S. Cerdán, R. Riguera and E. Fernandez-Megia, *Biomacromolecules*, 2011, **12**, 2902–2907.

44. J. Duane E. Prasuhn, R. M. Yeh, A. Obenaus, M. Manchester and M. G. Finn, *Chem. Commun.*, 2007, 1269–1271.

45. H. Wang, H. Wu, H. Shen, S. Geng, B. Wang, Y. Wang, X. Ma, G. Li and M. Tan, *J. Mater. Chem. B*, 2015, **3**, 8832–8841.

46. M. Othman, D. Desmaële, P. Couvreur, L. V. Elst, S. Laurent, R. N. Muller, C. Bourgaux, E. Morvan, T. Pouget, S. Lepêtre-Mouelhi, P. Durand and R. Gref, *Org. Biomol. Chem.*, 2011, **9**, 4367–4386.

47. J. L. Arias, L. H. Reddy, M. Othman, B. Gillet, D. Desmaële, F. Zouhiri, F. Dosio, R. Gref and P. Couvreur, *ACS Nano*, 2011, **5**, 1513–1521.

48. G. Liang, J. Ronald, Y. Chen, D. Ye, P. Pandit, M. L. Ma, B. Rutt and J. Rao, *Angew. Chem. Int. Ed.*, 2011, **50**, 6283–6286.

49. (a) L. Tei, G. Gugliotta, Z. Baranyai and M. Botta, *Dalton Trans.*, 2009, 9712–9714. (b) N. Kamaly, T. Kalber, A. Ahmad, M. H. Oliver, P.-W. So, A. H. Herlihy, J. D. Bell, M. R. Jorgensen and A. D. Miller, *Bioconjugate Chem.*, 2008, **19**, 118–129. (c) G. V. Martinez, S. Navath, K. Sewda, V. Rao, P. Foroutan, R. Alleti, V. E. Moberg, A. M. Ahad, D. Coppola, M. C. Lloyd, R. J. Gillies, D. L. Morse and E. A. Mash, *Bioorganic & ACS Med. Chem. Lett,* 2013, **23**, 2061–2064.

50. Z. Xu, S. Peng, Y.-Y. Wang, J.-K. Zhang, A. I. Lazar and D.-S. Guo, *Adv. Mater.*, 2016, **28**, 7666–7671.

51. H.J Bolink, E. Baranoff, M. Clemente-León, E. Coronado, N. Lardiést, A. Lopez-Muñoz, D.Repetto and Md. K. Nazeeruddin, *Langmuir*, 2010, **26**, 11461–11468.

52. K. Jie, Y. Zhou, Y. Yao and F. Huang, *Chem. Soc. Rev.*, 2015, **44**, 3568–3587.

53. C. Larpent, A. Laplace and T. Zemb, *Angew. Chem. Int. Ed.*, 2004, **43**, 3163–3167.

54. R. Ferreirós-Martínez, D. Esteban-Gómez, É. Tóth, A. de Blas, C. Platas-Iglesias and T. Rodríguez-Blas, *Inorg. Chem.*, 2011, **50**, 3772–3784.

55. *Macrocycle Synthesis: A Practical Approach*, ed. D. Parker, OUP, Oxford, 1996, p. 40-42.

56. R. Crossley, Z. Goolamali, J. J. Gosper and P. G. Sammes, *J. Chem. Soc., Perkin Trans. 2*, 1994, 513–520.

57. A. B. P. Lever, *J. Chem. Educ.*, 1968, **45**, 711.

58. P. Atkins, T. Overton, J. Rourke, M. Weller and F. Armstrong, *Shriver and Atkins' Inorganic Chemistry*, OUP Oxford, Oxford ; New York, 4 edition., 2006

59. M. Triest, G. Bussiére, H. Bélisle and C. Reber, *J. Chem. Edu. ACS,* 2000, **77**, 670 (Web-Ed article accessed June 2017).

60. A. B. P. Lever, *Inorganic Electronic Spectroscopy*, Elsevier Science, Amsterdam ; New York, 2 Sub edition., 1986.

61. (a) G. W. Gokel, W. M. Leevy and M. E. Weber, *Chem. Rev.*, 2004, **104**, 2723–2750. (b) C. Rodríguez-Infante, D. Esteban, F. Avecilla, A. de Blas, T. Rodríguez-Blas, J. Mahía, A. L. Macedo and C. F. G. C. Geraldes, *Inorg. Chim. Acta*, 2001, **317**, 190–198. (c) L. Vaiana, C. Platas-Iglesias, D. Esteban-Gómez, F. Avecilla, J. M. Clemente-Juan, J. A. Real, A. de Blas and T. Rodríguez-Blas, *Dalton Trans.*, 2005, 2031–2037.

62. (a) H. U. Rashid, M. A. U. Martines, J. Jorge, P. M. de Moraes, M. N. Umar, K. Khan and H. U. Rehman, *Bioorg. & Med. Chem.*, 2016, **24**, 5663–5684. (b) B. Jebasingh and V. Alexander, *Inorg. Chem.*, 2005, **44**, 9434–9443. (c) J.-M. Idée, M. Port, I. Raynal, M. Schaefer, S. Le Greneur and C. Corot, *Fundam. Clin. Pharmacol.*, 2006, **20**, 563–576.

63. B. Jagadish, G. L. Brickert-Albrecht, G. S. Nichol, E. A. Mash and N. Raghunand, *Tet. Lett.*, 2011, **52**, 2058–2061.

64. (a) T. Yokoyama, H. Kitagawa, H. Iwasawa and M. Zenki, *Inorg. Chim. Acta*, 1996, **253**, 1–6. (b) S. K. Sharma, G. Hundal and R. Gupta, *Eur. J. Inorg. Chem.*, 2010, **2010**, 621–636.

65. (a) W. C. E. Higginson, S. C. Nyburg and J. S. Wood, *Inorg. Chem.*, 1964, **3**, 463–467. (b) S. C. Nyburg and J. S. Wood, *Inorg. Chem.*, 1964, **3**, 468–476.

66. N. G. Connelly and W. E. Geiger, *Chem. Rev*., 1996, **96**, 877

Chapter Three

Acyclic Amphiphilic Ligand Architectures towards Micellar Systems

3.1 Introduction

This chapter describes the design, synthesis and characterisation of a range of acyclic amphiphilic ligands for metallosurfactants. Tensiometric studies were used to probe the self-assembly characteristics of the ligands and complexes into micellar systems, as well as to assess their microemulsion compatibility.

Although there is a fairly wide range of literature concerning acyclic ligand surfactants for a variety of applications, there has been a noticeable decline in interest over the past decade. Macrocyclic ligand surfactants have received attention due to their potentially higher binding affinity with metal ions. However, acyclic ligand surfactants generally offer a greater ease of synthesis and functionalisation over their macrocyclic analogues.

Multiple reports have considered the suitability of ethylenediamine-based ligands for use in metallosurfactants. For example, Tavares *et al.* describe a Pt(II) complex with an *N*-alkyl-ethylenediamine ligand which showed superior activity to cisplatin as a potential chemotherapy drug.[1] Similar ligands have also been reported for Pd(II) complexes which were synthesised from both mono-alkyl and bis-alkyl ligands, as shown in Figure 3.1.[2] The metallosurfactant complexes formed from the mono-alkyl ligands were found to be more soluble than those containing the bis-alkyl ligands as well as aggregating at lower concentrations and offering a greater degree of control over the physical properties of the complex.

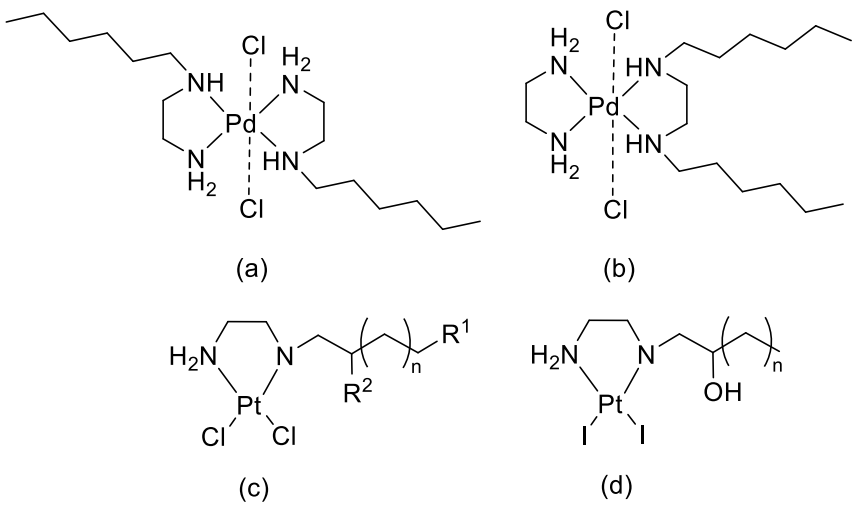

Figure 3.1 (a) and (b) Pd complexes of alkylated ethylenediamine-based ligands[2]; (c) and (d) Pt complexes of ethylenediamine-based ligands n = 7, 9, 11, 13; R^1 = H/OH; R^2 = H/OH[1]

In 2016 Qiao *et al.* reported the use of an *N*-lauroyl ethylenediamine triacetate ligand for the removal of Pb(II) and Zn(II) from contaminated soils. The aim was to be able to chelate the heavy metal ions using the amphiphilic ligand and therefore be able to "wash" them out of the soil. The authors proposed that the ligand coordinated to the metals *via* the carboxylic acid arms and one of the amines of the ethylenediamine backbone, as represented in Figure 3.2. The lipophilic dodecyl chain present on the ligand facilitated aggregation to form micelles. It was found that metal extraction was more efficient when the ligand was at a concentration above the CMC as alignment of ligand head groups at the micellar interface was found to increase metal binding.[3]

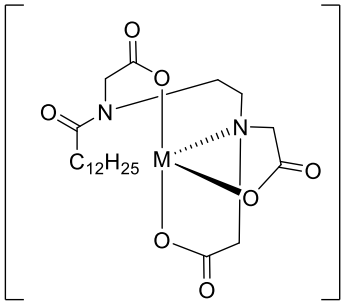

Figure 3.2 Proposed metallosurfactant structure (M = Pb(II)/Zn(II))[3]

Jaeger and co-workers have reported the use of similar ligands for Co(III) complexes. Co(III) is known to form diamagnetic octahedral complexes which are kinetically inert towards ligand substitution and can therefore be easily characterised *via* multinuclear NMR spectroscopy. An Ethylenediaminetetraacetic acid (EDTA) derived ligand was reported which coordinated to 5 out of 6 sites of the octahedral Co(III) complex as illustrated in Figure 3.3. A six-coordinate complex was discounted due to the high degree of ring-strain it would require. Functionalisation of these ligands with long alkyl chains created metallosurfactants capable of aggregation into "giant vesicles" (aggregates larger than micelles) and rods.[4,5,6]

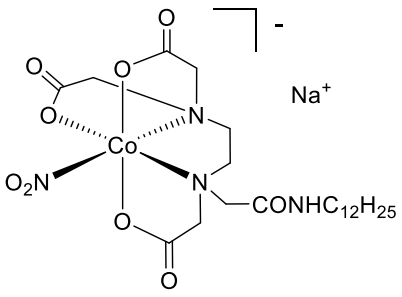

Figure 3.3 Proposed metallosurfactant structure[4]

One of the most commonly investigated metals used in metallosurfactants is Cu(II). It has been reported in an extensive range of applications mainly due to its redox active properties. A 2009 study by Polyzos *et al.* reports a Cu(II) complex with a tridentate ligand derived from diethethylenetriamine, bearing a tetradecyl chain. Various nitro-activated aryl ester hydrolysis reactions were tested in the presence of micelles of this metallosurfactant. The improved reaction rates observed were attributed to electrostatic interactions between the cationic micelles and the anion substrates as illustrated in Figure 3.4. These surfactants were also found to be capable of forming mixed surfactant systems with MTAB (myristyltrimethylammonium bromide) or Triton X-100 which were found to exhibit improved catalytic activity.[7]

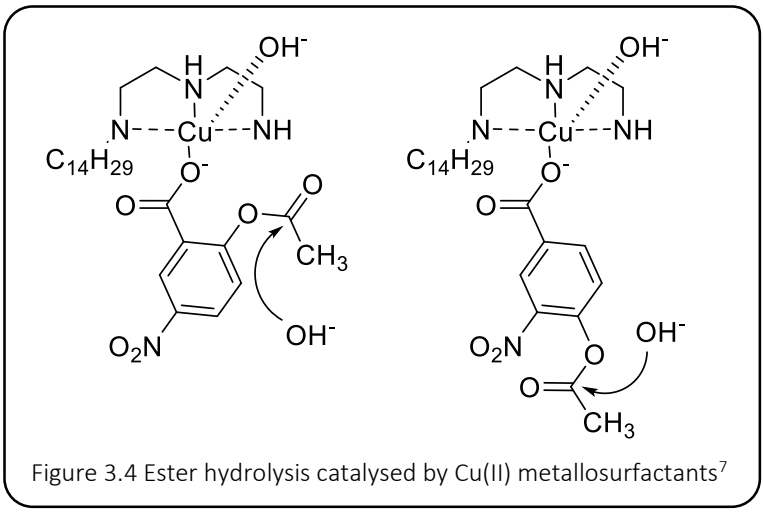

Figure 3.4 Ester hydrolysis catalysed by Cu(II) metallosurfactants[7]

A similar report describes lipophilic pyridine-based ligands capable of coordination to Cu(II) or Zn(II). These metallosurfactants catalysed carboxylic acid ester hydrolysis and formed micelles in the presence of a CTAB (cetyltrimethylammonium bromide) co-surfactant.[8]

The accessibility of the Cu(I)/Cu(II) redox pair has made it a common choice for fabrication of responsive materials, typically involving the formation of Langmuir-Blodgett films as precursors to highly ordered materials.[9,10,11,12,13] Verani and co-workers reported diimine amphiphiles of Cu(II) with single alkyl tails (C = 10, 14, 16, 18) for use as precursors to redox-active patterned Langmuir films for technological applications. These complexes were found to take on a distorted square planar geometry with Cl^-/Br^- ancillary ligands as shown in Figure 3.5. The length of alkyl chain and nature of halogen co-ligand were found to strongly influence characteristics, for example film formation only occurred for chain lengths of C_{16} or above.[14,15,16]

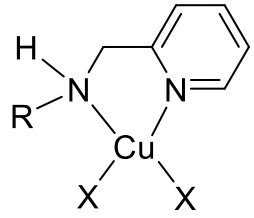

Figure 3.5 R = $C_{18}H_{37}$, $C_{16}H_{33}$, $C_{14}H_{29}$, $C_{10}H_{21}$; X = Br, Cl[14]

Transition metals including Cu(II) have also been reported to form vesicles, aggregated structures where surfactant molecules arrange in bilayers. For example, Luo *et al.* describe complexes of Co(II), Cu(II) and Ni(II) formed from a sodium hexadecyliminodiacetate (SHIDA) surfactant ligand (Figure 3.6). The ligand was found to be capable of self-aggregation to form micelles in aqueous media. However, addition of metal salts was found to alter the aggregate morphology, producing vesicles. It was found that the bidentate ligand coordinated to the metal ions in a 2:1 ligand:metal ratio to give double-chained surfactants. Transmission electron micrograph (TEM) studies showed these aggregates to have vesicle morphologies.[17] It is commonly found that whilst single-chained surfactants favour micelle formation, double-chained surfactants tend towards the formation of vesicles.[18,19]

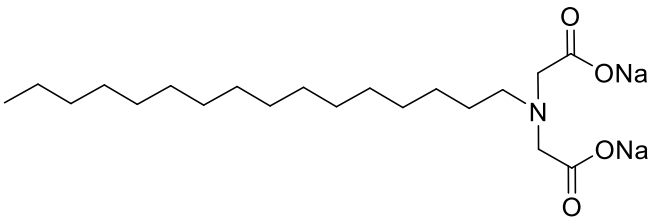

Figure 3.6 Sodium hexadecyliminodiacetate (SHIDA)[17]

Zha *et al*. report a similar range of surfactant molecules that aggregate into micelles on their own but form double-chained metallosurfactants upon addition of Cu(II). At relatively high concentrations these metallosurfactants formed vesicles which showed potential as delivery systems for chemotherapy drugs such as doxorubicin hydrochloride.[20]

Examples of metallosurfactants are not confined to Cu(II). Metals including Fe(III), Co(II), Zn(II) and Ni(II) have also been reported as forming metallosurfactants *via* coordination of acyclic amphiphiles with applications in areas such as thin-film fabrication for redox active materials and catalysts for water oxidation.[10,21,22,23]

3.2 Aims

The aim of this chapter was to synthesise a range of acyclic amphiphiles as analogues to the macrocyclic surfactants discussed elsewhere in this thesis. Cyclic surfactants have typically been found to be favourable due to the increased complex stability offered by the macrocyclic effect. However, the difficulties that arise in synthesising macrocycles and functionalising them to create amphiphiles raises the question as to whether their favourable qualities outweigh the difficulty in their synthesis.

The ligands and complexes reported in this chapter were synthesised *via* a much simpler process than their cyclic analogues, from readily available commercial starting materials. Ni(II) and Cu(II) complexes were formed *via* addition of metal salts to aqueous solutions of the ligands and were used to study the coordination geometry of the ligands *via* absorption spectroscopy. Characterisation *via* ^{1}H, $^{13}C\{^{1}H\}$ NMR and IR spectroscopy and mass spectrometry confirmed synthesis of ligands and complexes.

Drop volume tensiometry provided insight into the micellar systems of ligands and complexes, showing them to be capable of self-aggregation in aqueous solution. The effects of the head-group size, alkyl chain length and metal coordination were studied in order to fully characterise the micellar solutions.

One ligand was chosen to assess the microemulsion compatibility of the surfactants. This multidentate, dodecyl-functionalised ligand was doped into the $[MeImC_{12}]Br/BuOH/H_2O$ micellar system detailed in Chapter Two. This mixed-surfactant system was found to be capable of forming a stable microemulsion at room temperature with a toluene loading of ~10 wt%.

3.3 Results and Discussion

3.3.1 Design and Synthesis

The ligands studied in this chapter were designed to have multidentate head groups capable of metal binding and lipophilic moieties to create surfactant-like ligands and complexes with the ability to aggregate in aqueous media. As in other chapters of this thesis, the lipophilic character is provided by a range of alkyl chains of varying lengths whereas the head group was formed by functionalisation of a diamine or triamine backbone with multiple alcohol groups which not only provided sites for metal coordination, but also rendered the ligands water soluble.

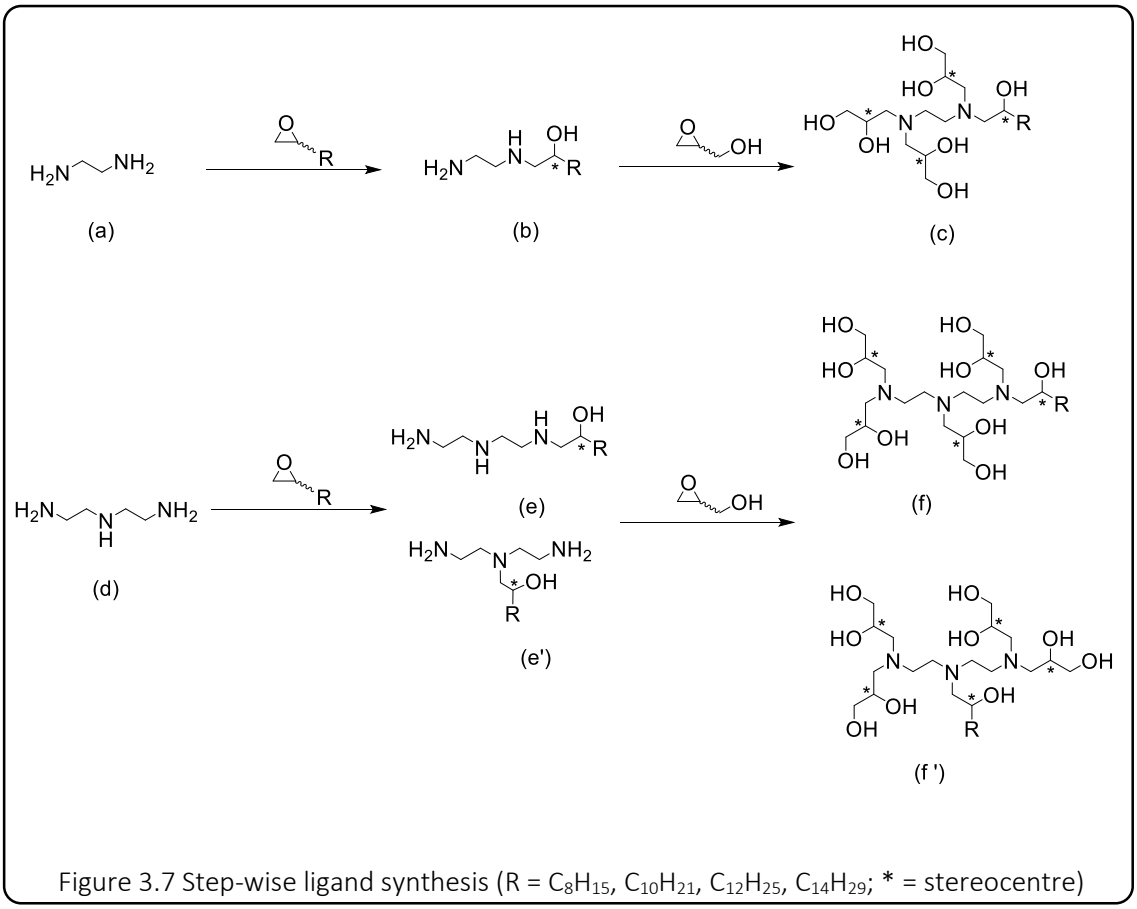

Figure 3.7 Step-wise ligand synthesis (R = C_8H_{15}, $C_{10}H_{21}$, $C_{12}H_{25}$, $C_{14}H_{29}$; * = stereocentre)

Ethylene diamine (**en**) based ligands were synthesised according to the above scheme (Figure 3.7, a-c). The initial reaction involved the addition of 10 equivalents of commercial **en** to the corresponding epoxide in EtOH. The mixture was left to stand in a foil-covered vessel for upwards of 5 days before the solvent was removed *in vacuo* and the excess **en** removed via bulb-to-bulb distillation (kugelrohr apparatus 118 °C). This gave a series of ligands with varying alkyl chain lengths, denoted **enC$_n$** (n = 8, 10, 12, 14), as off-white solids in yields of 65-83%.

The second step was achieved in an analogous manner, whereby an excess of glycidol was added to the **enC$_n$** ligand in EtOH and left to stand for at least 5 days. Bulb-to-bulb distillation (61-62 °C) was used to remove the unreacted glycidol, yielding the poly-alcohol functionalised ligands (denoted **polyEnC$_n$**) as yellow/brown oils in yields of 60-80%. Although the glycidol used in these reactions was obtained from commercial sources it is often known to degrade with time into glycerol. Pure glycidol was obtained *via* bulb-to-bulb distillation (61-62 °C) for use in subsequent reactions.

Diethylene triamine (**dien**) ligands were synthesised, according to the above scheme (Figure 3.7, d-f), in yields of 65-89%, analogously to the **enC$_n$** and **polyEnC$_n$** species. Unlike the **en** analogues, however, the presence of two inequivalent nitrogen environments capable of reacting with the epoxide led to the formation of the products as a mix of isomers (denoted f and f' in Figure 3.7).

The 1,2-epoxy-9-decene, 1,2-epoxydodecane and 1,2-epoxyhexadecane starting materials used in these reactions were obtained from commercial sources and used without further purification. However, the 1,2-epoxytetradecane was synthesised from racemic 1,2-tetradecane diol which first required repeated recrystallisation from EtOAc to remove any branched material. The diol was stirred in $CHCl_3$ with HBr/AcOH (45% w/v) for 24 hours under inert conditions. The reaction was quenched with water and the product extracted into DCM and dried *in vacuo* to give a white residue. This was then dissolved in dry MeOH and stirred for 2 hours in the presence of K_2CO_3. Again, the reaction was quenched with water, the product extracted into DCM and dried *in vacuo* to give a white residue. The crude product was purified using bulb-to-bulb distillation (95-96 °C) to give the desired racemic epoxide as a clear, colourless oil.[24] Methods are available for either separating the racemic mixture or for synthesising a single enantiomer, however, for our requirements the use of chiral epoxide was not deemed important so the material was simply used in its racemic form.

Complexes of the **polyEnC$_n$** and **polyDienC$_n$** ligands were formed by the addition of 1.1-1.5 equivalents of metal chloride salt to an aqueous solution of the ligand. In some cases mild heating or sonication was required to fully solubilise the ligand. It was noted that the C_{14} analogues of the ligands were the least soluble, requiring significantly more heating and sonication to dissolve than the other ligands. Ni(II) and Cu(II) complexes were made of each of the ligands in order to study their geometry and ligand field splitting. Sr(II) and Y(III) complexes were also made of the **polyDienC$_{12}$** ligand, as discussed in section **3.3.5**.

3.3.2 Spectroscopic Characterisation

The ligands were characterised primarily using ^{1}H, $^{13}C\{^{1}H\}$ NMR and IR spectroscopy and HR mass spectrometry. The successful addition of the alkyl chains to the amine precursors was identified by a series of characteristic peaks. The most obvious of these was a triplet around 0.59-0.87 ppm integrating to 3H which corresponds to the CH_3 group at the alkyl tail terminus. Secondly, a resonance around 1.48-1.08 ppm was observed corresponding to the C(OH)C***H***$_2$ at the start of the tail. Finally, a peak was observed, usually as a broad singlet around 1.33-0.97 ppm, representing the bulk of the protons in the alkyl tail which are all in very similar environments. Figure 3.8, below, demonstrates the process of characterisation *via* ^{1}H NMR spectroscopy. Although this holds true for the **C_{10}**, **C_{12}** and **C_{14}** alkane tails the mono-alkene **C_8** has its own set of characteristic peaks.

The ligands **enC_8** and **dienC_8** differ from the others as they have an alkene bond at the end of the lipophilic tail. This means that the ^{1}H NMR resonances arising from the chain are different to those of the alkanes described above. Firstly, instead of the triplet observed for CH_3 there is a multiplet around 5.85-5.75 ppm corresponding to $H_2C=C$***H***. The protons *cis* and *trans* to this proton produce resonances at ~4.98 ppm and ~4.92 ppm, respectively. Finally, as with the alkane analogues, the bulk chain is a broad singlet around 1.61-1.30 ppm. As discussed later the presence of an alkene rather than an alkane at the chain terminus had no notable effect on the properties of the amphiphile and its complexes.

As the epoxides and glycidol used in these reactions were all racemic, the final products contain a large number of stereogenic centres, as shown in Figure 3.7, above. **PolyEnC_n** ligands each contain 4 stereogenic centres which means that the product is a mixture of 16 stereoisomers. However, the **polyDienC_n** ligands each contain 5 stereogenic centres, hence 32 stereoisomers, but as there are two structural isomers present, the product will be a mixture of 64 isomers. The broad peaks observed in the ^{1}H NMR spectra can be attributed to these complex mixtures. While this did not hinder assignment of resonances in the case of **polyEnC_n** ligands, it did make full characterisation for the **dien** analogues much more complex.

One of the main reasons for introducing the poly-alcohol moieties to these ligands was to afford water solubility as the **enC_n** and **dienC_n** ligands were only very sparingly soluble in water. However, this means that direct comparisons cannot be drawn between the resonances of the ^{1}H NMR spectra as the **enC_n**/**dienC_n** spectra were recorded in $CDCl_3$ whereas the **polyEnC_n**/**polyDienC_n** spectra were recorded in D_2O. It is also worth noting that the exchangeable OH protons in D_2O led to peak broadening in the ^{1}H NMR spectra making detailed assignments difficult.

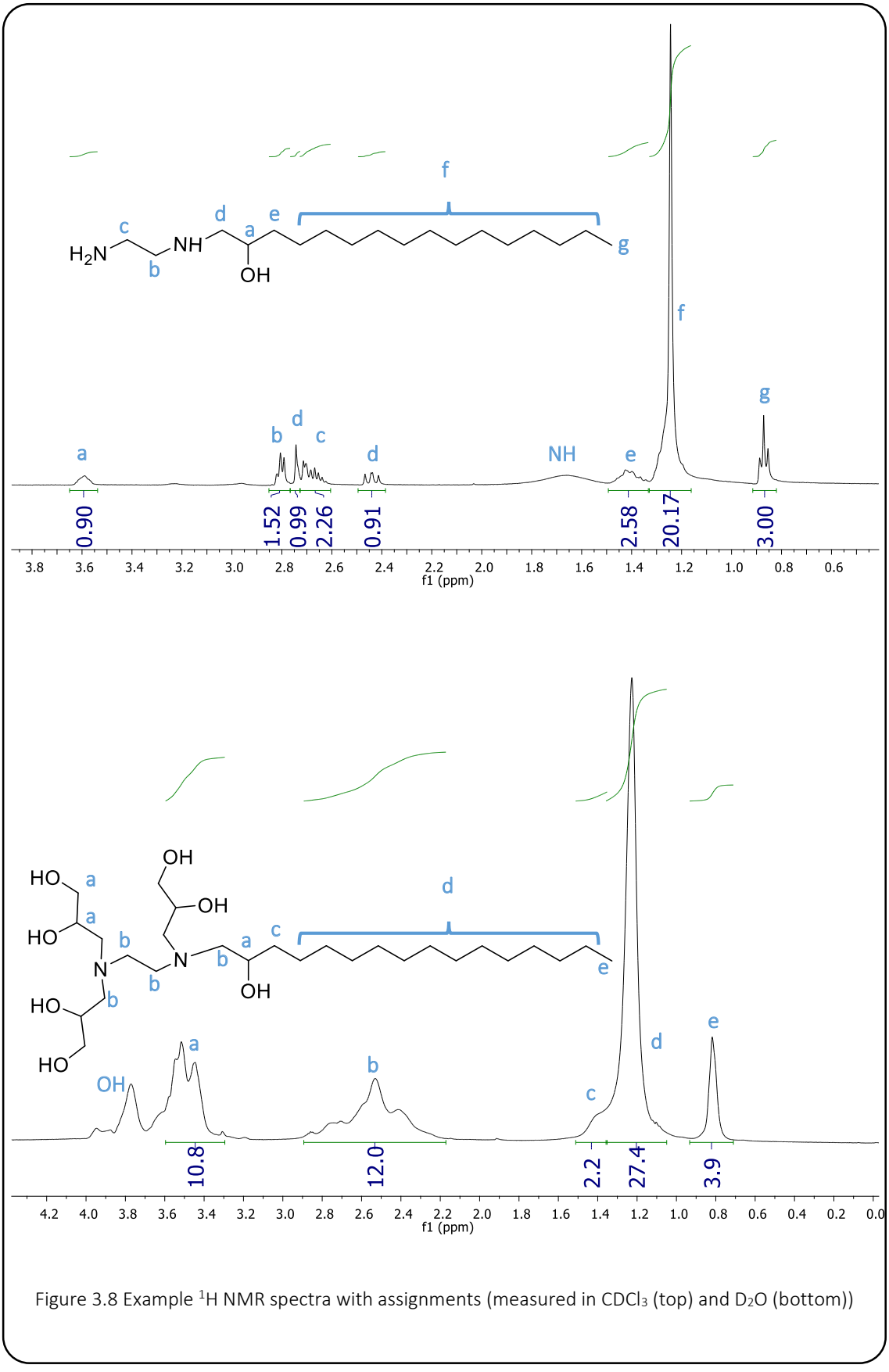

Figure 3.8 Example ^{1}H NMR spectra with assignments (measured in $CDCl_3$ (top) and D_2O (bottom))

It was expected that two isomers would be formed from the **dien** precursor as it possesses two inequivalent nitrogen environments. This theory was supported by the ^{1}H NMR spectra obtained as the proton resonances for the **dien** backbone and the poly-alcohol arms in **polyDienC$_n$** were seen as either overlapping resonances or indecipherable multiplets. However, the resonances for the bulk of the alkyl chain and the terminal methyl group could be identified. The complicated spectra meant that it was not possible to assign a ratio to the isomers present. Similarly, the $^{13}C\{^{1}H\}$ NMR spectra showed resonances corresponding to carbon environments in each of the different isomers although the majority of the carbon environments in the two isomers are either very similar or identical to one another and so were only seen as single peaks.

IR spectroscopy for the **enC$_n$** and **dienC$_n$** ligands identified alkane C-H stretches in the region of 2930-2840 cm^{-1} and the corresponding bending peaks around 1460 cm^{-1}. The alcohol C-O stretch was seen around 1123 cm^{-1} and the N-H bend observed in the region 1645-1560 cm^{-1}. Upon reaction of these species to form **polyEnC$_n$** and **polyDienC$_n$** the N-H bend disappeared as all of the primary and secondary amines in the ligands become tertiary. The other characteristic change observed was the appearance of a large, broad peak ranging from 3340-3280 cm^{-1} corresponding to the O-H stretch of the multiple alcohol groups now present in the ligands. There was also a shift in the C-O peak from around 1123 cm^{-1} to approximately 1036 cm^{-1}. However, no notable shifts were observed in any of the frequencies upon addition of Cu(II), Ni(II, Sr(II) or Y(III).

In octahedral geometries, Ni(II) is a paramagnetic metal ion which often makes NMR spectroscopy an inaccessible technique for its complexes. However, ^{1}H NMR spectra were recorded of the Ni(II) complexes of **polyEnC$_{12}$** and **polyDienC$_{12}$** in order to see whether the effect of metal coordination could be observed. The NMR spectra for these complexes showed resonances in very similar positions as the free ligands, however, the peaks were seen to broaden significantly. This effect is due to the metal's paramagnetism and is therefore indicative of successful coordination. This was confirmed by mass spectrometry, as discussed below.

Mass spectrometry of **enC$_n$/dienC$_n$** and their **polyEnC$_n$/polyDienC$_n$** analogues consistently showed peaks corresponding to either the parent cation or the $[M+H]^+$ species. Whereas the Ni(II) and Cu(II) complexes generally showed peaks corresponding to the $[M-H]^+$ species, confirming metal coordination and suggesting deprotonation of an alcohol group upon binding. However, for the **polyDienC$_{12}$** Sr(II) and Y(III) complexes peaks were only observed for the free ligand $[M-X+H]^+$ (X = Sr(II), Y(III)), which could be indicative of unsuccessful metal coordination or due to fragmentation during the measurement.

3.3.3 Electronic Properties

UV-Vis absorption spectra were recorded for the Ni(II) and Cu(II) complexes of the **polyEnC$_n$**, and **polyDienC$_n$** ligands in water in order to investigate the complex geometry afforded by metal coordination.

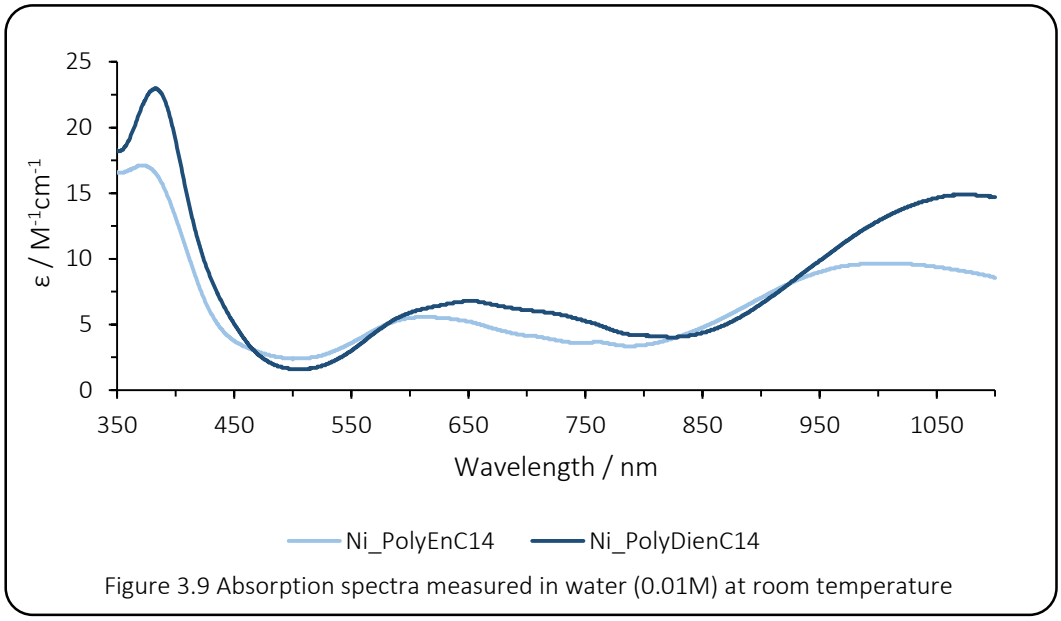

Figure 3.9 Absorption spectra measured in water (0.01M) at room temperature

Figure 3.9, above, shows the absorption spectra of the Ni(II) **polyEnC$_{14}$** and **polyDienC$_{14}$** complexes. The spectra of both complexes show three clear absorption bands corresponding to the *d-d* transitions $^3A_{2g}$ → $^3T_{2g}$ (~950-1050 nm), $^3A_{2g}$ → $^3T_{1g}$(F) (~550-650 nm) and $^3A_{2g}$ → $^3T_{1g}$(P) (~380 nm). Although there is a slight difference between the **polyEnC$_n$** and the **polyDienC$_n$** complex absorption profiles they both have similar peak ratios and λ_{max} values to the absorption spectrum of $[Ni(H_2O)_6]^{2+}$ (see Figure 2.10, Chapter Two[25]). This suggests that complexes of both **en** and **dien** ligands adopt octahedral (or near-octahedral) geometries. It was observed that variation in the length of the lipophilic alkyl chain had very little effect on the absorption spectra, hence only one example of each ligand is shown in Figure 3.9.

For some of the Ni(II) complexes there was a second peak visible in the same region as the $^3A_{2g}$ → $^3T_{1g}$(F) absorption corresponding to the spin-forbidden $^3A_{2g}$ → ^1E_g transition. The $^3T_{1g}$(F) and ^1E_g states lie close enough together in energy for spin-coupling to allow the spin-forbidden transition to gain intensity from the spin-allowed transition leading to the observation of two close peaks in the absorption spectrum. In some cases these two peaks are observed but in others only a single broad peak is seen as technically these two states are scrambled by spin-orbit coupling and therefore cannot be separated.[26]

From the spectra, it was possible to assign the octahedral field splitting parameter (Δ_{oct}) which is given by the lowest energy transition (ν_1) and therefore calculate the Racah B parameter for each ligand based on the equation:

——————.....Equation 3.1 [27]

From the Racah B parameter of the complex it is possible to calculate to nephelauxetic effect (β) of the ligands given that the free ion value of B for Ni(II) is known to be 1082 cm^{-1} (Equation 3.2). For the free ion B is a measure of electron-electron repulsion within the *d*-orbitals. Upon complexation the occupied molecular orbitals become delocalised over the ligands and thus away from the metal ion. This reduces inter-electron repulsion by expanding the electron cloud which increases the average separation between the *d*-electrons. The extent of delocalisation depends on the covalent character of the complex, therefore the value of β can provide information on the relative covalency of the metal-ligand bonds.

——————.....Equation 3.2

Table 3.1 shows that although the nephelauxetic parameter is very similar for all of the ligands, the value is slightly smaller for the **polyEnC$_n$** Ni(II) complexes than for the **polyDienC$_n$** analogues. The smaller the value of β the larger the delocalisation of *d*-electrons over the ligands. Therefore the data suggests that the **polyEnC$_n$** ligands are slightly more covalent in character than the **polyDienC$_n$** ligands.[28]

Ligand Name	ν_1 / cm^{-1}	ν_2 / cm^{-1}	ν_3 / cm^{-1}	Racah B / cm^{-1}	β
polyEnC$_8$	10020	16667	26455	871	0.805
polyEn$_{10}$	10060	16667	26385	858	0.793
polyEn$_{12}$	9166	15198	26316	934	0.863
polyEn$_{14}$	10111	16313	26385	824	0.762
polyDienC$_8$	9259	15314	25773	887	0.820
polyDien$_{10}$	9268	15198	25773	878	0.811
polyDien$_{12}$	9407	15337	25907	868	0.802
polyDien$_{14}$	9276	15291	25907	891	0.823

Table 3.1 Ligand field parameters for Ni(II) complexes

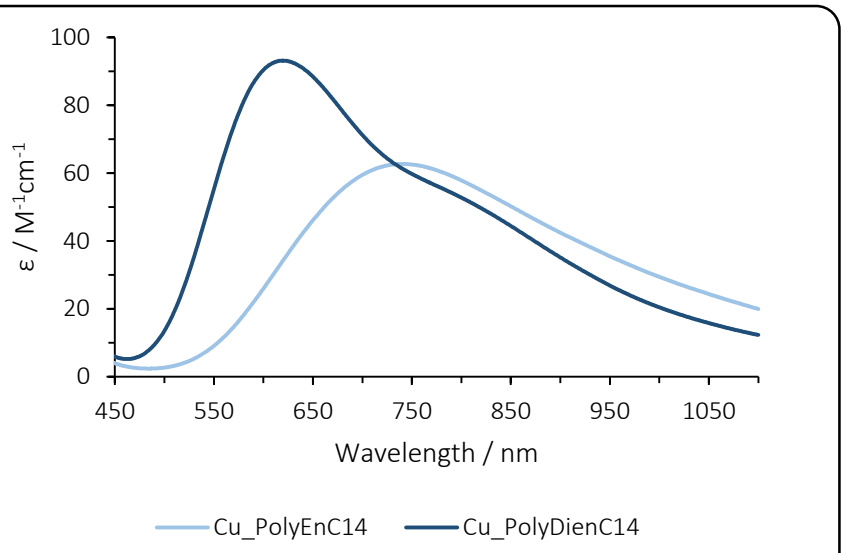

Figure 3.10 Absorption spectra measured in water (0.01M) at room temperature

The absorption spectra of the Cu(II) complexes of each ligand were measured in water at room temperature (Figure 3.10). As for the Ni(II) complexes the length of the alkyl chain was seen to cause little variation in the complex absorption spectra, hence only one example of each ligand is shown. However, the nature of the head group was seen to significantly influence the absorption. The position of the absorption bands for the **polyEnC$_n$** complexes, with λ_{max} at ~760 nm, are typical of octahedral Cu(II) complexes, whereas those for the **polyDienC$_n$** ligands, with λ_{max} of ~580 nm, are more typical of complexes with square pyramidal geometry.[29] This may be explained as a tetragonal distortion arising from the Jahn-Teller effect which is a common occurrence in octahedrally-coordinated d^9 metals such as Cu(II). In this case, the distortions cause a change in complex geometry from octahedral for the **polyEnC$_n$** complexes to square pyramidal for the **polyDienC$_n$** analogues. Tetragonal distortion results from elongation of the bonds along the z-axis which causes orbitals with a z-component (, ,) to reduce in energy while bonds in the x- and y-directions (,) shorten causing an increase in orbital energy. Although it is more common for this process to result in a distorted 6-coordinate complex, the absorption spectra for the Cu(II) **polyDienC$_n$** complexes suggest that one of the ligands on the z-axis is lost, resulting in a square pyramidal complex geometry. Despite the change in complex geometry, the splitting parameter remains the same for the two complexes.[30,31]

3.3.4 Micellar Systems

Surface tension studies were carried out *via* drop volume tensiometry (DVT). By measuring the change in surface tension of a micellar system with respect to concentration, it is possible to determine the critical micelle concentration (CMC) and therefore the average area per molecule (APM) of the system. Both parameters are able to give insights into the structure of aggregates in the micellar solution. Measurements were carried out using milliQ ultra-pure water to ensure no unwanted surface active compounds were present.

Table 3.2 shows the CMC values measured for each system and the APM values subsequently calculated. It is assumed that the ligands are non-ionic species, therefore calculations using a Gibb's prefactor of n=1 provide the most accurate APM values. The results for the complexes are likely to lie somewhere between n=1 and n=2 as it is not known whether the complexes form charged surfactants or whether the ligands are sufficiently deprotonated upon coordination to form neutral surfactants. Also, if the metallosurfactants are ionic, a Gibb's prefactor of n=2 assumes complete dissociation of the counter ion from the complex, however the degree of dissociation cannot be estimated by tensiometry but rather requires a technique such as small angle X-ray scattering in order to be quantified.

Due to the time-consuming nature of these tensiometry measurements, systems were chosen which could give the largest range of insight into the effects of varying parameters. Table 3.2 shows the ligands and complexes selected for analysis. From this cross-section comparisons can be made between chain length, head groups size, presence of polyol groups, ligands *vs.* complexes and nature of metal ion.

System	CMC / mM (±0.1)	APM (n=1) / Å^2 (±1)	APM (n=2) / Å^2 (±2)
polyDienC_{14}	0.32	27	54
Ni-polyDienC_{14}	0.59	18	36
Cu-polyDienC_{14}	1.23	20	40
Ni-dienC_{14}	2.91	24	48
polyDienC_{10}	1.43	39	78
Ni-polyDienC_{10}	7.52	29	58
Ni-polyEnC_{10}	9.10	27	54
polyDienC_{12}	0.27	27	54
Ni-polyDienC_{12}	24.5	23	46

Table 3.2 CMC and APM values

The surfactants reported here are considered "non-classical" in terms of micellisation behaviour as there is no obvious relationship between the lengths of the alkyl tail of a surfactant with the CMCs of their micellar systems. "Classical" behaviour expects the CMC of a micellar system to decrease as the length of the surfactant tail increases. Here, however, the CMC is seen to decrease from 1.43 mM for **polyDienC$_{10}$** to 0.27 mM for **polyDienC$_{12}$** as expected, but increase again to 0.32 mM for **polyDienC$_{14}$**. Comparison of the Ni(II) complexes of these ligands also shows "non-classical" behaviour.[32]

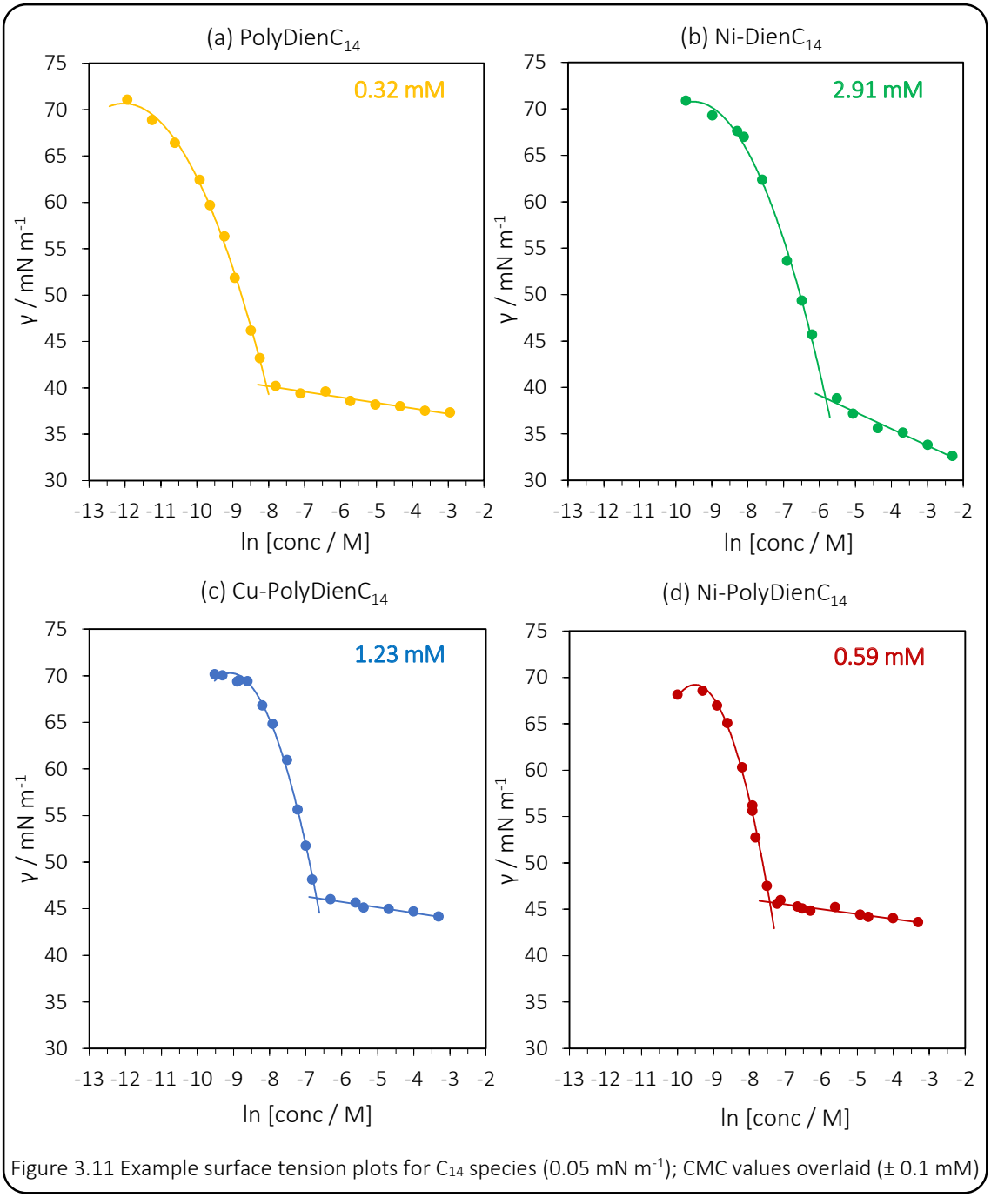

Figure 3.11 Example surface tension plots for C_{14} species (0.05 mN m^{-1}); CMC values overlaid (± 0.1 mM)

Comparison of the parameters for **polyDienC$_{14}$** with its Ni(II) and Cu(II) complexes shows that the CMC increases upon addition of the metal, thus indicating a significant change in the micelle morphology. It is known that surfactants with bulkier head groups have lower CMCs as the larger amount of curvature afforded by each surfactant means fewer aggregates are required to form micelles. This suggests that the free ligand has a larger head group than the metal complexes. Coordination of a metal ion is likely to restrict the mobility of the polyol arms of the ligand resulting in an overall reduction in the size of the ligand head group. This theory also applies when comparing the CMC values of **Ni(II)-polyDienC$_{14}$** and **Ni(II)-DienC$_{14}$**. The polyol-functionalised ligand will have a much bulkier head group which accounts for the much lower CMC of 0.59 mM compared to 2.91 mM for the smaller **DienC$_{14}$** ligand.

Variations in CMC values are also afforded by changes in the electrostatic repulsion between surfactant head groups. A reduction in electrostatic repulsion allows surfactants to pack more tightly which would increase the amount of surfactants required to form micelles thus increasing the CMC.

The similarity in the APM values for both the Ni(II) and Cu(II) complexes of **polyDienC$_{14}$** may be attributed to the similarity in their atomic radii and their identical charge. Despite this, the CMC values for the Ni(II) and Cu(II) systems are significantly different meaning the micelles have very different morphologies. This may be due to the binding geometry of the ligand as the absorption data discussed in section **3.3.3**, above, suggested that for the **polyDienC$_n$** species the Ni(II) complexes have an octahedral geometry whereas the Cu(II) complexes are square pyramidal which may significantly affect the packing of surfactants in the micelle.

Comparison for the decyl Ni(II) complexes shows that the CMC is lower for the **polyDienC$_{10}$** species (7.52 mM) than for the **polyEnC$_{10}$** system (9.10 mM). However, the APM values for each system show the **Ni(II)-polyDienC$_{10}$** head group to be only marginally bigger than that of **Ni(II)-polyEnC$_{10}$** (29 *vs.* 27 Å^2 for n=1 or 58 *vs.* 54 Å^2 for n=2). Therefore, the head groups are of almost equal size whereas the CMC values are significantly different. This may be due to a difference in the charge-stabilising effect between the two ligands. The fact that the CMC value is lower for the **polyDienC$_{10}$** complex suggests that metal coordination causes a greater reduction in electrostatic repulsion between surfactants compared to the **polyEnC$_{10}$** complex meaning that the **dien** based complexes are able to pack more tightly than the **en** analogues.

As discussed in section **3.3.2** the **polyDienC$_n$** ligands are present as a mixture of two isomers, one symmetric and one asymmetric. This did not seem to cause problems for the tensiometric analysis of the free ligand in aqueous solution as a clear CMC point was visible on the plot and no

impurities were observed, this suggests that the isomers form mixed micelles. However, when studying the Ni(II)-doped system the difference between the two isomers became apparent.

When 1.05 equivalents of Ni(II) salt were added to the **polyDienC$_{14}$** system the tensiometry plot showed a deviation from linearity in the high concentration region, characteristic of the presence of a surface active impurity. However, when 1.50 equivalents of Ni(II) were added to the solution this impurity was found to disappear, leaving a linear relationship post-CMC. This result (illustrated in Figure 3.12) suggests that one of the isomers has a higher binding affinity for Ni(II) meaning that at low metal concentrations one ligand isomer coordinates to the metal but the other does not. The fact that this is detected as an impurity suggests that the ligand with the higher binding affinity is the bulk surfactant and the other ligand is in the minority. If a 1:1 ratio of ligands were present the tensiometry plot would more likely be a random scattering of data rather than the clear curve seen in Figure 3.12. It can also be concluded that this impurity does not come from any exterior source as if this were the case it would have been observed in the free **polyDienC$_{14}$** ligand CMC plot.

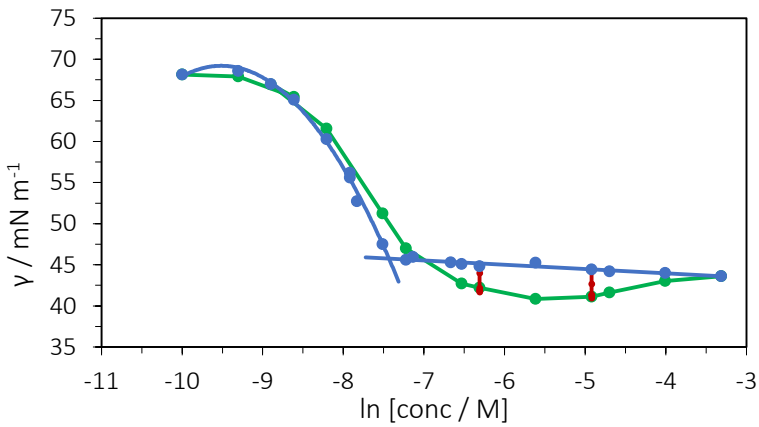

Figure 3.12 polyDienC$_{14}$ with 1.05 eq. Ni(II) (green) and with 1.50 eq. Ni(II) (blue); tests of [Ni(II)] *vs.* ln[conc] (red) (error = ± 0.05 mN m^{-1})

Equivalents Ni(II)	ln[conc] = -4.92 M γ /mNm^{-1}	ln[conc] = -6.31 M γ /mNm^{-1}
0.25	40.96	41.86
0.50	41.28	41.71
0.75	41.36	41.90
1.00	41.34	42.18
1.25	42.67	44.01
1.50	44.19	44.52
2.00	44.26	44.56

Table 3.3 Effect of Ni(II) concentration on surface tension

To confirm the effect of increasing metal concentration on the surface tension of the solution, Ni(II) salt was added incrementally and the surface tension measured. Two solution concentrations were chosen which were known to lie above the CMC point, in the region where the impurity was detectable. The surface tension of these solutions was measured over a range of Ni(II) concentrations from 0.25 to 2.0 equivalents relative to the ligand concentration. It was observed that each sequential addition of Ni(II) increased the surface tension of the solution up until a limiting surface tension was reached at 1.5 equivalents of Ni(II). Table 3.3 collates the data from these tests which are also shown on the tensiometry plot in Figure 3.12.

3.3.5 Microemulsion Compatibility

Although the ligand architectures described above were capable of forming micellar systems both as free ligands and metal complexes the oil-solubilising ability of the solutions was found to be extremely low at around 2 wt%. Therefore the **polyDienC$_{12}$** ligand was doped into the [MeImC$_{12}$]Br/BuOH/H_2O (1:1:7) micellar system described previously, which has a characteristically high toluene loading of ~25 wt%, in order to create a compromise between metal-binding ability and oil loading capacity. The **polyDienC$_{12}$** ligand was selected as it demonstrated a high metal-binding efficiency and has the optimal alkyl tail length for micellisation.

Surface tension analysis *via* DVT was used to assess the effects of doping the carrier micellar system with **polyDienC$_{12}$**. It was observed that the order of formulation was vital to creating an isotropic micellar system. Initially the **polyDienC$_{12}$** ligand was added to a pre-made [MeImC$_{12}$]Br/BuOH/H_2O mixture. However, tensiometry studies showed no clear CMC point for this system suggesting that either the ligand was simply dissolved in the aqueous phase, therefore acting as a surface-active impurity, or that it was forming discrete micelles of its own, meaning that there was more than one type of micelle present in the solution.

In order to counter-act this the solutions were formulated by combining all of the non-aqueous components into a homogenous mixture prior to solubilisation in ultra-pure water. The surface tension measurements for this system (Figure 3.13c) showed a single CMC point and no surface-active impurities therefore indicating the successful formation of mixed-surfactant micelles within the system.

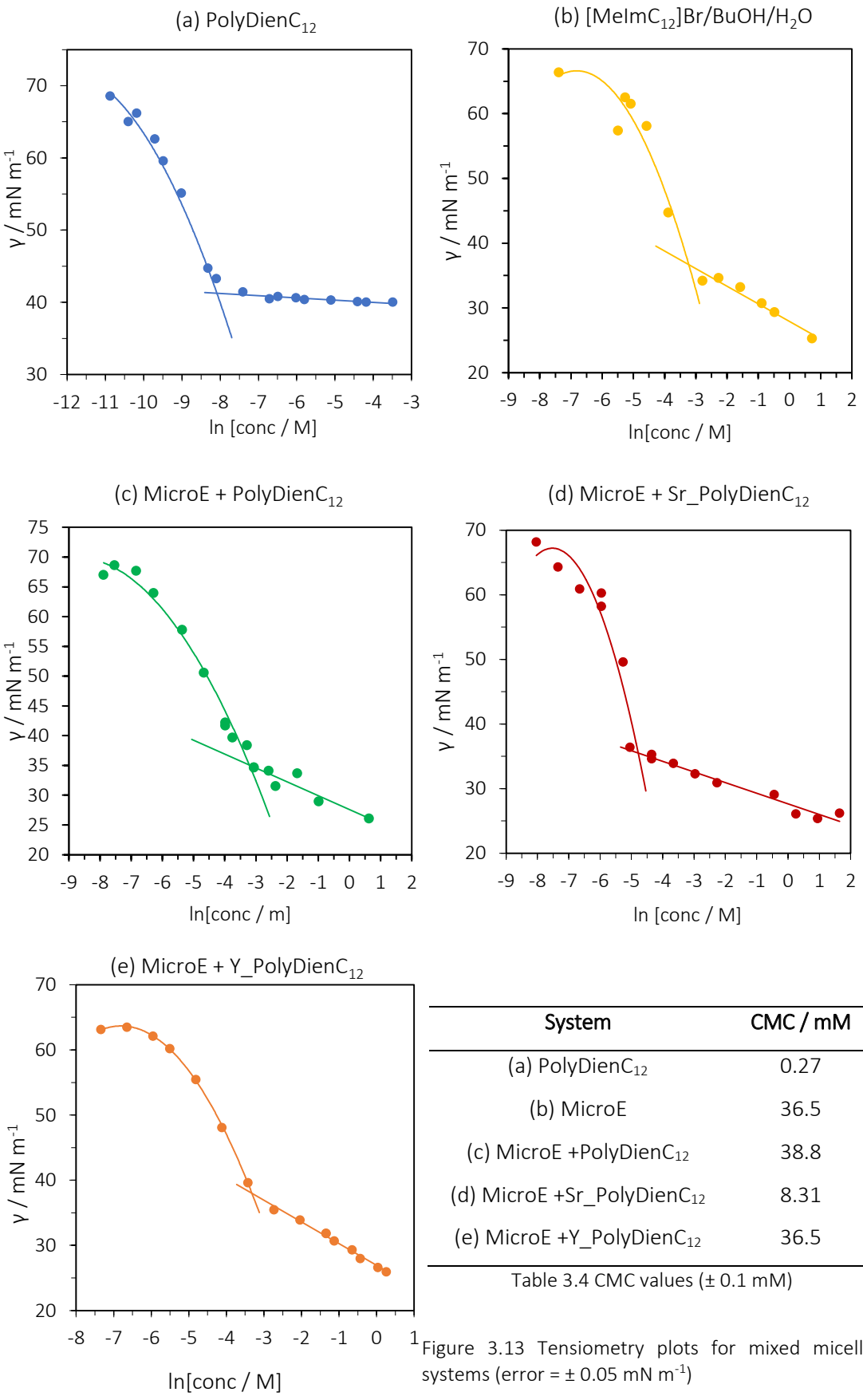

System	CMC / mM
(a) PolyDienC$_{12}$	0.27
(b) MicroE	36.5
(c) MicroE +PolyDienC$_{12}$	38.8
(d) MicroE +Sr_PolyDienC$_{12}$	8.31
(e) MicroE +Y_PolyDienC$_{12}$	36.5

Table 3.4 CMC values (± 0.1 mM)

Figure 3.13 Tensiometry plots for mixed micellar systems (error = ± 0.05 mN m^{-1})

(MicroE = stock microemulsion MeIm/BuOH/UPW)

Figure 3.13 shows the surface tension plots for **polyDienC$_{12}$** (a), [MeImC$_{12}$]Br/BuOH/H_2O (b) and the doped system (c). There is a small difference in the CMC values of the carrier micellar system (36.5 mM) and that doped with the surfactant ligand (38.8 mM). The magnitude of this difference is likely due to the fact that there is only 2 wt% dopant in the system. Larger variations in the CMC would be expected for higher doping. Tensiometry was also used to study the effect of metal addition to the doped micellar system. Figure 3.13 shows the data for the system upon addition of Sr(II) (d) or Y(III) (e). The solutions were formulated by the addition of 1.1 equivalents of the corresponding metal chloride during formulation.

Firstly, the change in the CMC of the system upon the addition of metal ion is indicative of binding. This is a useful result as mass spectrometry and NMR spectroscopy could not definitively confirm binding of Sr(II) or Y(III) to the **polyDienC$_{12}$** ligand. The CMC is notably lower for the Sr(II) system (8.31 mM) than for Y(III) (36.5 mM). As the atomic radii of these ions are very similar the difference in CMC may be due to the charge difference of the ions or a difference in coordination geometry.

3.4 Conclusions

This chapter describes a series of novel acyclic amphiphilic ligands synthesised from ethylenediamine and diethylenetriamine precursors. These ligands were functionalised with pendent alcohol groups to form surfactant ligands capable of metal binding. Tensiometry was used to assess the ability of these ligands to form micelles as well as to study how varying different parameters affected properties such as the CMC and average APM.

Ni(II) and Cu(II) salts were added to solutions of the ligands to study metal coordination and ligand field parameters. The poly-alcohol functionalised ligands all showed similar absorption profiles on addition of Ni(II) which were indicative of the formation of octahedral (or near-octahedral) complexes. However, the addition of Cu(II) to the same systems resulted in a clear distinction between the absorption profiles of the **polyEnC$_n$** and **polyDienC$_n$** systems. The **Cu(II)-polyEnC$_n$** complexes exhibited absorption profiles with λ_{max} at ~760 nm, typical of octahedral complexes. However, for the **Cu(II)-polyDienC$_n$** complexes λ_{max} was ~580 nm, indicating a preference for complexes of square pyramidal geometry. This change in coordination environment was attributed to Jahn-Teller distortions sometimes seen for d^9 metals such as Cu(II).

Despite the fact that the poly-alcohol ligands formed micelles on their own the oil-loading capacity of these systems was extremely low. Therefore **polyDienC$_{12}$** was doped into the [MeImC$_{12}$]Br/BuOH/H_2O micellar system described previously to create a compromise between oil-loading capacity and metal-binding ability. Tensiometric studies of this system showed a slight decrease in the CMC of the carrier system from 36.5 mM to 38.8 mM on addition of the doped ligand. Addition of Sr(II) and Y(III) to this system resulted in changes in the CMC suggestive of metal binding.

The **polyDienC$_{12}$** doped micellar system was found to be capable of forming stable microemulsions solubilising up to 10 wt% toluene.

3.5 Experimental

Synthesis of 1,2-epoxytetradecane[24]

1,2-Tetradecane diol* (8.00 g, 34.7 mmol) was added to HBr/AcOH (45% w/v) in $CHCl_3$ (375 mL, 1:7 v/v) and stirred overnight under a N_2 atmosphere. Water was added, the product extracted into DCM and dried *in vacuo* to give a yellow oil (5.46 g, 16.3 mmol). The oil was dissolved in dry MeOH (60 mL) and K_2CO_3 (8.00 g, 57.9 mmol) added, the solution was stirred overnight under a N_2 atmosphere. The reaction was quenched with water, extracted into DCM and dried *in vacuo*. Bulb-to-bulb distillation of the crude product (Kugelrohr apparatus 95-96 °C) isolated the product as a colourless oil. Yield: 1.79 g, 8.43 mmol, 24%. ^{1}H NMR (400 MHz, $CDCl_3$): δ_H = 3.74-3.59 (2H, br. s, OC***H***$_2$), 3.46-3.37 (1H, br. s, OC***H***(CH_2)), 2.87-2.66 (2H, br. s, OCHC***H***$_2$), 1.46-1.36 (2H, br. s, OCHCH_2C***H***$_2$), 1.24 (18H, s, -(C***H***$_2$)$_9$-), 0.87 (3H, app. s, C***H***$_3$) ppm.

(*commercial 1,2-tetradecane diol was recrystallised multiple times from EtOAc in order to remove branched material.)

3.5.1 Primary Ligands

General Synthesis

Ligands were synthesised by addition of either diethylene triamine (dien) or ethylene diamine (en) (10 eq.) to the corresponding epoxide (1 eq.) in EtOH. The solution was then left to stand at room temperature in a foil-covered vessel for 5-7 days. Solvent was removed *in vacuo* and excess amine removed *via* bulb-to-bulb distillation (Kugelrohr apparatus) to give the ligands as white or pale yellow waxy solids.

En ligands

Synthesis of EnC_8

Yield: 5.02 g, 23.4 mmol, 71%. ^{1}H NMR (400 MHz, $CDCl_3$): δ_H = 5.85-5.75 (1H, m, C***H***=CH_2), 4.99 (1H, dd, J_{HH} = 1.9, 17.2 Hz, H_{cis}), 4.92 (1H, dd, J_{HH} = 1.0, 10.1 Hz, H_{trans}), 3.63-3.57 (1H, m, C***H***(OH)), 2.83-2.80 (2H, m, NHC***H***$_2$$CH_2$$NH_2$), 2.75-2.63 (3H, m, NH_2C***H***$_2$$CH_2$NHC***H***H), 2.44 (1H, dd, J_{HH} = 9.5, 12.1 Hz, CH_2NHC***H***H), 2.03 (2H, q, $^3J_{HH}$ = 6.7 Hz, H_2C=CHC***H***$_2$), 1.91-1.63 (br. s, N***H***/O***H***), 1.43-1.30 (10H, m, -(C***H***$_2$)$_5$-) ppm. ^{13}C{^{1}H} NMR (75 MHz, $CDCl_3$) δ_C = 138.9, 114.0, 55.5, 52.0, 41.5, 35.3, 33.6, 29.4, 28.9, 28.7, 25.6 ppm. LRMS (ES^+) found *m/z* 215.21, calculated 215.21 for $[M+H]^+$. HRMS (AP^+) found *m/z* 215.2113, calculated 215.2123 for $[C_{12}H_{27}N_2O]^+$. IR (solid/cm^{-1}): *v* 3336, 3283 (N-H/O-H), 2924, 2847 (C-H), 1645 (N-H), 1466, 1437 (C-H), 1128 (C-O).

Synthesis of EnC_{10}

Yield: 5.60 g, 22.9 mmol, 83%. ^{1}H NMR (400 MHz, $CDCl_3$): δ_H = 3.67-3.52 (1H, br. s, C***H***(OH)), 2.79-2.76 (2H, m, NHC***H***$_2$CH$_2$NH$_2$), 2.67-2.58 (3H, m, NH$_2$C***H***$_2$CH$_2$NHC***H***H), 2.48-2.31 (1H, m, CH$_2$NHCH***H***), 1.45-1.36 (2H, m, C***H***$_2$-(CH$_2$)$_8$-), 1.24 (16H, s, -(C***H***$_2$)$_8$-), 0.86 (3H, t, $^{3}J_{HH}$ = 6.8 Hz, C***H***$_3$) ppm. ^{13}C{^{1}H} NMR (75 MHz, $CDCl_3$) δ_C = 69.5 (***C***O), 55.5, 52.1, 41.6, 35.3, 31.8, 29.7, 29.5, 29.3, 25.7, 22.6, 14.0 ppm. LRMS (AP$^+$) found *m/z* 245.29, calculated 245.26 for [M+H]$^+$. HRMS (AP$^+$) found *m/z* 245.2582, calculated 245.2585 for [$C_{14}H_{33}N_2O$]$^+$. IR (solid/cm^{-1}): *v* 3292 (N-H/O-H), 2913, 2847 (C-H), 1635, 1557 (N-H), 1465, 1420 (C-H), 1113, 1049 (C-O).

Synthesis of EnC_{12}

Yield: 4.82 g, 17.7 mmol, 78%. ^{1}H NMR (400 MHz, $CDCl_3$): δ_H = 3.22 (1H, app. t, J_{HH} = 8.7 Hz, C***H***(OH)), 2.84-2.61 (3H, m, NC***H***$_2$), 2.47-2.37 (3H, m, NC***H***$_2$), 1.48-1.36 (2H, m, C***H***$_2$(CH$_2$)$_{10}$), 1.33-1.14 (20H, m, -(C***H***$_2$)$_{10}$-), 0.86 (3H, t, $^{3}J_{HH}$ = 6.6 Hz, C***H***$_3$) ppm. ^{13}C{^{1}H} NMR (125 MHz, $CDCl_3$) δ_C = 70.4 (***C***O), 59.1, 33.3, 32.1, 29.8, 29.7, 29.5, 25.8, 25.7, 22.8, 14.3 ppm. HRMS (ES$^+$) found *m/z* 273.2901, calculated 273.2900 for [$C_{16}H_{37}N_2O$]$^+$. IR (solid/cm^{-1}): *v* 3331 (NH/OH), 2916, 2847 (C-H), 1558 (N-H), 1466, 1427 (C-H), 1111 (C-O).

Synthesis of EnC_{14}

Yield: 3.44 g, 11.4 mmol, 65%. ^{1}H NMR (400 MHz, $CDCl_3$): δ_H = 3.61-3.57 (1H, br. m, C***H***(OH)), 2.82-2.80 (2H, m, NHC***H***$_2$CH$_2$NH$_2$), 2.74-2.62 (3H, m, NH$_2$C***H***$_2$CH$_2$NHC***H***H), 2.44 (1H, app. dd, J_{HH} = 9.6, 11.9 Hz, CH$_2$NHC***H***H), 1.91-1.51 (br. s, N***H***/O***H***), 1.45-1.37 (2H, m, C***H***$_2$(CH$_2$)$_{13}$), 1.24 (24H, s, -(C***H***$_2$)$_{12}$-), 0.87 (3H, t, $^{3}J_{HH}$ = 6.7 Hz, C***H***$_3$) ppm. ^{13}C{^{1}H} NMR (75 MHz, $CDCl_3$) δ_C = 69.8 (***C***O), 55.5, 52.1, 41.8, 35.3, 32.0, 29.9, 29.8, 29.5, 25.8, 22.8, 14.2 ppm. LRMS (ES$^+$) found *m/z* 301.32, calculated 301.32 for [M+H]$^+$. HRMS (AP$^+$) found *m/z* 301.3210, calculated 301.3209 for [$C_{18}H_{41}N_2O$]$^+$. IR (solid/cm^{-1}): *v* 3333 (N-H/O-H), 2922, 2849 (C-H), 1638 (N-H), 1464 (C-H), 1123 (C-O).

Dien Ligands

Due to the mix of isomers the ^{1}H NMR assignments do not contain peak integrations.

Synthesis of $DienC_8$

Yield: 6.04 g, 23.5 mmol, 72%. ^{1}H NMR (400 MHz, $CDCl_3$): δ_H = 5.85-5.75 (m, C***H***=CH$_2$), 4.98 (app. d, J_{HH} = 17.9 Hz, H_{cis}), 4.92 (app. d, J_{HH} = 10.1 Hz, H_{trans}), 3.62-3.56 (m, C***H***OH), 2.82-2.78 (m, NC***H***),

2.76-2.70 (m, NC***H***), 2.68-2.66 (m, NC***H***), 2.44 (dd, J_{HH} = 9.7, 11.9 Hz, NC***H***), 2.03 (q, $^{3}J_{HH}$ = 6.6 Hz, H_2C=CHC***H***$_2$), 1.81-1.61 (br. s, N***H***/O***H***), 1.61-1.30 (m, -(C***H***$_2$)$_5$-) ppm. $^{13}C\{^{1}H\}$ NMR (75 MHz, $CDCl_3$) δ_C = 139.1, 114.2, 69.6 (***C***O), 57.5, 55.6, 52.1, 49.1, 41.5, 35.3, 33.8, 29.6, 29.1, 28.8, 25.7 ppm. LRMS (ES^+) found *m/z* 258.24, calculated 258.25 for $[M+H]^+$. HRMS (AP^+) found *m/z* 258.2534, calculated 258.2538 for $[C_{14}H_{32}N_3O]^+$; found *m/z* 280.2315, calculated 280.2358 for $[C_{14}H_{31}N_3ONa]^+$. IR (solid/cm^{-1}): *v* 3282 (N-H/O-H), 2922, 2853 (C-H), 1645, 1610 (N-H), 1466 (C-H), 1123 (C-O).

Synthesis of DienC$_{10}$

Yield: 4.65 g, 16.2 mmol, 70%. ^{1}H NMR (400 MHz, $CDCl_3$) δ_H = 3.62-3.56 (m, C***H***OH), 2.82-2.77 (app. q, J_{HH} = 2.3 Hz, NC***H***), 2.77-2.71 (m, NC***H***), 2.68 (app. q, J_{HH} = 6.1 Hz, NC***H***), 2.44 (app. dd, J_{HH} = 9.5, 12.1 Hz, NC***H***), 1.85-1.54 (br. s, N***H***/O***H***), 1.47-1.36 (m -C***H***$_2$-), 1.31-1.25 (m, -(C***H***$_2$)$_n$-), 0.87 (t, $^{3}J_{HH}$ = 6.8 Hz, C***H***$_3$) ppm. $^{13}C\{^{1}H\}$ NMR (75 MHz, $CDCl_3$) δ_C = 69.7 (***C***O), 55.5, 52.0, 49.2, 49.1, 41.6, 35.3, 32.0, 29.9, 29.7, 29.4, 25.8, 22.8, 14.2 ppm. LRMS (AP^+) found *m/z* 288.30, calculated 288.30 for $[M+H]^+$. HRMS (ES) found *m/z* 288.3008, calculated 288.3015 for $[C_{16}H_{38}N_3O]^+$; found *m/z* 310.2800, calculated 310.2834 for $[C_{16}H_{37}N_3ONa]^+$. IR (solid/cm^{-1}): *v* 3273 (N-H/O-H), 2918, 2851 (C-H), 1608 (N-H), 1465(C-H), 1123 (C-O).

Synthesis of DienC$_{12}$

Yield: 1.93 g, 6.13 mmol, 77%. ^{1}H NMR (300 MHz, $CDCl_3$) δ_H = 3.38-3.26 (m, C***H***OH), 2.50-2.33 (m, NC***H***), 2.30-2.08 (m, NC***H***), 1.27-1.08 (m, CH(OH)C***H***$_2$CH$_2$), 1.05-0.97 (m, -(C***H***$_2$)$_{10}$-), 0.59 (t, $^{3}J_{HH}$ = 7.8 Hz, C***H***$_3$) ppm. $^{13}C\{^{1}H\}$ NMR (75 MHz, $CDCl_3$) δ_C = 69.6 (***C***O), 55.9, 51.9, 49.0, 41.4, 35.4, 31.9, 29.8, 29.7, 29.4, 25.8, 22.7, 14.1 ppm. LRMS (AP^+) found *m/z* 316.32, calculated 316.33 for $[M+H]^+$. HRMS (AP^+) found *m/z* 316.3323, calculated 316.3322 for $[C_{18}H_{42}N_3O]^+$. IR (solid/cm^{-1}): *v* 2916, 2847 (C-H), 1568 (N-H), 1464 (C-H), 1124 (C-O).

Synthesis of DienC$_{14}$

Yield: 4.34 g, 13.2 mmol, 75%. ^{1}H NMR (400MHz, $CDCl_3$) δ_H = 3.61-3.56 (m, C***H***OH), 2.82-2.78 (m, NC***H***), 2.76-2.70 (m, NC***H***), 2.67 (t, $^{3}J_{HH}$ = 5.78 Hz, NC***H***), 2.44 (app. dd, J_{HH} = 9.5, 12.1 Hz, NC***H***), 1.93-1.67 (br. s, N***H***), 1.47-1.36 (m CH(OH)C***H***$_2$CH$_2$), 1.29-1.24 (m, -(C***H***$_2$)$_{12}$-), 0.87 (t, $^{3}J_{HH}$ = 6.8 Hz, C***H***$_3$) ppm. $^{13}C\{^{1}H\}$ NMR (75 MHz, $CDCl_3$) δ_C = 69.6 (***C***O), 57.3, 55.6, 51.7, 48.9, 41.2, 39.5, 35.5, 35.0, 31.9, 29.9, 29.7, 29.4, 25.8, 22.7, 14.1 ppm. LRMS (ES^+) found *m/z* 344.35, calculated 344.36 for $[M+H]^+$. HRMS (ES) found *m/z* 344.3633, calculated 344.3641 for $[C_{20}H_{46}N_3O]^+$; found *m/z*

366.3439, calculated 366.3461 for $[C_{20}H_{45}N_3ONa]^+$. IR (solid/cm^{-1}): *v* 3294, 3256 (N-H/O-H), 2918, 2851 (C-H), 1464 (C-H), 1126 (C-O).

3.5.2 Secondary Ligands

General Synthesis

Primary ligands synthesised above were added to glycidol* (approx. 5 eq.) in EtOH and the solution left to stand at room temperature in a foil-covered vessel for 5-7 days. Solvent was removed *in vacuo* and excess glycidol removed *via* bulb-to-bulb distillation (Kugelrohr apparatus 61-62 °C) to give the ligands as yellow oils.

*glycidol was obtained *via* bulb-to-bulb distillation (Kugelrohr apparatus 61-62 °C) to separate it from the glycerol (degradation product) present in commercial glycidol

PolyEnC$_n$

Synthesis of PolyEnC$_8$

Yield: 0.51 g, 1.16 mmol, 50%. ^{1}H NMR (400 MHz, D_2O) δ_H = 5.83-5.72 (1H, m, H_2C=C***H***), 4.94 (1H, app. d, J_{HH} = 17.2 Hz, H_{cis}), 4.87 (1H, app. d, J_{HH} = 10.9 Hz, H_{trans}), 3.96-3.63 (5H, m, C***H***(OH) & C(OH)C***H***$_2$), 3.51-3.40 (5H, m, C***H***(OH) & C(OH)C***H***$_2$), 2.71-2.39 (12H, m, NC***H***$_2$), 1.97 (2H, q, $^3J_{HH}$ = 6.8 Hz, H_2C=CHC***H***$_2$), 1.35-1.23 (10H, m, -(C***H***$_2$)$_5$-) ppm. ^{13}C{^{1}H} NMR (125 MHz, $CDCl_3$) δ_C = 139.2, 114.4, 77.4 (***C***O), 77.2 (***C***O), 72.6 (***C***O), 71.0 (***C***O), 70.9 (***C***O), 69.7 (***C***O), 65.0, 64.8, 63.5, 63.4, 50.5, 33.9, 29.9, 29.8, 29.2, 29.0, 25.8, 15.3 ppm. HRMS (AP^+) found *m/z* 437.3224, calculated 437.3227 for $[C_{21}H_{45}N_2O_7]^+$. IR (solid/cm^{-1}): *v* 3327 br. (O-H), 2924, 2853, 1460 (C-H), 1030 (C-O).

Synthesis of PolyEnC$_{10}$

Yield: 0.59 g, 1.26 mmol, 62%. ^{1}H NMR (400 MHz, D_2O) δ_H = 3.82-2.75 (br. s, N***H***/O***H***), 3.60-3.40 (10H, m, C***H***(OH) & C(OH)C***H***$_2$), 2.88-2.27 (12H, m, NC***H***$_2$), 1.46-1.36 (2H, br. s, C(OH)C***H***$_2$), 1.27-1.08 (16H, br. s, -(C***H***$_2$)$_8$-), 0.82 (3H, t, $^3J_{HH}$ = 6.6 Hz, C***H***$_3$) ppm. ^{13}C{^{1}H} NMR (125 MHz, $CDCl_3$) δ_C = 70.9 (***C***O), 70.8 (***C***O), 70.2 (***C***O), 70.0 (***C***O), 69.7 (***C***O), 69.2 (***C***O), 69.0 (***C***O), 68.8, 67.8, 65.1, 65.0, 64.8, 64.7, 64.6, 63.5, 58.2, 57.5, 54.2, 35.3, 35.2, 34.9, 32.1, 30.1, 30.0, 29.9, 29.8, 29.5, 25.9, 22.8, 14.3 ppm. HRMS (AP^+) found *m/z* 467.3694, calculated 467.3696 for $[C_{23}H_{51}N_2O_7]^+$. IR (solid/cm^{-1}): *v* 3331 br., 3281 br. (O-H), 2922, 2847, 1462 (C-H), 1121, 1047 (C-O).

Synthesis of PolyEnC$_{12}$

Yield: 0.55 g, 1.11 mmol, 58%. ^{1}H NMR (400 MHz, D_2O) δ_H = 3.61-3.48 (10H, m, C***H***(OH) & C(OH)C***H***$_2$), 2.87-2.35 (12H, m, NC***H***$_2$), 1.49-1.37 (2H, br. s, C(OH)C***H***$_2$), 1.34-1.19 (20H, br. s, -(C***H***$_2$)$_{10}$-), 0.85 (3H, app. s, C***H***$_3$) ppm. ^{13}C{^{1}H} NMR (125 MHz, $CDCl_3$) δ_C = 72.7 (***C***O), 71.1 (***C***O), 64.7, 63.4, 32.1, 29.8, 29.5, 25.9, 22.8, 14.3 ppm. HRMS (ES$^+$) found *m/z* 495.3993, calculated 495.3995 [$C_{25}H_{55}N_2O_7$]$^+$. IR (solid/cm^{-1}): *v* 3298 br. (O-H), 2920, 2851, 1456 (C-H), 1088, 1043 (C-O).

PolyEnC$_{14}$

Yield: 0.48 g, 0.92 mmol, 55%. ^{1}H NMR (400 MHz, D_2O) δ_H = 3.84-3.73 (br. s, N***H***/O***H***), 3.57-3.41 (10H, m, C***H***(OH) & C(OH)C***H***$_2$), 2.88-2.27 (12H, m, NC***H***$_2$), 1.47-1.37 (2H, br. s, C(OH)C***H***$_2$), 1.35-1.12 (24H, br. s, -(C***H***$_2$)$_{12}$-), 0.82 (3H, t, $^{3}J_{HH}$ = 6.6 Hz, C***H***$_3$) ppm. ^{13}C{^{1}H} NMR (125 MHz, $CDCl_3$) δ_C = 70.9 (***C***O), 70.8 (***C***O), 70.2 (***C***O), 70.0 (***C***O), 69.7 (***C***O), 69.3 (***C***O), 69.0 (***C***O), 68.8, 67.8, 65.1, 65.0, 64.8, 64.7, 64.6, 58.2, 57.5, 54.2, 35.4, 35.0, 32.1, 30.1, 30.0, 29.9, 29.8, 29.5, 25.9, 22.8, 14.3 ppm. HRMS (AP$^+$) found *m/z* 523.4327, calculated 523.4322 for [$C_{27}H_{59}N_2O_7$]$^+$. IR (solid/cm^{-1}): *v* 3339 br. (O-H), 2920, 2853, 1454 (C-H), 1036 (C-O).

PolyDienC$_n$

Due to the mix of isomers the ^{1}H NMR resonance assignments do not contain peak integrations.

Synthesis of PolyDienC$_8$

Yield: 0.77 g, 1.39 mmol, 71%. ^{1}H NMR (400 MHz, D_2O) δ_H = 5.88-5.78 (m, H_2C=C***H***), 4.97 (dd, J_{HH} = 1.7, 17.2 Hz, H_{cis}), 4.90 (dd, J_{HH} = 2.2, 10.1 Hz, H_{trans}), 3.59-3.40 (m, HOC***H*** & HOC***H***$_2$), 2.73-2.38 (m, NC***H***), 1.99 (q, $^{3}J_{HH}$ = 6.9 Hz, H_2C=CHC***H***$_2$), 1.36-1.26 (m, -(C***H***$_2$)$_5$-) ppm. ^{13}C{^{1}H} NMR (125 MHz, $CDCl_3$) δ_C = 139.2, 114.4, 71.0 (***C***O), 70.1 (***C***O), 69.4 (***C***O), 64.9 (***C***O), 64.6 (***C***O), 63.5, 63.4, 58.7, 58.0, 53.0, 50.5, 35.2, 34.9, 33.9, 29.8, 29.0, 25.8 ppm. HRMS (AP$^+$) found *m/z* 554.4020, calculated 554.4016 for [$C_{26}H_{56}N_3O_9$]$^+$. IR (solid/cm^{-1}): *v* 3335 br. (O-H), 2930, 2853, 1454 (C-H), 1038 (C-O).

Synthesis of PolyDienC$_{10}$

Yield: 0.70 g, 1.20 mmol, 69%. ^{1}H NMR (400 MHz, D_2O) δ_H = 3.85-3.70 (br. s, N***H***/O***H***), 3.60-3.37 (m, HOC***H***/HOC***H***$_2$), 2.75-2.38 (m, NC***H***), 1.45-1.37 (br. s, HOCC***H***$_2$), 1.32-1.25 (br. s, -(C***H***$_2$)$_8$-), 0.83 (app. s, C***H***$_3$) ppm. ^{13}C{^{1}H} NMR (125 MHz, $CDCl_3$) δ_C = 72.7 (***C***O), 70.1 (***C***O), 69.4 (***C***O), 64.9 (***C***O), 64.7 (***C***O), 63.4, 58.6, 53.0, 50.7, 35.3, 35.0, 32.1, 30.1, 29.9, 29.8, 29.5, 26.0, 22.8, 14.3 ppm.

HRMS found *m/z* 584.4489, calculated 584.4486 for $[C_{28}H_{62}N_3O_9]^+$. IR (solid/cm^{-1}): *v* 3329 br., 3281 br. (O-H), 2916, 2847, 1462 (C-H), 1119, 1047 (C-O).

Synthesis of PolyDienC$_{12}$

Yield: 3.96 g, 6.48 mmol, 89%. ^{1}H NMR (300 MHz, D_2O) δ_H = 3.85-3.73 (br. s, N***H***/O***H***), 3.61-3.39 (m, HOC***H***/HOC***H***$_2$), 2.86-2.40 (m, NC***H***), 1.46-1.38 (br. s, HOCC***H***$_2$), 1.35-1.16 (br. s, -(C***H***$_2$)$_{10}$-), 0.84 (app. s, C***H***$_3$) ppm. ^{13}C{^{1}H} NMR (75 MHz, D_2O) δ_C = 72.0 (***C***O), 71.0 (***C***O), 70.3 (***C***O), 66.8 (***C***O), 62.6, 57.3, 52.2, 51.5, 49.4, 46.0, 39.4, 32.0, 30.0, 29.5, 22.7, 14.0 ppm. ^{13}C{^{1}H} NMR (125 MHz, $CDCl_3$) δ_C = 72.1 (***C***O), 71.0 (***C***O), 70.8 (***C***O), 70.4 (***C***O), 67.0 (***C***O), 64.2, 59.1, 33.2, 32.0, 29.8, 29.7, 29.5, 29.4, 25.9, 25.6, 22.8, 15.2, 14.2 ppm. LRMS (AP^+) found *m/z* 612.49, calculated 612.48 for $[M+H]^+$. HRMS (AP^+) found *m/z* 612.4780, calculated 612.4794 for $[C_{30}H_{66}N_3O_9]^+$. IR (solid/cm^{-1}): *v* 3319 br. (O-H), 2920, 2851, 1456 (C-H), 1032 (C-O).

Synthesis of PolyDienC$_{14}$

Yield: 0.67 g, 1.05 mmol, 72%. ^{1}H NMR (400 MHz, D_2O) δ_H = 3.82-3.70 (br. s, N***H***/O***H***), 3.62-3.38 (m, HOC***H***/HOC***H***$_2$), 2.80-2.30 (m, NC***H***), 1.46-1.38 (br. s, HOCC***H***$_2$), 1.33-1.15 (br. s, -(C***H***$_2$)$_{12}$-), 0.83 (app. s, C***H***$_3$) ppm. ^{13}C{^{1}H} NMR (125 MHz, $CDCl_3$) δ_C =72.6 (***C***O), 70.0 (***C***O), 69.3 (***C***O), 64.8 (***C***O), 64.6 (***C***O), 63.3, 58.6, 58.0, 52.7, 50.3, 35.3, 34.9, 33.3, 32.0, 30.1, 29.8, 29.5, 22.8, 14.2 ppm. HRMS (ES^-) found *m/z* 638.4937, calculated 638.4938 for $[C_{32}H_{68}N_3O_9]^-$. IR (solid/cm^{-1}): *v* 3331 br. (O-H), 2920, 2853, 1458 (C-H), 1036 (C-O).

3.5.3 Complexes

General Synthesis

1.05 eq. of the corresponding hexahydrate metal chloride salt were added to aqueous solutions of the ligand. The samples were warmed and/or sonicated to allow for complete dissolution of ligands. Characterisation was performed directly using these solutions, except for IR spectroscopy where aliquots of each sample were dried prior to analysis.

PolyEnC$_n$ Complexes

Cu-PolyEnC$_8$

HRMS (ES^+) found *m/z* 498.2360, calculated 498.2355 for $[C_{21}H_{43}N_2O_7Cu]^+$. UV/Vis (CH_3CN): λ_{max}/nm (ε/$M^{-1}cm^{-1}$) = 726 (50). IR (solid/cm^{-1}): *v* 2923, 1454 (C-H), 1036 (C-O).

Cu-PolyEnC$_{10}$

HRMS (AP$^+$) found *m/z* 528.2823, calculated 528.2823 for $[C_{23}H_{49}N_2O_7Cu]^+$. UV/Vis (CH_3CN): λ_{max}/nm (ε/M^{-1}cm^{-1}) = 724 (57). IR (solid/cm^{-1}): *v* 2922, 1452 (C-H), 1047 (C-O).

Cu-PolyEnC$_{12}$

HRMS (ES$^+$) found *m/z* 556.3163, calculated 556.3149 for $[C_{25}H_{53}N_2O_7Cu]^+$. UV/Vis (CH_3CN): λ_{max}/nm (ε/M^{-1}cm^{-1}) = 779 (64). IR (solid/cm^{-1}): *v* 3337 br. (O-H), 2922, 2851, 1456 (C-H), 1038 (C-O)

Cu-PolyEnC$_{14}$

HRMS (ES$^+$) found *m/z* 584.3458, calculated 584.3462 for $[C_{27}H_{57}N_2O_7Cu]^+$. UV/Vis (CH_3CN): λ_{max}/nm (ε/M^{-1}cm^{-1}) = 736 (63). IR (solid/cm^{-1}): *v* 2920 (C-H), 1452 (C-H), 1047 (C-O).

Ni-PolyEnC$_8$

HRMS (AP$^+$) found *m/z* 493.2429, calculated 493.2424 for $[C_{21}H_{43}N_2O_7Ni]^+$. UV/Vis (CH_3CN): λ_{max}/nm (ε/M^{-1}cm^{-1}) = 998 (10), 600 (5), 380 (17). IR (solid/cm^{-1}): *v* 2927 (C-H), 1465 (C-H), 1037 (C-O).

Ni-PolyEnC$_{10}$

HRMS (AP$^+$) found *m/z* 523.2899, calculated 523.2893 for $[C_{23}H_{49}N_2O_7Ni]^+$. UV/Vis (CH_3CN): λ_{max}/nm (ε/M^{-1}cm^{-1}) = 994 (13), 600 (6), 379 (21). IR (solid/cm^{-1}): *v* 2924 (C-H), 1462 (C-H), 1037 (C-O).

Ni-PolyEnC$_{12}$

^{1}H NMR (300 MHz, D_2O): δ_H = 4.00-3.91 (br. s), 3.87-3.80 (br. s), 3.63-3.46 (br. m, NC***H***$_2$), 1.23-1.04 (br. s, -(C***H***$_2$)$_n$-), 0.81-0.69 (br. s, C***H***$_3$) ppm. HRMS (ES$^+$) found *m/z* 551.3224, calculated 551.3206 for $[C_{25}H_{53}N_2O_7Ni]^+$. UV/Vis (CH_3CN): λ_{max}/nm (ε/M^{-1}cm^{-1}) = 1091 (18), 726 (6), 658 (7), 380 (25 IR (solid/cm^{-1}): *v* 3237 br. (O-H), 2920, 2853, 1456 (C-H), 1040 (C-O).

Ni-PolyEnC$_{14}$

HRMS (ES$^+$) found *m/z* 579.3508, calculated 579.3504 for $[C_{27}H_{57}N_2O_7Ni]^+$. UV/Vis (CH_3CN): λ_{max}/nm (ε/M^{-1}cm^{-1}) = 989 (9), 613 (4), 379 (16). IR (solid/cm^{-1}): *v* 2924 (C-H), 1467 (C-H), 1037 (C-O).

PolyDienC$_n$ Complexes

Cu-PolyDienC$_8$

HRMS (ES$^+$) found *m/z* 615.3166, calculated 615.3157 for $[C_{26}H_{54}N_3O_9Cu]^+$. UV/Vis (CH_3CN): λ_{max}/nm (ε/M^{-1}cm^{-1}) = 615 (95). IR (solid/cm^{-1}): *v* 2930, 1462 (C-H), 1053 (C-O).

Cu-PolyDienC$_{10}$

HRMS (ES$^+$) found *m/z* 645.3646, calculated 645.3626 for $[C_{28}H_{60}N_3O_9Cu]^+$. UV/Vis (CH_3CN): λ_{max}/nm (ε/M^{-1}cm^{-1}) = 618 (98). IR (solid/cm^{-1}): *v* 2925, 1454 (C-H), 1049 (C-O).

Cu-PolyDienC$_{12}$

HRMS (ES$^+$) found *m/z* 673.3969, calculated 673.3939 for $[C_{30}H_{64}N_3O_9Cu]^+$. UV/Vis (CH_3CN): λ_{max}/nm (ε/M^{-1}cm^{-1}) = 615 (79). IR (solid/cm^{-1}): *v* 3308 br. (O-H), 2922, 2853, 1456 (C-H), 1036 (C-O).

Cu-PolyDienC$_{14}$

HRMS (ES$^+$) found *m/z* 701.4255, calculated 701.4252 for $[C_{32}H_{68}N_3O_9Cu]^+$. UV/Vis (CH_3CN): λ_{max}/nm (ε/M^{-1}cm^{-1}) = 615 (93). IR (solid/cm^{-1}): *v* 2924, 1454 (C-H), 1031 (C-O).

Ni-PolyDienC$_8$

HRMS (AP$^+$) found *m/z* 610.3226, calculated 601.3214 for $[C_{26}H_{54}N_3O_9Ni]^+$.UV/Vis (CH_3CN): λ_{max}/nm (ε/M^{-1}cm^{-1}) = 1080 (15), 653 (6), 388 (21). IR (solid/cm^{-1}): *v* 2923, 1467 (C-H), 1043 (C-O).

Ni-PolyDienC$_{10}$

HRMS (AP$^+$) found *m/z* 640.3676, calculated 640.3683 for $[C_{28}H_{60}N_3O_9Ni]^+$. UV/Vis (CH_3CN): λ_{max}/nm (ε/M^{-1}cm^{-1}) = 1079 (18), 658 (7), 388 (25). IR (solid/cm^{-1}): *v* 2925, 1458 (C-H), 1035 (C-O).

Ni-PolyDienC$_{12}$

^{1}H NMR (300 MHz, D_2O): δ_H = 3.89-3.60 (m), 3.52-3.33 (br. s, NC***H***$_2$), 1.21-1.04 (br. s, -(C***H***$_2$)$_n$-), 0.72-0.64 (br. s, C***H***$_3$) ppm. HRMS (ES$^+$) found *m/z* 668.3965, calculated 668.3979 for $[C_{30}H_{64}N_3O_9Ni]^+$. UV/Vis (CH_3CN): λ_{max}/nm (ε/M^{-1}cm^{-1}) = 1063 (11), 652 (4), 386 (16). IR (solid/cm^{-1}): *v* 3244 br. (O-H), 2922, 2853, 1456, 1338 (C-H), 1053, 1038 (C-O).

Ni-PolyDienC$_{14}$

HRMS (AP$^+$) found *m/z* 696.4329, calculated 696.4307 for $[C_{32}H_{68}N_3O_9Ni]^+$. UV/Vis (CH_3CN): λ_{max}/nm (ε/$M^{-1}cm^{-1}$) = 1078 (15), 654 (7), 389 (22). IR (solid/cm^{-1}): *v* 2922, 1454 (C-H), 1039 (C-O).

Sr-PolyDienC$_{12}$

^{1}H NMR (300 MHz, D_2O) δ_H = 3.71-3.40 (br. m, NC***H***$_2$), 2.97-2.19 (br. m, HOC***H***/HOC***H***$_2$), 1.55-1.37 (m, HOCC***H***$_2$), 1.18-1.36 (br. s, -(C***H***$_2$)$_{10}$-), 0.85 (app. s, C***H***$_3$) ppm. LRMS (ES$^+$) found *m/z* 612.48, calculated 612.48 for [M-Sr+H]$^+$. IR (solid/cm^{-1}): *v* 3283 br. (O-H), 2922, 2853 (C-H), 1636 (N-H), 1456 (C-H), 1040 (C-O).

Y-PolyDienC$_{12}$

^{1}H NMR (300 MHz, D_2O) δ_H = 3.65-3.38 (br. m, NC***H***$_2$), 3.21-2.62 (br. m, HOC***H***/HOC***H***$_2$), 1.51-1.32 (br. s, -(C***H***$_2$)$_{10}$-), 0.79 (app. s, C***H***$_3$) ppm. LRMS (ES$^+$) found *m/z* 612.48, calculated 612.48 for [M-Y+H]$^+$. IR (solid/cm^{-1}): *v* 3227 br. (O-H), 2922, 2853 (C-H), 1647 (N-H), 1456, 1107 (C-H), 1035 (C-O).

3.6 References

1. T. T. Tavares, G. F. Teixeira, C. M. Lopes, W. T. G. Novato, H. Silva, M. T. P. Lopes, M. V. De Almeida, R. M. Grazul, H. F. Dos Santos and A. P. S. Fontes, *J. Inorg. Biochem.*, 2012, **115**, 13–19.

2. H. Er, S. Ohkawa and M. Iida, *Colloids Surf. A*, 2007, **301**, 189–198.

3. H. Qiao, B. Zhao, J. Diao, L. Huang, J. Zhong and F. Ma, *CLEAN*, 2016, **44**, 1191–1197.

4. D. A. Jaeger, X. Zeng and Y. Wang, *Colloids Surf. A*, 2006, **289**, 158–162.

5. D. A. Jaeger, M. F. Peacock and D. S. Bohle, *Langmuir*, 2003, **19**, 4859–4862.

6. M. J. Danks, M. E. Light and D. W. Bruce, *Eur. J. Inorg. Chem.*, 2009, **2009**, 4232–4239.

7. A. Polyzos, A. B. Hughes and J. R. Christie, *Langmuir*, 2007, **23**, 1872–1879.

8. D. Juan, J. Bingying, K. Xingming, Z. Xiancheng and X. Qingxiang, *J. Colloid Interface Sci.*, 2002, **256**, 428–434.

9. G. Ghirlanda, P. Scrimin, A. E. Kaifer and L. A. Echegoyen, *Langmuir*, 1996, **12**, 3695–3701.

10. C. N. Verani, R. Shanmugam, F. R. Xavier, M. M. Allard and K. K. Kpogo, *Dalton Trans.*, 2013, **42**, 15296–15306.

11. P. Scrimin, P. Tecilla, U. Tonellato and T. Vendrame, *J. Org. Chem.*, 1989, **54**, 5988–5991.

12. G. Ghirlanda, P. Scrimin and L. A. Echegoyen, *Langmuir*, 1996, **12**, 5188–5194.

13. G. Ghirlanda, P. Scrimin, P. Tecilla and A. Toffoletti, *Langmuir*, 1998, **14**, 1646–1655.

14. J. A. Driscoll, M. M. Allard, L. Wu, M. J. Heeg, S. R. P. da Rocha and C. N. Verani, *Chem. Eur. J.*, 2008, **14**, 9665–9674.

15. F. D. Lesh, S. S. Hindo, M. J. Heeg, M. M. Allard, P. Jain, B. Peng, L. Hryhorczuk and C. N. Verani, *Eur. J. Inorg. Chem.*, 2009, **2009**, 345–356.

16. C. N. Verani, J. Driscoll, P. H. Keyes and M. J. Heeg, *Inorg. Chem.*, 2014, **53**, 5647–5655.

17. X. Luo, S. Wu and Y. Liang, *Chem. Commun.*, 2002, 492–493.

18. J. N. Israelachvili, D. J. Mitchell and B. W. Ninham, *J. Chem. Soc., Faraday Trans. 2*, 1976, **72**, 1525–1568.

19. R. Kaur and S.K. Mehta, *Coord. Chem. Rev*., 2014, **262**, 37– 54.

20. Q. Zha, Q. Xie, Y. Hu, J. Han, L. Ge and R. Guo, *Colloid Polym. Sci.*, 2016, **294**, 841–849.

21. A. M. Ako, J. P. Hill, C. E. Anson, K. Ariga and A. K. Powell, *J. Coord. Chem.*, 2016, **69**, 3182–3191.

22. S. Gonawala, V. R. Leopoldino, K. Kpogo and C. N. Verani, *Chem. Commun.*, 2016, **52**, 11155–11158.

23. S. Gonawala, H. Baydoun, L. Wickramasinghe and C. N. Verani, *Chem. Commun.*, 2016, **52**, 8440–8443.

24. P. C. Griffiths, I. A. Fallis, D. J. Willock, A. Paul, C. L. Barrie, P. M. Griffiths, G. M. Williams, S. M. King, R. K. Heenan and R. Görgl, *Chem. Eur. J.*, 2004, **10**, 2022–2028.

25. M. Triest, G. Bussiére, H. Bélisle and C. Reber, *J. Chem. Edu. ACS,* 2000, **77**, 670.

26. A. B. P. Lever, *Inorganic Electronic Spectroscopy*, Elsevier Science, Amsterdam ; New York, 2 Sub edition., 1986.

27. P. C. Griffiths, I. A. Fallis, C. James, I. R. Morgan, G. Brett, R. K. Heenan, R. Schweins, I. Grillo and A. Paul, *Soft Matter*, 2010, **6**, 1981–1989.

28. P. Atkins, T. Overton, J. Rourke, M. Weller and F. Armstrong, *Shriver and Atkins' Inorganic Chemistry*, OUP Oxford, Oxford ; New York, 4 edition., 2006

29. C. Jubert, A. Mohamadou, C. Gérard, S. Brandes, A. Tabard and J.-P. Barbier, *J. Chem. Soc., Dalton Trans.*, 2002, 2660–2669.

30. H.A Jahn and E. Teller, *Proc. R. Soc. Lond.*, 1937, **161**, 220-235.

31. S. Roy, P. Mitra and A. K. Patra, *Inorg. Chim. Acta*, 2011, **370**, 247–253.

32. P. C. Griffiths, I. A. Fallis, T. Tatchell, L. Bushby and A. Beeby, *Adv. Colloid Interface Sci.*, 2008, **144**, 13–23.

Chapter Four

Cationic Iridium(III) Metallosurfactants for Luminescent Micellar Systems

4.1 Introduction

4.1.1 Luminescence

Luminescence is the observed radiative decay process of an excited state molecule. When a luminescent molecule absorbs a photon the electrons in the S_0 ground state are promoted to the highest vibrational level of the S_1 or S_2 excited state. The excited energy state is unstable and must therefore lose excess energy. This occurs *via* internal conversion (IC), a non- radiative (NR) decay process which causes relaxation to the lowest vibrational energy of the excited state, typically through molecular vibrations and/or loss of heat.

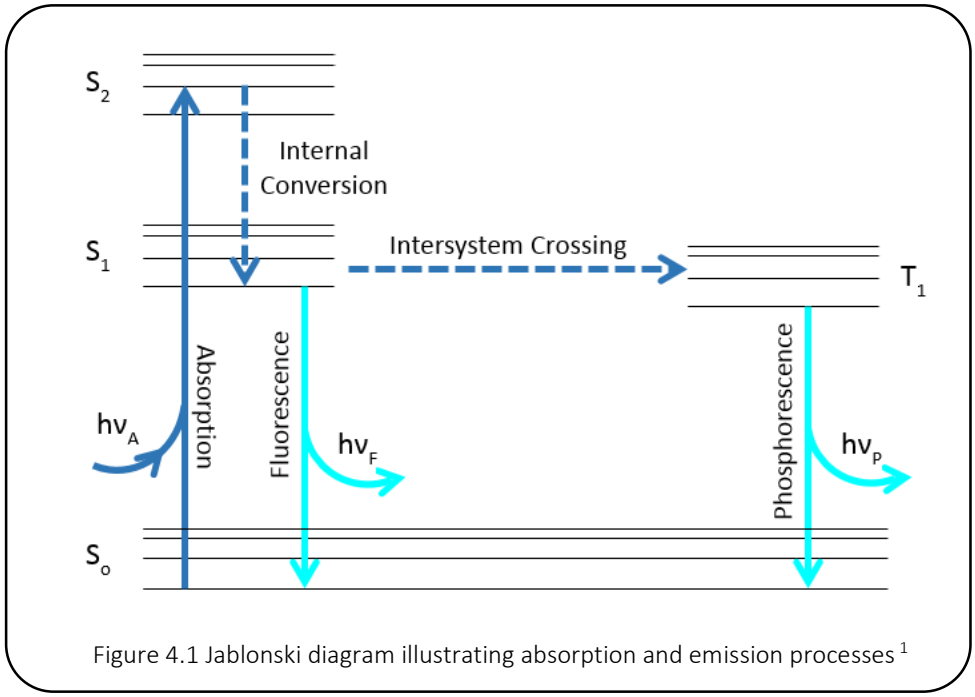

Figure 4.1 Jablonski diagram illustrating absorption and emission processes [1]

From this point, two processes may occur. Firstly, the system may undergo fluorescence, a radiative decay from the excited S_1 state to the ground S_0 state. This process is rapid as the transition is Laporte- and spin-allowed as it occurs between states of the same spin multiplicity and therefore fluorescence lifetimes are typically very short (<10 ns). Fluorescence emissions have characteristically small Stokes' shifts as the only energy difference between the absorbed and emitted light is that which is lost *via* IC.

Alternatively, the electrons in the excited S_1 state may undergo intersystem crossing (ISC), a NR decay process, allowing electrons to occupy the lower-energy T_1 excited state. ISC can only occur when the excited S_1 and T_1 states have similar energies. It is a spectroscopically forbidden process,

but can be facilitated by spin-orbit coupling from heavy atoms such as transition metals or heavy halides. Radiative decay from this state, known as phosphorescence, is spin-forbidden as it occurs between states of different spin multiplicities and therefore phosphorescence lifetimes can be much longer than those of fluorescence (milliseconds to seconds). Phosphorescence emission is characterised by a large Stokes' shift as the wavelength of emitted light is much longer than that of the absorbed light, due to the large loss of energy during ISC.[1]

4.1.2 Luminescence of Transition Metal Complexes

Octahedral d^6 transition metal complexes have been widely studied with regard to their luminescence as they afford highly tuneable photophysical properties as well as being kinetically inert and thermodynamically stable. Transition metals have five degenerate d-orbitals which are split into the excited state e_g^* set and the ground state t_{2g} set by coordination of ligands. Low spin d^6 complexes incorporating heavy metals such as iridium(III), rhenium(I) and ruthenium(II) exhibit large ligand field splitting between these two states. Such complexes often absorb light through intraligand (IL) and metal-to-ligand charge transfer (^{1}MLCT) processes and commonly emit *via* ^{3}MLCT phosphorescence.

The MLCT process initially involves ^{1}MLCT absorption where electrons are promoted from the metal t_{2g} orbital to a vacant π* orbital of the coordinated ligand. This is followed by ISC mediated by the heavy atom effect exhibited by 2nd and 3rd row transition metals by which spin-orbit coupling promotes ISC leading to population of the triplet excited state, therefore permitting ^{3}MLCT emission. Since the ^{3}MLCT state is lower in energy than the ^{1}MLCT state, the triplet emission is of a much longer wavelength, hence a large Stokes' shift is observed. This process formally oxidises the metal and effectively reduces the ligand to a radical anion. Therefore in order to have good MLCT character a complex requires an easily oxidisable metal of low oxidation state and a strongly π-accepting ligand which can stabilise the radical anion, such as polyaromatic ligands which are able to delocalise the negative charge over the highly conjugated system.

IL transitions are observed at shorter wavelengths than MLCT as they correspond to transitions between π-π* orbitals of the ligand system. IL emission is generally characterised by relatively short lifetimes and small Stokes' shifts as it is a spin-allowed process with relatively little energy loss. In large conjugated systems the molecular orbitals of the ligand can lie close enough in energy to be sensitised by long wavelength light – even into the visible region. IL transitions are

localised on the coordinated ligand and are therefore less affected by the nature of the metal centre in a complex.[1]

4.1.3 Design of Luminescent Iridium(III) Complexes

Cyclometallated iridium(III) complexes are those in which the organic ligand is coordinated to the metal centre *via* a metal-carbon interaction. There have been many recent investigations into the use of cyclometallated complexes in photophysical applications (see section **4.1.4**) as they have been found to exhibit high photoluminescence efficiencies as well as relatively high quantum yields.[2,3,4,5,6] The nature of the cyclometallating and ancillary ligands can be varied extensively to allow a high degree of control over both the physical and photophysical characteristics of the complex.

Cyclometallated iridium(III) complexes typically fall into two categories: neutral *tris*-cyclometallates, in which all three of the bidentate ligands are cyclometallating or cationic *bis*-cyclometallates, in which the ancillary ligand is non-cyclometallating (typically a conjugated diimine). Density functional theory (DFT) calculations have shown that the highest occupied molecular orbital (HOMO) is located primarily on the iridium 5(d) centre and the cyclometallated units, while the lowest unoccupied molecular orbital (LUMO) is located primarily on the diimine ligand. Variation in the types of ligands coordinated to the metal therefore allows independent tuning of these energy levels, hence *bis*-cyclometallates offer a higher degree of control over photophysical character than *tris*-cyclometallates.[7]

Iridium(III) cyclometallates are advantageous in terms of promoting triplet emission as σ-donation from the metallated aryl rings raises the energy of the metal orbitals, increasing their contribution to the excited state, which promotes ISC, thereby increasing triplet emission and hence leading to lifetimes in excess of 500 ns.[8,9]

In 1974 Nonoyama reported the synthesis of a chloro-bridged iridium(III) dimer which could be used as a convenient starting material for cationic *bis*-cyclometallated iridium(III) complexes.[10] The dimer was synthesised by the reaction of $IrCl_3.xH_2O$ with 2.2 equivalents of a cyclometallating ligand. Reaction of this chloro-bridged dimer with 2.2 equivalents of ancillary ligand afforded the desired complex. This is a useful synthesis as it allows for the step-wise addition of ligands to the iridium(III) centre which allows for fine-tuning of the complexes' physical and photophysical

properties as a wide range of cyclometallating and diimine ligands can be added to one iridium(III) centre.[11]

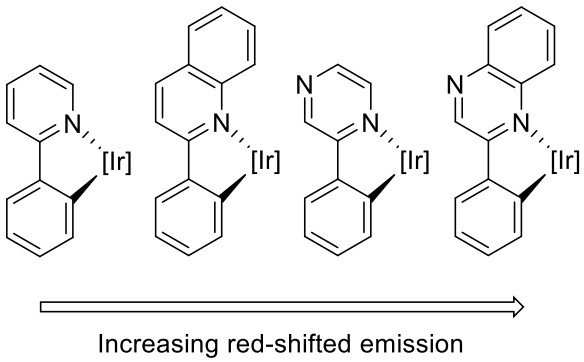

Figure 4.2 The effect of altering the cyclometallating ligand on the wavelength of emission.[6]

Phenyl pyridine is a typical example of a cyclometallating ligand, though it has been reported that increasing the π-conjugation of the pyridine unit has a strong influence on the photophysical properties of the complex. For example, addition of an aromatic ring to the pyridine moiety – to afford phenyl quinoline – altered the emission as the increased conjugation decreased the energy of the band gap, thus red-shifting the $^{3}\pi$-π and ^{3}MLCT emission of the complex. The emission wavelength was also found to be red-shifted further by substituting phenyl quinoline for phenyl quinoxaline.[6]

4.1.4 General Applications of Luminescent Ir(III) Complexes

Cyclometallated iridium(III) complexes exhibit good photostability and high photoluminescence efficiency, they are also kinetically inert and thermodynamically stable. They have therefore been reported for a wide range of applications.

One well studied applications of iridium(III) complexes is as bio-probes for fluorescence imaging due to their high sensitivity, resolution and selectivity. They can be easily tuned to control both their physical and photophysical properties and their large Stokes' shift removes interference from autofluorescence and self-adsorption.[3,6,8,9,12,13,14,15,16]

Iridium(III) complexes have been reported as singlet oxygen sensitizers for photooxidation reactions. Photoexcitation populates the singlet excited states of Ir(III), ISC arising from the heavy atom effect leads to population of the triplet excited states. Triplet-triplet energy transfer can

then produce singlet O_2, as the ground state of O_2 is the triplet state, which can then take part in oxidation reactions. For example, Sun *et al*. reported the use of $[Ir(ppy)_2(N^N)](PF_6)$ complexes (where ppy = 2-phenylpyridine and N^N = polyaromatic diimine) for the photooxidation of 1,5-dihydroxynaphthalene, as illustrated in Figure 4.3.[17,18,19,20,21]

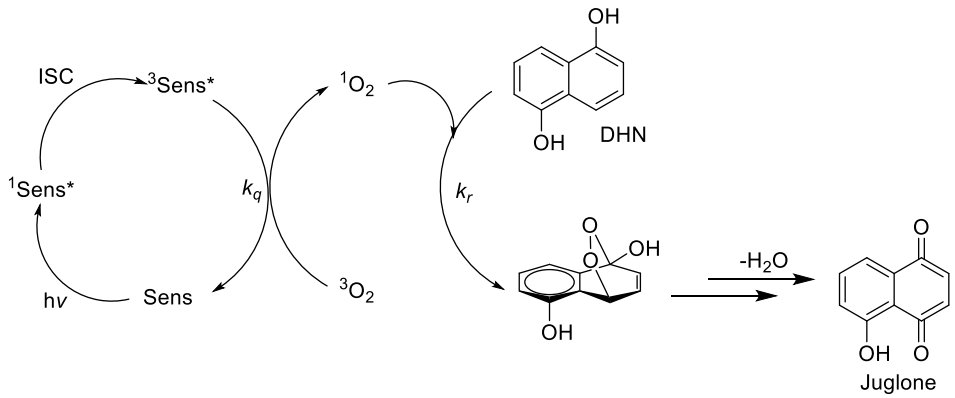

Figure 4.3 Mechanisms for photooxidation of 1,5-dihydroxynaphthalene (DHN) with an iridium(III) singlet oxygen photosensitiser (Sens)[18]

Complexes incorporating azacrown ether ligands, such as those shown in Figure 4.4, have been exploited as ion sensors as they have been found to show a marked change in luminescence upon binding of an ion into the host site. Sensors have been reported for ions including Zn^{2+},[22] Ca^{2+},[23] Mg^{2+},[24] Ba^{2+} and Ag^{2+},[25] however, they are disadvantaged by their poor solubility in water.[26]

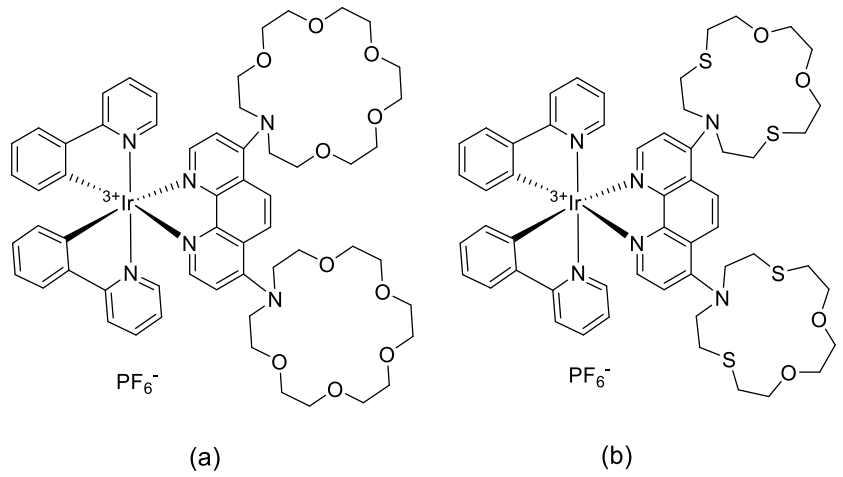

Figure 4.4 Structures of *bis*-cyclometallated iridium(III) complexes with crown ether pendants.[25,27]

One of the most widely-studied applications of iridium(III) complexes arises from the ability to readily tune their emission wavelengths *via* the nature of the coordinated ligands. Organic Light Emitting Diodes (OLEDs) have been reported which incorporate complexes such as $[Ir(ppy)_2(bpy)]^+$, *fac*-$[Ir(ppy)_3]$ and *fac*-$[Ir(thpy)_3]$ ((ppy = 2-phenylpyridine, bpy = 2,2'-bipyridine, thpy = 2-(thiophen-2-yl)pyridine) which can emit over a wide range of colours such as green,[5,28,29] yellow,[30] red[31,32] and blue.[33]

4.1.5 Amphiphilic Iridium(III) Complexes

Despite the extensive applications of iridium(III) complexes outlined in the section above, literature exploring their uses as metallosurfactants is relatively scarce. The majority of work considering iridium(III) amphiphiles in micellar systems report *bis*- or *tris*- cyclometallated complexes as precursors for mesoporous materials,[28,34] Langmuir films[32,35,36] and OLEDs.[21,37]

Guerrero-Martinez *et al.* reported the doping of iridium(III) and ruthenium(II) amphiphiles into CTAB (cetyltrimethylammonium bromide) micellar systems. Micelles which contained both metallosurfactants were found to exhibit dual-emissive properties arising from an Ir-donor/Ru-acceptor system which could be readily tuned *via* control of the metallosurfactant concentrations and hence spacial proximity within the micelle. Enhanced QYs were observed for the aggregated systems which were believed to be related to protection of the ^{3}MLCT state against oxygen diffusion and a reduction in NR decay afforded by the aggregate formation.[38,39]

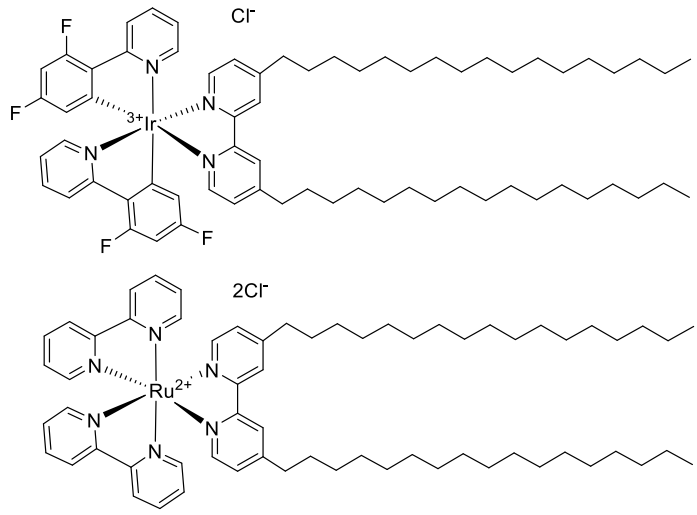

Figure 4.5 Iridium(III) and ruthenium(II) donor/acceptor metallosurfactants[30]

The 2016 study by McGoorty *et al.* investigated two *bis*-cyclometallated iridium(III) complexes containing SO_3^- moieties, added to aid solubility in water.[40] The excited state properties were found to be enhanced by concentration-induced aggregation leading to a blue-shift in photoluminescence emission attributed to the immediate environment of the chromophore being less polar than that of the solvated water. As in the Guerrero-Martinez study above the complex lifetime was found to be mono-exponential pre-CMC and bi-exponential post-CMC.[30] This suggests that the micellar structure prevents quenching of the chromophore excited state by oxygen diffusion and supresses NR decay, leading to higher QYs and longer lifetimes.[41]

4.1.6 Other d-block Amphiphiles

Although iridium(III) amphiphiles have received relatively little attention, other d-block metals have been reported in a wide range of micellar systems. For example, zinc(II) has been described as a catalyst for various hydrolysis reactions. Phenanthroline-based zinc(II) complexes incorporating long alkyl chains have been reported as catalysts for the hydrolysis of PNPP, PNPO and PNPD (*p*-nitrophenyl picolinate/octanoate/dodecanoate). Similarly, zinc(II) metallosurfactants derived from cyclen macrocycles have been reported for the hydrolysis of lipophilic esters. However, in both cases it was found necessary to use co-surfactants (CTAB and Triton X-100, respectively) in order to form micellar systems.[42,43]

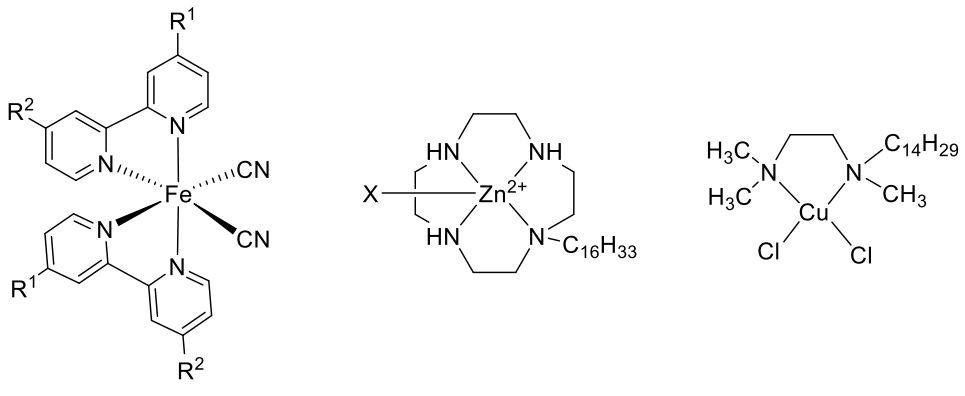

Figure 4.6 Examples of d-block metallosurfactants (i) R^1=R^2= i-C_4H_9, R^1=R^2= n-C_5H_{11}, R^1=R^2= n-C_7H_{15}, R^1= CH_3 R^2= n-C_7H_{15}, R^1= CH_3 R^2= n-C_5H_{15};[45] (ii) X = OH_2, OH^-;[43] (iii)[47]

Other such investigations include amphiphilic phosphines which have been reported as ligands for palladium(II) metallosurfactants which exhibited potential for applications in catalysis.[44] Iron(II)-containing complexes of the form $[Fe(CN)_2L_2]$ (where L is a symmetric or asymmetric bipyridine analogue functionalised with various length alkyl chains) have been investigated as potential solvatochromic probes in organised media.[45]

Triazacyclododecane derived surfactants have been reported which incorporate polymerisable vinylbenzene arms which are capable of forming metallosurfactants with Ni(II), Cu(I) and (II), and Co(II).[46] Cu(II)-containing surfactants have also been found to be effective catalysts in the hydrolysis of the nerve agent Sarin along with other similar phosphates.[47]

One of the more commonly studied d-block metals for metallosurfactants is ruthenium(II). Bowers *et al.* undertook a three-part investigation into the use of $[Ru(bpy)_3](2Cl)$ based complexes incorporating long alkyl chains for applications in the formulation of thin films for heterogeneous catalysis. Their initial study investigated double-chained molecules *via* SANS which showed a change in micelle morphology from oblate ellipsoid to spherical as the length of the alkyl chain increased (n = 12 to 15, 19).[48]

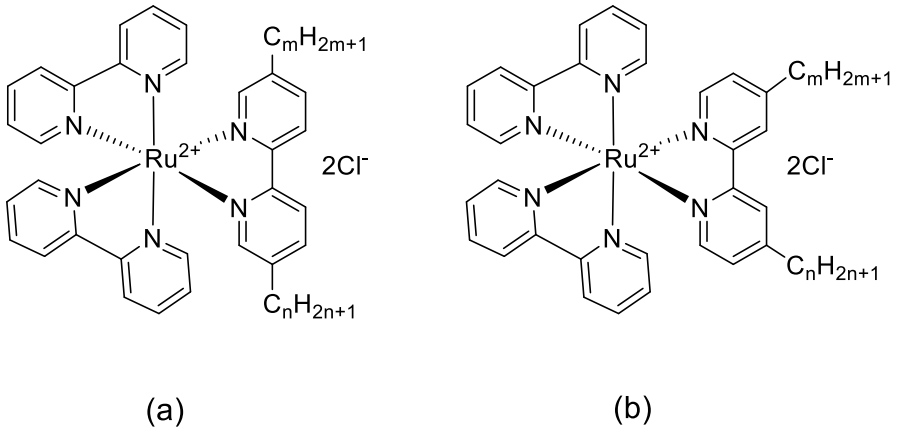

Figure 4.7 Ruthenium(II) metallosurfactants (a) n=m=12-15,19; m=1, n=19 (b) n=m=19, n=1, m=19.[48,49,50]

Subsequent investigations concerned time-dependent adsorption in thin film fabrication, the number of head-groups observed per adsorption site and the effect of chain length and orientation on the structure of the adsorbed films. It was found that single-chained species exhibited time-dependent adsorption whereas adsorption of double-chained analogues was independent of time. It was also established that racemic films were observed to have more closely-packed ruthenium(II) head-groups than the single isomer alternatives.[49,50] Such complexes are useful for thin film fabrication as the metallosurfactants are used as a template, upon calcination the metal-containing particles are deposited into pores producing highly ordered mesoporous materials for catalysis.[51,52]

4.2 Aims

Despite the existence of comprehensive literature on cyclometallated iridium(III) complexes and their applications there is relatively little information concerning iridium(III) metallosurfactants in micellar solutions and microemulsions.

The aim of this chapter was to synthesise a range of novel, luminescent amphiphiles based on cationic *bis*-cyclometallated iridium(III) complexes. Lipophilicity was afforded by bipyridine-based ancillary ligands functionalised with alkyl chains, whilst cyclometallating ligands known to afford water solubility upon deprotection provided hydrophilicity.

The microemulsion compatibility of the metallosurfactants was assessed *via* tensiometric measurements and related photophysical studies. The dodecyl-functionalised complexes were successfully doped into a carrier micellar system and exhibited marked changes in the emission properties upon micellisation. The solutions were found to be capable of solubilising up to 10 wt% toluene to form stable microemulsions at room temperature.

4.3 Results and Discussion

4.3.1 Synthesis

4.3.1.1. Synthesis of Ligands

The three diimine ligands reported in this chapter were made from a commercial 4,4'-dimethyl-2,2'-bipyridine starting material. This precursor was converted to the mono-acid analogue *via* a multi-step synthesis beginning with oxidation of one of the methyl moieties *via* reaction with SeO_2 in refluxing 1,4-dioxane for 24 hours. The crude product was then stirred overnight with $AgNO_3$ in water before being isolated as an off-white solid.[53] The mono-acid was then converted to the acid chloride *via* reaction with thionyl chloride and DMF in refluxing $CHCl_3$ for 24 hours. The solvent was removed *in vacuo* and used in further reactions without purification or characterisation due to its moisture sensitivity. Reaction of the acid chloride precursor with the corresponding 1-alkylamine in the presence of *N,N*-diisopropylethylamine (DIEA) yielded the desired ligands as brown solids in yields of 31-34%.

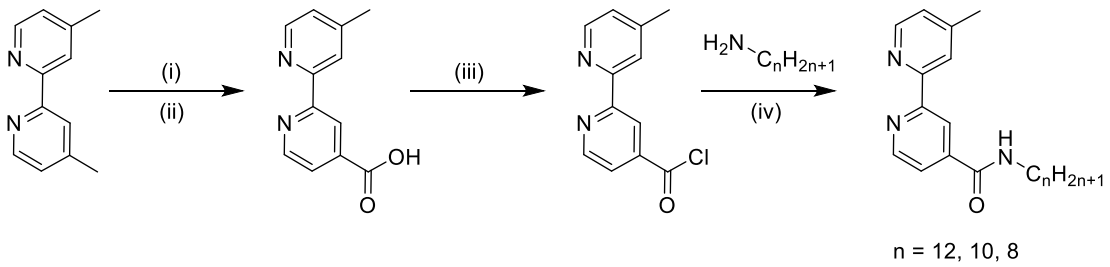

Figure 4.8 Synthesis of diimine ligands (n = 8, 10, 12). Reactions conditions: (i) SeO_2, 1,4-dioxane, (ii) $AgNO_3$ aq., NaOH, EtOH, (iii) $SOCl_2$, $CHCl_3$, DMF, (iv) DIEA, MeCN.

The two cyclometallating ligands used in this chapter were synthesised in simple single-step reactions. Ethyl-2-phenylquinoline-4-carboxylate (**epqcH**) was synthesised from a commercial 1-phenylquinoline-4-carboxylic-acid precursor *via* 24 hour reaction in refluxing EtOH with conc. H_2SO_4.[54] Ethyl-4-methylphenylthiazole-5-carboxylate (**emptzH**) was synthesised from the reaction of thiobenzamide with ethyl-2-chloroacetoacetate in refluxing EtOH.[55]

4.3.1.2 Synthesis of Iridium(III) Complexes

Chloro-bridged iridium(III) dimers of **emptz** and **epqc** where synthesised according to the literature procedure.[10] These dimers were split *via* a light-sensitive reaction in MeCN in the presence of $AgBF_4$ to yield the intermediate complexes **$[Ir(C^N)_2(MeCN)_2](BF_4)$** (where C^N =

emptz or **epqc**). The *bis*-MeCN complexes where then stirred at reflux in $CHCl_3$ with the corresponding diimine ligand to give the desired cationic *bis*-cyclometallated complexes as bright red to dark brown solids in yields of 24-87%. This procedure was chosen over the traditional splitting-procedure used by Nonoyama[10] as it was found to lead to higher purity products, removing the need to purify *via* column chromatography, therefore affording higher yields. It also meant that the counter-ion exchange (from Cl^- to BF_4^-) did not need to be performed in the separate step but instead took place during the coordination reaction.

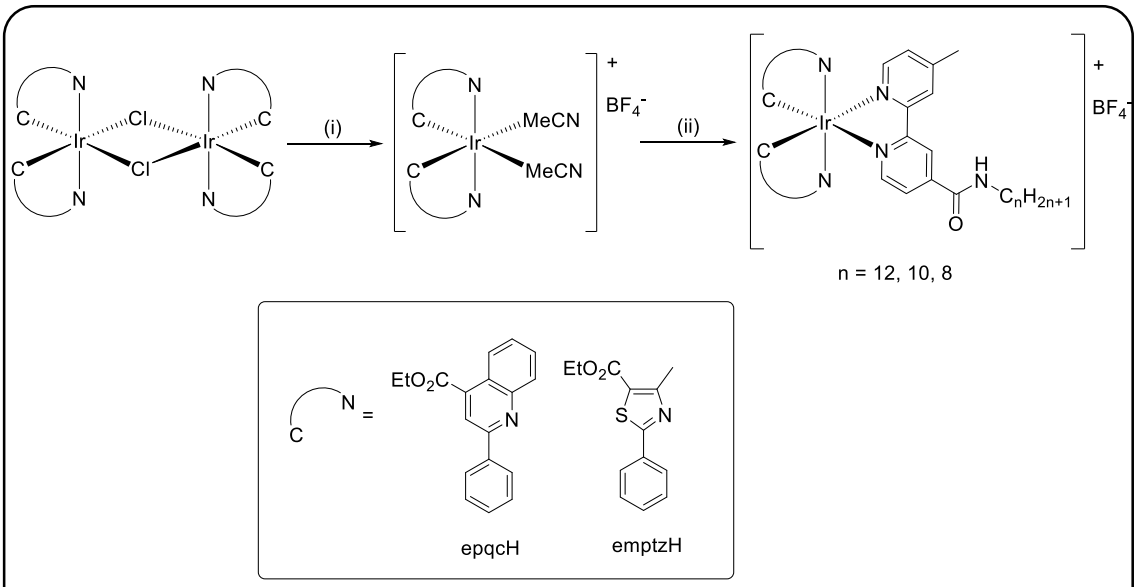

Figure 4.9 Synthesis of amphiphilic iridium(III) complexes. Reaction conditions (i) $AgBF_4$, MeCN, (ii) 1 eq. N^N, $CHCl_3$ [10,54,55]

4.3.1.3 Deprotection of Iridium(III) Complexes

The iridium(III) complexes containing the dodecyl chain functionalisation were deprotected to afford water solubility and thus assess their microemulsion compatibility. The protected complexes were stirred at reflux in acetone for 24 hours in the presence of KOH (1 M) before being neutralised with HCl (1 M) and the solvent removed *in vacuo*. The crude product was dissolved in MeOH and filtered to remove inorganic salts to afford the complexes **$[Ir(pqca)_2(BpyC_{12})]Cl$** and **$[Ir(mptca)_2(BpyC_{12})]Cl$** (**pqca** = 2-phenyl-quinoline-4-carboxylic acid, **mptca** = 4-methyl-2-phenylthiazole-5-carboxylic acid) from **$[Ir(epqc)_2(BpyC_{12})](BF_4)$** and **$[Ir(emptz)_2(BpyC_{12})](BF_4)$** respectively.[54]

4.3.2 Structural Characterisation

All of the ligands and complexes described herein were characterised via UV-Vis, IR, ^{1}H and $^{13}C\{^{1}H\}$ NMR spectroscopy and mass spectrometry. The iridium(III) complexes were difficult to fully characterise *via* ^{1}H NMR spectroscopy due to the numerous overlapping signals in the aromatic region. However, for the MeCN precursors and complexes it was possible to identify the proton on the carbon atom adjacent to the cyclometallating bond. This peak is simple to identify as it is significantly upfield-shifted (in the region of ~5.9 ppm) by shielding from the metal and therefore stands apart from the other aromatic signals. The complexes were also characterised *via* LR and HR mass spectrometry. All exhibited either the parent cation peak $[M\text{-}X]^{+}$ or $[M\text{-}X+H]^{+}$ (X = BF_4/Cl) with the signature iridium(III) isotope pattern.

During synthesis, **$[Ir(epqc)_2(MeCN)_2](BF_4)$** was purified *via* precipitation from DCM and Et_2O yielding bright red crystals suitable for X-ray diffraction studies (Figure 4.10). The same precipitation method afforded similar crystals of the corresponding complex **$[Ir(epqc)_2(BpyC_{12})](BF_4)$** (Figure 4.11).

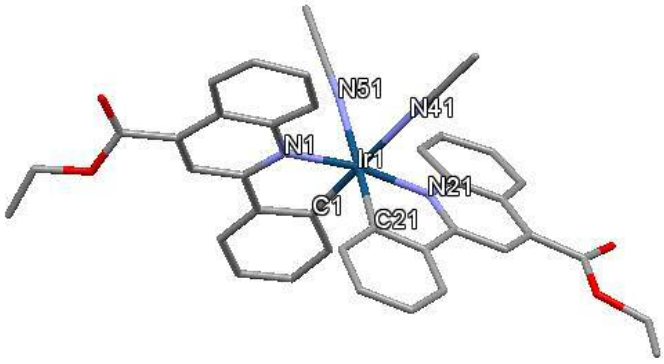

Figure 4.10 Crystal structure of **$[Ir(epqc)_2(MeCN)_2](BF_4)$** precursor (counter ion and protons omitted for clarity)

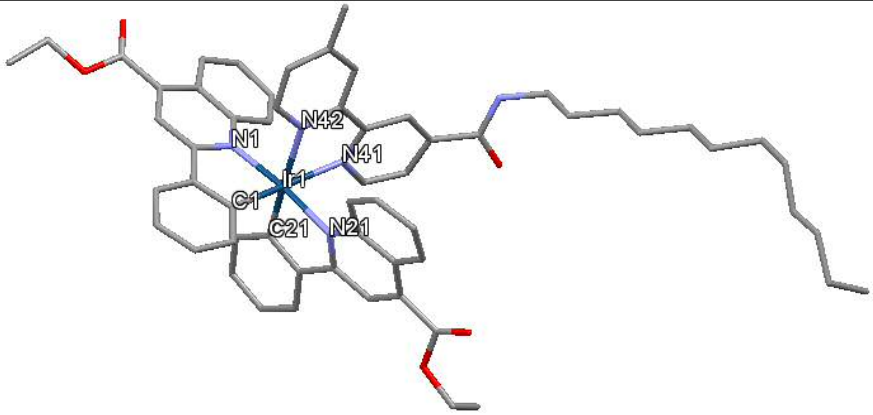

Figure 4.11 Crystal structure of **$[Ir(epqc)_2(BpyC_{12})](BF_4)$** (counter ion and protons omitted for clarity)

Sample	$[Ir(epqc)_2(MeCN)_2](BF_4)$		$[Ir(epqc)_2(BpyC_{12})](BF_4)$	
Empirical formula	$C_{44}H_{44}BF_4IrN_4O_5$		$C_{62}H_{68}BF_4IrN_5O_{5.50}$	
Formula weight	987.84		1250.22	
Temperature	100(2) K		100(2) K	
Wavelength	0.71073 Å		0.71073 Å	
Crystal system	Triclinic		Triclinic	
Space group	*P*–1		*P*–1	
Unit cell dimensions	*a* = 8.743(2) Å	α = 119.06(5)°	*a* = 9.710(0) Å	α = 100.36(2)°
	b = 16.461(2) Å	β = 91.75(2)°	*b* = 16.272(1) Å	β = 91.40(2)°
	c = 16.553(5) Å	γ = 102.72(2)°	*c* = 18.627(9) Å	γ = 104.59(4)°
Volume	2004.68(13) $Å^3$		2794.29(12) $Å^3$	
Z	2		2	
Density (calculated)	1.637 Mg / m^3		1.486 Mg / m^3	
Absorption coefficient	3.401 mm^{-1}		2.458 mm^{-1}	
F(000)	988		1274	
Crystal	Needle; red		Plate; Red	
Crystal size	0.160 × 0.010 × 0.010 mm^3		0.140 × 0.100 × 0.010 mm^3	
θ range for data collection	2.470 – 27.490°		2.361 – 27.484°	
Index ranges	$-11 \le h \le 11$, $-21 \le k \le 21$, $-21 \le l \le 21$		$-10 \le h \le 12$, $-21 \le k \le 21$, $-24 \le l \le 24$	
Reflections collected	38177		48070	
Independent reflections	9082 [R_{int} = 0.0375]		12767 [R_{int} = 0.0320]	
Completeness to θ = 25.242°	98.9 %		99.9 %	
Absorption correction	Semi–empirical from equivalents		Semi–empirical from equivalents	
Max. and min. transmission	1.00000 and 0.79516		1.00000 and 0.81267	
Refinement method	Full-matrix least-squares on F^2		Full-matrix least-squares on F^2	
Data/ restraints / parameters	9082 / 159 / 632		12767 / 429 / 940	
Goodness-of-fit on F^2	1.073		1.029	
Final R indices [$F^2 > 2\sigma(F^2)$]	*R1* = 0.0294, *wR2* = 0.0719		*R1* = 0.0328, *wR2* = 0.0788	
R indices (all data)	*R1* = 0.0337, *wR2* = 0.0739		*R1* = 0.0389, *wR2* = 0.0816	
Extinction coefficient	n/a		n/a	
Largest diff. peak and hole	1.700 and –1.280 e $Å^{-3}$		1.648 and –1.182 e $Å^{-3}$	

Table 4.1 Crytallographic data for **$[Ir(epqc)_2(MeCN)_2](BF_4)$** and **$[Ir(epqc)_2(BpyC_{12})](BF_4)$**

The X-ray crystal structures shown in Figures 4.10 and 4.11, show that the complexes adopt a distorted octahedral geometry. The cyclometallating ligands retain the *cis*-C, *trans*-N coordination of the chloro-bridged dimer precursor with bond angles of 88.1(5)° and 172.6(2)°, respectively for **$[Ir(epqc)_2(BpyC_{12})](BF_4)$** (Figure 4.11). The diimine ligand is coordinated *trans* to the cyclometallated phenyl rings with Ir-N bond lengths (2.16 Å) slightly longer than those of the **epqc** ligands (2.085 Å). These parameters are in good agreement with those of the analogous complexes reported previously, for example complexes of the type **$[Ir(epqc)_2(N\text{^}N)](PF_6)$** (N^N = 4,4'-dimethyl-2,2'-bipyridine and 4,7-diphenyl-1,10-phenanthroline) had *trans*-N bond angles in the range 168.0(3)° to 174.9(3)°. They also had bond lengths of 2.094(8) to 2.112(8) Å for the **epqc** Ir-N bonds which were shorter than those observed for the diimine Ir-N bonds. It is also noteworthy that in the **$[Ir(epqc)_2(BpyC_{12})]^+$** complex there was no disorder seen along the dodecyl chain.[54,56,57]

4.3.3 Electrochemistry

The electrochemical characteristics of the **$[Ir(C\text{^}N)_2(BpyC_n)](BF_4)$** complexes were studied in de-oxygenated DCM. The cyclic voltammograms, measured at a platinum disc electrode (scan rate $v = 200$ mV s^{-1}, $1x10^{-3}$ M solutions, 0.1 M $[NBu_4][PF_6]$ as a supporting electrolyte) generally showed one non-fully reversible oxidation around +1.57 V (for **C^N = epqc**) and +1.44 V (for **C^N = emptz**) which were assigned to the $Ir^{3+/4+}$ couple.

Complex	E_{ox} / V	E_{red} / V
$[Ir(emptz)_2(BpyC_8)](BF_4)$	+1.57	-1.22
$[Ir(emptz)_2(BpyC_{10})](BF_4)$	+1.57	-1.22
$[Ir(emptz)_2(BpyC_{12})](BF_4)$	+1.56	-1.41
$[Ir(epqc)_2(BpyC_8)](BF_4)$	+1.45	-1.16
$[Ir(epqc)_2(BpyC_{10})](BF_4)$	+1.42	-1.15
$[Ir(epqc)_2(BpyC_{12})](BF_4)$	+1.46	-1.15

Table 4.2 Electrochemical studies (calibrated with Fc/Fc^+ as an internal standard)

Previous studies involving the two cyclometallating ligands reported here have found the non-fully reversible oxidation for the $Ir^{3+/4+}$ couple to lie around +1.38 to +1.45 V for **C^N = epqc** and +1.55 V for **C^N = emptz**[54,55] and are therefore in good agreement with the figures in Table 4.2. As in previous studies, the data shown here for the oxidation potentials for the $Ir^{3+/4+}$ couple are higher for the **emptz** complexes than for **epqc** analogues suggesting that the iridium(III) ion is relatively more stable in the former. Five complexes also showed a fully or partially reversible

reduction wave at around -1.22 V for **C^N = emptz** and -1.16 V for **C^N = epqc** which are typically assigned to ligand-centred processes involving the diimine ligands but with the potential for some contribution from the cyclometallating ligands. The complex **$[Ir(emptz)_2(BpyC_{12})](BF_4)$** showed an anomalous reduction peak at -1.41 V.

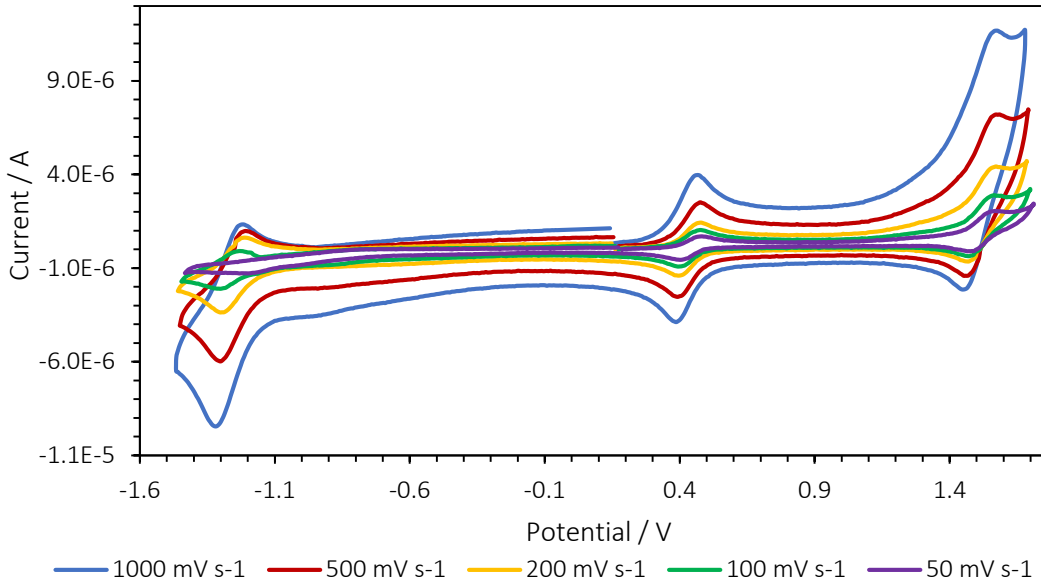

Figure 4.12 Cyclic voltammograms for **$[Ir(emptz)_2(BpyC_8)](BF_4)$** at varying scan rates (calibrated with Fc/Fc^+ as an internal standard)

Figure 4.12 illustrates an example set of data showing the variation in the cyclic voltammograms of **$[Ir(emptz)_2(BpyC_8)](BF_4)$** over a range of different scan rates. It can be seen that there are subtle changes in both the oxidation and reduction potentials with varying scan rates, this observation is indicative of non-fully reversible redox processes

4.3.4 Photophysical Characterisation

4.3.4.1 UV-Vis Absorption Spectroscopy

Absorption spectroscopy was undertaken in aerated MeCN solutions (10^{-5} M) at room temperature. Figure 4.13 shows the absorption profiles of **[Ir(epqc)$_2$(BpyC$_{12}$)](BF$_4$)**, **[Ir(emptz)$_2$(BpyC$_{12}$)](BF$_4$)** and their constituent ligands. The free ligands **BpyC$_{12}$**, **epqcH** and **emptzH** show strong absorption bands in the high energy region (200-400 nm) which were assigned to n-π*and π-π* transitions. It was observed that variation in the length of the alkyl chain on the diimine ligand had a negligible effect on the absorption properties. The complexes show a combination of the spin-allowed ligand-centred transitions (slightly red-shifted by perturbation from the coordinated metal) from both the cyclometallating and diimine ligands. The weaker bands at 470 nm (ε ~2700) and 435 nm (ε ~8000) for **[Ir(epqc)$_2$(BpyC$_{12}$)](BF$_4$)** and **[Ir(emptz)$_2$(BpyC$_{12}$)](BF$_4$)**, respectively, were assigned to the spin-allowed ^{1}MLCT transitions. These values correlate well with those reported for the bipyridine analogues of 470 (ε ~4500) and 442 (ε ~6700), respectively.[54,55]

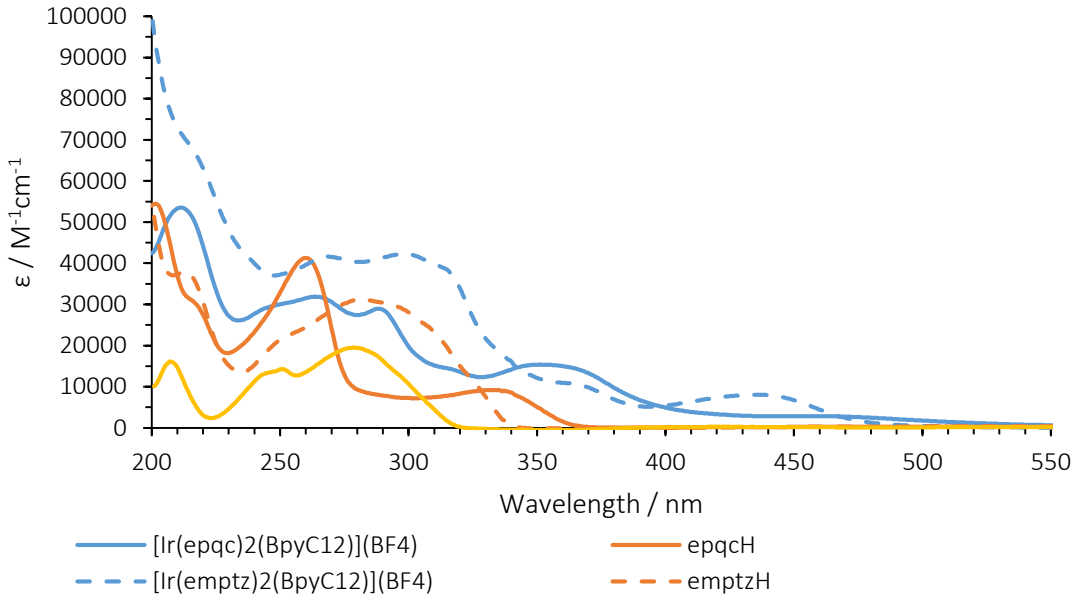

Figure 4.13 Absorption spectra of iridium(III) complexes and constituent ligands (10^{-5} M MeCN solutions, room temperature)

4.3.4.2 Luminescence Spectroscopy

The room temperature steady state emission measurements were carried out in aerated MeCN solutions (10^{-5} M). Figure 4.14 shows the normalised emission spectra of **$[Ir(epqc)_2(BpyC_{12})](BF_4)$** and its constituent ligands as well as the low temperature emission spectrum for the complex (measured at 77 K on a 1:1 EtOH/MeOH glass). The precursors, **epqcH** and **$BpyC_{12}$**, show typical ligand-centred emission in the high energy region (~300-550 nm) and exhibit short-lived lifetimes (~0.01 – 4 ns) consistent with fluorescence emission. The room temperature emission of the complex shows weak ligand-centred fluorescence at ~510 nm and much stronger ^{3}MLCT phosphorescence at ~630 nm consistent with the reported 2,2'-bipyridine and 4,4'-dimethyl-2,2'-bipyridine analogues which both show ^{3}MLCT emission at ~630 nm under the same conditions. Emission from the complex is long-lived (189 ns) as it originates from a spin-forbidden triplet-singlet transition and lies in the same region as the analogous complexes (211-219 ns).[54] These emission characteristics were retained across the range of different **epqc** complexes as the minor variations in the alkyl chain length were found to have a negligible effect on the photophysical properties.

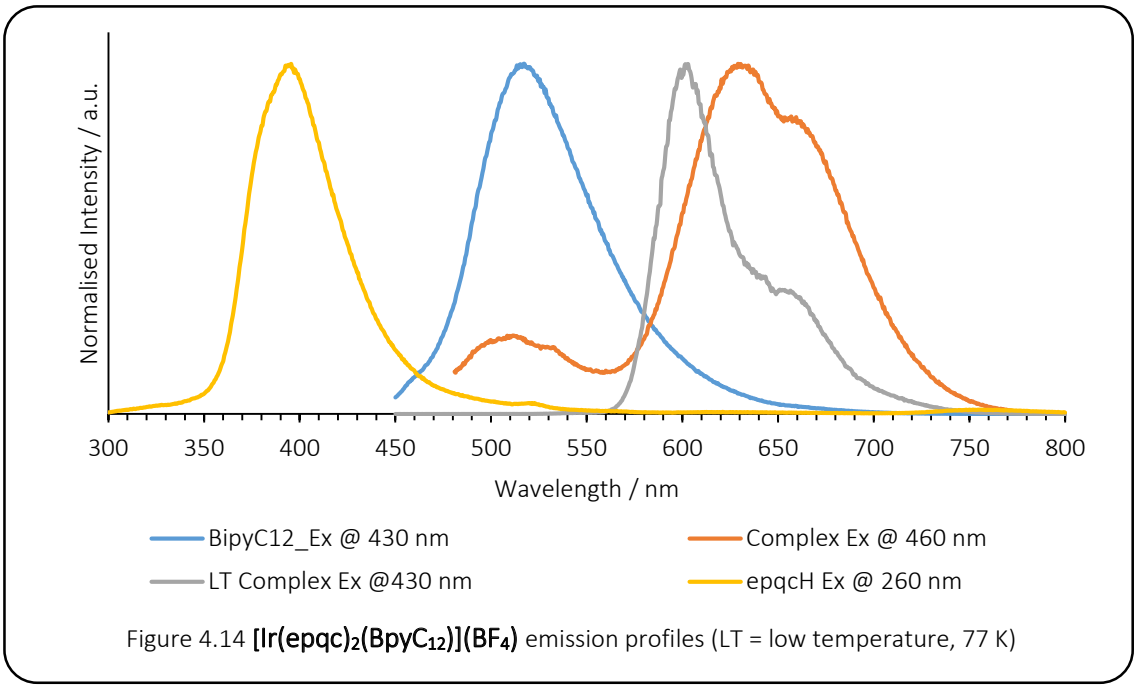

Figure 4.14 **$[Ir(epqc)_2(BpyC_{12})](BF_4)$** emission profiles (LT = low temperature, 77 K)

The room temperature steady state emission measurements for **[Ir(emptz)$_2$(BpyC$_{12}$)](BF$_4$)** show the same pattern as the **epqc** analogue described above. The key difference is the lack of ligand-centred emission in the complex profile, though this is consistent with other complexes incorporating the **emptz** cyclometallating ligand. The complex ^{3}MLCT emission at ~560 nm is consistent with the reported 2,2'-bypyridine and 4,4'-dimethyl-2,2'-bipyridine analogues which emit at 549 nm. The low temperature spectrum of the complex (measured at 77 K on a MeOH-EtOH (1:1) glass) shows a highly structured emission profile. Similar to the previously reported **emptz** complexes the low temperature spectrum shows vibronic structure which can be attributed to the ligand-centred triplet component of the cyclometallating ligand which also contributes to the emission observed at room temperature.[55]

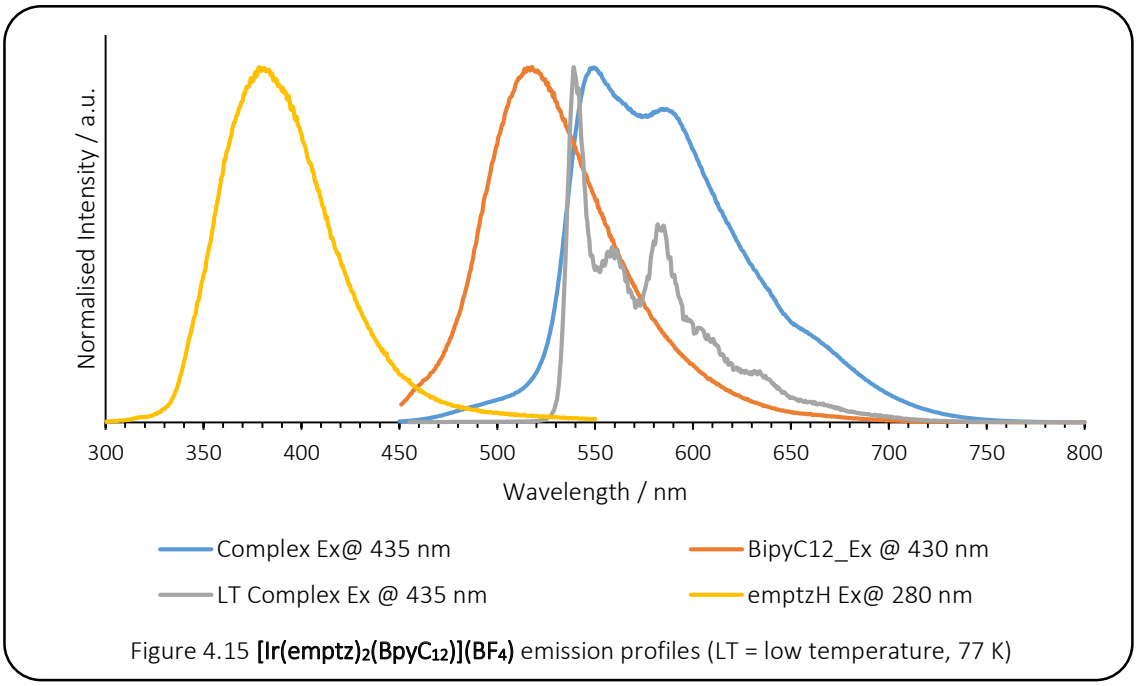

Figure 4.15 **[Ir(emptz)$_2$(BpyC$_{12}$)](BF$_4$)** emission profiles (LT = low temperature, 77 K)

The emission lifetimes were obtained in aerated MeCN for both ligands (<1-5 ns) and complexes (176-270 ns) and were consistent with an emitting state of singlet and triplet character, respectively. The complex emission lifetimes where generally longer for the **emptz** complexes than the **epqc** which concurs with literature values.

The Ir(III) complexes were seen to exhibit modest quantum yields (Φ) of around 1-3% in aerated MeCN at room temperature. These values are in line with previously reported species bearing the **epqc**[56] and **emptz**[55] cyclometallating ligands.

Complex/ Ligand	λ_{abs}/nm [a]	λ_{em}/ nm [a]	τ/ns [a]	Low Temp. /nm [b]	Φ[c]
epqcH	335 (9200), 259 (41200), 216 sh. (30900), 201 (54300)	394	1.01 (39%) 0.01 (61%)	-	0.002
emptzH	281 (31200), 250 sh. (21200), 213 (37900)	378	< 1 ns	-	0.005
$BpyC_{12}$	278 (19400), 250 (14200), 245 sh. (13300), 206 (15800)	513, 412	3.58	-	0.006
$BpyC_{10}$	277 (23000), 250 (16000), 245 sh. (14900), 206 (16900)	514, 410	3.56	-	0.009
$BpyC_8$	284 (9500), 250 sh. (8900), 243 (9200), 208 (13600)	514, 409	4.45	-	0.008
$[Ir(epqc)_2(BpyC_{12})](BF_4)$	468 (2700), 354 (15300), 288 (28900), 262 (31800), 247 (29600), 211 (53400)	630, 511	189	651 sh., 601	0.009
$[Ir(epqc)_2(BpyC_{10})](BF_4)$	461 (2600), 355 (14000), 289 (25900), 267 (29900), 247 (26600), 210 (47700)	630, 511	176	656 sh., 639 sh., 600	0.016
$[Ir(epqc)_2(BpyC_8)](BF_4)$	461 (4500), 351 (25400), 289 (63000), 264 (70500), 208 (92300)	631, 514	186	659 sh., 640 sh., 601	0.031
$[Ir(emptz)_2(BpyC_{12})](BF_4)$	435 (8000), 299 (42300), 269 (41600)	585, 549	199 (97%) 6.39 (3%)	630 sh., 607 sh., 585, 561, 539	0.023
$[Ir(emptz)_2(BpyC_{10})](BF_4)$	436 (7100), 368 (9200), 308 (33000), 269 (27800), 209 (50900)	586 sh., 547, 511	263	635 sh., 604 sh., 583, 560, 540	0.023
$[Ir(emptz)_2(BpyC_8)](BF_4)$	434 (6100), 365 (7000), 315 sh. (29300), 298 (34100), 273 (34900), 212 (39300)	584 sh., 546, 515	238 (99%) 5.15 (1%)	633 sh., 605 sh., 584, 562, 540	0.023
$[Ir(mptca)_2(BpyC_{12})]Cl$	417 (2000), 311 (4100), 281 (5300), 251 (9900), 216 (37900)	596, 451,	270 (173)[d]	628, 600 sh., 578, 556, 534	0.016
$[Ir(pqca)_2(BpyC_{12})]Cl$	457 (700), 355 (1600), 288 (3000), 239 (6800)	623, 449	230 (332)[d]	601, 559	0.031

Table 4.3 [a] measurements obtained in aerated 10^{-5} M MeCN solutions at 293 K; [b] EtOH-MeOH (1:1) glass at 77 K; [c] $[Ru(bpy)_3](PF_6)_2$ as reference of 0.016 in aerated MeCN; [d] comparative values in parentheses recorded in water.

The complexes were also assessed for their efficacy to sensitise triplet oxygen. Protected complexes (**[Ir(epqc)$_2$(BpyC$_n$)](BF$_4$)**, n = 8, 12 and **[Ir(emptz)$_2$(BpyC$_n$)](BF$_4$)**, n = 8, 10) in aerated MeCN showed an emission at ~1270 nm which was assigned to the characteristic emission from $^1O_2$, indicating that they could be employed in photooxidation reactions. However, the water-soluble complexes showed no peak either in MeCN, water, or in a micellar solution.

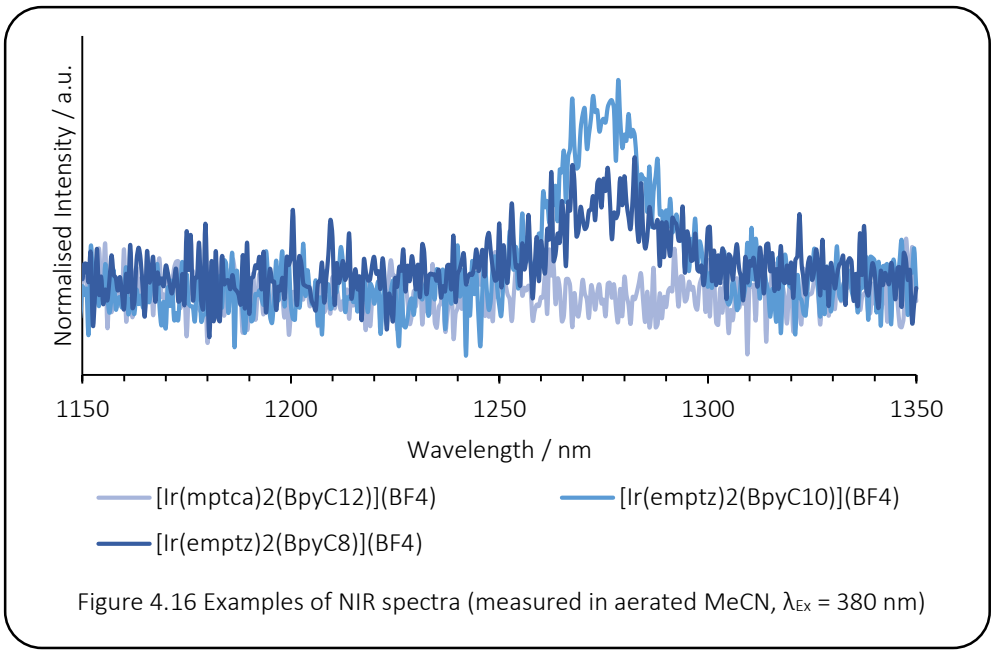

Figure 4.16 Examples of NIR spectra (measured in aerated MeCN, λ_{Ex} = 380 nm)

Examples of the observed NIR spectra are shown in Figure 4.16. Peaks corresponding to $^1O_2$ emission can be seen for the two protected complexes but not for the deprotected analogue. Although these complexes have differing alkyl chain lengths, earlier studies showed that this had no noticeable effect on the photophysical properties therefore direct comparisons may be drawn between the complexes.

4.3.5 Microemulsion Compatibility

4.3.5.1 Tensiometry

Previous studies involving the cyclometallated ligands reported here state that solubility in water is afforded by deprotection of the ethyl ester moieties to give hydrophilic carboxylic acids.[54] Although deprotection of **[Ir(epqc)$_2$(BpyC$_{12}$)](BF$_4$)** and **[Ir(emptz)$_2$(BpyC$_{12}$)](BF$_4$)** to give **[Ir(pqca)$_2$(BpyC$_{12}$)]Cl** and **[Ir(mptca)$_2$(BpyC$_{12}$)]Cl**, respectively, did afford water solubility at low concentrations the complexes were not soluble enough to form micelles on their own, *i.e.* the CMC lies at a point where the complex is no longer soluble. Previous studies involving long-chain

amphiphiles have attributed their poor solubility in water to the hydrophobic moiety coiling around the hydrophilic head-group and thus shielding it from the aqueous environment.[58,59]

Due to these solubility limitations the deprotected iridium(III) complexes were doped into the [MeImC$_{12}$]Br/BuOH/H$_2$O carrier-solution described previously (Chapter Two). The tensiometry plots (Figure 4.17) confirmed the effective doping as a clear CMC point was shown for each complex and the linearity of the post-CMC surface tension measurements is indicative of a lack of impurities. As the components are in an aqueous environment it is assumed that they orientate with the lipophilic chains on the interior of the micelle and thus away from the water. The carrier micellar system was doped with 2 wt% of each iridium(III) complex individually, which gave rise to highly-coloured orange solutions and were capable of solubilising at least 10 wt% toluene to give stable microemulsions at room temperature.

From the surface tension plots shown in Figure 4.17, it can be seen that the presence of the iridium(III) complexes slightly raises the CMC of the micellar system. The subtlety of the change in CMC can be attributed to the fact that the iridium(III) complexes are only present at 2 wt% meaning it is unlikely that each micelle contains more than one complex, thus the overall perturbation of the system is relatively small. The subtle change may be due to a number of factors such as the charge of the metal complex or the large steric bulk of the complex head group when it is incorporated into the carrier micelle.

For a single-surfactant micellar system it is possible to calculate the average area on the surface of the micelle occupied by each surfactant head group (area per molecule, APM). However, for a system comprising two or more surfactants it is not possible to determine the individual areas as the APM for a surfactant and a co-surfactant (e.g. [MeImC$_{12}$]Br and BuOH) is not simply the sum of the two individual APM measurements. This is due to the fact that the presence of a co-surfactant alters the physical properties of the system (such as the CMC).

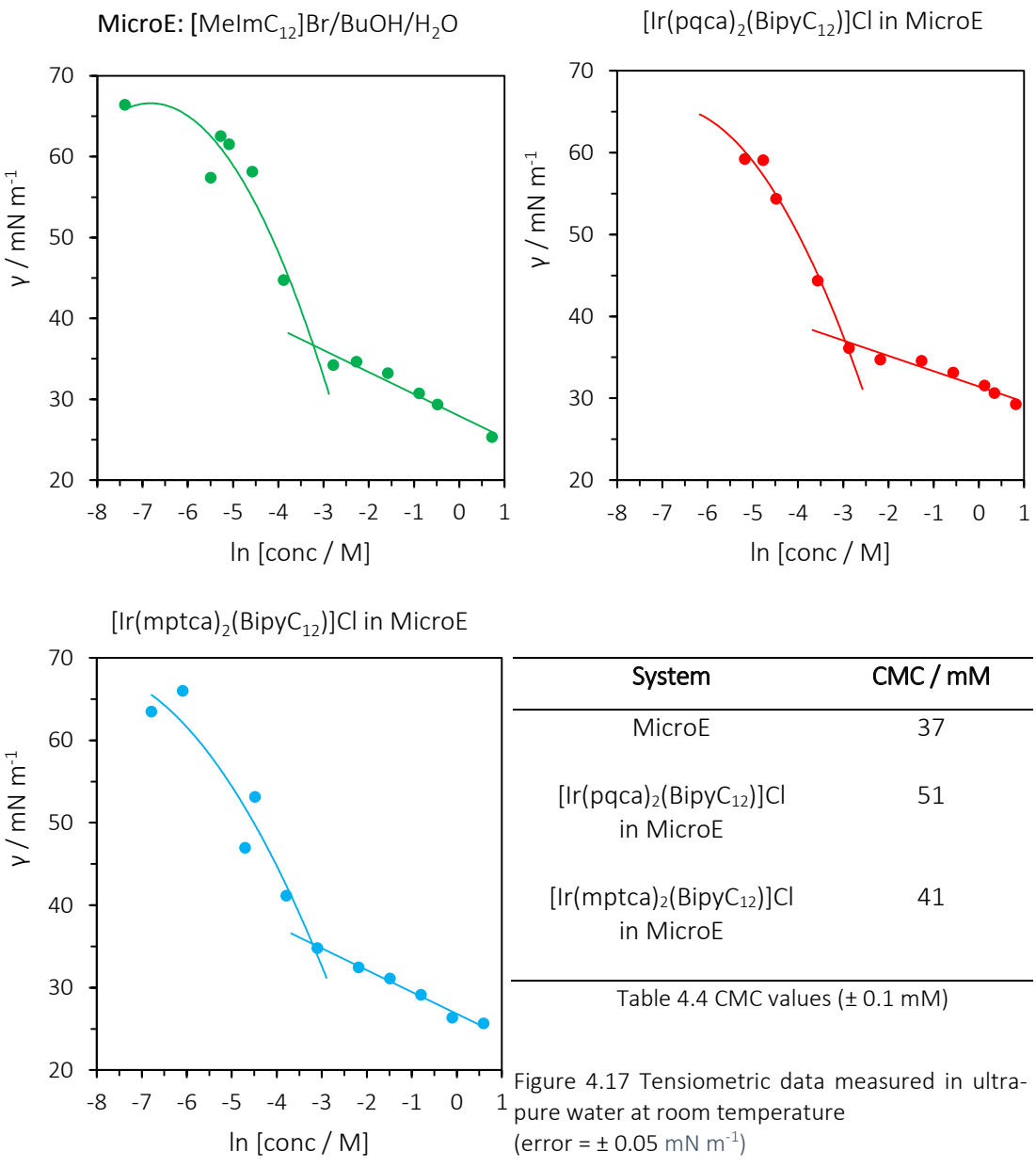

System	CMC / mM
MicroE	37
$[Ir(pqca)_2(BipyC_{12})]Cl$ in MicroE	51
$[Ir(mptca)_2(BipyC_{12})]Cl$ in MicroE	41

Table 4.4 CMC values (± 0.1 mM)

Figure 4.17 Tensiometric data measured in ultra-pure water at room temperature (error = ± 0.05 mN m^{-1})

4.3.5.2 Photophysical Studies of Micellar Solutions

The luminescent nature of the iridium(III) complexes allowed for a combined tensiometric/luminescence spectroscopy study involving measurement of steady state luminescence and lifetimes both below and above the CMC. Measurements were carried out in ultra-pure water so that emission data could be directly correlated with the tensiometry measurements.

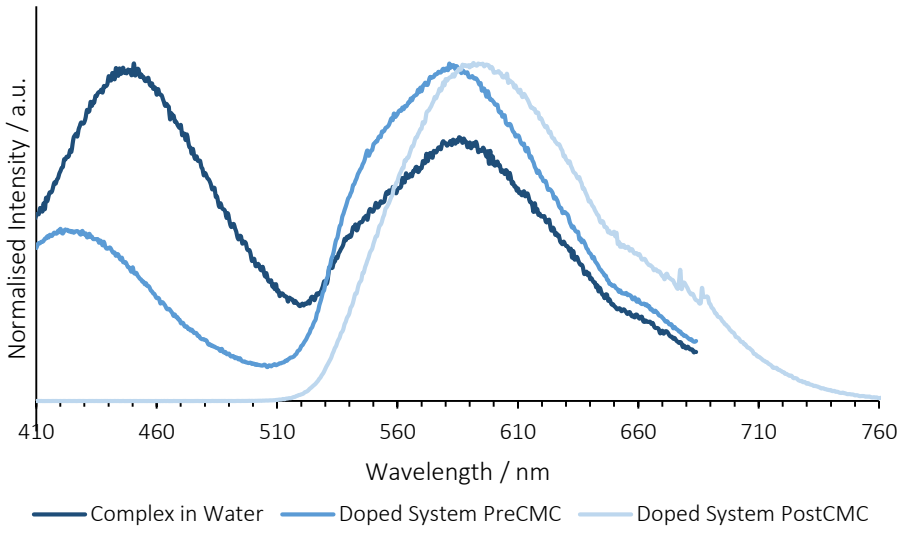

Figure 4.18 Normalised emission of $[Ir(mptca)_2(BpyC_{12})]Cl$ with respect to CMC (measured in ultra-pure water at room temperature, λ_{Ex} = 390 nm)

Figure 4.18 above shows the steady state emission for **$[Ir(mptca)_2(BpyC_{12})]Cl$** in three different environments: (i) complex in water (ii) 2 wt% doping in $[MeImC_{12}]Br/BuOH/H_2O$ below the CMC and (iii) 2 wt% doping in $[MeImC_{12}]Br/BuOH/H_2O$ above the CMC. It is clear from these spectra that the emission properties vary greatly with the concentration relative to the CMC. Both the pure complex in water and the doped system pre-CMC show both ligand centred emission (~410-520 nm) and ^{3}MLCT (~520-670 nm). However, for the doped system post-CMC only ^{3}MLCT emission is observed.

Although the above spectra are normalised, which removes concentration as a variable, the relative ratios between the ligand-centred fluorescence and the ^{3}MLCT phosphorescence peaks are able to provide an insight into the photophysical changes occurring with respect to the CMC. Due to the normalisation it is not easy to tell if the change in ratios is due to aggregation caused quenching (ACQ) of the ligand-centred transitions or aggregation induced emission (AIE) of the ^{3}MLCT.

Some studies report that AIE originates from the micellar structure preventing oxygen diffusion to the chromophores and therefore eliminating quenching. From photophysical studies of the deprotected iridium(III) complexes it was found that they do not act as singlet oxygen sensitisers either as dilute aqueous solutions or as structured micelles. Therefore it may be more probable that the complexes in the micellar environment are undergoing some sort of AIE mechanism.

However, most studies that report AIE of d-block lumophores compare solution with aggregation into the solid state, therefore this in an area which requires further study before definitive conclusions can be made.[60]

Complex	τ in MeCN / ns	τ in water / ns	τ PreCMC / ns*	τ PostCMC / ns
$[Ir(pqca)_2(BpyC_{12})]Cl$	230	332	-	210
$[Ir(mptca)_2(BpyC_{12})]Cl$	270	173	-	159

Table 4.5 Lifetimes of deprotected iridium(III) complexes measured in water; λ_{Ex} = 580-590 nm, measurement error ~10 % (* solutions too dilute to obtain results)

Previous studies have reported a change from single to bi-exponential lifetimes upon aggregation,[30] though for these systems the pre-CMC solutions were too dilute to obtain a lifetime value. However, decrease was observed in the emission lifetime post-CMC compared to the free metallosurfactant in water, suggesting there is some sort of quenching mechanism occurring when the complex is incorporated into the carrier micellar system.

4.4 Conclusions

This chapter reports the synthesis and characterisation of three novel bipyridine-based ligands incorporating lipophilic alkyl chains. These ligands were successfully coordinated to iridium(III) as the ancillary ligands in six novel *bis*-cyclometallated complexes where the cyclometallating ligand could be deprotected to afford hydrophilicity, thus making amphiphilic complexes. These complexes exhibited good ^{3}MLCT emission and long phosphorescence lifetimes in line with previously reported analogues.

Despite ligand-deprotection affording water solubility the complexes were not soluble enough to form micelles on their own. Instead they were successfully doped into the [MeImC_{12}]Br/BuOH/H_2O carrier system described previously. Surface tension measurements showed successful doping of 2 wt% iridium(III) complex into the carrier system which yielded micellar systems with clear, discernible CMC points. These solutions were found to be capable of solubilising at least 10 wt% toluene to form stable microemulsions at room temperature.

Combined tensiometric and photophysical studies provided an insight into the iridium(III)-containing micellar systems. It was found that aggregation of surfactants had a noted effect on the ratio of ligand-centred and ^{3}MLCT emission. This suggests one of two mechanisms occurring above the CMC, either a quenching of ligand-centred fluorescence or an enhancement of ^{3}MLCT emission upon aggregation. However, further studies are needed in order to determine which of these two mechanisms is occurring.

Micellar systems such as these may find roles in applications such as probes for bio-imaging, OLEDs or precursors to mesoporous materials and Langmuir-Blodgett films.

4.5 Experimental

4.5.1 Precursors

Synthesis of 4-methyl-[2,2'-bipyridine]-4'-carboxylic acid[53]

4,4'-Dimethyl-2,2'-bipyridine (4.00 g, 21.7 mmol) and SeO_2 (2.89 g, 26.0 mmol) in 1,4-dioxane (200 mL) were heated to reflux for 24 hours under a N_2 atmosphere. The mixture was filtered hot to remove Se(0), dried *in vacuo* and the crude product suspended in EtOH (100 mL). $AgNO_3$ (4.03 g, 23.5 mmol) in water (40 mL) was added and NaOH (1 M, 100 mL) added dropwise over approx. 30 minutes. The mixture was stirred at RT for 24 hours under a N_2 atmosphere in a foil-covered vessel. The solution was filtered through celite to remove Ag(0) and EtOH removed *in vacuo*. The residue was washed with NaOH (1.3 M, 60 mL) and water, followed by $CHCl_3$ (3x30 mL) to remove unreacted 4,4'-dimethyl-2,2'-bipyridine. The pH of the combined aqueous phases was adjusted to 3.5 using HCl/AcOH (1:1) and the resulting solution filtered to give the title compound as an off-white solid. Yield: 0.9706 g, 4.53 mmol, 18%. ^{1}H NMR (400 MHz, CD_3OD) δ_H = 7.26-7.24 (2H, m, NC(***H***)C(H)C(CO_2H)), 7.07 (1H, d, $^3J_{HH}$ = 5.0 Hz, C(Me)C(***H***)CC), 6.67 (1H, s, C(CO_2H)C(***H***)CC), 6.40 (1H, dd, J_{HH} = 1.5, 5.0 Hz, NC(***H***)C(H)C(Me)), 5.85 (1H, d, $^3J_{HH}$ = 5.3 Hz, NC(H)C(***H***)C(Me)), 1.03 (3H, s, C$\boldsymbol{H}_3$) ppm.

Synthesis of 4-methyl-[2,2'-bipyridine]-4'-carbonyl chloride

4-Methyl-[2,2'-bipyridine]-4'-carboxylic acid (0.18 g, 0.84 mmol) was dissolved in $CHCl_3$ (5 mL). DMF (approx. 4 drops) and thionyl chloride (5 mL) were added and the solution stirred at 60 °C for 24 hours under a N_2 atmosphere. The reaction was cooled to RT and dried *in vacuo* to give the title compound as an orange/red solid. Yield (crude): 0.1932 g, 0.83 mmol, 98%. Due to the moisture sensitivity of the product it was used in in subsequent reactions without purification or characterisation.

Synthesis of ethyl-2-phenylquinoline-4-carboxylate (epqcH)[54]

2-Phenylquinoline-4-carboxylic acid (1.04 g, 4.17 mmol) was dissolved in EtOH (10 mL) and conc. H_2SO_4 (1 mL). The reaction was heated to reflux for 24 hours under a N_2 atmosphere. The solvent was removed *in vacuo* and the crude product dissolved in DCM, washed with water and dried over $MgSO_4$. Solvent was removed *in vacuo* to give the title compound as a yellow oil. Yield: 0.8480 g, 3.06 mmol, 76 %. ^{1}H NMR (400 MHz, $CDCl_3$): δ_H = 8.75 (1H, app. d, $^3J_{HH}$ = 8.5 Hz, $H_{quin.}$), 8.39 (1H, s, C(CO_2Et)C(***H***)), 8.25 (1H, d, $^3J_{HH}$ = 8.4 Hz, $H_{quin.}$), 8.21 (2H, d, $^3J_{HH}$ = 7.2 Hz, $H_{quin.}$), 7.77

(1H, app. t, $^3J_{HH}$ = 7.6 Hz, $H_{phenyl.}$), 7.76 (1H, app. t, $^3J_{HH}$ = 7.6 Hz, $H_{phenyl.}$), 7.54 (2H, app. t, $^3J_{HH}$ = 7.1 Hz, $H_{phenyl.}$), 7.49, (1H, d, $^3J_{HH}$ = 7.0 Hz, $H_{phenyl.}$), 4.54 (2H, q, $^3J_{HH}$ = 7.1 Hz, C***H***$_2$CH$_3$), 1.49 (3H, t, $^3J_{HH}$ = 7.1 Hz, CH$_2$C***H***$_3$) ppm. ^{13}C{^{1}H} NMR (100 MHz, $CDCl_3$) δ_C = 165.7 (***C***O), 156.0, 148.6, 138.1, 135.5, 129.7, 129.5, 129.4, 128.5, 127.4, 127.1, 125.1, 123.7, 119.8, 61.5, 14.0 ppm. LRMS (EI$^+$) found *m/z* 277.11, calculated 277.11 for [M]$^+$. HRMS (EI$^+$) found *m/z* 277.1103, calculated 277.1103 for [$C_{18}H_{15}NO_2$]$^+$. UV/Vis (CH_3CN): λ_{max}/nm (ε/M^{-1}cm^{-1}) = 335 (9200), 259 (41200), 216 sh. (30900), 201 (54300). IR (solid/cm^{-1}): *v* 3057, 2980 (C-H), 1719 (C=O), 1589 (C=C), 1341, 1231, 1192, 1148 (C-O), 766, 691 (C-H).

Synthesis of ethyl-methyl-2-phenylthiazole-5-carboxylate (emptzH)[55]

Thiobenzamide (2.01 g, 14.7 mmol) and ethyl-2-chloroacetoacetate (2.39 g, 14.5 mmol) were heated to reflux in EtOH (30 mL) for 4 hours under a N_2 atmosphere. Solvent was removed *in vacuo* and the crude product dissolved in DCM, washed with aqueous $NaHCO_3$ solution and water, dried over $MgSO_4$ and the solvent removed *in vacuo*. The crude product was recrystallised from MeOH to give the title compound as a white crystalline solid. Yield: 2.4601 g, 9.90 mmol, 68%. ^{1}H NMR (400 MHz, $CDCl_3$) δ_H = 7.96-7.94 (2H, m, $H_{phenyl.}$), 7.45-7.43 (3H, m, $H_{phenyl.}$), 4.34 (2H, q, $^3J_{HH}$ = 7.1 Hz, C***H***$_2$CH$_3$), 2.77 (3H, s, C***H***$_3$), 1.38 (3H, t, $^3J_{HH}$ = 7.1 Hz, CH$_2$C***H***$_3$) ppm. ^{13}C{^{1}H} NMR (100 MHz, $CDCl_3$) δ_C = 170.0, 162.4 (***C***O), 161.1, 133.0, 131.1, 129.1, 126.9, 121.9, 61.3, 17.7, 14.4 ppm. LRMS (EI$^+$) found *m/z* 247.07, calculated 247.07 for [M-2H]$^+$. HRMS (EI$^+$) found m/z 247.0664, calculated 247.0667 for [$C_{13}H_{13}NO_2S$]$^+$. UV/Vis (CH_3CN): λ_{max}/nm (ε/M^{-1}cm^{-1}) = 281 (31200), 250 sh. (21200), 213 (37900). IR (solid/cm^{-1}): *v* 2976 (C-H), 1711 (C=O), 1422 (C=C), 1366, 1321, 1263 br. (C-O), 1096, 1090 (C=S), 768, 756, 687, 656 (C-H).

Synthesis of [Ir(epqc)$_2$(μ-Cl)Ir(epqc)$_2$][10]

$IrCl_3.xH_2O$ (0.18 g, 0.60 mmol) was added to **epqcH** (0.40 g, 1.44 mmol) in 2-methoxyethanol (6 mL) and water (2 mL). The reaction was heated to reflux for 48 hours under a N_2 atmosphere before being cooled to RT. The product was precipitated with water (approx. 20 mL) and filtered to give the title compound as an orange solid. Yield (crude): 0.4687 g, 0.30 mmol, 83%. Product was used without further characterisation or purification.

Synthesis of [Ir(emptz)$_2$(μ-Cl)Ir(emptz)$_2$][10]

Made similarly to **[Ir(epqc)$_2$(μ-Cl)Ir(epqc)$_2$]** but using $IrCl_3.xH_2O$ (0.21 g, 0.70 mmol) and **emptzH** (0.35 g 1.42 mmol) in 2-methoxyethanol (6 mL) and water (2 mL). The product was obtained as

brown solid. Yield (crude): 0.4811 g, 0.33 mmol, 94%. Product was used without further characterisation or purification.

Synthesis of $[Ir(epqc)_2(MeCN)_2](BF_4)$

$AgBF_4$ (0.02 g, 0.10 mmol) in MeCN (10 mL) was added to **$[Ir(epqc)_2(\mu\text{-}Cl)_2Ir(epqc)_2]$** (0.08 g, 0.05 mmol) in MeCN (25 mL) and the solution heated to reflux for 2 hours under a N_2 atmosphere. The solvent was removed *in vacuo* and the product precipitated with DCM/Et_2O to give the title compound as a red crystalline solid. Yield: 0.0600 g, 0.06 mmol, 64% .^{1}H NMR (400 MHz, $CDCl_3$) δ_H = 9.12 (2H, d, $^3J_{HH}$ = 8.9 Hz, $H_{quin.}$), 8.72 (2H, d, $^3J_{HH}$ = 8.4 Hz, $H_{quin.}$), 8.35 (2H, s, $H_{quin.}$), 8.05-7.95 (2H, m, $H_{quin.}$), 7.72 (2H, app. t, $^3J_{HH}$ = 7.7 Hz, H_{phenyl}), 7.60 (2H, d, $^3J_{HH}$ = 7.7 Hz, H_{quin}), 6.87 (2H, app. t, $^3J_{HH}$ = 7.4 Hz, H_{phenyl}), 6.64 (2H, app. t, $^3J_{HH}$ = 7.5 Hz, H_{phenyl}), 5.70 (2H, d, $^3J_{HH}$ = 7.2 Hz, C(Ir)C(***H***)), 4.58 (4H, q, $^3J_{HH}$ = 7.2 Hz, OC***H***$_2CH_3$), 2.24 (6H, s, C***H***$_3$CN), 1.51 (6H, t, $^3J_{HH}$ = 7.2 Hz, OCH_2C***H***$_3$) ppm. $^{13}C\{^1H\}$ NMR (125 MHz, $CDCl_3$) δ_C = 165.5 (***C***O), 149,1, 145.9, 132.7, 131.4, 130.4, 128.6, 128.4, 127.0, 126.5, 126.3, 124.8, 122.3, 118.1, 70.1, 65.9, 63.4, 62.8, 59.2, 14.7, 3.5, 1.1 ppm. HRMS (ES^+) found *m/z* 745.1664, calculated 745.1671 for $[IrC_{36}H_{28}N_2O_4]^+$. UV/Vis (CH_3CN): λ_{max}/nm ($\varepsilon/M^{-1}cm^{-1}$) = 313 (29300), 273 (59000), 234 (67400). IR (solid/cm^{-1}): *v* 2980, 2963 (C-H), 2372, 2311 (C≡N), 1717 (C=O), 1541 (N-H), 1375 (C-H), 1261, 1242 (C-O), 1057, 1016 br. (B-F), 793, 762 (C-H).

Synthesis of $[Ir(emptz)_2(MeCN)_2](BF_4)$

Made similarly to **$[Ir(epqc)_2(MeCN)_2](BF_4)$** but using **$[Ir(emptz)_2(\mu\text{-}Cl)_2Ir(emptz)_2]$** (0.10 g, 0.07 mmol) in MeCN (25 mL) with $AgBF_4$ (0.03 g, 0.15 mmol) in MeCN (10 mL) to give the title compound as an orange crystalline solid. Yield: 0.0894 g, 0.10 mmol, 75%. ^{1}H NMR (400 MHz, $CDCl_3$) δ_H = 7.53 (2H, d, $^3J_{HH}$ = 5.6 Hz, H_{phenyl}), 6.94 (2H, app. t, $^3J_{HH}$ = 6.0 Hz, H_{phenyl}), 6.84 (2H, app. t, $^3J_{HH}$ = 8.0 Hz, H_{phenyl}), 6.22 (2H, d, $^3J_{HH}$ = 7.4 Hz, C(Ir)C(***H***)), 4.47 (4H, q, $^3J_{HH}$ = 5.8 Hz, OC***H***$_2CH_3$), 3.08 (6H, s, C***H***$_3$CN), 2.43 (6H, s, (C)C***H***$_3$), 1.47 (6H, t, $^3J_{HH}$ = 9.5 Hz, OCH_2C***H***$_3$) ppm. $^{13}C\{^1H\}$ NMR (125 MHz, $CDCl_3$) δ_C = 182.1, 160.9 (***C***O), 159.9, 143.0, 140.4, 132.5, 131.7, 125.3, 123.5, 121.7, 120.1, 62.4, 17.3, 14.5, 3.68 ppm. HRMS (ES^+) found *m/z* 767.1328, calculated 767.1331 for $[IrC_{30}H_{30}N_4O_4S_2]^+$. UV/Vis ($CH_3CN$): λ_{max}/nm ($\varepsilon/M^{-1}cm^{-1}$) = 414 (18000), 306 (56300), 254 (33200). IR (solid/cm^{-1}): *v* 2986, 2980 (C-H), 2374, 2322 (C≡N), 1715 (C=O), 1558 (N-H), 1379 (C-H), 1290, 1263 (C-O), 1055 (B-F), 761, 731 (C-H).

4.5.2 Ligands

Synthesis of *N*-dodecyl-4'-methyl-[2,2'-bipyridine]-4-carboxamide ($BpyC_{12}$)

4'-Methyl-[2,2'-bipyridine]-4-carbonyl chloride (0.19 g, 0.82 mmol) and 1-dodecylamine (0.15 g, 0.81 mmol) were dissolved in MeCN (5 mL) with *N,N*-diisopropylethylamine (0.48 mL, 2.76 mmol) and stirred at 60 °C for 24 hours under a N_2 atmosphere. The solvent was removed *in vacuo* and the crude product dissolved in DCM, washed with water and dried over $MgSO_4$. Solvent was removed *in vacuo* to give the title compound as a brown solid. Yield: 0.1018 g, 0.27 mmol, 33%. ^{1}H NMR (400 MHz, $CDCl_3$) δ_H = 8.75 (1H, d, $^3J_{HH}$ = 5.0 Hz, NC(***H***)C(H)C(CO)), 8.57 (1H, s, C(Me)C(***H***)C), 8.49 (1H, d, $^3J_{HH}$ = 5.0 Hz, NC(***H***)C(H)C(Me)), 1.23 (1H, s, C(CO)C(***H***)C), 7.75 (1H, dd, J_{HH} = 1.7, 5.0 Hz, C(CO)C(***H***)C(H)), 7.15 (1H, dd, J_{HH} = 0.6, 4.9 Hz, C(Me)C(***H***)C(H)), 6.76-6.72 (1H, m, N***H***), 3.48 (2H, q, $^3J_{HH}$ = 6.2 Hz, N(H)C***H***$_2$-), 2.85 (3H, s, (C)C***H***$_3$), 1.69-1.60 (2H, m, N(H)CH$_2$C***H***$_2$-), 1.39-1.15 (18H, br. m, -(C***H***$_2$)$_9$-), 0.85 (3H, t, $^3J_{HH}$ = 6.8 Hz, CH$_2$C***H***$_3$) ppm. ^{13}C{^{1}H} NMR (100 MHz, $CDCl_3$) δ_C = 165.6 (***C***O), 156.7, 155.1, 150.3, 149.0, 148.9, 143.2, 125.4, 122.6, 122.2, 117.6, 40.4, 32.0, 29.8, 29.7, 29.6, 29.5, 29.4, 27.1, 22.8, 21.4, 14.2 ppm. LRMS (ES$^+$) found m/z 382.29, calculated 382.29 for [M+H]$^+$. HRMS (ES$^+$) found m/z 382.2851, calculated 382.2850 for [$C_{24}H_{36}N_3O$]$^+$. UV/Vis (CH_3CN): λ_{max}/nm (ε/M^{-1}cm^{-1}) = 278 (19400), 250 (14200), 245 sh. (13300), 206 (15800). IR (solid/cm^{-1}): *v* 3306 (N-H), 2940, 2918, 2849 (C-H), 1632 (C=O), 1526 (N-H), 1258 (C-H).

Synthesis of *N*-decyl-4'-methyl-[2,2'-bipyridine]-4-carboxamide ($BpyC_{10}$)

Made similarly to **$BpyC_{12}$** but using 4'-methyl-[2,2'-bipyridine]-4-carbonyl chloride (0.44 g, 1.89 mmol), 1-decylamine (0.42 mL, 2.10 mmol) and *N,N*-diisopropylethylamine (1.12 mL, 6.43 mmol) in MeCN (5 mL) to give the title compound as a brown solid. Yield: 0.2040 g, 0.58 mmol, 31%. ^{1}H NMR (400 MHz, $CDCl_3$) δ_H = 8.74 (1H, d, $^3J_{HH}$ = 5.0 Hz, NC(***H***)C(H)C(CO)), 8.57 (1H, s, C(Me)C(***H***)C), 8.49 (1H, d, $^3J_{HH}$ = 5.0 Hz, NC(***H***)C(H)C(Me)), 8.22 (1H, s, C(CO)C(***H***)C), 7.74 (1H, app. dd, J_{HH} = 1.7, 5.0 Hz, C(CO)C(***H***)C(H)), 7.13 (1H, d, $^3J_{HH}$ = 4.2 Hz, C(Me)C(***H***)C(H)), 6.76-6.73 (1H, br. s, N***H***), 3.43 (2H, q, $^3J_{HH}$ = 6.8 Hz, N(H)C***H***$_2$-), 2.43 (3H, s, (C)C***H***$_3$), 1.59 (2H, app. t, $^3J_{HH}$ = 7.1 Hz, N(H)CH$_2$C***H***$_2$-), 1.33-1.23 (14H, br. m, -(C***H***$_2$)$_7$-), 0.85 (3H, t, $^3J_{HH}$ = 6.8 Hz, CH$_2$C***H***$_3$) ppm. ^{13}C{^{1}H} NMR (100 MHz, $CDCl_3$) δ_C = 165.8 (***C***O), 156.9, 155.2, 150.1, 149.0, 148.6, 143.0, 125.3, 122.3, 122.0, 117.4, 41.1, 40.4, 36.2, 32.0, 30.5, 29.6, 29.4, 27.1, 22.8, 21.3, 14.2 ppm. LRMS (ES$^+$) found m/z 354.26, calculated 354.25 for [M+H]$^+$. HRMS (ES$^+$) found m/z 354.2538, calculated 354.2538 for [$C_{22}H_{32}N_3O$]$^+$. UV/Vis (CH_3CN): λ_{max}/nm (ε/M^{-1}cm^{-1}) = 277 (23000), 250 (16000), 245 sh. (14900),

206 (16900). IR (solid/cm^{-1}): *v* 3304 (N-H), 2955, 2920, 2849 (C-H), 1630 (C=O), 1526 (N-H), 1267 (C-H).

Synthesis of *N*-octyl-4'-methyl-[2,2'-bipyridine]-4-carboxamide ($BpyC_8$)

Made similarly to **$BpyC_{12}$** but using 4'-methyl-[2,2'-bipyridine]-4-carbonyl chloride (0.47 g, 2.02 mmol), 1-octylamine (0.37 g, 2.86 mmol) and *N,N*-diisopropylamine (1.20 mL, 6.89 mmol) in MeCN (5 mL) to give the title compound as a brown solid. Yield: 0.2247 g, 0.69 mmol, 34%. ^{1}H NMR (400 MHz, $CDCl_3$) δ_H = 8.76 (1H, d, $^3J_{HH}$ = 5.0 Hz, NC(***H***)C(H)C(CO)), 8.57 (1H, s, C(Me)C(***H***)C), 8.50 (1H, d, $^3J_{HH}$ = 5.0 Hz, NC(***H***)C(H)C(Me)), 8.24 (1H, s, C(CO)C(***H***)C), 7.75 (1H, app. dd, J_{HH} = 1.7, 5.0 Hz, C(CO)C(***H***)C(H)), 7.16-7.14 (1H, m, C(Me)C(***H***)C(H)), 6.67-6.59 (1H, br. s, N***H***), 3.44 (2H, q, $^3J_{HH}$ = 6.8 Hz, N(H)C***H***$_2$-), 2.43 (3H, s, (C)C***H***$_3$), 1.62-1.58 (2H, m, N(H)CH_2C***H***$_2$-), 1.35-1.25 (10H, br. s, -(C***H***$_2$)$_5$-), 0.85 (3H, t, $^3J_{HH}$ = 6.8 Hz, CH_2C***H***$_3$) ppm. ^{13}C{^{1}H} NMR (100 MHz, $CDCl_3$) δ_C = 165.7 (***C***O), 156.9, 155.1, 150.0, 148.9, 148.5, 143.0, 125.2, 122.2, 121.8, 117.5, 40.4, 31.8, 29.5, 29.2, 27.0, 22.7, 21.2, 14.1 ppm. LRMS (ES^+) found m/z 326.22, calculated 326.22 for $[M+H]^+$. HRMS (ES^+) found m/z 326.2227, calculated 326.2226 for $[C_{20}H_{28}N_3O]^+$. UV/Vis (CH_3CN): λ_{max}/nm ($\varepsilon/M^{-1}cm^{-1}$) = 284 (9500), 250 sh. (8900), 243 (9200), 208 (13600). IR (solid/ cm^{-1}): *v* 3302 (N-H), 2922, 2940, 2847 (C-H), 1630 (C=O), 1526 (N-H), 1258 (C-H).

4.5.3 Complexes

Synthesis of $[Ir(emptz)_2(BpyC_{12})](BF_4)$

$[Ir(emptz)_2(MeCN)_2](BF_4)$ (0.05 g, 0.06 mmol) and **$BpyC_{12}$** (0.02 g, 0.06 mmol) were dissolved in $CHCl_3$ (8 mL). The reaction was heated to reflux for 24 hours under a N_2 atmosphere. Solvent was removed *in vacuo* and the product precipitated from DCM/Et_2O to give the title compound as a red/orange solid. Yield: 0.0160 g, 0.01 mmol, 24%. ^{1}H NMR (400 MHz, $CDCl_3$) δ_H = 9.01 (1H, s, H_{N^N}), 8.84 (1H, s, H_{N^N}), 8.25 (1H, app. t, $^3J_{HH}$ = 5.0 Hz, H_{N^N}), 7.96 (2H, q, $^3J_{HH}$ = 6.9 Hz, H_{N^N}), 7.71-7.68 (2H, m, H_{C^N}), 7.22 (1H, d, $^3J_{HH}$ = 5.4 Hz, H_{N^N}), 7.09 (2H, q, $^3J_{HH}$ = 6.1 Hz, H_{C^N}), 6.98 (2H, q, $^3J_{HH}$ = 6.2 Hz, H_{C^N}), 6.42 (2H, d, $^3J_{HH}$ = 7.6 Hz, C(Ir)C(***H***)), 4.32 (4H, q, $^3J_{HH}$ = 6.3 Hz, OC***H***$_2$$CH_3$), 3.47 (2H, q, $^3J_{HH}$ = 6.8 Hz, NHC***H***$_2$), 2.67 (3H, s, C***H***$_{3\ N^N}$), 1.85 (3H, s, C***H***$_{3\ C^N}$), 1.83 (3H, s, C***H***$_{3\ C^N}$), 1.71 (2H, app. t, $^3J_{HH}$ = 6.9 Hz, $NHCH_2$C***H***$_2$), 1.34 (6H, t, $^3J_{HH}$ = 7.0 Hz, OCH_2C***H***$_3$), 1.23-1.21 (18H, br. m, -(C***H***$_2$)$_9$-), 0.86 (3H, t, $^3J_{HH}$ = 6.4 Hz, $(CH_2)_{12}$C***H***$_3$) ppm. ^{13}C{^{1}H} NMR (100 MHz, $CDCl_3$) δ_C = 182.4, 182.2, 162.9 (***C***O), 160.4 (***C***O), 160.3 (***C***O) 158.5, 158.4, 157.1, 155.6, 153.7, 150.5, 149.4, 149.3, 149.1, 145.4, 133.2, 132.5, 132.4, 129.3, 127.3, 127.1, 126.2, 126.1, 123.8, 123.7, 121.6, 120.6, 120.5, 66.0, 62.4, 41.1, 32.0, 29.8, 29.7, 29.5, 29.1, 22.8, 21.4, 15.5, 15.4, 15.1, 14.3, 14.2 ppm.

LRMS (ES^+) found *m/z* 1066.35, calculated 1066.36 for $[M\text{-}BF_4]^+$. HRMS (ES^+) found m/z 1066.3556, calculated 1066.3573 for $[IrC_{50}H_{59}N_5O_5S_2]^+$. UV/Vis ($CH_3CN$): λ_{max}/nm ($\varepsilon/M^{-1}cm^{-1}$) = 435 (8000), 299 (42300), 269 (41600). IR (solid/cm^{-1}): *v* 2924, 2853 (C-H), 1717, 1699 (C=O), 1543, 1541 (C=C), 1456, 1373 (C-O), 1288, 1258 (C=O), 1098, 1057 (B-F), 669 (C-H).

Synthesis of $[Ir(emptz)_2(BpyC_{10})](BF_4)$

Made similarly to **$[Ir(emptz)_2(BpyC_{12})](BF_4)$** but using **$[Ir(emptz)_2(MeCN)_2](BF_4)$** (0.05 g, 0.06 mmol) and **$BpyC_{10}$** (0.02 g, 0.06 mmol) in $CHCl_3$ (8 mL) to give the title compound as red/orange solid. Yield: 0.0520 g, 0.05 mmol, 77%. ^{1}H NMR (400 MHz, $CDCl_3$) δ_H = 9.03 (1H, s, H_{N^N}), 8.86 (1H, s, H_{N^N}), 8.29-8.24 (1H, br. s, H_{N^N}), 7.98 (1H, dd, J_{HH} = 1.6, 5.7 Hz, H_{N^N}), 7.93 (1H, d, $^3J_{HH}$ = 5.8 Hz, H_{N^N}), 7.71 (1H, qd, J_{HH} = 0.9, 4.0 Hz, H_{C^N}), 7.67 (1H, d, $^3J_{HH}$ =5.6 Hz, H_{C^N}), 7.21 (1H, dd, J_{HH} = 0.7, 5.5 Hz, H_{N^N}), 7.10 (2H, qd, J_{HH} = 1.1, 8.6 Hz, H_{C^N}), 6.99 (2H, qd, J_{HH} = 1.4, 6.8 Hz, H_{C^N}), 6.42 (2H, d, $^3J_{HH}$ = 7.6 Hz, C(Ir)C(***H***)), 4.37-4.29 (4H, m, OC***H***$_2$CH$_3$), 3.49 (2H, q, $^3J_{HH}$ = 6.8 Hz, NC***H***$_2$), 2.69 (3H, s, C***H***$_{3\ N^N}$), 1.86 (3H, s, C***H***$_{3\ C^N}$), 1.84 (3H, s, C***H***$_{3\ C^N}$), 1.72 (2H, app. t, $^3J_{HH}$ = 7.1 Hz, NHCH$_2$C***H***$_2$), 1.35 (6H, q, $^3J_{HH}$ = 7.0 Hz, OCH$_2$C***H***$_3$), 1.27-1.24 (14H, br. m, -(C***H***$_2$)$_7$-), 0.86 (3H, t, $^3J_{HH}$ = 6.9 Hz, (CH$_2$)$_{10}$C***H***$_3$), ppm. ^{13}C{^{1}H} NMR (100 MHz, $CDCl_3$) δ_C = 182.4, 182.2, 163.1 (***C***O), 160.4 (***C***O), 158.5, 158.4, 157.1, 155.6, 153.7, 150.5, 149.5, 149.3, 149.1, 148.7, 147.2, 145.5, 140.0, 140.0, 133.3, 132.6, 132.5, 129.3, 127.4, 127.1, 126.2, 126.1, 123.8, 123.7, 121.7, 120.7, 120.5, 62.5, 62.4, 41.1, 32.1, 29.8, 29.5, 29.2, 27.2, 22.8, 21.5, 15.6, 15.1, 14.3 ppm. HRMS (ES^+) found m/z 1038.3240, calculated 1038.3261 for $[IrC_{48}H_{55}N_5O_5S_2]^+$. UV/Vis ($CH_3CN$): λ_{max}/nm ($\varepsilon/M^{-1}cm^{-1}$) = 436 (7100), 368 (9200), 308 (33000), 269 (27800), 209 (50900). IR (solid/cm^{-1}): *v* 2941, 2926, 2853 (C-H), 1717 (C=O), 1541 (N-H), 1373 (C-H), 1288, 1256 (C-O), 1092, 1026 br. (B-F), 799, 762 (C-H).

Synthesis of $[Ir(emptz)_2(BpyC_8)](BF_4)$

Made similarly to **$[Ir(emptz)_2(BpyC_{12})](BF_4)$** but using **$[Ir(emptz)_2(MeCN)_2](BF_4)$** (0.05 g, 0.06 mmol) and **$BpyC_8$** (0.02 g, 0.06 mmol) in $CHCl_3$ (8 mL) to give the title compound as a red/orange solid. Yield: 0.0447 g, 0.04 mmol, 68%. ^{1}H NMR (400 MHz, $CDCl_3$) δ_H = 9.00 (1H, s, H_{N^N}), 8.84 (1H, s, H_{N^N}), 8.23 (1H, app. t, $^3J_{HH}$ = 5.7 Hz, H_{N^N}), 7.96 (2H, app. dd, J_{HH} = 5.7, 16.3 Hz, H_{N^N}), 7.72-7.69 (2H, m, H_{C^N}), 7.22 (1H, d, $^3J_{HH}$ = 5.5 Hz, H_{N^N}), 7.10 (2H, dd, J_{HH} = 7.4, 12.5 Hz, H_{C^N}), 6.99 (2H, dd, J_{HH} =7.4, 13.5 Hz, H_{C^N}), 6.42 (2H, d, $^3J_{HH}$ = 7.6 Hz, C(Ir)C(***H***)), 4.32 (4H, q, $^3J_{HH}$ = 6.9 Hz, OC***H***$_2$CH$_3$), 3.39 (2H, q, $^3J_{HH}$ = 6.7 Hz, NHC***H***$_2$), 2.68 (3H, s, C***H***$_{3\ N^N}$), 1.86 (3H, s, C***H***$_{3\ C^N}$), 1.84 (3H, s, C***H***$_{3\ C^N}$), 1.71 (2H, app. t, $^3J_{HH}$ = 7.2 Hz, NHCH$_2$C***H***$_2$), 1.35 (6H, t, $^3J_{HH}$ = 7.1 Hz, OCH$_2$C***H***$_3$), 1.28-1.24 (10H, br. m, -(C***H***$_2$)$_5$-), 0.85 (3H, t, $^3J_{HH}$ = 6.7 Hz, (CH$_2$)$_5$C***H***$_3$) ppm. ^{13}C{^{1}H} NMR (100 MHz, $CDCl_3$) δ_C = 182.4, 182.2, 163.0 (***C***O), 160.4 (***C***O), 160.3 (***C***O), 158.5, 158.4, 157.1, 155.6, 153.7, 150.5, 149.5, 149.3,

149.1, 145.4, 140.0, 133.3, 132.6, 132.5, 129.3, 127.4, 127.1, 126.2, 123.8, 123.7, 121.6, 120.6, 120.5, 62.5, 62.4, 41.1, 32.0, 29.4, 29.1, 27.2, 22.8, 21.5, 15.5, 15.1, 14.3 ppm. HRMS (ES^+) found m/z 1010.2933, calculated 1010.2949 for $[IrC_{46}H_{51}N_5O_5S_2]^+$. UV/Vis ($CH_3CN$): λ_{max}/nm ($\varepsilon/M^{-1}cm^{-1}$) = 434 (6100), 365 (7000), 315 sh. (29300), 298 (34100), 273 (34900), 212 (39300). IR (solid/cm^{-1}): *v* 2961, 2926 (C-H), 1717 (C=O), 1541 (N-H), 1373 (C-H), 1288, 1258 (C-O), 1090, 1011 br. (B-F), 797, 762 (C-H).

Synthesis of $[Ir(epqc)_2(BpyC_{12})](BF_4)$

Made similarly to **$[Ir(emptz)_2(BpyC_{12})](BF_4)$** but using **$[Ir(epqc)_2(MeCN)_2](BF_4)$** (0.05 g, 0.05 mmol) and **$BpyC_{12}$** (0.02 g, 0.05 mmol) in $CHCl_3$ (8 mL) to give the title compound as a red/brown solid. Yield: 0.0485 g, 0.04 mmol, 73%. ^{1}H NMR (400 MHz, $CDCl_3$) δ_H = 8.61 (1H, d, $^3J_{HH}$ = 15.3 Hz, H_{C^N}), 8.61 (1H, s, H_{N^N}), 8.56 (1H, s, H_{N^N}), 8.53 (1H, d, $^3J_{HH}$ = 8.4 Hz, H_{C^N}), 8.41 (1H, s, H_{C^N}), 8.18 (1H, d, $^3J_{HH}$ = 5.8 Hz, H_{N^N}), 8.14-8.10 (1H, m, $H_{arom.}$), 8.06 (2H, app. t, $^3J_{HH}$ = 8.5 Hz, $H_{arom.}$), 8.00 (1H, d, $^3J_{HH}$ = 5.3 Hz, $H_{arom.}$), 7.90 (1H, d, $^3J_{HH}$ = 5.5 Hz, H_{N^N}), 7.45-7.38 (4H, m, H_{C^N}), 7.22-7.17 (3H, m, $H_{arom.}$), 7.07 (1H, app. t, $^3J_{HH}$ = 7.5 Hz, H_{C^N}), 7.00 (1H, app. t, $^3J_{HH}$ = 7.8 Hz, H_{C^N}), 6.84 (2H, q, $^3J_{HH}$ = 6.5 Hz, H_{C^N}), 6.50 (2H, d, $^3J_{HH}$ = 7.0 Hz, C(Ir)C(***H***)), 4.60 (4H, q, $^3J_{HH}$ = 6.9 Hz, OC***H***$_2CH_3$), 3.41 (2H, q, $^3J_{HH}$ = 6.8 Hz, NC***H***$_2$), 2.52 (3H, s, CC***H***$_3$), 1.65-1.62 (2H, m, NCH_2C***H***$_2$), 1.55 (6H, t, $^3J_{HH}$ = 6.6 Hz, OCH_2C***H***$_3$), 1.28-1.19 (18H, m, -(C***H***$_2)_9$-), 0.86 (3H, t, $^3J_{HH}$ = 6.3 Hz, $(CH_2)_9C$***H***$_3$) ppm. $^{13}C\{^1H\}$ NMR (100 MHz, $CDCl_3$) δ_C = 169.5 (***C***O), 165.2 (***C***O), 165.0 (***C***O), 156.4, 155.0, 153.4, 151.1, 151.0, 148.3, 148.2, 147.9, 146.4, 145.2, 145.1, 144.7, 138.9, 138.8, 134.9, 134.8, 131.9, 131.6, 131.5, 131.4, 128.8, 128.6, 128.3, 127.6, 127.3, 127.1, 126.9, 126.4, 125.2, 125.1, 124.6, 124.4, 123.6, 123.4, 121.2, 118.9, 118.5, 66.0, 63.0, 62.9, 41.0, 32.0, 29.8, 29.7, 29.5, 29.4, 29.1, 27.2, 22.8, 21.3, 15.4, 14.5, 14.2 ppm. LRMS (ES^+) found *m/z* 1126.45, calculated 1126.45 for $[M\text{-}BF_4]^+$. HRMS (ES^+) found *m/z* 1126.4438, calculated 1126.4443 for $[IrC_{60}H_{63}N_5O_5]^+$. UV/Vis (CH_3CN): λ_{max}/nm ($\varepsilon/M^{-1}cm^{-1}$) = 468 (2700), 354 (15300), 354 (15300), 288 (28900), 262 (31800), 247 (29600), 211 (53400). IR (solid/cm^{-1}): *v* 2961, 2922 (C-H), 1719 (C=O), 1539 (N-H), 1375 (C-H), 1260, 1240 (C-O), 1078. 1013 br. (B-F), 791, 764 (C-H).

Synthesis of $[Ir(epqc)_2(BpyC_{10})](BF_4)$

Made similarly to **$[Ir(emptz)_2(BpyC_{12})](BF_4)$** but using **$[Ir(epqc)_2(MeCN)_2](BF_4)$** (0.05 g, 0.05 mmol) and **$BpyC_{10}$** (0.02 g, 0.05 mmol) in $CHCl_3$ (8 mL) to give the title compound as a red/brown solid. Yield: 0.0492 g, 0.04 mmol, 83%. ^{1}H NMR (400 MHz, $CDCl_3$) δ_H = 8.63-8.56 (3H, m, $H_{arom.}$), 8.56 (1H, s, H_{N^N}), 8.54 (1H, dd, J_{HH} = 1.0, 8.5 Hz, H_{C^N}), 8.43 (1H, s, H_{C^N}), 8.17 (1H, d, $^3J_{HH}$ = 5.6 Hz, H_{N^N}), 8.11-8.04 (3H, m, $H_{arom.}$), 8.01 (1H, dd, J_{HH} = 1.6, 5.7 Hz, $H_{arom.}$), 7.89 (1H, d, $^3J_{HH}$ = 5.8 Hz,

H_{N^N}), 7.49-7.43 (2H, m, H_{C^N}), 7.39 (2H, app. t, $^3J_{HH}$ = 7.9 Hz, H_{C^N}), 7.19 (2H, app. t, $^3J_{HH}$ = 7.3 Hz, $H_{arom.}$), 7.09-7.05 (1H, m, H_{C^N}), 7.02-6.98 (1H, m, H_{C^N}), 6.87-6.82 (2H, m, H_{C^N}), 6.50 (2H, d, $^3J_{HH}$ = 8.0 Hz, C(Ir)C(***H***)), 4.62 (4H, q, $^3J_{HH}$ = 7.1 Hz, OC***H***$_2$CH$_3$), 3.41 (2H, q, $^3J_{HH}$ = 6.7 Hz, NC***H***$_2$), 2.54 (3H, s, CC***H***$_3$), 1.66-1.62 (2H, m, NCH$_2$C***H***$_2$), 1.56 (6H, app. td, J_{HH} = 2.2, 7.1 Hz, OCH$_2$C***H***$_3$), 1.29-1.22 (14H, m, -(C***H***$_2$)$_7$-), 0.85 (3H, t, $^3J_{HH}$ = 6.9 Hz, (CH$_2$)$_7$C***H***$_3$) ppm. ^{13}C{^{1}H} NMR (100 MHz, $CDCl_3$) δ_C = 169.4 (***C***O), 165.1 (***C***O), 162.5 (***C***O), 156.4, 155.0, 153.4, 148.2, 147.9, 145.2, 145.1, 138.9, 132.0, 131.5, 128.9, 128.6, 127.1, 126.9, 125.2, 124.6, 123.6, 121.2, 118.9, 118.5, 63.0, 32.0, 29.7, 27.2, 22.8, 21.3, 14.5, 14.3 ppm. HRMS (ES$^+$) found m/z 1098.4111, calculated 1098.4131 for $[IrC_{58}H_{59}N_5O_5]^+$. UV/Vis (CH_3CN): λ_{max}/nm (ε/M^{-1}cm^{-1}) = 461 (2600), 355 (14000), 289 (25900), 267 (29900), 247 (26600), 210 (47700). IR (solid/cm^{-1}): *v* 2961, 2926, 2853 (C-H), 1719 (C=O), 1375 (C-H), 1539 (N-H), 1261, 1240 (C-O), 1065, 1016 br. (B-F), 760, 762 (C-H).

Synthesis of [Ir(epqc)$_2$(BpyC$_8$)](BF$_4$)

Made similarly to **[Ir(emptz)$_2$(BpyC$_{12}$)](BF$_4$)** but using **[Ir(epqc)$_2$(MeCN)$_2$](BF$_4$)** (0.05 g, 0.05 mmol) and **BpyC$_8$** (0.02 g, 0.05 mmol) in $CHCl_3$ (8 mL) to give the title compound as a red/brown solid. Yield: 0.0503 g, 0.04 mmol, 87%. ^{1}H NMR (400 MHz, $CDCl_3$) δ_H = 8.62 (1H, dd, J_{HH} = 0.9, 14.0 Hz, H_{C^N}), 8.61 (1H, s, H_{N^N}), 8.57 (1H, s, H_{N^N}), 8.54 (1H, dd, J_{HH} = 1.0, 8.5 Hz, H_{C^N}), 8.41 (1H, s, H_{C^N}), 8.19 (1H, d, $^3J_{HH}$ = 5.8 Hz, H_{N^N}), 8.12 (1H, app. t, $^3J_{HH}$ = 5.7 Hz, $H_{arom.}$), 8.06 (2H, app. t, $^3J_{HH}$ = 8.2 Hz, $H_{arom.}$), 8.01 (1H, dd, J_{HH} = 1.6, 5.8 Hz, $H_{arom.}$), 7.90 (1H, d, $^3J_{HH}$ = 5.7 Hz, H_{N^N}), 7.48-7.36 (4H, m, H_{C^N}), 7.20 (3H, q, $^3J_{HH}$ = 7.6 Hz, $H_{arom.}$), 7.09-7.05 (1H, m, H_{C^N}), 7.02-6.98 (1H, m, H_{C^N}), 6.87-6.81 (2H, m, H_{C^N}), 6.50 (2H, dd, J_{HH} = 2.7, 7.1 Hz, C(Ir)C(***H***)), 4.61 (4H, q, $^3J_{HH}$ = 7.1 Hz, OC***H***$_2$CH$_3$), 3.44-3.39 (2H, m, NC***H***$_2$), 2.52 (3H, s, CC***H***$_3$), 1.64 (2H, app. t, $^3J_{HH}$ = 6.9 Hz, NCH$_2$C***H***$_2$), 1.55 (6H, app. td, J_{HH} = 2.2, 7.2 Hz, OCH$_2$C***H***$_3$), 1.28-1.21 (10H, br. m, -(C***H***$_2$)$_5$-), 0.83 (3H, t, $^3J_{HH}$ = 6.8 Hz, (CH$_2$)$_5$C***H***$_3$) ppm. ^{13}C{^{1}H} NMR (125 MHz, $CDCl_3$) δ_C = 169.6 (***C***O), 165.1 (***C***O), 162.6 (***C***O), 156.4, 155.0, 153.4, 151.1, 151.0, 148.3, 148.2, 147.9, 145.1, 144.8, 139.0, 138.9, 134.9, 132.0, 131.7, 131.6, 131.5, 129.1, 128.9, 128.6, 128.3, 127.7, 127.3, 127.2, 126.9, 126.5, 146.4, 63.0, 41.1, 32.0, 29.4, 29.1, 27.2, 22.8, 21.3, 14.5, 14.2, 1.2 ppm. HRMS (ES$^+$) found m/z 1070.3805, calculated 1070.3819 for $[IrC_{56}H_{55}N_5O_5]^+$. UV/Vis (CH_3CN): λ_{max}/nm (ε/M^{-1}cm^{-1}) = 461 (4500), 351 (25400), 289 (63000), 264 (70500), 208 (92300). IR (solid/cm^{-1}): *v* 2963, 2924 (C-H), 1719 (C=O), 1373 (C-H), 1539 (N-H), 1259, 1238 (C-O), 1078, 1015 br. (B-F), 793, 762 (C-H).

4.5.4 Deprotected Complexes

Synthesis of $[Ir(mptca)_2(BpyC_{12})]Cl$

$[Ir(emptz)_2(BpyC_{12})](BF_4)$ (0.03 g, 0.03 mmol) and KOH (1 M, 10 mL) in acetone (10 mL) were stirred at RT for 24 hours under a N_2 atmosphere. Solvent was removed *in vacuo*, water (approx. 20 mL) was added and the solution neutralised with HCl (1 M). Water was removed *in vacuo* and the crude product dissolved in MeOH (10 mL). The solution was filtered to remove salts and dried *in vacuo* to give the title compound as an orange solid. Yield: 0.0243 g, 0.02 mmol, 85%. ^{1}H NMR (400 MHz, CD_3OD) δ_H = 8.98 (1H, s, H_{N^N}), 8.61 (1H, s, H_{N^N}), 8.08 (1H, d, $^3J_{HH}$ = 5.8 Hz, H_{N^N}), 7.81 (2H, app. t, $^3J_{HH}$ = 4.5 Hz, H_{N^N}), 7.70 (2H, d, $^3J_{HH}$ = 7.7 Hz, H_{C^N}), 7.67 (1H, d, $^3J_{HH}$ = 5.5 Hz, H_{N^N}), 7.02 (2H, app. t, $^3J_{HH}$ = 7.1 Hz, H_{C^N}), 6.91 (2H, app. t, $^3J_{HH}$ = 7.5 Hz, H_{C^N}), 6.44 (2H, app. t, $^3J_{HH}$ = 7.4 Hz, C(Ir)C(***H***)), 3.38 (2H, app. t, $^3J_{HH}$ = 7.1 Hz, NHC***H***$_2$), 2.57 (3H, s, C***H***$_{3\ N^N}$), 1.81 (6H, s, C***H***$_{3\ C^N}$), 1.64-1.55 (2H, m, $NHCH_2CH_2$), 1.29-1.24 (18H, m, -(C***H***$_2$)$_9$-), 0.85 (3H, t, $^3J_{HH}$ = 6.3 Hz, $(CH_2)_9CH_3$) ppm. ^{13}C{^{1}H} NMR (100 MHz, CD_3OD) δ_C = 180.8, 166.7 (***C***O), 165.9 (***C***O), 158.9 (***C***O), 157.1, 154.5, 153.8, 152.1, 151.0, 149.9, 149.8, 146.0, 142.3, 142.2, 134.3, 134.1, 132.2, 130.5, 126.8, 126.3, 124.2, 123.2, 41.5, 30.8, 30.7, 30.5, 30.4, 30.2, 28.2, 21.4, 20.9, 15.2, 15.0, 14.4 ppm. LRMS (ES$^+$) found *m/z* 1010.30, calculated 1010.30 for $[M\text{-}BF_4]^+$. HRMS (ES$^+$) found *m/z* 1010.2956, calculated 1010.2961 for $[IrC_{46}H_{51}N_5O_5S_2]^+$. UV/Vis ($CH_3CN$): λ_{max}/nm (ε/M^{-1}cm^{-1}) = 417 (2000), 311 (4100), 281 (5300), 251 (9900), 216 (37900). IR (solid/cm^{-1}): *v* 3289 br. (O-H), 2922, 2851 (C-H), 1653 (C=O), 1541 (C=C), 1437, 1350, 1279, 1238 (C-O), 754, 739 (C-H).

Synthesis of $[Ir(pqca)_2(BpyC_{12})]Cl$

Made as for **$[Ir(mptca)_2(BpyC_{12})]Cl$** but using **$[Ir(epqc)_2(BpyC_{12})](BF_4)$** (0.02 g, 0.02 mmol) and KOH (1 M, 10 mL) in acetone (10 mL) to give the title compound as an orange solid. Yield: 0.0183 g, 0.02 mmol, 96%. ^{1}H NMR (400 MHz, CD_3OD) δ_H = 8.61 (1H, s, H_{N^N}), 8.37-8.35 (3H, m, $H_{arom.}$), 8.26 (1H, s, $H_{arom.}$), 8.20 (2H, d, $^3J_{HH}$ = 8.6 Hz, $H_{arom.}$), 8.16 (2H, d, $^3J_{HH}$ = 9.4 Hz, $H_{arom.}$), 8.10 (1H, d, $^3J_{HH}$ = 5.7 Hz, $H_{arom.}$), 7.88-7.83 (1H, m, H_{N^N}), 7.43-7.38 (3H, m, H_{C^N}), 7.34 (2H, app. t, $^3J_{HH}$ = 7.6 Hz, H_{C^N}), 7.18-7.14 (2H, m, H_{C^N}), 7.02-6.96 (2H, m, H_{C^N}), 6.79 (2H, app. td, J_{HH} = 2.7, 7.4 Hz, H_{C^N}), 6.54-6.51 (2H, m, C(Ir)C(***H***)), 3.61-3.60 (2H, m, NC***H***$_2$), 2.47 (3H, s, CC***H***$_3$), 1.59-1.56 (2H, m, NCH_2CH_2), 1.34-1.27 (18H, br. m, -(C***H***$_2$)$_9$-), 0.89 (3H, t, $^3J_{HH}$ = 6.7 Hz, $(CH_2)_9CH_3$) ppm. ^{13}C{^{1}H} NMR (100 MHz, CD_3OD) δ_C = 170.6 (***C***O), 170.4 (***C***O), 165.6 (***C***O), 158.0, 157.9, 156.2, 153.6, 151.8, 149.6, 149.2, 149.1, 148.5, 147.5, 147.4, 147.3, 145.7, 135.7, 135.6, 131.6, 131.5, 129.0, 128.3, 128.0, 127.6, 126.2, 124.1, 124.0, 122.5, 115.8, 115.7, 73.8, 71.7, 70.8, 64.4, 57.0, 55.1, 41.4, 30.0, 30.8, 30.7, 30.6, 30.5, 29.9, 28.1, 24.2, 23.7, 22.0, 21.7, 21.2, 14.4 ppm. LRMS (ES$^+$) found

m/z 1070.39, calculated 1070.38 for $[M\text{-}BF_4]^+$. HRMS (ES^+) found m/z = 1070.3835, calculated 1070.3831 for $[IrC_{56}H_{55}N_5O_5]^+$. UV/Vis (CH_3CN): λ_{max}/nm ($\varepsilon/M^{-1}cm^{-1}$) = 457 (700), 355 (1600), 288 (3000), 239 (6800). IR (solid/cm^{-1}): *v* 3391 br. (O-H), 2970, 2926 (C-H), 1589 br. (C=C), 1379, 1375, 1339 (C-O), 768, 662 (C-H).

4.5.5 Details of X-ray Crystallography

Diffractometer: *Rigaku AFC12* goniometer equipped with an enhanced sensitivity (HG) *Saturn724+* detector mounted at the window of an *FR-E+ SuperBright* molybdenum rotating anode generator with VHF *Varimax* optics (70µm focus). **Cell determination and data collection**: *CrystalClear-SM Expert 3.1 b27* (Rigaku, 2013). **Data reduction, cell refinement and absorption correction**: *CrysAlisPro* 1.171.38.41 (Rigaku Oxford Diffraction, 2015). **Structure solution**: *SUPERFLIP* (Palatinus, L. & Chapuis, G. (2007). J. Appl. Cryst. 40, 786-790.) **Structure refinement**: *SHELXL-2014* (G Sheldrick, G.M. (2008). Acta Cryst. A64, 112-122.). **Graphics:** *ORTEP3 for Windows* (L. J. Farrugia, J. Appl. Crystallogr. 1997, 30, 565 and *OLEX2* (O.V. Dolomanov, L.J. Bourhis, R. J. Gildea, J.A.K. Howard, H. Puschmann, H., (2009). *J. Appl. Cryst.*, 42, 339-341).

Special details: **$[Ir(epqc)_2(MeCN)](BF_4)$:** Both the BF_4^- anion and ether molecule are disordered over 2 positions. As such various geometrical (SAME) and displacement (RIGU) restraints were applied. **$[Ir(epqc)_2(BpyC_{12})](BF_4)$:** There is disorder of the ethyl ester groups. This leads to whole molecule disorder for one of the ligands. Due to this various geometrical (SAME, SADI) and displacement (RIGU) restraints were employed. Also there is a molecule of disordered ether lying over an inversion centre. To model this, both geometric (AFIX) and displacement (EADP) constraints were applied to its atoms.

4.6 References

1. J. R. Lakowicz, *Principles of Fluorescence Spectroscopy*, Springer Science & Business Media, 2007.

2. E. Baranoff, J.-H. Yum, M. Graetzel, and M. K. Nazeeruddin, *J. Organomet. Chem.*, 2009, **694**, 2661–2670.

3. L. Murphy, A. Congreve, L.-O. Pålsson, and J. A. G. Williams, *Chem. Commun.*, 2009, **46**, 8743–8745.

4. A. Tsuboyama, H. Iwawaki, M. Furugori, T. Mukaide, J. Kamatani, S. Igawa, T. Moriyama, S. Miura, T. Takiguchi, S. Okada, M. Hoshino, and K. Ueno, *J. Am. Chem. Soc.*, 2003, **125**, 12971–12979.

5. M. A. Baldo, S. Lamansky, P. E. Burrows, M. E. Thompson, and S. R. Forrest, *Appl. Phys. Lett.*, 1999, **75**, 4–6.

6. E. E. Langdon-Jones, A. J. Hallett, J. D. Routledge, D. A. Crole, B. D. Ward, J. A. Platts, and S. J. A. Pope, *Inorg. Chem.*, 2013, **52**, 448–456.

7. F. De Angelis, S. Fantacci, N. Evans, C. Klein, S. M. Zakeeruddin, J.-E. Moser, K. Kalyanasundaram, H. J. Bolink, M. Grätzel, and M. K. Nazeeruddin, *Inorg. Chem.*, 2007, **46**, 5989–6001.

8. F. L. Thorp-Greenwood, R. G. Balasingham, and M. P. Coogan, *J. Organomet. Chem.*, 2012, **714**, 12–21.

9. E. Baggaley, J. A. Weinstein, and J. A. G. Williams, *Coord. Chem. Rev.*, 2012, **256**, 1762–1785.

10. M. Nonoyama, *Bull. Chem. Soc. Jpn.*, 1974, **47**, 767–768.

11. A. Kapturkiewicz, *Anal Bioanal. Chem.*, 2016, **408**, 7013–7033.

12. B. M. Zeglis, V. C. Pierre, and J. K. Barton, *Chem. Commun. (Camb.)*, 2007, 4565–4579.

13. K. K.-W. Lo, M.-W. Louie, and K. Y. Zhang, *Coord. Chem. Rev.*, 2010, **254**, 2603–2622.

14. A. E. Friedman, J. C. Chambron, J. P. Sauvage, N. J. Turro, and J. K. Barton, *J. Am. Chem. Soc.*, 1990, **112**, 4960–4962.

15. V. Fernández-Moreira, F. L. Thorp-Greenwood, and M. P. Coogan, *Chem. Commun.*, 2009, **46**, 186–202.

16. P.-K. Lee, H.-W. Liu, S.-M. Yiu, M.-W. Louie, and K. K.-W. Lo, *Dalton Trans.*, 2011, **40**, 2180–2189.

17. A. J. Hallett, N. White, W. Wu, X. Cui, P. N. Horton, S. J. Coles, J. Zhao, and S. J. A. Pope, *Chem. Commun.*, 2012, **48**, 10838–10840.

18. J. Sun, J. Zhao, H. Guo, and W. Wu, *Chem. Commun.*, 2012, **48**, 4169–4171

19. J. Sun, W. Wu, H. Guo, and J. Zhao, *Eur. J. Inorg. Chem.*, 2011, **2011**, 3165–3173.

20. D. Aiello, A. Maria Talarico, F. Teocoli, E. I. Szerb, I. Aiello, F. Testa and M. Ghedini, *New J. Chem.*, 2011, **35**, 141–148.

21. H.J. Bolink, E. Baranoff, M. Clemete-León, E. Coronado, N. Lardiés, Á. López-Muñoz, D. Repetto and Md. K. Nazeeruddin, *Langmuir*, 2010, **26**, 11461–11468.

22. J. C. Araya, J. Gajardo, S. A. Moya, P. Aguirre, L. Toupet, J. A. G. Williams, M. Escadeillas, H. L. Bozec, and V. Guerchais, *New J. Chem.*, 2010, **34**, 21–24.

23. M.-L. Ho, F.-M. Hwang, P.-N. Chen, Y.-H. Hu, Y.-M. Cheng, K.-S. Chen, G.-H. Lee, Y. Chi, and P.-T. Chou, *Org. Biomol. Chem.*, 2006, **4**, 98–103.

24. J. Brandel, M. Sairenji, K. Ichikawa, and T. Nabeshima, *Chem. Commun.*, 2010, **46**, 3958.

25. H. Lin, M. E. Cinar, and M. Schmittel, *Dalton Trans.*, 2010, **39**, 5130–5138.

26. V. Guerchais and J.-L. Fillaut, *Coord. Chem. Rev.*, 2011, **255**, 2448–2457.

27. M. Schmittel, H. Lin, *Inorg. Chem.,* 2007, **46**, 9139.

28. P. Coppo, E. A. Plummer, and L. D. Cola, *Chem. Commun.*, 2004, 1774–1775.

29. G. Zhou, W.-Y. Wong, B. Yao, Z. Xie, and L. Wang, *Angew. Chem. Int. Ed.*, 2007, **46**, 1149–1151.

30. M. G. Colombo, T. C. Brunold, T. Riedener, H. U. Guedel, M. Fortsch, and H.-B. Buergi, *Inorg. Chem.*, 1994, **33**, 545–550.

31. G. Zhang, H.-H. Chou, X. Jiang, P. Sun, C.-H. Cheng, Y. Ooyama, and Y. Harima, *Org. Electron.*, 2010, **11**, 632–640.

32. M. Clemente-León, E. Coronado, Ángel López-Muñoz, D. Repetto, T. Ito, T. Konya, T. Yamase, E. C. Constable, C. E. Housecroft, K. Doyle, and S. Graber*, Langmuir* 2010, **26(2)**, 1316–1324

33. M. A. Baldo, M. E. Thompson, and S. R. Forrest, *Nature*, 2000, **403**, 750–753.

34. M. de B. e S. Botelho, J. M. Fernandez-Hernandez, T. B. de Queiroz, H. Eckert, L. D. Cola and A. S. S. de Camargo, *J. Mater. Chem.*, 2011, **21**, 8829–8834.

35. C. Roldán-Carmona, A. M. González-Delgado, A. Guerrero-Martínez, L. D. Cola, J. J. Giner-Casares, M. Pérez-Morales, M. T. Martín-Romero and L. Camacho, *Phys. Chem. Chem. Phys.*, 2011, **13**, 2834–2841.

36. J. M. Fernández-Hernández, L. De Cola, H. J. Bolink, M. Clemente-León, E. Coronado, A. Forment-Aliaga, A. López-Muñoz and D. Repetto, *Langmuir*, 2014, **30**, 14021–14029.

37. C.-H. Yang, S.-H. Yang and C.-S. Hsu, *Nanotechnology*, 2009, **20**, 315601.

38. A. Guerrero-Martínez, Y. Vida, D. Domínguez-Gutiérrez, R. Q. Albuquerque and L. De Cola, *Inorg. Chem.*, 2008, **47**, 9131–9133.

39. J. J. Rack, T. M. McCleskey and E. R. Birnbaum, *J. Phys. Chem. B*, 2002, **106**, 632–636.

40. M. M. McGoorty, R. S. Khnayzer and F. N. Castellano, *Chem. Commun.*, 2016, **52**, 7846–7849.

41. C. Cebrián, M. Natali, D. Villa, M. Panigati, M. Mauro, G. D'Alfonso and L. D. Cola, *Nanoscale*, 2015, **7**, 12000–12009.

42. J. G. J. Weijnen, A. Koudijs, G. A. Schellekens and J. F. J. Engbersen, *J. Chem. Soc., Perkin Trans. 2*, 1992, 829–834.

43. E. Kimura, H. Hashimoto and T. Koike, *J. Am. Chem. Soc.*, 1996, **118**, 10963–10970.

44. E. Valls, A. Solsona, J. Suades, R. Mathieu, F. Comelles and C. López-Iglesias, *Organometallics*, 2002, **21**, 2473–2480.

45. P. Gameiro, E. Pereira, P. Garcia, S. Breia, J. Burgess and B. de Castro, *Eur. J. Inorg. Chem.*, 2001, 2755–2761.

46. N. J. Long, D. G. Parker, P. R. Speyer, A. J. P. White and D. J. Williams, *J. Chem. Soc., Dalton Trans.*, 2002, 2142–2150.

47. R. W. Hay, N. Govan and K. E. Parchment, *Inorg. Chem. Commun.*, 1998, **1**, 228–231.

48. J. Bowers, M. J. Danks, D. W. Bruce and R. K. Heenan, *Langmuir*, 2003, **19**, 292–298.

49. J. Bowers, M. J. Danks, D. W. Bruce and J. R. P. Webster, *Langmuir*, 2003, **19**, 299–305.

50. J. Bowers, K. E. Amos, D. W. Bruce and J. R. P. Webster, *Langmuir*, 2005, **21**, 1346–1353.

51. H. B. Jervis, D. W. Bruce, M. E. Raimondi, J. M. Seddon, T. Maschmeyer and R. Raja, *Chem. Commun.*, 1999, 2031–2032.

52. M. J. Danks, H. B. Jervis, M. Nowotny, W. Zhou, T. A. Maschmeyer and D. W. Bruce, *Catal. Lett.*, 2002, **82**, 95–98.

53. D. G. McCafferty, B. M. Bishop, C. G. Wall, S. G. Hughes, S. L. Mecklenberg, T. J. Meyer and B. W. Erickson, *Tetrahedron*, 1995, **51**, 1093–1106.

54. R. A. Smith, E. C. Stokes, E. E. Langdon-Jones, J. A. Platts, B. M. Kariuki, A. J. Hallett and S. J. A. Pope, *Dalton Trans.*, 2013, **42**, 10347–10357.

55. E. C. Stokes, E. E. Langdon-Jones, L. M. Groves, J. A. Platts, P. N. Horton, I. A. Fallis, S. J. Coles and S. J. A. Pope, *Dalton Trans.*, 2015, **44**, 8488–8496.

56. E. E. Langdon-Jones, A. J. Hallett, J. D. Routledge, D. A. Crole, B. D. Ward, J. A. Platts and S. J. A. Pope, *Inorg. Chem.*, 2013, **52**, 448

57. J. D. Routledge, A. J. Hallett, J. A. Platts, P. N. Horton, S. J. Coles and S. J. A. Pope, *Eur. J. Inorg. Chem.*, 2012, 4065

58. A. D. Pidwell, S. R. Collinson, S. J. Coles, M. B. Hursthouse, M. Schröder and D. W. Bruce, *Chem. Commun.*, 2000, 955–956

59. L. J. Farrugia, P. A. Lovatt, R. D. Peacock, *Acta Cryst. C*, 1993, **49**, Part 12, 2164

60. A. J. Howarth, R. Patia, D. L. Davies, F. Lelj, M. O. Wolf and K. Singh *Eur. J. Inorg. Chem.,* 2014, 3657–3664

Chapter Five

Amphiphilic Lanthanide(III) Complexes for Luminescent Micellar Systems

5.1 Introduction

5.1.1 Sensitisation of Lanthanides

In the lanthanide elements the valence electrons are located in the 4*f* orbital. Although *f* → *f* transitions between different energy levels of the 4*f* orbitals are formally forbidden by the Laporte rule they may occur due to spin orbit coupling. This is a result of the coupling of the angular momentum of the spin of an electron with the angular momentum of its orbital and can be described using Russell-Saunders coupling with the term symbol:

$$^{(2S+1)}L_J$$

Where *S* is the total spin angular momentum, *L* is the total orbital angular momentum and *J* is the total angular momentum. Spin orbit coupling means that those transitions considered to be 'forbidden' may be referred to more appropriately as simply being of low probability with respect to the 'allowed' transitions.[1]

As the atomic number of the lanthanides increases there is a larger than expected decrease in the ionic radii of the atoms, referred to as 'lanthanide contraction'. This results in the 4*f* orbitals being core-like as they are shielded by the 5*s* and 5*p* orbitals leading to weak ligand interactions.

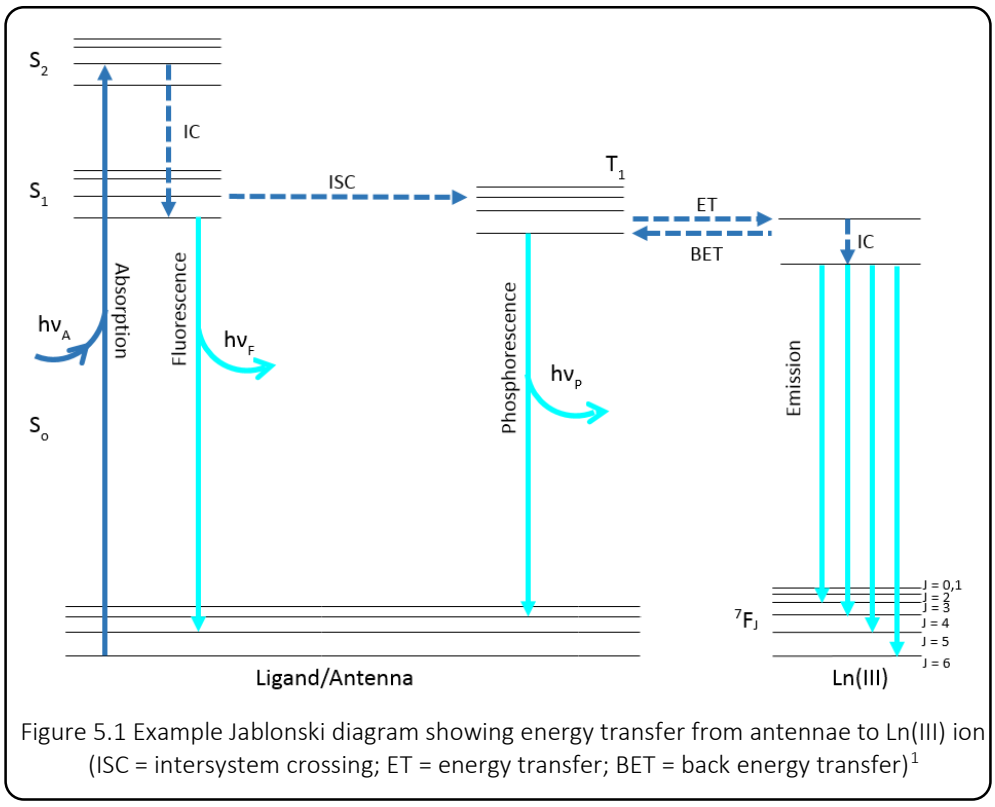

Figure 5.1 Example Jablonski diagram showing energy transfer from antennae to Ln(III) ion (ISC = intersystem crossing; ET = energy transfer; BET = back energy transfer)[1]

The photophysics of lanthanide ions is dominated by the Laporte-forbidden 4*f*-4*f* transitions which have low molar absorption coefficients. As a result direct excitation of the Ln(III) ion results only in weak emission, therefore a donor chromophore or "antenna" is required to indirectly sensitise the Ln(III) ion. The antenna is typically a highly-conjugated aromatic species that can absorb in the UV-Vis region of the spectrum.

Figure 5.1 illustrates the absorption and emission processes of antenna-mediated sensitisation of lanthanide emission. Initial excitation occurs when light is absorbed by the chromophore, promoting an electron to the excited singlet state. Conversion to the ligand triplet state occurs *via* ISC, a non-radiative process mediated by spin orbit coupling arising from the heavy-atom effect of the lanthanide. From this point energy transfer may occur from the ligand triplet state to the excited triplet state of the lanthanide. This process requires the triplet state of the ligand to be higher in energy than that of the lanthanide in order for energy transfer to be favourable. If the energy gap between these two states is too small (<2000 cm^{-1}), thermally activated back energy transfer may occur, which deactivates the Ln(III) luminescence and renders it sensitive to quenching by dissolved oxygen. Emission from the Ln(III) excited state is typically long-lived and lies in the visible or NIR regions of the spectrum. The emission of each Ln(III) ion has a unique 'fingerprint' comprising line-like spectra which lie in a specific region of the spectrum and provide information about the coordination sphere of the ion.[1]

5.1.2 Hyperfine Transitions

One of the characteristic features of lanthanide chemistry that influences characterisation *via* electronic spectroscopy is the appearance of hyperfine transitions. These are often seen as well-defined line-like spectra which can be used to provide information about the coordination sphere of an ion. These transitions are observed due to the weak crystal field effect of the lanthanides arising from shielding of the 4*f* valence orbitals by the 5*s* and 5*p* orbitals. This leads to considerably weaker absorbance and thus weak phosphorescence on relaxation of the excited states in comparison to transition metal (*d*-block) complexes. The weak crystal field effect gives rise to the well-defined transitions that can be seen to vary only slightly in energy between different compounds. However, the relative ratios of these peaks can provide important information about either the lanthanide coordination sphere or the complex environment.

Numerous factors can influence energy transfer from antenna to metal but two mechanisms exist for non-radiative transfer. Förster transfer is an entirely through-space effect arising from dipole-

dipole mechanisms whereas Dexter transfer requires efficient overlap in the donor and acceptor electron clouds in order to invoke electron exchange.[2]

Hyperfine transitions may be observed for several lanthanides, however Eu(III) and Tb(III) are the most notable. The Eu(III) emission spectrum is dominated by the $^5D_0 \rightarrow {}^7F_J$ transitions (J = 0 – 4). The J = 1 transition is mostly insensitive to the ligand field as it relates to magnetic dipole character whereas for J = 0, 2, 4 the transitions are of electric dipole and are therefore sensitive to ligand field splitting.

As for Eu(III), Tb(III) also gives rise to line-like spectra relating to the $^5D_4 \rightarrow {}^7F_J$ (J = 6 – 3) transitions. However, these emission bands can rarely be fully resolved, making it harder to infer as much about the local ion symmetry as is possible for Eu(III) from fine structure analysis. Back transfer from the Ln(III) triplet state to the antenna singlet state is much more likely for Tb(III) than Eu(III) however, as the $^5D_4$ state is substantially closer in energy to the donor singlet state than the $^5D_0$ state of Eu(III) is, meaning the energy gap can be more easily bridged and thus the Tb(III) emission more easily quenched.

5.1.3 Quenching and Hydration Factor

Quenching is defined as any mechanism, chemical and/or electronic, which reduces the intensity of a luminescent signal. Deactivation processes of lanthanide ions include ISC, electron exchange and photochemical transfer and may be determined by coordination environment. Electron-deficient molecules, amines, halogens and oxygen can deactivate the excited state of a lumophore *via* collisions in solution.

Halides and heavy atoms may also act as quenchers as spin-orbit coupling (mediated by the heavy-atom effect) promotes ISC to the triplet excited state. Phosphorescence from this state is long-lived and thus readily quenched by the processes outlined above. Another possible mechanism is static quenching whereby non-emissive complexes form between fluorophores and quenchers. This process is independent of diffusion or molecular collisions and occurs in the ground state of the molecule.[3]

Whereas some of these quenching pathways can be circumvented, (*e.g.* oxygen quenching can be avoided by de-aeration of the solutions prior to luminescence measurements, leading to enhanced luminescence lifetimes) other may be used to provide information about the luminescent species.

The emissive properties of a molecule can provide an insight into the coordination environment of a metal ion in a complex. One of the key mechanisms for deactivation of luminescence is quenching which is a non-radiative energy transfer to surrounding molecules' vibrational modes. For lanthanide complexes in water the emission lifetime is drastically quenched by interactions with O-H oscillators of solvent molecules both in the outer and inner spheres. Quenching of an aqueous Ln(III) ion occurs via energy transfer to the O-H stretching vibrations of water at a rate that is proportional to the number of O-H oscillators associated with the metal. However, Knapp and Windsor established that energy transfer to O-D vibrations is much less efficient than to O-H as D_2O has a smaller vibrational stretching frequency. This give rise to more intense luminescence in D_2O than water and thus the lifetime of a species in solvent can be used to calculated the number of water molecules associated with a Ln(III) ion.[4]

Quenching *via* inner sphere water molecules has a quantifiable effect on the lifetimes of lanthanide luminescence meaning the degree of solvation of the Ln(III) ions in complexes can be calculated.[5] Horrocks *et al.* found that the number of inner sphere solvent molecules can be calculated by comparison of the decay rate constant in deuterated and non-deuterated solvents as the lifetimes linearly correlate with the hydration factor *q*, which can be expressed as:

—— —— …….Equation 5.1

—— —— …….Equation 5.2

Horrocks equation modified for Eu(III), Yb(III) and Tb(III)[5,6,7]

Ln(III)	A	B
Eu(III)	1.25 ms	0.25 ms^{-1}
Tb(III)	5.00 ms	0.06 ms^{-1}
Yb(III)	1.00 µs	0.20 μs^{-1}

Table 5.1 Horrocks equation values for A and B for various Ln(III) ions in water[7]

Where *A* and *B* relate to the efficiency of quenching *via* interactions with O-H oscillations of surrounding solvent molecules and is experimentally determined for each particular lanthanide ion. *A* refers to the inner sphere correction factor while *B* is the outer sphere correction factor.

These equations can be modified in order to account for the quenching effects of outer sphere molecules on Eu(III), Tb(III) and Yb(III) and the effect of C-H and N-H oscillators which have also been found to quench emission but to a lesser extent than O-H vibrations. Nd(III) has been found to be particularly sensitive to C-H oscillator quenching, therefore the above equation can be modified further to account for this. The results of this modification have been found to be more accurate for ligands with a high number of C-H bonds close to the Ln(III) ion but anomalous for ligands with a limited number of these bonds.[8,9,10,11]

…….Equation 5.3

Horrocks equation modified for Nd(III)[12]

5.1.4 Suitable ligands for lanthanides

The chemistry of the lanthanides is dominated by the 3+ oxidation state and the most common coordination numbers are 8-9. Lanthanides are hard Lewis acids and therefore prefer ligands with hard donors such as nitrogen and oxygen and bonds of low covalency and high lability. Even with hard donors monodentate ligands coordinated to lanthanide ions are very labile and therefore a chelating or macrocyclic ligand system is desirable for the formation of kinetically inert complexes.

The greater the number of donor atoms there are in a ligand the higher the stability of the corresponding complex as a greater number of water molecules are liberated upon metal coordination. This is an entropy driven process known as the 'chelate effect'.

A similar ligand effect is the 'macrocyclic effect' where the restricted prearrangement of donors in a cyclic ligand makes dissociation unfavourable as the simultaneous breaking of several donor-metal bonds induces unfavourable strain across the ring system.

The binding of multidentate ligands to a Ln(III) ion are also capable of shielding the metal from surrounding water molecules. This reduces deactivation *via* vibrational energy transfer to water molecules and therefore optimises the luminescence lifetime and efficiency.

Common ligands for lanthanide complexes are based around cyclen derivatives such as DO3A (1,4,7,10-tetraazacyclododecane-1,4,7-triacetic acid) which provides three amine-bonded carboxylic acid groups capable of binding *via* oxygen coordination as well as leaving the fourth amine group free for further functionalisation. This free sight may be functionalised with an amide

group which acts as a linker to further functionality. In such case either the N-atom or the carbonyl O-atom of the amide has the potential to coordinate to the lanthanide ion, thus increasing the overall stability of the complex. Other similar ligands, shown in Figure 5.2, include DOTA (1,4,7,10-tetraazacyclododecane-1,4,7,10-triaceticacid), DTPA (diethylenetriamine pentaaceticacid) and NOTA (1,4,7-triazacyclononande-1,4,7-tiaceticacid), which meet the demands of hard, polarising Ln(III) ions and commonly form polyhedra of square anti-prismatic or dodecahedral geometry.[13]

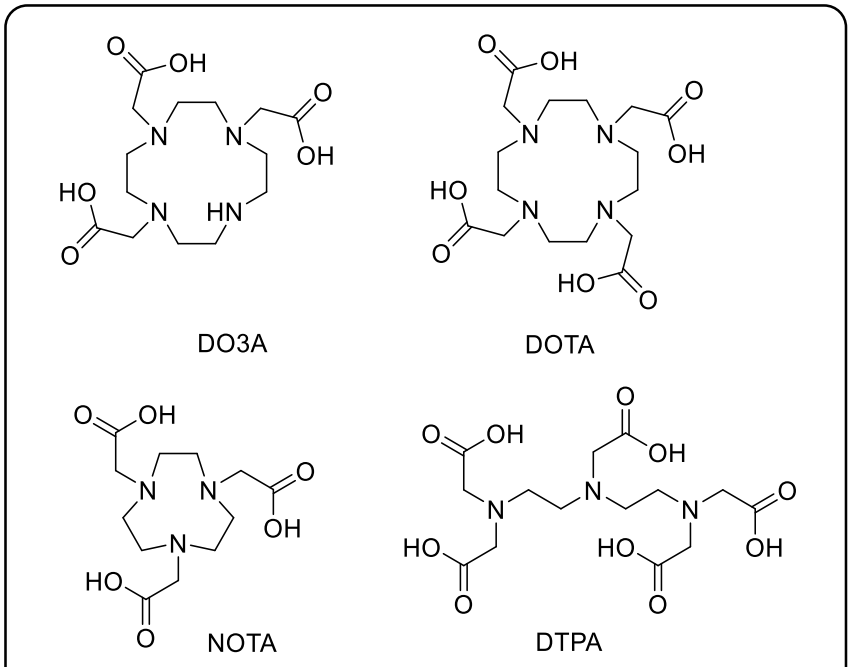

Figure 5.2 Multidentate chelating ligands for lanthanides

DO3A based compounds are commonly used as ligands for lanthanide ions as they exhibit both the macrocyclic effect (from the 4 N-atoms) and the chelate effect (from the carboxylic acid O-atoms) which together provide good stability for the resulting complex. Such ligands have high formation constants and are kinetically inert to proton- or cation-mediated dissociation; the free amine site of the DO3A macrocycle also allows for further functionalisation. This ligand environment also allows for the coordination of a small number of water molecules, the number of which can be determined *via* the luminescence lifetimes as explained in section **5.1.3** above, the binding effect of the ligand can also have a direct effect on the luminescence of the complex.

5.1.5 Applications

Lanthanide complexes have been reported for many applications including permanent magnets,[14] homogeneous catalysts,[15] phosphorescent dyes[16] and lasers.[17] However, recently they have been most widely investigated as biological probes for diagnostic and therapeutic medicine.[18,19]

In biological applications they have been reported for detection of small peptides,[20] nucleic acid strands[21] and cyclodextrins.[22,23] Solution assays have been used as alternatives to radioimmunoassays in biological media as their chemistry is similar to ^{90}Y and they exhibit long-lived emission under ambient conditions.[24,25,26,27,28]

Gd(III) complexes have been comprehensively studied as contrast agents (CAs) for magnetic resonance imaging (MRI), a medical diagnostic technique which affords greater tissue penetration than fluorescence imaging microscopy and allows whole body imaging. The key requirement for a Gd(III) complex to be an MRI CA is the presence of inner-sphere water molecules as it is the relative difference in the relaxivity of these water molecules and those in the bulk phase that gives rise to the contrast required.[21]

However, Ln(III) ions are toxic as they mimic calcium coordination chemistry in the body. They therefore require ligands with high binding efficiencies. Therefore macrocyclic chelating ligands have proved to be extremely effective carriers for Ln(III) ions in biological applications due to their thermodynamic stability and kinetic inertness.[29]

Ln(III) complexes are suited to applications as optical CAs as their long-lived emission and large Stokes' shift mean their signals can be readily distinguished from interference from biological autofluorescence. Ln(III) complexes can be designed to emit in the NIR region which is beneficial for biological applications as such signals can penetrate tissue without causing damage.

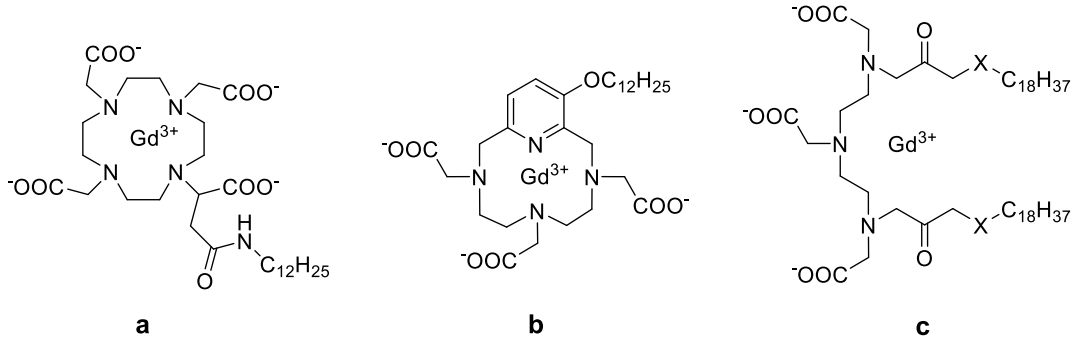

Figure 5.3 Examples of Gd(III) metallosurfactants (a[21] b[20] c[24])

In terms of *f*-block metallosurfactants, Gd(III) CAs are the most widely reported. The chelating ligands reported previously for such applications (DO3A, DOTA *etc.*) allow for functionalisation to form amphiphilic complexes. These have been employed as MRI CAs with promising results. Amphiphilic Gd(III) complexes which self-assemble into micelles in aqueous solution have been reported with a relatively low CMC of 0.15 mM and may also be incorporated into mixed-micelle liposomes.[30] These aggregates were found to increase the relaxivity time of the CAs due to increases in the rotational correlation time of the Ln(III) complexes. However, the long relaxivity time was found to be partially quenched by the slow dissociative exchange of water molecules from the coordination site to the bulk phase.[31]

Gd(III) complexes have also been incorporated into liposome drug carriers as a means to deliver the MRI CAs to selective sites. As opposed to the traditional method of delivering the CA encapsulated in the aqueous core of the liposomes, DTPA derivatives with alkyl side chains have been reported which are incorporated into the membranes of liposomal vesicles. Such complexes are good candidates for these roles as they are analogous in structure to the phospholipids which comprise the liposomal membranes. These liposomes can be designed to deliver the CAs to specific organs, such as the liver, ultimately leading to images of greater contrast.[32] It is also generally accepted that neither the incorporation of alkyl chains into the chelating ligand nor micellisation affect the ability of the ligand to bind the Ln(III) ion.[33,34] The exchange of water is also unaffected by micellisation as the chelated headgroup lies on the surface of the micelle and is therefore in contact with the bulk aqueous phase; also the water molecules are able to penetrate the first one or two methylene residues of the alkyl chain meaning the head group is fully hydrated.[29,33]

5.2 Aims

The aim of this chapter was to explore the possibility of creating a microemulsion with a lanthanide ion bound and localised on the surface of the micellar droplet. It was hoped that the incorporation of luminescent handles into the ligand architecture in the form of a pendent chromophore would provide information about lanthanide binding and localisation of the complexes within a microemulsion.

The amphiphilic ligands were designed to act as surfactant molecules with a lanthanide-binding head group and a hydrophobic tail. The head group was designed around the DO3A framework commonly used in lanthanide chemistry which incorporates a cyclen macrocycle with three carboxylic acid arms thus combining the chelate and macrocyclic effects. The tail group comprised a dodecyl chain combined with a pendent chromophore which were both attached to the head group *via* an amide linker.

A range of pendent chromophores were incorporated into the ligand architectures and thus a wide range of lanthanide complexes synthesised. The complexes were characterised *via* structural and photophysical studies as solubilised free species and in single-surfactant micellar systems. Selected complexes were also investigated for their microemulsion compatibility *via* tensiometric measurements and related luminescence studies.

5.3 Results and Discussion

5.3.1 Synthesis

The reductive amination of aldehydes (two commercial and one synthesised, see Figure 5.4) with dodecyl amine afforded the secondary amine precursors for the ligand chromophores. The aldehyde was stirred in DCE for 5 hours with dodecyl amine prior to the addition of tris(acetoxy)borohydride. The resulting solution was stirred for 2-5 days at room temperature under a N_2 atmosphere before being neutralised and the products isolated as orange/brown oils in yields of 68-97%.

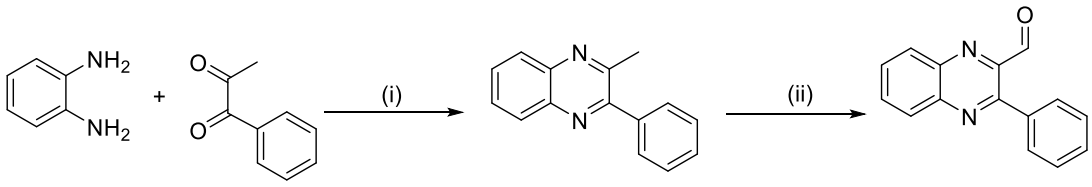

Figure 5.4 Synthesis of phenylquinoxaline precursor;
reaction conditions (i) AcOH, EtOH, 78 °C, 48 hrs; (ii) SeO_2, 1,4-dioxane, 101 °C, 3 hours.

The non-commercial aldehyde, shown in Figure 5.4, was synthesised *via* the addition of concentrated glacial AcOH to 1,2-phenylene diamine and 1-phenyl-1,2-propandione in EtOH. This solution was heated to reflux for 48 hours under inert conditions before being neutralised and the product isolated as a yellow oil. This oil was then stirred in 1,4-dioxane at 101 °C for 3 hours in the presence of SeO_2 before being filtered to remove elemental selenium and dried *in vacuo* to give the aldehyde precursor as a red/brown solid in good yields (93-99%).

The chloroacetamides where synthesised *via* the dropwise addition of chloroacetyl chloride to the corresponding secondary amine at 0 °C in the presence of NEt_3 in MeCN. The reaction was stirred for 2-4 days at room temperature under an inert atmosphere. The crude products were washed with water and isolated as oils which were purified by precipitation using DCM and Et_2O to give the desired compounds in yields of 62-68%.

The surfactant-based ligands were synthesised in accordance to the literature procedure.[35] The triester of cyclen (made from commercial cyclen[36]) and Cs_2CO_3 were stirred in MeCN at 50 °C for 30 minutes. The corresponding chloroacetamide in MeCN was added and the reaction stirred at reflux for 72 hours under inert conditions. The resulting solution was cooled to room temperature and the caesium salts removed by filtration. Recrystallisation from boiling toluene was used where necessary to remove unreacted macrocycle to give the ligands in their triester protected form.

Deprotection was achieved using standard *tert*-butyl cleavage conditions (1:1 TFA:DCM) to give the free ligands as highly hygroscopic TFA adducts. Attempts to precipitate the product from the mother liquor gave only oils, therefore the remaining solvent was decanted and the oil dried *in vacuo*. In some cases a precipitate formed but was too fine to filter using traditional filtration-under-vacuum methods so again, the solvent was removed and the product dried under reduced pressure.

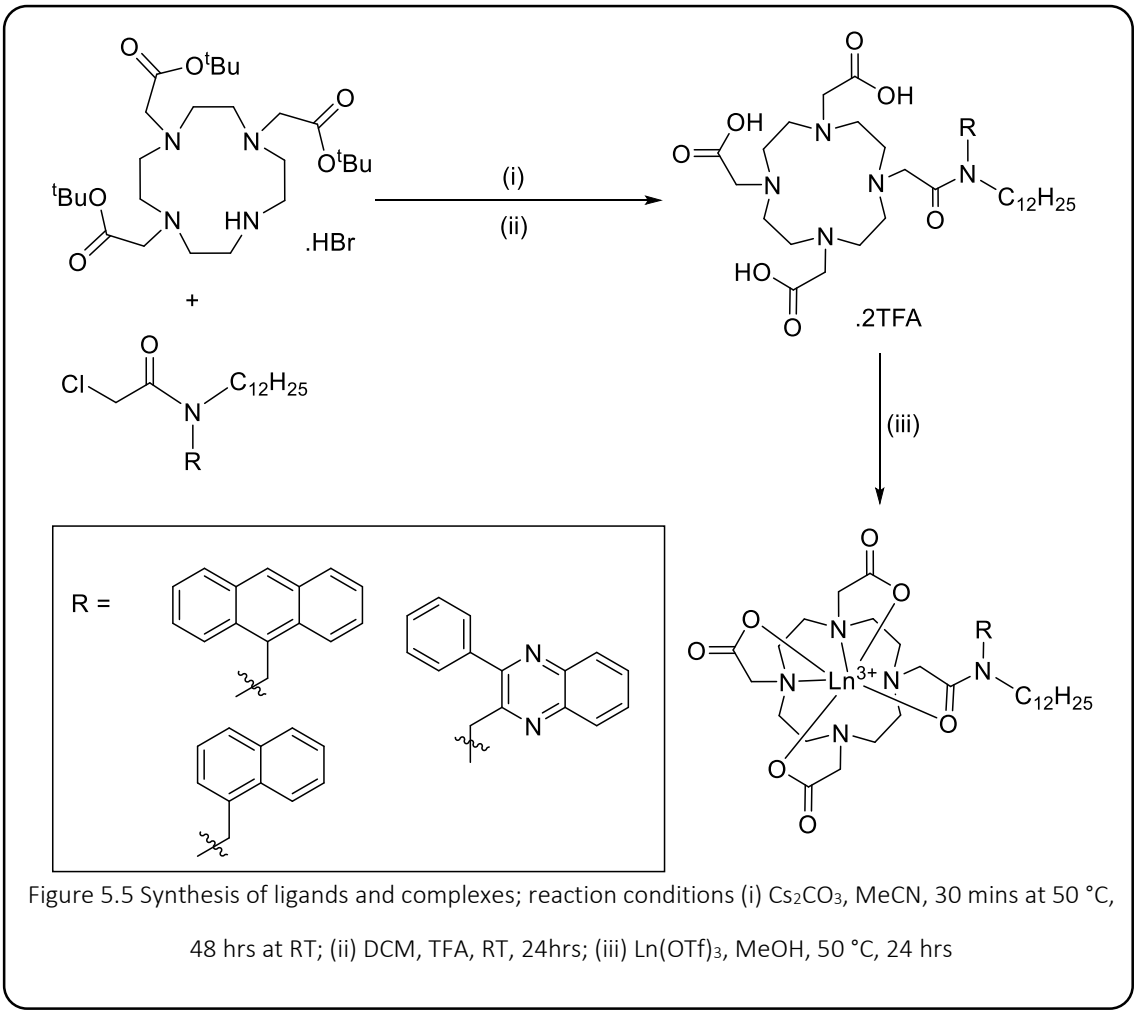

Figure 5.5 Synthesis of ligands and complexes; reaction conditions (i) Cs_2CO_3, MeCN, 30 mins at 50 °C, 48 hrs at RT; (ii) DCM, TFA, RT, 24hrs; (iii) $Ln(OTf)_3$, MeOH, 50 °C, 24 hrs

Complexes were formed *via* the addition of the corresponding lanthanide triflate to the ligand in MeOH. The resulting mixture was stirred overnight at 50 °C under a N_2 atmosphere. Attempts to precipitate the product by reducing the volume of the reaction mixture and adding it dropwise to stirring Et_2O at 0 °C resulted in formation of oils. These residues were washed with fresh Et_2O, the solvent decanted and the product dried *in vacuo* to give light to dark brown solids. Although the precursors were air stable the deprotected ligands and corresponding lanthanide complexes were highly hygroscopic and therefore required storage under nitrogen.

5.3.2 Structural Characterisation

Figure 5.6 outlines the synthesis of the **DO3AQuinC$_{12}$** ligand as followed by ^{1}H NMR spectroscopy. This is also representative of the other two analogues however, for reasons described below, the quinoxaline ligand afforded the most well-resolved spectra. The 2-methyl-3-phenyl quinoxaline precursor (Figure 5.6a) was characterised from the ^{1}H NMR spectrum as the methyl group at 1.56 ppm is easily identified and integrates with the aromatic multiplets seen from 6.23-6.93 ppm.

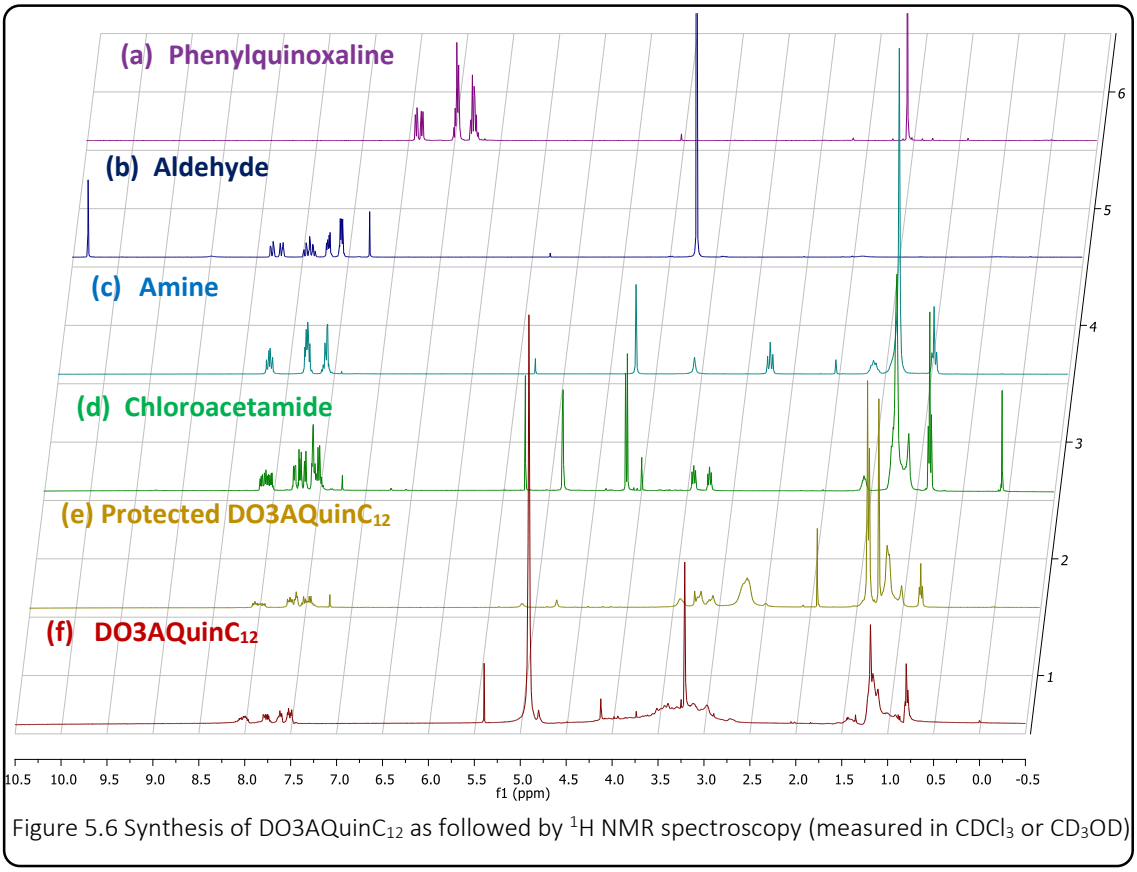

Figure 5.6 Synthesis of DO3AQuinC$_{12}$ as followed by ^{1}H NMR spectroscopy (measured in $CDCl_3$ or CD_3OD)

The reaction of this precursor with SeO_2 yielded the aldehyde as shown by the characteristic $CO_2\boldsymbol{H}$ resonance at 10.33 ppm in Figure 5.6b which is accompanied by the disappearance of the methyl resonance seen on the previous spectrum. Reductive amination of the aldehyde species with 1-dodecylamine afforded the lipophilic chromophore precursor *N*-((3-phenylquinoxalin-2-yl)methyl)dodecan-1-amine.

Figure 5.6c shows the ^{1}H NMR spectrum for the amine species. It can be seen that the splitting of the aromatic region remains unchanged but the resonances now lie between 7.41-8.09 ppm. A key indication that this reaction was successful is the lack of aldehyde peak at ~10 ppm and the appearance of a singlet resonance at 4.05 ppm which corresponds to the methyl linker between

the aromatic chromophore and the secondary amine. Additionally, peaks corresponding to the dodecyl chain are visible in the aliphatic region of the spectrum. The protons of the first two methyl linkers in the chain (NH-C***H***$_2$-C***H***$_2$) are seen as a triplet resonance at 2.58 ppm and a broad multiplet at 1.52-1.41 ppm, respectively. The bulk of the chain protons, being in very similar environments, are seen as a singlet resonance at 1.24 ppm which corresponds to 18H. The terminal methyl group was observed as a characteristic triplet at 0.80 ppm integrating to 3H.

Reaction of the secondary amine with chloroacetyl chloride afforded the chloroacetamide product (Figure 5.6d) which gives rise to an additional resonance at 4.85 ppm corresponding to the Cl-C***H***$_2$ group. The presence of the chloroacetamide group also creates an inequivalence between the protons of the first chain methyl linker (N-C***H***$_2$-CH$_2$), creating two triplet peaks at 3.42 and 3.25 ppm integrating to one proton each.

When the chloroacetamide is combined with the protected cyclen the quality of the ^{1}H NMR spectra obtained noticeably decreases (Figure 5.6e). The aromatic protons are still identifiable between 8.10-7.34 ppm and the dodecyl chain protons are seen at 1.25 ppm for the bulk of the chain protons and 0.79 ppm for the terminal methyl group. However, the resonances arising from the macrocyclic protons are broad and difficult to decipher. Resonances within the range of 3.21-2.62 ppm integrate to 28 protons and were therefore assigned to all NC***H***$_2$ environments within the ligand including the macrocyclic protons, those of the ^{t}Bu-ester arms and those in the amide/chromophore/chain linker. The ^{t}Bu-protected esters gave rise to a series of resonances around 1.38-1.35 ppm as although their protons are in similar environments, they are not exactly equivalent.

Similarly to the protected ligand, the ^{1}H NMR spectrum of the deprotected ligand (Figure 5.6f) is difficult to assign in great detail. As before the aromatic resonances of the chromophore and the aliphatic resonances of the dodecyl chain can be deciphered and the broad peaks in the range of 4.22-2.61 ppm integrate to the 28 NC***H***$_2$ protons. The key difference between the protected spectrum (Figure 5.6e) and the final ligand spectrum is the lack of peaks around 1.38-1.35 ppm in the latter, meaning that there are no ^{t}Bu protons present and thus deprotection has been successful.

The ligand synthesis was also followed *via* MS which was most relevant for the final two ^{1}H NMR spectra as their quality was poorer than their precursors' spectra. HRMS showed peaks corresponding to $[M+Na]^+$ for the protected species and $[M+H]^+$ for the deprotected species, suggesting successful synthesis of the target ligand.

All of the lanthanide ions studied in this chapter (Eu(III), Gd(III), Nd(III), Tb(III), Yb(III)) have unpaired electrons in the 4*f* state, giving rise to their paramagnetism. The magnitude of the spin orbit coupling present for these ions make the excited states thermally inaccessible therefore the paramagnetism is determined by the electron configuration of the ground state. This makes characterisation *via* NMR spectroscopy difficult, therefore characterisation focussed on IR and UV-Vis spectroscopy and MS. ^{1}H NMR spectra were recorded for the Eu(III) complexes of **DO3AQuinC$_{12}$** and **DO3ANaphC$_{12}$** but were not of sufficient quality to provide information on complex properties, they are therefore not included in this thesis.

For the **DO3AQuinC$_{12}$** ligand the MS for all of the lanthanide complexes formulated generally showed peaks for $[M+H]^+$, assuming the three carboxylic acid groups become deprotonated upon coordination. Similar MS results were seen for the complexes of **DO3ANaphC$_{12}$**. Although these results are convincing evidence for successful lanthanide coordination, comparison of the IR spectra of the free ligand and the complexes show very little change upon addition of the lanthanide salt. The free **DO3AQuinC$_{12}$** ligand showed peaks at 1730 and 1652 cm^{-1} for the C=O bonds, 1381 cm^{-1} for C-N and 1088 cm^{-1} for C-O . The complexes similarly showed peak in the regions of 1739-1591 cm^{-1}, 1416-1377 cm^{-1} and 1084-1080 cm^{-1} for C=O, C-N and C-O, respectively.

Despite the inconclusive IR spectroscopy results, the MS results suggest successful complex formulation and this is further supported by the tensiometry results discussed below (section **5.3.4**).

Synthesis of the **DO3AAnthC$_{12}$** ligand was followed in much the same way as **DO3AQuinC$_{12}$**. ^{1}H NMR spectroscopy was used to track subsequent reactions starting with 9-anthraldehyde *via* the same set of reactions to give the target ligand. ^{1}H NMR spectroscopy gave very similar spectra to those seen in Figure 5.6 while MS typically showed peaks for $[M+H]^+$ or $[M+Na]^+$ for all of the products up until the ligand deprotection. As for the **DO3AQuinC$_{12}$** analogue, the ^{1}H NMR spectrum for the target ligand was broad and difficult to assign, but unlike the analogue, the MS for **DO3AAnthC$_{12}$** only showed a peak at *m/z* = 727.31 corresponding to $[M\text{-}AnthCH_2+2H]^+$ which may be a sign of fragmentation during the MS process but may also be due to product degradation upon deprotection of the triester moieties.

Unlike the **DO3AAnthC$_{12}$** and **DO3AQuinC$_{12}$** ligands an impurity was seen in the precursors of the **DO3ANaphC$_{12}$** analogue that appeared after formation of the secondary amine and persisted throughout the rest of the ligand synthesis. ^{1}H and ^{13}C{^{1}H} NMR showed a more complex aromatic region than was expected for a naphthyl moiety but MS suggested that the desired product had

been formed. DVT studies, discussed below (section **5.3.4**) indicated that the impurity was surface active, *i.e.* it had a dodecyl chain moiety. Initially it was thought that the impurity was a structural isomer of the target ligand, however, when crystals were obtained from the final product they showed that the impurity was in fact a tertiary amine by-product of the reductive amination reaction between 1-naphthaldehyde and 1-dodecylamine. Figure 5.7 shows the X-ray crystal structure obtained.

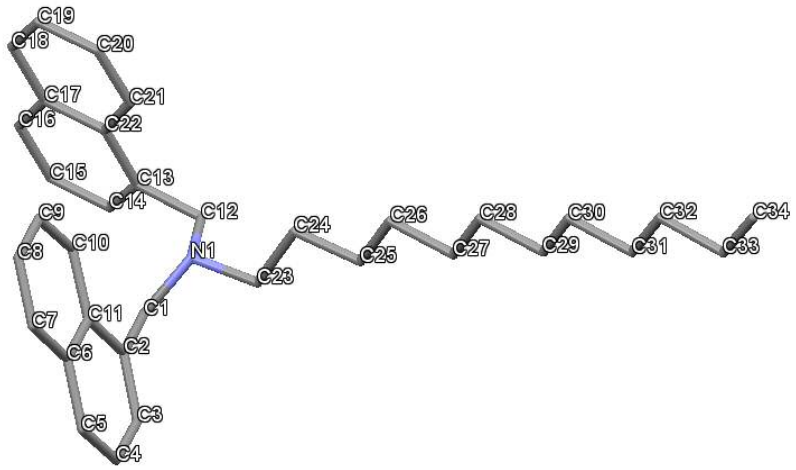

Figure 5.7 Crystal structure of impurity (H atoms omitted for clarity; details in appendix) crystals suitable for X-ray diffraction studies obtained by slow evaporation of product in MeCN at room temperature

This species was also present in some of the MS spectra recorded for the free ligand and complexes, seen as peaks at *m/z* = 466.34 and 467.3993, corresponding to $[M+H]^+$ and $[M+2H]^+$ in LR and HRMS, respectively.

Bond	Angle/°
C(1)-N(1)-C(12)	110.21(8)
C(1)-N(1)-C(23)	111.40(8)
C(12)-N(1)-C(23)	109.64(8)
N(1)-C(1)-C(2)	113.79(8)
N(1)-C(12)-C(13)	114.13(8)
N(1)-C(23)-C(24)	113.20(8)

Table 5. 2 Selected bond angles for the X-ray crystal structure shown in Figure 5.7

Table 5.2 shows selected bond angles for the structure obtained. It can be seen that the C-N-C angles around the tertiary amine are all very similar as are the N-C-C bond angles for each arm, showing that there is no steric competition between the two naphthyl groups and the dodecyl

chain. The N-C bond lengths are also very similar, with values of 1.469 Å, 1.470 Å and 1.468 Å for N(1)-C(1), N(1)-C(12) and N(1)-C(23), respectively.

5.3.3 Photophysical Characterisation

5.3.3.1. Absorption Spectroscopy

The absorption spectra shown in Figure 5.8 were measured in aerated MeCN solution (10^{-5} M) at room temperature. The **DO3ANaphC$_{12}$** ligand spectrum shows $^{1}\pi$-π^* absorption with some vibronic structure in the lower energy region corresponding to intraligand charge transfer. Although the absorption profile for **DO3AQuinC$_{12}$** shows the same peaks they are red-shifted compared to those of **DO3ANaphC$_{12}$**. This can possibly be attributed to the extended conjugation which is known to bring the π levels closer together meaning that they can be sensitised by wavelengths of lower energy, even into the visible region.[37] The absorption spectrum of **DO3AQuinC$_{12}$** shows a π-π* transition at ~235 nm and a π-π*or n-π* transition at ~320 nm. It is noticeable that the difference in relative peak intensity is markedly larger for **DO3ANaphC$_{12}$** than **DO3AQuinC$_{12}$**. Unlike the other spectra the profile for **DO3AAnthC$_{12}$** shows only one absorption peak with no vibronic structure. This signal can be attributed to π-π* absorption within the pendent anthracene moiety. The positioning of the peak may be attributed to the extended conjugation of the anthracene's three-ring system.

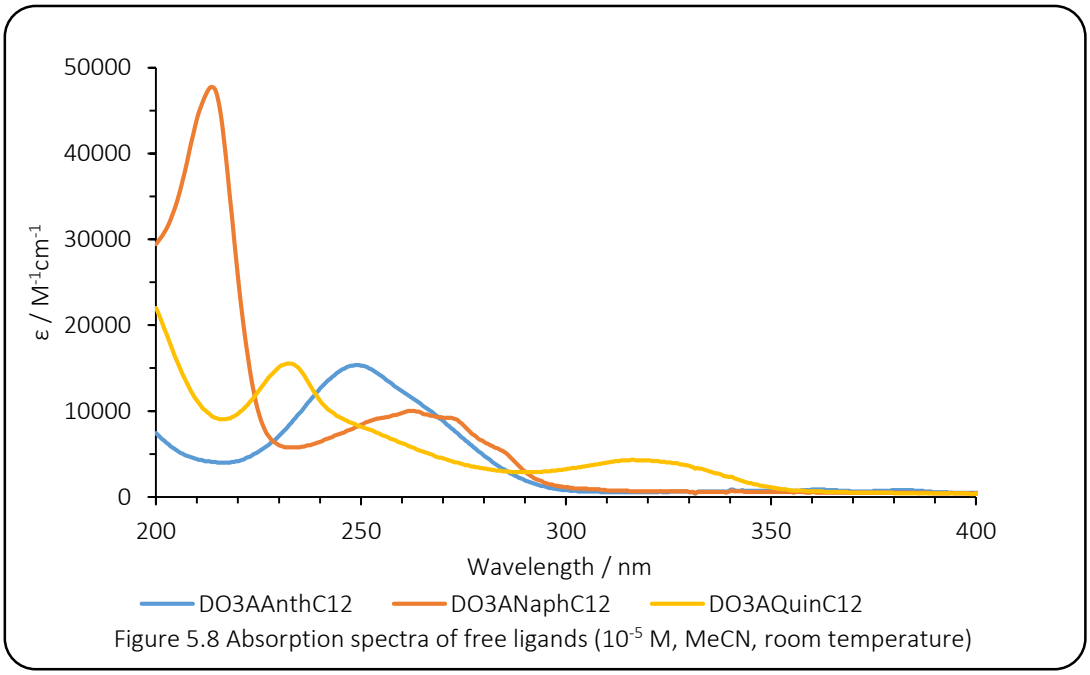

Figure 5.8 Absorption spectra of free ligands (10^{-5} M, MeCN, room temperature)

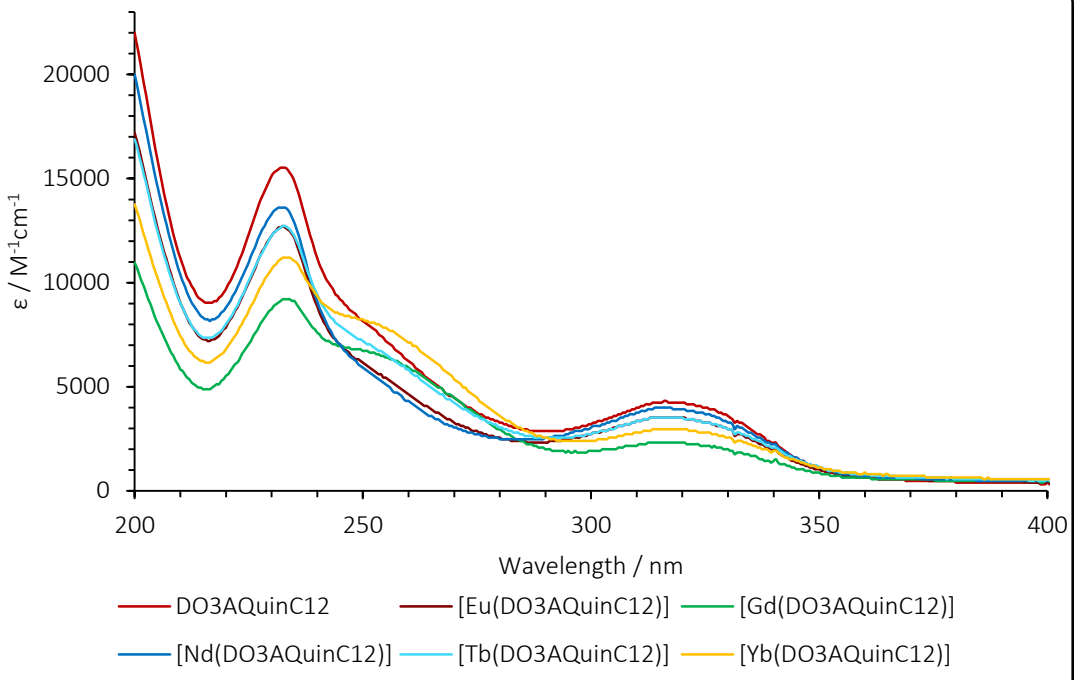

Figure 5.9 Absorption spectra of DO3AQuinoxC_{12} and complexes (10^{-5} M, MeCN, room temperature)

Figure 5.9 above, is an example of how complexation of the free ligands to lanthanide ions has very little effect on the absorption profile; this was also seen for **DO3ANaphC$_{12}$** and **DO3AAnthC$_{12}$** complexes. The absorption characteristics of all the ligands and complexes are dominated by the n-π* and π-π* transitions of the chromophoric antenna species.

Ligand/Complex	λ_{abs} /nm[a]	λ_{em} /nm [a]	λ_{em} /nm 77 K [b]	τ [c]	q [d]
DO3ANaphC$_{12}$	286 (5000), 274 (9000), 263 (10000), 253 (9000), 214 (47700).	653 (weak), 399, 340 sh., 327 sh.	-	3.53 ns (7%) 38.5 ns (93%)	-
DO3AAnthC$_{12}$	390 (3800), 252 (17400).	668 (weak), 623 (weak), 440, 418.	-	1.19 ns (36%) 5.36 ns (64%)	-
DO3AQuinC$_{12}$	318 (4200), 254 sh. (7400), 233 (15500).	439	-	0.294 ns (52%) 2.01 ns (48%)	-
[Eu(DO3ANaphC$_{12}$)]	285 (2600), 273 (3100), 266 (3100), 215 (24200)	701, 689, 683, 655, 616, 594, 580, 416, 396, 340.	-	425 µs (H_2O) 480 µs (D_2O)	0.02
[Gd(DO3ANaphC$_{12}$)]	273 (5700), 263 (6100), 253 (5400), 215 (31500)	654 (weak), 398, 345 sh., 327 sh.	(675), (665), 645, (636), 549, 511, (487), 475, (367 sh.), 349, 337, 323	2.04 ns (43%) 8.04 ns (57%)	-
[Yb(DO3ANaphC$_{12}$)]	285 (3000), 273 (4600), 262 (4600), 215 (29100).	NIR: no peaks	-	1.413 µs (H_2O) 6.343 µs (D_2O)	0.35
[Tb(DO3ANaphC$_{12}$)]	284 (4200), 272 (6800), 262 (7400), 215 (37800)	651, 397, 344 sh., 327 sh.	-	No signal	-
[Nd(DO3ANaphC$_{12}$)]	284 (2800), 273 (5000), 262 (6000), 215 (20600).	NIR: no peaks	-	78 ns (H_2O) 335 ns (D_2O)	2.45
[Gd(DO3AAnthC$_{12}$)]	392 sh. (3800), 253 (17400).	421	(509), (469), 441, (423 sh.), 415, (397 sh.), 391, (381)	7.97 ns	-

Ligand/Complex	λ_{abs} /nm[a]	λ_{em} /nm [a]	λ_{em} /nm 77 K [b]	τ [c]	q [d]
[Yb(DO3AAnthC$_{12}$)]	265 sh. (13100), 247 (21500).	-	-	0.396 ns (H_2O) 4.560 µs (D_2O)	2.11
[Eu(DO3AQuinC$_{12}$)]	318 (3500), 233 (12600).	701, 689, 685, 655, 616, 594, 581, 421, 398, 341.	-	486 µs (H_2O) 754 µs (D_2O)	0.60
[Gd(DO3AQuinC$_{12}$)]	318 (2300), 257 sh. (6200), 235 (9100).	654 (weak), 398, 345 sh., 327 sh.	(560 sh.), 524, 492, 433	2.30 ns (59%) 0.465 ns (41%)	-
[Yb(DO3AQuinC$_{12}$)]	317 (3000), 256 sh. (7700), 235 (11100).	NIR: 1028, 1000, 984	-	2.248 µs (H_2O) 8.060 µs (D_2O)	0.12
[Tb(DO3AQuinC$_{12}$)]	318 (2300), 258 sh. (6000), 234 (12600).	544, 489, 429.	-	No signal	-
[Nd(DO3AQuinC$_{12}$)]	317 (4000), 233 (12600).	NIR: (905), (878), 1064	-	209 ns (H_2O) 484 ns (D_2O)	0.39

Table 5.3 [a] measurements obtained in aerated 10^{-5} M UPW solutions at 293 K; [b] EtOH-MeOH (1:1) glass at 77 K; [c] lifetimes measured in H_2O unless otherwise stated, error ~10 %; [d] hydration factors calculated according to equations outlined in section **5.1.3**.

5.3.3.2. Emission Spectroscopy

Steady state measurements of the ligands and complexes were carried out in ultra-pure water (UPW). The emission spectra of the free ligands (Figure 5.10) show only broad, fairly structureless fluorescence from the pendent chromophores. There was no evidence for triplet emission from these ligands and this can be attributed to dissolved oxygen which quenches the T→S relaxation pathway at room temperature meaning only the $S_1 \rightarrow S_0$ relaxation is observed at short wavelengths with short fluorescence lifetimes.

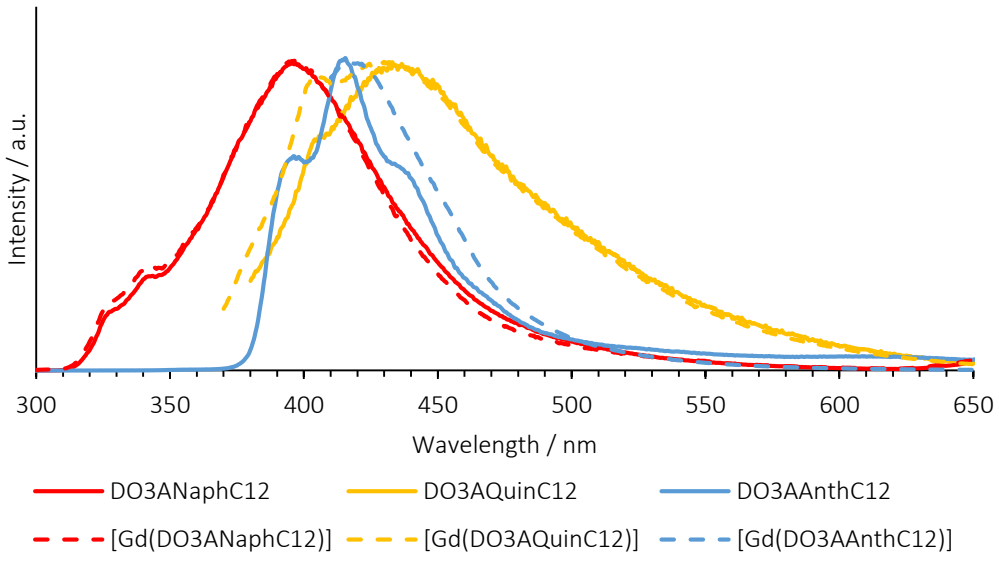

Figure 5.10 Steady State emission spectra of free ligands and Gd(III) complexes (measured in UPW at 293 K)

The dashed lines in Figure 5.10 show the emission profiles of the Gd(III) complexes. As for the free ligands, only chromophoric fluorescence is observed as energy transfer to the excited state of Gd(III) is not energetically favourable. However, a small shift was observed between the Gd(III) complexes and the free ligands which can be attributed to perturbation as a result of metal coordination.

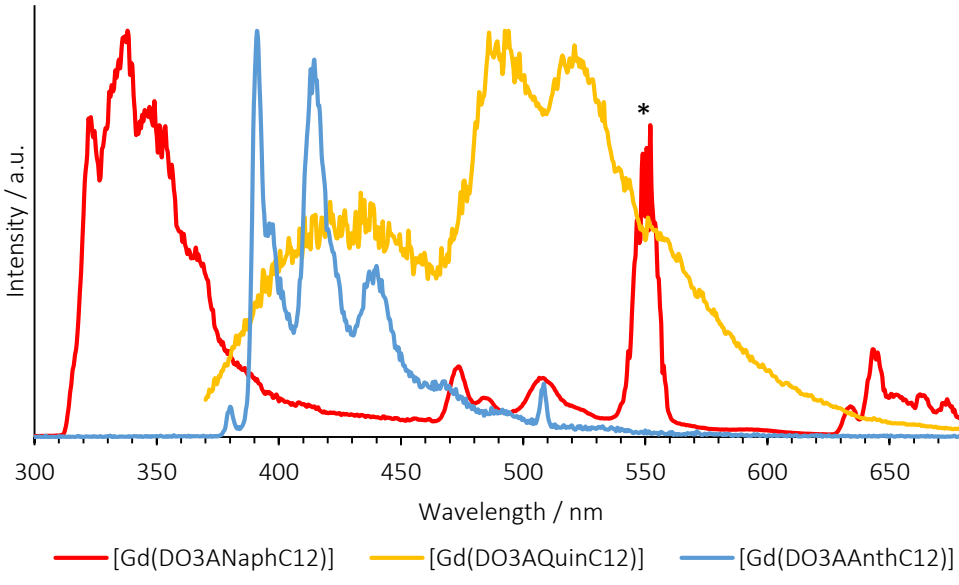

Figure 5.11 Low temperature emission spectra of Gd(III) complexes (measured on EtOH-MeOH glass at 77K; *double excitation harmonic peak)

The low temperature emission spectra of the Gd(III) complexes were measured at 77 K on an EtOH-MeOH (1:1) glass (Figure 5.11) in order to identify the triplet levels of the different chromophores. The lowest excited state energy level for Gd(III) is 32,000 cm^{-1} therefore it cannot accept energy from long-wavelength chromophores.[38]

The **[Gd(DO3ANaphC$_{12}$)]** spectrum shows $^{1}\pi$-π* emission in the 300-400 nm region but also demonstrates vibronically structured triplet emission from the naphthyl antenna with an onset around 21,500 cm^{-1} which is in good agreement with previously reported values.[39] **[Gd(DO3AQuinC$_{12}$)]** shows a similar emission profile with $^{1}\pi$-π* emission around 370-460 nm and an onset of triplet emission which matches that of the naphthyl analogue.

The reason for the residual singlet emission is the fact that ISC to the triplet state is not 100% efficient. Transfer is directly related to the physical distance between the chromophore antenna and the Ln(III) ion because spin orbit coupling, mediated by the heavy atom effect of the Ln(III) ion, is responsible for promoting ISC. In these complexes the ion and the antenna are separated by an amide linker which creates a relatively large physical separation.

The low temperature emission spectra suggest that **DO3ANaphC$_{12}$** and **DO3AQuinC$_{12}$** will be capable of sensitising a range of Ln(III) ions as their triplet states lie above those of Eu(III) ($^{5}D_1$ 19,020 cm^{-1} and $^{5}D_1$ 17,250 cm^{-1}),[40] Tb(III) (20,430 cm^{-1})[41] and Yb(III) (10,300 cm^{-1}),[12,42] therefore energy transfer from the chromophore to the Ln(III) ion will be possible.

For the **[Gd(DO3AAnthC$_{12}$)]** complex, however, no triplet level is observed in the low temperature spectrum. Instead only fluorescence is observed at 77 K, though the emission spectrum is well resolved, showing vibronic structure corresponding to the anthryl chromophore. Although no triplet emission was observed for the anthryl species, literature studies report it to be around 14,500 cm^{-1} meaning that it cannot sensitise Tb(III) or Eu(III).[43]

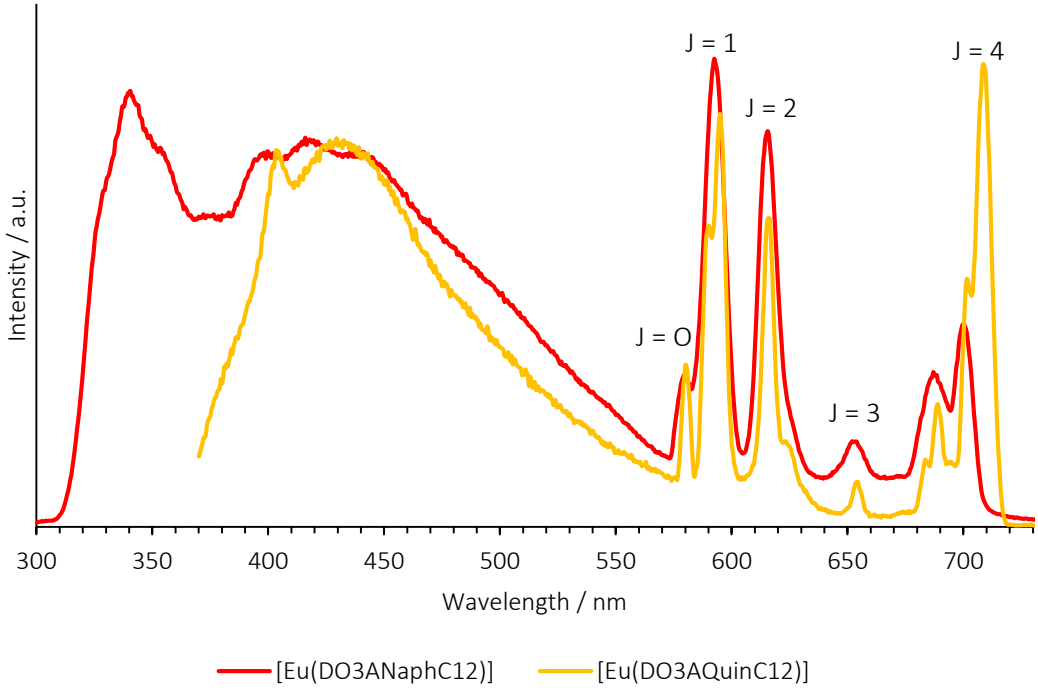

Figure 5.12 Steady state total emission spectra of Eu(III) complexes

(measured in UPW at 293 K; λ_{Ex} = 275 nm (Naph) and 355 nm (Quin) based on emission maxima)

Figure 5.12, above, shows the steady state total emission spectra for the Eu(III) complexes of **DO3ANaphC$_{12}$** and **DO3AQuinC$_{12}$**. In each case both Eu(III) sensitised emission (~560-720 nm) and residual chromophore fluorescence (~300-560 nm) of similar intensities are observed. This shows that the energy transfer process from the chromophore is not 100% efficient. The efficiency of ISC is directly related to the physical distance between the chromophore and the Ln(III) ion. In the complexes reported here the presence of a methyl linker to the pendent chromophore creates a separation between the Ln(III) ion and the antenna which also prevents the chromophore from coordinating to the metal resulting in an apparent reduction in energy transfer efficiency.

It is possible to assign the hyperfine transitions for the region of the Eu(III) complex spectra above 570 nm, as shown in Figure 5.12. These peaks correspond to emission from the $^5D_0$ state and are well resolved thus the transitions can be distinguished without then need to time-gate the emission (see Table 5.4 below). As the transitions are indicative of the metal coordination environment the observed change in the relative ratios of the hyperfine structure corresponds to a change in the Eu(III) coordination sphere. This is to be expected as the nature of the ligand has changed even though the chelating parts of the ligand remain the same. This can also be related to the value of the hydration state, *q*, discussed later.

Complex	J=0	J=1	J=2	J=3	J=4
[Eu(DO3ANaphC$_{12}$)]	580 nm	593 nm	616 nm	653 nm	688, 701 nm
[Eu(DO3AQuinC$_{12}$)]	581 nm	595 nm	617 nm	654 nm	689, 709 nm

Table 5.4 Sensitised Eu(III) transitions from steady state emission measurements

Figure 5.13, below, illustrates the emission spectra for the Tb(III) complexes of **DO3AQuinC$_{12}$** and **DO3ANaphC$_{12}$** measured in UPW. Although Tb(III) emission would be expected for the **DO3ANaphC$_{12}$** complex, it is not observed in this case. However, the **DO3AQuinC$_{12}$** analogue shows some very weak hyperfine structure on the shoulder of the chromophore fluorescence peak that can be assigned J=6 (490 nm) and J=5 (550 nm) corresponding to the $^5D_4 \rightarrow {}^7F_6$ and $^5D_4 \rightarrow {}^7F_5$ transitions, respectively.[44]

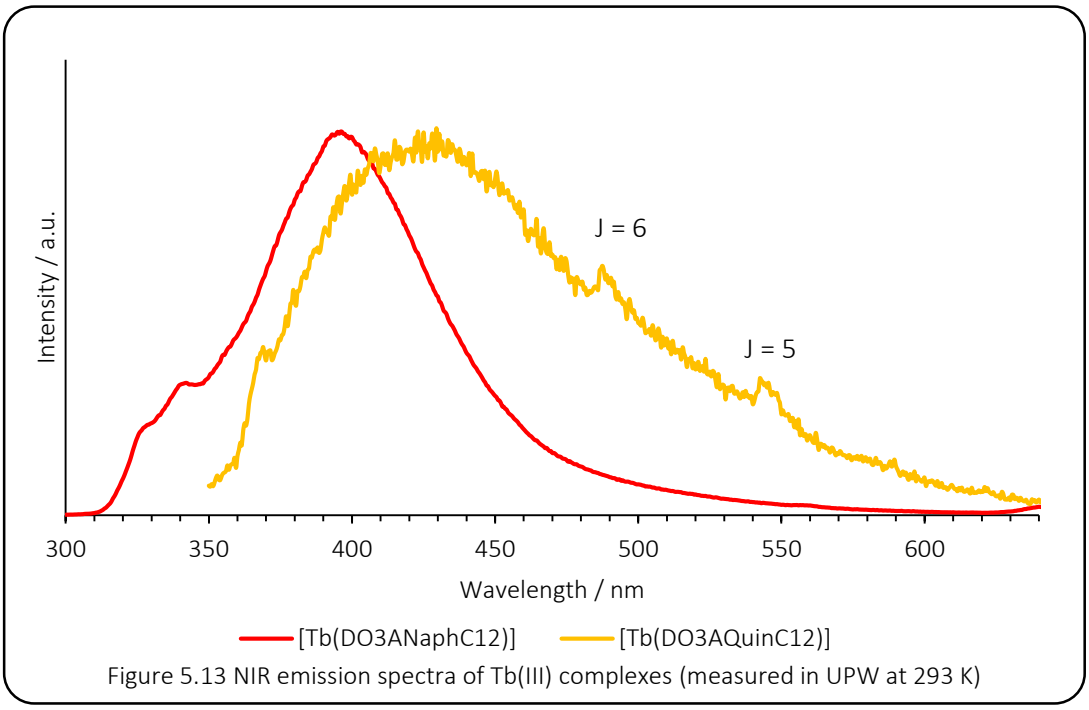

Figure 5.13 NIR emission spectra of Tb(III) complexes (measured in UPW at 293 K)

The lack of sensitisation for **DO3ANaphC$_{12}$** and the weak structure seen for **DO3AQuinC$_{12}$** may be due to the fact that the triplet level for Tb(III) lies at 20,430 cm^{-1} which is very close to the triplet levels determined for the ligand chromophores which both lie at 21,500 cm^{-1}.[41] If the energy levels lie close together then thermally activated back energy transfer is more likely which will lead to a reduction in emission observed from the Ln(III) ion.

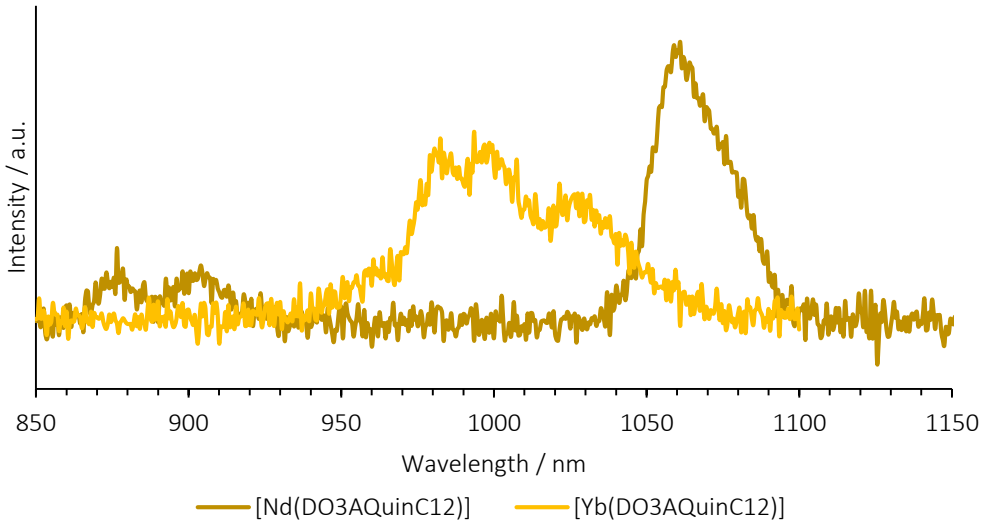

Figure 5.14 NIR emission spectra of DO3AQuinC$_{12}$ complexes (measured in UPW at 293 K)

The NIR emission spectra were recorded for the Yb(III) and Nd(III) complexes of **DO3AQuinC$_{12}$** and **DO3ANaphC$_{12}$**. For the **DO3ANaphC$_{12}$** analogue no lanthanide signals were observed for either metal. However, for **DO3AQuinC$_{12}$** peaks were seen for both Yb(III) and Nd(III) emissions (Figure 5.14, above). The Nd(III) spectrum shows a peak at around 1063 nm corresponding to the $^4F_{3/2} \rightarrow {}^4I_{11/2}$ transition. The Yb(III) analogue, however, shows a peak around 984 nm characteristic of the $^2F_{5/2} \rightarrow {}^2F_{7/2}$ transition along with a lower energy peak at 1030 nm corresponding to ligand field induced splitting of the $^2F_{7/2}$ manifold.

The luminescent lifetime values were recorded for the Eu(III), Yb(III) and Nd(III) complexes in both H_2O and D_2O in order to determine the hydration factors (q) for the metallosurfactants. Water molecules that are associated with the Ln(III) ion cause quenching due to energy transfer from the Ln(III) ion to the O-H oscillations. The rate at which the emission lifetime is quenched is proportional to the number of O-H oscillators associated with the Ln(III) ion. When H_2O is substituted for D_2O more intense emission is observed as O-D oscillators have much smaller vibrational stretching frequencies thus energy transfer from the Ln(III) ion is much less efficient. By measuring the emission lifetimes of a species in both H_2O and D_2O the hydration factor (q) can be quantified (see section **5.1.3**) which correlates linearly with the number of inner sphere water molecules associated with a Ln(III) ion and therefore provides important information about the coordination geometry of the metal.

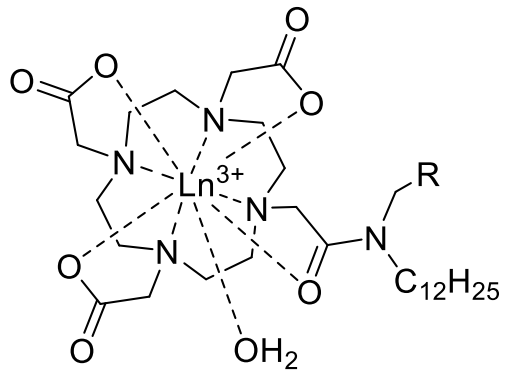

Figure 5.15 Example of hydrated lanthanide complex;
R = naphthyl, anthryl, quinyl, Ln = Eu, Gd, Nd, Yb, Tb

The calculated hydration factors are listed with the photophysical data in Table 5.3. For the **DO3AQuinC$_{12}$** and **DO3ANaphC$_{12}$** complexes studied the hydration factors were between 0.02 and 0.60 which suggests the presence of 0-1 inner sphere water molecules (with the exception of **[Nd(DO3ANaphC$_{12}$)]** as discussed below). Although a number of studies described direct coordination of chromophoric N-atoms to the lanthanide this is not possible for the systems reported here as the amide linker creates a physical distance too large to be spanned. Instead, the O-atom of the amide contributes to the coordination sphere which, along with 4 macrocyclic N-atoms and 3 carboxylate O-atoms provide 8 binding sites from the ligand framework. This agrees with the expected degree of solvation as Ln(III) ions are generally reported to favour a coordination number of 9 therefore 8 ligand binding sites and one inner sphere water molecule correlates with this hypothesis.[4,45]

The hydration factor for the Nd(III) complexes of **DO3ANaphC$_{12}$** and **DO3AQuinC$_{12}$** were calculated according to the modified Horrock's equation (section **5.1.3**). Although the equations used for the other complexes consider quenching by C-H and N-H oscillators, Nd(III) is more sensitive to the quenching effect of C-H oscillations than other lanthanide ions, which is taken into account by the modified equation. While the hydration factor of **[Nd(DO3AQuinC$_{12}$)]** correlates with those of its analogous complexes, indicating 0-1 inner sphere water molecules, the value obtained for the **[Nd(DO3ANaphC$_{12}$)]** complex was 2.45 which would suggest 2-3 inner sphere water molecules. This anomalous result is most likely due to the limitations created by the sensitivity of Nd(III) to quenching and the C-H quenching contributions which are difficult to quantify.

5.3.4 Microemulsion Compatibility

The microemulsion compatibility of the **DO3AQuinC$_{12}$** ligand and its Eu(III), Gd(III) and Tb(III) complexes were investigated, initially using drop volume tensiometry (DVT). Figure 5.16 shows the surface tension *vs.* ln[concentration in UPW] relationships of the systems studied.

For the free ligand (Figure 5.16a) there is a polynomial decrease in surface tension with increasing concentration up until 0.10 mM after which the decrease is linear and very subtle. The point at which the state of the decrease changes is recognised as the critical micelle concentration (CMC), the concentration at which the surface active species begin to aggregate into micelles. This parameter is characteristic of each particular micellar system. The presence of a clear, single CMC point suggests only one type of micelle is forming within the solution and the linear nature of the plot after this point is an indication of purity. As these measurement were performed in a purely aqueous environment it can be assumed that the hydrophobic tail groups will aggregate together on the inside of the micelle and the lanthanide-binding head groups will align on the surface.

The value of the CMC for a particular micellar system can be used to calculate the surface area of the micelle occupied by one surfactant *via* use of the equations described in section **1.5** of Chapter One. Table 5.5 shows the CMC values and calculated APM values given a Gibbs Prefactor (n) of 1 or 2. In reality the APM value is likely to lie somewhere between these values as they represent a non-ionic system (n=1) and a fully dissociated ionic system (n=2), whereas the real situation is likely to be somewhere between these two extremes. These three lanthanide ions were chosen for this study as they form a consecutive row on the Periodic Table. The calculated CMC and APM parameters show a clear difference between each of the surfactants, however, no discernible trend can be found relating to the size of the lanthanide ion and the effect it has on the APM. This result was also described by Fallis and Griffiths *et al.* who studied various lanthanide metallosurfactants and found the APM to be unrelated to ionic radius.[46]

It is also noteworthy that while the **DO3AQuinC$_{12}$** ligand and the Eu(III) complex were readily soluble in UPW at concentrations above the CMC, the Gd(III) and Tb(III) complexes were poorly soluble at high concentrations. This may be responsible for a degree of error in their CMC values as it significantly limited the amount of measurements possible after the CMC.

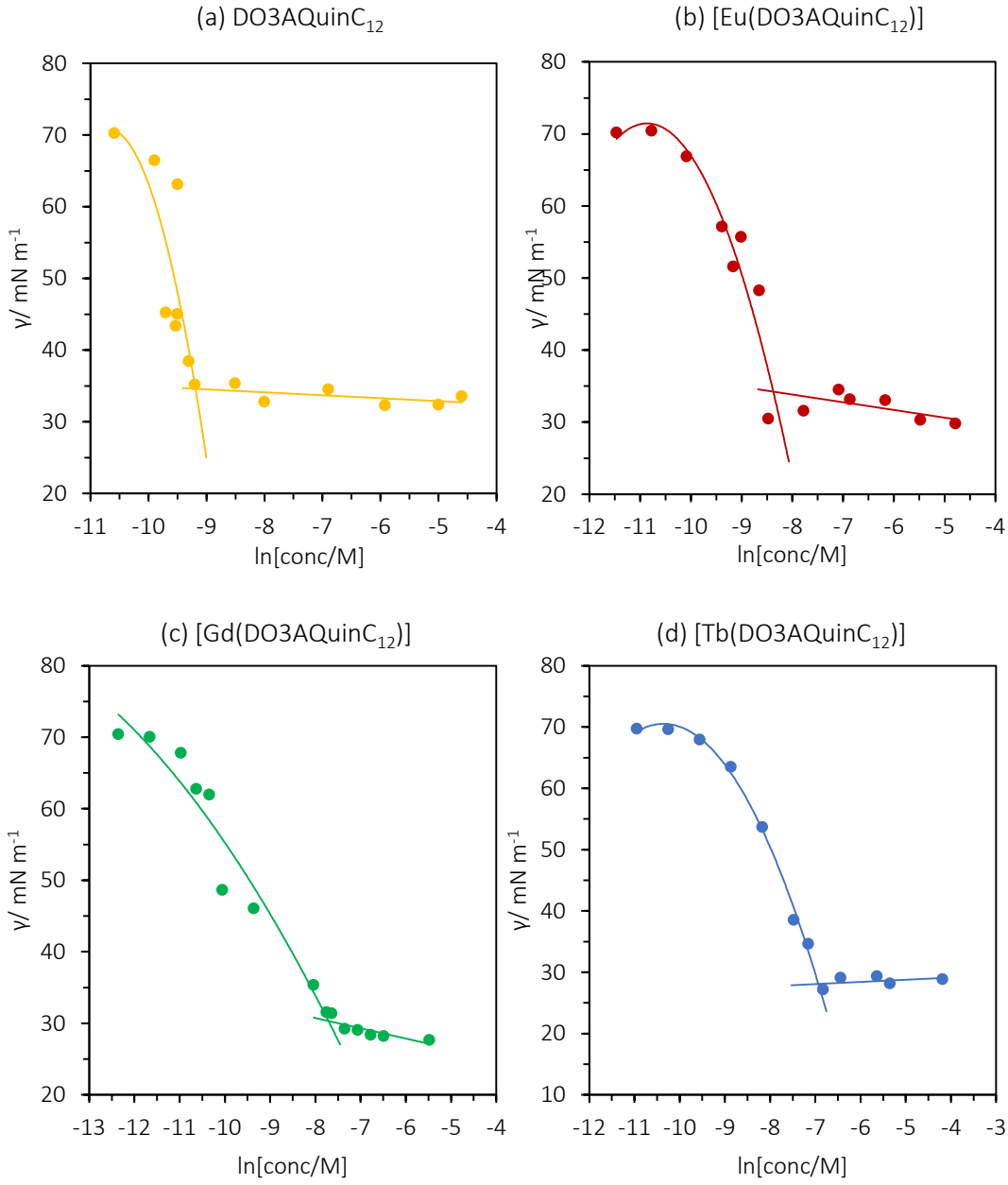

Figure 5.16 Tensiometry data (surface tension *vs.* ln [conc/M]) for the $DO3AQuinC_{12}$ ligand and its complexes (error = ± 0.05 mN m^{-1})

Species	CMC / mM (± 0.1)	APM (n=1) / Å^2 (± 1)	APM (n=2) / Å^2 (± 2)
$DO3AQuinC_{12}$	0.10	8	17
[Eu($DO3AQuinC_{12}$)]	0.22	14	27
[Gd($DO3AQuinC_{12}$)]	0.45	32	65
[Tb($DO3AQuinC_{12}$)]	0.99	16	33

Table 5.5 CMC and APM data for $DO3AQuinC_{12}$ ligand and complexes

A second microemulsion compatibility investigation was undertaken involving the **[Eu(DO3AQuinC$_{12}$)]** complex in order to study the effect of micellisation on the coordination environment of the lanthanide and the lifetime of the emission.

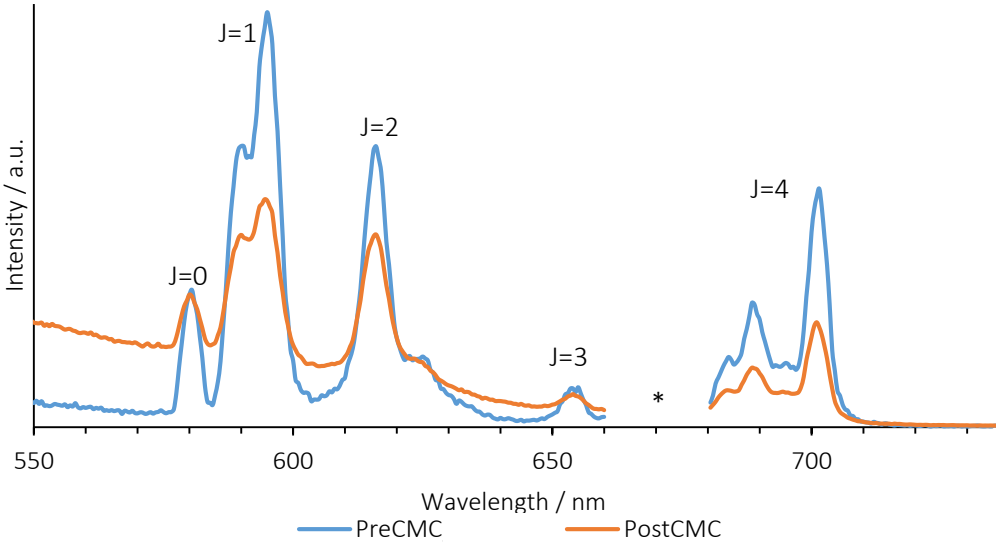

Figure 5.17 Hyperfine structure comparison of steady state emisson of [Eu(DO3AQuinC$_{12}$)]; measured in UPW at 293 K; (*harmonic peaks omitted for clarity)

Once the CMC of the **[Eu(DO3AQuinC$_{12}$)]** system had been established the effects of micellisation could be studied. Figure 5.17, above, shows the hyperfine structure for the Eu(III) transitions recorded both pre- and post-CMC. The position of the peaks are consistent between the two samples but there is a change in the relative intensities. For example pre-CMC J=1 and J=2 have a relative ratio of roughly 7:5 whereas post-CMC they are closer to 1:1. The similarity in peak position indicates that the ligand coordination is unchanged, this is to be expected as the 8-coordinate, macrocyclic **DO3AQuinC$_{12}$** ligand has a high binding efficiency to the Eu(III) ion which is not expected to alter upon aggregation. However, the change in relative ratios suggests a change in the local environment of the complex. This is a logical conclusion as pre-CMC the complex is in an aqueous environment surrounded by water molecules, whereas post-CMC water molecules are displaced by micellisation and the immediate environment of the complex has changed significantly as it is now in close proximity to other complex molecules.

The emission lifetimes for these species are presented in Table 5.6 and illustrated in Figure 5.18. It can be see that the lifetime pre-CMC is a mono-exponential decay whereas post-CMC it is bi-exponential. This trend was also observed for McGoorty *et al.* when studying cyclometallated Ir(III) complexes in micellar systems. It has been suggested that this arises because the self-assembled aggregates shield the metal from quenching *via* oxygen diffusion.[47]

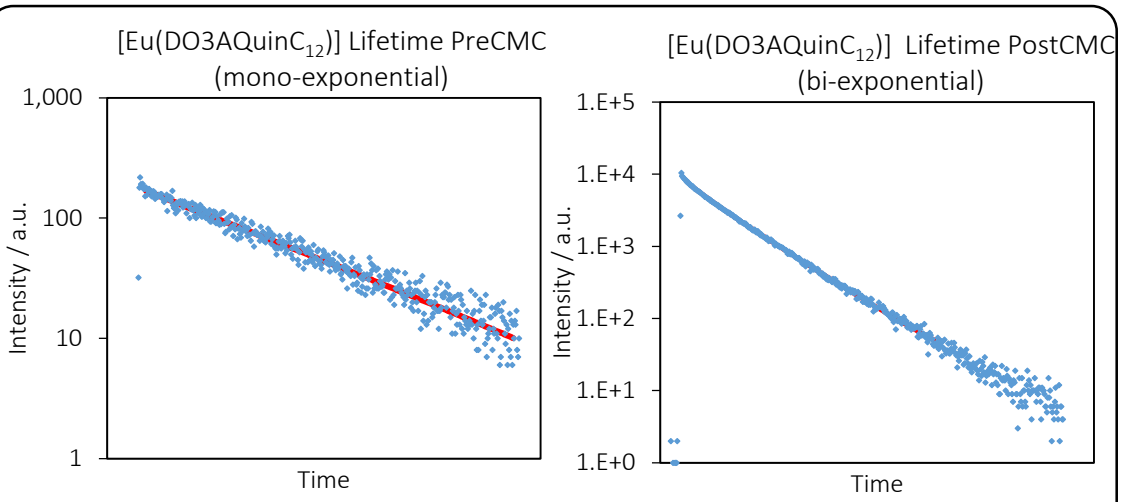

Figure 5.18 Lifetime plots for [Eu(DO3AQuinC$_{12}$)] complexes pre- and post-CMC (measured in UPW at 293 K, errors ~10 %)

[Eu(DO3AQuinC$_{12}$)]	Lifetime / µs
Pre-CMC	653
Post-CMC	188 (6.33%), 486 (93.67%)

Table 5.6 Lifetime values for [Eu(DO3AQuinC$_{12}$)] relative to the CMC

5.4 Conclusions

This chapter reports the design and synthesis of three novel amphiphilic ligands for lanthanides incorporating macrocyclic chelating head groups, pendent chromophores and dodecyl chains. The ligands were generally found to form 8-coordinate complexes with Ln(III) ions with hydration states suggesting 0-1 coordinated inner sphere water molecules.

Photophysical characterisation showed sensitised lanthanide emission in the visible and NIR regions for a number of complexes. Lack of sensitisation for some of the complexes was attributed to the large distance between the antenna and the metal ion caused by the presence of an amide linker group.

The **DO3AQuinC$_{12}$** ligand was chosen for microemulsion compatibility studies as it showed the most conclusive physical characterisation and the most promising photophysical properties. Tensiometry measurements concluded that micellisation occurred for the ligand as well as its Eu(III), Gd(III) and Tb(III) complexes. Investigations into the photophysical properties of the Eu(III) complex showed subtle changes in the hyperfine structure of the emission spectra suggesting a consistent coordination structure but a change in the local metal environment below and above the CMC. It was also noted that the lifetime changed from mono- to bi-exponential decay upon micellisation consistent with previous studies involving d-block metallosurfactants.

5.5 Experimental

5.5.1 Precursors

General Precursors

Synthesis of 1,4,7-tris(tert-butoxycarbonyl methyl)-1,4,7,10-tetrazacyclododecane[36]

Sodium acetate (1.57 g, 19.1 mmol) was added to 1,4,7,10-tetrazacyclododecane (1.00 g, 5.80 mmol) in DMA (10 mL) and cooled to -20 °C. *tert*-butyl bromoacetate (3.73 g, 19.1 mmol) in DMA (10 mL) was added dropwise over approx. 30 minutes. The reaction was allowed to reach RT and stirred overnight under a N_2 atmosphere. The mixture was poured over water (approx. 60 mL) and additional water (approx. 70 mL) was added until the formation of a clear solution. $KHCO_3$ (3.00 g, 30.0 mmol) was added portion wise until the formation of the title compound as a white precipitate (HBr salt). Yield: 2.87 g, 4.82 mmol, 83%. ^{1}H NMR (400 MHz, $CDCl_3$): δ_H = 10.19-9.86 (1H, br. s, N***H***), 3.36 (4H, s, 1,7-C***H***$_2$CO$_2^t$Bu), 3.27 (2H, s, 4-C***H***$_2$CO$_2^t$Bu), 3.14-3.05 (4H, br. m, 9,11-NC***H***$_2$), 2.96-2.83 (12H, br. m, 2,3,5,6,8,12-C***H***$_2$), 1.45-1.44 (27H, m, C(C***H***$_3$)$_3$) ppm.

Synthesis of 2-methyl-3-phenyl quinoxaline

1-phenyl-1,2-propandione (2.00 mL, 14.9 mmol) was added to 1,2-phenylene diamine (1.60 g, 14.8 mmol) in EtOH (30 mL) with AcOH (approx. 10 drops). The reaction was stirred at 78 °C for 48 hrs under a N_2 atmosphere. The mixture was cooled to RT and the solvent removed *in vacuo*. The crude product was dissolved in DCM, neutralised with NaOH soln. (2 M) and washed with water and brine. The collected organic phases were dried over $MgSO_4$ and the solvent removed *in vacuo* to give the title compound as a yellow oil. Yield: 3.06 g, 13.9 mmol, 93%. ^{1}H NMR (400 MHz, $CDCl_3$): δ_H = 7.22-7.14 (2H, m, H_{phenyl}), 6.79-6.74 (4H, m, $H_{qunox.}$), 6.62-6.56 (3H, m, H_{phenyl}), 1.86 (3H, s, C***H***$_3$) ppm. IR (solid/cm^{-1}): *v* 1479 (C=C), 1339 (C-H), 1003 (C=C), 756, 698 (C-H).

Synthesis of 3-phenylquinoxaline-2-carbaldehyde

SeO_2 (2.60 g, 23.4 mmol) was added to 2-methyl-3-phenylquinoxaline (3.06 g, 13.9 mmol) in 1,4-dioxane (15 mL) and the mixture stirred at 101 °C for 48 hrs under a N_2 atmosphere. The reaction was cooled to RT and filtered to remove Se(0). Solvent was removed *in vacuo* to give the title compound as a waxy red-brown solid. Yield: 3.23 g, 13.8 mmol, 99%. ^{1}H NMR (250 MHz, $CDCl_3$):

δ_H = 10.35 (1H, s, C(O)***H***), 8.35-8.32 (1H, m, H_{phenyl}), 8.25-8.21 (1H, m, H_{phenyl}), 7.99-7.86 (2H, m, $H_{quinox.}$), 7.74-7.69 (2H, m, $H_{quinox.}$), 7.60-7.27 (3H, m, H_{phenyl}) ppm. IR (solid/cm^{-1}): *v* 2862 (C-H), 1709 (C=O), 760, 687 (C-H).

Secondary Amines

Synthesis of *N*-(naphthalen-1-ylmethyl)dodecan-1-amine

1-Naphthaldehyde (3 mL, 22.1 mmol) and 1-dodecylamine (4.52 g, 24.4 mmol) were stirred in DCE (25 mL) for 5 hrs at RT. Sodium tris(acetoxy)borohydride (5.15 g, 24.3 mmol) was added and the solution stirred for 5 days under a N_2 atmosphere (reaction followed by TLC). The reaction was neutralised with sat. $NaHCO_3$ soln. and extracted into $CHCl_3$. The combined organic phases were washed with water and brine and dried over $MgSO_4$. The solvent was removed *in vacuo* to give the title compound as a yellow-orange oil which solidified on standing. Yield: 4.88 g, 15.0 mmol, 68%. ^{1}H NMR (400 MHz, $CDCl_3$): δ_H = 8.12 (1H, app. d, J_{HH} = 8.3 Hz, $H_{arom.}$), 7.87 (1H, app. d, J_{HH} = 8.4 Hz, $H_{arom.}$), 7.77 (1H, app. d, J_{HH} = 8.0 Hz, $H_{arom.}$), 7.54-7.42 (4H, m, $H_{arom.}$), 4.24 (2H, s, arom-C***H***$_2$-NH), 2.74 (2H, t, $^3J_{HH}$ = 7.3 Hz, NH-C***H***$_2$-CH_2), 1.56-1.54 (2H, m, NH-CH_2-C***H***$_2$), 1.40 (18H, br. s, -(C***H***$_2$)$_9$-),0.92 (3H, t, $^3J_{HH}$ = 6.8 Hz, C***H***$_3$) ppm. ^{13}C{^{1}H} NMR (75 MHz, $CDCl_3$) δ_C = 133.9, 131.8, 131.3, 129.0, 128.0, 126.8, 126.1, 125.5, 123.3, 49.1, 48.2, 32.0, 29.7, 29.5, 28.2, 27.2, 22.8, 14.3 ppm. HRMS (ES^+) found *m/z* 326.2845, calculated *m/z* 326.2842 for $[C_{23}H_{36}N]^+$. IR (solid/cm^{-1}): *v* 2928, 2835 (C-H), 1470, 1445 (C=C), 1336 (C-H), 1149 (C-N), 1112 (C=C), 894, 726 (C-H).

Synthesis of *N*-(anthracen-9-ylmethyl)dodecan-1-amine

Prepared ***N*-(naphthalen-1-ylmethyl)dodecan-1-amine** but using 9-anthraldehyde (3.01 g, 14.6 mmol) and 1-dodecylamine (2.97 g, 16.0 mmol) with sodium tris(acetoxy)borohydride (3.39 g, 16.0 mmol) in DCE (25 mL) to give the title compound as a dark brown oil which solidified on standing. Yield: 5.29 g, 14.1 mmol, 97%. ^{1}H NMR (400 MHz, $CDCl_3$): δ_H = 8.40 (3H, app. t, J_{HH} = 7.9 Hz, H_{arom}(1,8,10)), 8.03 (2H, d, $^3J_{HH}$ = 8.4 Hz, H_{arom}(4,5)), 7.58 (2H, td, J_{HH} = 7.6, 1.1 Hz, H_{arom}(2,7)), 7.50 (2H, app. t, J_{HH} = 7.4 Hz, H_{arom}(3,6)), 4.74 (2H, s, arom-C***H***$_2$-NH), 2.91 (2H, t, $^3J_{HH}$ = 7.3 Hz, NC***H***$_2$$CH_2$), 1.63 (2H, app. t, J_{HH} = 6.9 Hz, NCH_2C***H***$_2$), 1.32 (18H, s, -(C***H***$_2$)$_9$-), 0.66 (3H, t, $^3J_{HH}$ = 6.8 Hz, C***H***$_3$) ppm. ^{13}C{^{1}H} NMR (75 MHz, $CDCl_3$) δ_C = 134.2, 133.6, 131.5, 130.8, 129.4, 129.0, 128.4, 127.3, 126.8, 125.2, 123.9, 48.9, 44.1, 32.0, 29.7, 29.6, 29.5, 29.4, 27.2, 22.8, 14.3 ppm. HRMS (ES^+) found *m/z* 376.3000, calculated *m/z* 376.2999 for $[C_{27}H_{38}N]^+$. IR (solid/cm^{-1}): *v* 2920, 2845 (C-H), 1466, 1445 (C=C), 1339 (C-H), 1155 (C-N), 1111 (C=C), 891, 731 (C-H).

Synthesis of *N*-((3-phenylquinoxalin-2-yl)methyl)dodecan-1-amine

Prepared as ***N*-(naphthalen-1-ylmethyl)dodecan-1-amine** but using 3-phenylquinoxaline-2-carbaldehyde (3.24 g, 13.8 mmol) and 1-dodecylamine (3.04 g, 16.4 mmol) with sodium tris(acetoxy)borohydride (3.23 g, 15.2 mmol) in DCE (30 mL) to give the title compound as a dark brown oil. Yield: 4.15 g, 10.3 mmol, 74%. ^{1}H NMR (250 MHz, $CDCl_3$): δ_H = 8.07-8.00 (2H, m, H_{phenyl}), 7.65-7.60 (4H, m, $H_{quinox.}$), 7.43-7.40 (3H, m, H_{phenyl}), 4.05 (2H, s, arom-C***H***$_2$-NH), 3.46-3.37 (1H, br. s, N**H**), 2.58 (2H, t, $^{3}J_{HH}$ = 7.1 Hz, NC***H***$_2$CH$_2$), 1.52-1.41 (2H, br. m, NCH$_2$C***H***$_2$), 1.24 (18 H, s, -(C***H***$_2$)$_9$-), 0.80 (3H, t, $^{3}J_{HH}$ = 6.6 Hz, C***H***$_3$) ppm. ^{13}C{^{1}H} NMR (75 MHz, $CDCl_3$) δ_C = 144.7, 130.0, 129.4, 128.9, 128.5, 122.6, 121.6, 120.7, 32.0, 29.8, 29.5, 22.8, 14.3 ppm. LRMS (ES$^+$) found *m/z* 618.36, calculated 618.36 for [M+(phenylquinoxaline)-4H]$^+$. IR (solid/cm^{-1}): *v* 3312, 3059 (N-H), 2920, 2850 (C-H), 1655, 1464 (C=C), 1341 (C-N), 760, 696 (C-H).

Chloroacetamides

Synthesis of 2-chloro-*N*-dodecyl-*N*-(naphthalen-1-ylmethyl)acetamide[48]

NEt_3 (3.37 mL, 24.0 mmol) was added to *N*-(naphthalen-1-ylmethyl)dodecan-1-amine (7.17 g, 22.0 mmol) in MeCN (30 mL) and cooled to 0 °C. Chloroacetyl chloride (2.95 mL, 37.0 mmol) in MeCN (20 mL) was added dropwise. The reaction was allowed to reach room temperature and stirred for 72 hrs under a N_2 atmosphere. The solvent was removed *in vacuo*, the crude residue was dissolved in DCM, washed with water and dried over $MgSO_4$. The solvent was removed *in vacuo* and the title compound as a light brown oil. Yield: 6.04 g, 15.0 mmol, 68%. ^{1}H NMR (250 MHz, $CDCl_3$): δ_H = 7.90-7.08 (7H, m, $H_{arom.}$), 4.98 (2H, s, Cl-C***H***$_2$), 4.05 (2H, s, arom-C***H***$_2$-N), 3.02 (2H, t, $^{3}J_{HH}$ = 7.6 Hz, N-C***H***$_2$-CH$_2$), 1.42-1.39 (2H, m, NH-CH$_2$-C***H***$_2$), 1.13 (18H, s, -(C***H***$_2$)$_9$-), 0.79-0.75 (3H, m, C***H***$_3$) ppm (signals from impurity excluded). ^{13}C{^{1}H} NMR (75 MHz, $CDCl_3$) δ_C = 166.6, 134.1, 132.0, 131.7, 130.6, 128.8, 128.7, 128.5, 126.8, 126.7, 126.6, 126.2, 125.3, 123.7, 49.2, 46.9, 46.4, 41.5, 39.8, 32.1, 29.8, 29.5, 26.9, 22.8, 14.3 ppm. LRMS (ES$^+$) found *m/z* 402.26, calculated 402.26 for [M+H]$^+$. HRMS (ES$^+$) found *m/z* 402.2564, calculated 402.2556 for [$C_{25}H_{36}NOCl$+H]$^+$. UV-Vis (CH_3CN): λ_{max}/nm (ε/M^{-1} cm^{-1}) = 277 (2900), 220 (12800). IR (solid/cm^{-1}): *v* 3292, 2916, 2849, 2470 (C-H), 1643 (C=O), 1463 (C=C), 1375 (C-N), 775 (C-H).

Synthesis of 2-chloro-*N*-dodecyl-*N*-(anthracen-9-ylmethyl)acetamide

Prepared similarly to **2-chloro-*N*-dodecyl-*N*-(naphthalen-1-ylmethyl)acetamide** but using NEt_3 (2.18 mL, 15.5 mmol) and *N*-(anthracen-9-ylmethyl)dodecan-1-amine (5.29 g, 14.1 mmol) with chloroacetyl chloride (1.91 mL, 24.0 mmol) in MeCN (45 mL). The crude product was dissolved in DCM and precipitated with Et_2O to give the title compound as a dark brown oil which solidified on standing. Yield: 4.12 g, 9.11 mmol, 65%. ^{1}H NMR (250 MHz, $CDCl_3$): δ_H = 8.42 (1H, s, H_{arom}(10)), 8.21 (2H, d, $^3J_{HH}$ = 8.9 Hz, H_{arom}(1,8)), 7.98 (2H, d, $^3J_{HH}$ = 8.4 Hz H_{arom}(4,5)), 7.54-7.43 (4H, m, H_{arom}(2,3,7,6)), 5.66 (2H, s, Cl-C***H***$_2$), 4.12 (2H, s, arom-C***H***$_2$-N), 2.79 (2H, t, $^3J_{HH}$ = 8.2 Hz, NC***H***$_2$CH$_2$), 1.25-1.06 (20H, br. s, -(C***H***$_2$)$_{10}$-), 0.89 (3H, t, $^3J_{HH}$ = 6.6 Hz, C***H***$_3$) ppm. ^{13}C{^{1}H} NMR (75 MHz, $CDCl_3$) δ_C = 166.6 (***C***O), 134.2, 133.6, 131.5, 129.4, 128.7, 127.3, 127.2, 126.9, 125.3, 124.0, 45.7, 41.5, 40.3, 32.0, 29.7, 29.6, 29.5, 29.3, 28.8, 26.6, 22.8, 14.3 ppm. LRMS (AP$^+$) found *m/z* 474.29, calculated 474.25 for [M+Na]$^+$. HRMS (AP$^+$) found *m/z* 452.2712, calculated 452.2711 for [$C_{29}H_{39}NOCl$]$^+$. UV-Vis (CH_3CN): λ_{max}/nm (ε/M^{-1} cm^{-1}) = 280 (2800), 256 (12800). IR (solid/cm^{-1}): *v* 2920, 2849 (C-H), 1651 (C=O), 1464, 1427 (C=C), 1221, 1123 (C-N), 893, 783, 733 (C-H).

Synthesis of 2-chloro-*N*-dodecyl-*N*-((3-phenylquinoxalin-2-yl)methyl)acetamide

Prepared similarly to **2-chloro-*N*-dodecyl-*N*-(naphthalen-1-ylmethyl)acetamide** but using NEt_3 (1.6 mL, 11.4 mmol) and *N*-((3-phenylquinoxalin-2-yl)methyl)dodecan-1-amine (4.15 g, 10.3 mmol) with chloroacetyl chloride (1.40 mL, 17.6 mmol) in MeCN (40 mL) to give the title compound as a dark brown oil. Yield: 3.08 g, 6.42 mmol, 62%. ^{1}H NMR (250 MHz, $CDCl_3$): δ_H = 8.11-8.01 (2H, m, H_{phenyl}), 7.79-7.64 (3H, m, H_{phenyl}), 7.59-7.48 (4H, m, $H_{quinox.}$), 4.85 (2H, s, Cl-C***H***$_2$), 4.15 (2H, app. d, J_{HH} = 4.5 Hz arom-C***H***$_2$-N), 3.42 (1H, t, $^3J_{HH}$ = 7.7 Hz, N-C***H***H-CH_2), 3.25 (1H, t, $^3J_{HH}$ = 7.5 Hz, N-CH***H***-CH_2), 1.67-1.41 (2H, br. m, NCH_2C***H***$_2$), 1.36-1.15 (18H, br. s, (C***H***$_2$)$_9$), 0.84 (3H, t, $^3J_{HH}$ = 6.6 Hz, C***H***$_3$) ppm. ^{13}C{^{1}H} NMR (75 MHz, $CDCl_3$) δ_C = 170.3 (***C***O), 159.9, 153.9, 152.6, 141.7, 137.5, 129.7, 129.2, 125.0, 120.8, 32.0, 29.7, 29.5, 22.8, 14.3 ppm. LRMS (ES$^+$) found *m/z* 480.27, calculated 480.28 for [M+H]$^+$. UV-Vis (CH_3CN): λ_{max}/nm (ε/M^{-1} cm^{-1}) = 261 (2700). IR (solid/cm^{-1}): *v* 2922, 2851 (C-H), 1655 (C=C), 1607 (C=O), 1445 (C=C), 760, 575 (C-H).

5.5.2 Surfactant Ligands[49]

Synthesis of tri-*tert*-butyl-2,2',2''-(10-(2-(dodecyl(naphthalen-1-ylmethyl)amino)-2-oxoethyl)-1,4,7,10-tetraazacyclododecane-1,4,7-triyl)triacetate Protected DO3ANaphC$_{12}$

Cs_2CO_3 (0.57 g, 1.75 mmol) was added to 1,4,7-tris(tert-butoxycarbonyl methyl)-1,4,7,10-tetrazacyclododecane (0.52 g, 0.87 mmol) in MeCN (10 mL) and stirred at 50 °C for approx. 30 minutes. 2-chloro-*N*-dodecyl-*N*-(naphthalen-1-ylmethyl)acetamide (0.42 g, 1.04 mmol) in MeCN (5 mL) was added and the mixture stirred at 82°C for 72 hrs under a N_2 atmosphere. The reaction was cooled to RT and filtered to remove Cs_2CO_3. The solvent was removed *in vacuo* to give a brown residue. Unreacted macrocycle was removed via recrystallisation from toluene to isolate the title compound as a brown oil. Yield: 0.52 g, 0.54 mmol, 62%. ^{1}H NMR (400 MHz, $CDCl_3$): δ_H = 8.13-7.88 (1H, br. m, $H_{arom.}$), 7.8-7.67 (2H, br. m, $H_{arom.}$), 7.54-7.08 (4H, br. m, $H_{arom.}$), 3.58-2.39 (28H, br. m, NC***H***$_2$), 1.44-1.31 (27H, m, C(C***H***$_3$)$_3$), 1.15 (20H, br. s, -(C***H***$_2$)$_{10}$-), 0.82-0.76 (3H, m, C***H***$_3$) ppm (signals from impurity excluded). ^{13}C{^{1}H} NMR (125 MHz, $CDCl_3$) δ_C = 170.6 (***C***O), 170.5 (***C***O), 165.1 (***C***O), 164.7 (***C***O), 135.5, 133.8, 132.5, 131.7, 128.8, 128.2, 127.8, 126.9, 126.1, 125.4, 125.3, 125.2, 125.0, 123.5, 122.5, 81.0, 59.9, 57.7, 56.2, 54.2, 52.6, 46.6, 44.4, 31.9, 29.6, 29.3, 28.2, 27.4, 26.2, 22.7, 14.1 ppm. HRMS (ES$^+$) found *m/z* 902.6334, calculated 902.6341 for $[C_{51}H_{85}N_5O_7Na]^+$. UV-Vis (CH_3CN): λ_{max}/nm (ε/M^{-1} cm^{-1}) = 274 (15100), 210 (68800). IR (solid/cm^{-1}): *v* 2924, 2847, 2789 (C-H), 1730, 1506 (C=O), 1460 (C=C), 1369 (C-N), 1167, 1120 (C-O), 970 (C=C), 792, 773, 733 (C-H).

Synthesis of 2,2',2''-(10-(2-(dodecyl(naphthalen-1-ylmethyl)amino)-2-oxoethyl)-1,4,7,10-tetraazacyclododecane-1,4,7-triyl)triacetic acid DO3ANaphC$_{12}$

Deprotection was achieved by adding TFA (approx. 6 mL) to the triester (0.52 g, 0.54 mmol) in DCM (7 mL) and stirring the solution for 48 hrs at RT. The solvent was removed *in vacuo* and the residue washed with MeOH (3 x 20 mL) and dried *in vacuo*. The crude product was dissolved in DCM and hexane was added to give a dark brown oil. The mother liquor was decanted and the oil dried *in vacuo* to give the TFA salt of the title compound as a brown solid. Yield: 0.44 g, 0.47 mmol, 87%. ^{1}H NMR (400 MHz, CD_3CN): δ_H = 6.69-6.34 (3H, br. m, H_{arom}), 6.26-5.41 (4H, br. m, H_{arom}), 3.69-1.39 (28H, br. m, NC***H***$_2$), -0.09—0.41 (20H, br. m, -(C***H***$_2$)$_{10}$-), 0.56—0.58 (3H, t, $^3J_{HH}$ = 3.3 Hz, C***H***$_3$) ppm (signals from impurity excluded). ^{13}C{^{1}H} NMR (175 MHz, CD_3CN) δ_C = 161.2 (***C***O), 160.9 (***C***O), 160.6 (***C***O), 160.3 (***C***O), 134.7, 132.3, 131.6, 129.8, 129.6, 129.3, 128.9, 127.7, 127.5, 127.1, 126.5, 124.4, 123.5, 55.8, 54.2, 51.9, 49.7, 47.3, 46.9, 32.6, 30.3, 30.0, 29.7, 28.4, 27.6,

27.2, 23.3, 14.3 ppm. HRMS (ES^+) found *m/z* 710.4478, calculated 710.4498 for $[C_{39}H_{60}N_5O_7]^+$. UV-Vis (CH_3CN): λ_{max}/nm ($\varepsilon/M^{-1}\,cm^{-1}$) = 286 (5000), 274 (9000), 263 (10000), 253 (9000), 214 (47700). IR (solid/cm^{-1}): *v* 2980, 2926, 2855 (C-H), 1730, 1652 (C=O), 1458 (C=C), 1381 (C-N), 1165, 1132, 1088 (C-O), 797, 719 (C-H).

Synthesis of tri-*tert*-butyl-2,2'2''-(10-(2-((anthracen-9-ylmethyl)(dodecyl)amino)-2-oxoethyl)-1,4,7,10-tetraazacyclododecane-1,4,7-triyl)triacetate Protected DO3AAnthC$_{12}$

Prepared as **Protected DO3ANaphC$_{12}$** but using Cs_2CO_3 (0.77 g, 2.36 mmol), 1,4,7-tris(tert-butoxycarbonyl methyl) 1,4,7,10-tetrazacyclododecane (0.68 g, 1.14 mmol) and 2-chloro-*N*-dodecyl-*N*-(anthracen-1-ylmethyl)acetamide (0.62 g, 1.37 mmol) in MeCN (15 mL). The title compound was obtained as a brown oil. Yield: 0.44 g, 0.44 mmol, 38%. ^{1}H NMR (400 MHz, $CDCl_3$): δ_H = 8.34 (1H, s, $H_{arom.}$), 8.27-8.18 (2H, m, $H_{arom.}$), 7.86 (2H, app. d, J_{HH} = 8.2 Hz, $H_{arom.}$), 7.57-7.32 (4H, m, $H_{arom.}$) 3.40-2.56 (28H, br. m, NC***H***$_2$), 1.35-1.31 (27H, m, C(C***H***$_3$)$_3$), 1.20-1.14 (20H, br. m, -(C***H***$_2$)$_{10}$-), 0.79 (3H, t, $^3J_{HH}$ = 6.6 Hz, C***H***$_3$) ppm. ^{13}C{^{1}H} NMR (125 MHz, CDCl3) δ_C = 170.9 (***C***O), 170.7 (***C***O), 165.5 (***C***O), 164.8 (***C***O), 134.1, 131.3, 129.3, 127.2, 126.8, 125.1, 124.0, 123.7, 80.9, 56.7, 53.5, 52.7, 51.9, 39.4, 31.9, 29.6, 29.3, 28.2, 22.7, 14.1 ppm. LRMS (ES^+) found *m/z* 930.66, calculated 930.67 for $[M+H]^+$. HRMS (ES^+) found *m/z* 952.6496, calculated 952.6498 for $[C_{55}H_{87}N_5O_7Na]^+$. UV-Vis (CH_3CN): λ_{max}/nm ($\varepsilon/M^{-1}\,cm^{-1}$) = 380 (1300), 360 (1400), 342 (980), 326 (560), 247 (23000). IR (solid/cm^{-1}): *v* 2970, 2924, 2852 (C-H), 1728, 1636 (C=O), 1456 (C=C), 1366 (C-N), 1217, 1150 (C-N), 733 (C-H).

Synthesis of 2,2',2''-(10-(2-((anthracen-9-ylmethyl)(dodecyl)amino)-2-oxoethyl)-1,4,7,10-tetraazacyclododecane-1,4,7-triyl)triacetic acid DO3AAnthC$_{12}$

Deprotected as for **DO3ANaphC$_{12}$** using TFA (approx. 6 mL) and triester (0.44 g, 0.44 mmol) in DCM (7 mL) to give the title compound as a dark brown solid. Yield: 0.25 g, 0.25 mmol, 58%. ^{1}H NMR (400 MHz, CD_3CN): δ_H = 8.38 (1H, s, $H_{arom.}$), 8.23-8.18 (2H, br. m, $H_{arom.}$), 7.95-7.89 (2H, br. m, $H_{arom.}$), 7.69-7.67 (4H, br. m, $H_{arom.}$), 3.96-3.02 (28H, br. m, NC***H***$_2$), 1.26-1.09 (20H, br. s, -(C***H***$_2$)$_{10}$-), 0.81-0.78 (3H, m, C***H***$_3$) ppm. ^{13}C{^{1}H} NMR (175 MHz, CD_3CN) δ_C = 161.0 (***C***O), 160.8 (***C***O), 160.5 (***C***O), 160.2 (***C***O), 135.5, 133.8, 132.5, 128.1, 127.8, 125.4, 125.3, 125.2, 125.0, 62.1, 59.9, 57.7, 56.2, 54.2, 52.6, 46.4, 44.4, 40.2, 39.5, 38.9, 31.9, 29.6, 29.3, 28.2, 27.5, 26.2, 22.7, 14.1 ppm. LRMS (ES^+) found *m/z* 572.40, calculated 572.40 for [M-AnthMe+2H]$^+$. HRMS (ES^+) found *m/z* 572.4010, calculated 572.4023 for $[C_{28}H_{54}N_5O_7]^+$. UV-Vis (CH_3CN): λ_{max}/nm ($\varepsilon/M^{-1}\,cm^{-1}$) = 390

(3800), 252 (17400). IR (solid/cm^{-1}): *v* 3082 br., 2924, 2855 (C-H), 1730, 1668 (C=O), 1458, 1387 (C-N), 1182, 1132, 1087 (C-O) 7999, 719, 692 (C-H).

Synthesis of tri-*tert*-butyl-2,2',2''-(10-(2-(dodecyl((3-phenylquinoxalin-2-yl)methyl)amino)-2-oxoethyl)-1,4,7,10-tetraazacyclododecane-1,4,7-triyl)triacetate Protected DO3AQuinC_{12}

Prepared as **Protected DO3ANaphC_{12}** but using Cs_2CO_3 (0.89 g, 2.73 mmol), 1,4,7-tris(tert-butoxycarbonyl methyl)-1,4,7,10-tetrazacyclododecane (0.81 g, 1.36 mmol) and 2-chloro-*N*-dodecyl-*N*-((3-phenylquinoxalin-2-yl)methyl)acetamide (0.78 g, 1.62 mmol) in MeCN (25 mL). The title compound was obtained as a brown oil. Yield: 0.98 g, 0.94 mmol, 69%. ^{1}H NMR (400 MHz, $CDCl_3$): δ_H = 8.16-7.91 (2H, br. m, H_{phenyl}), 7.73-7.56 (3H, br. m, H_{phenyl}) 7.52-7.29 (4H, br. m, $H_{quniox.}$), 3.21-2.62 (28H, br. m, NC***H***$_2$), 1.38-1.35 (27H, m, C(C***H***$_3$)$_3$), 1.25 (20H, s, -(C***H***$_2$)$_{10}$-), 0.79 (3H, t, $^3J_{HH}$ = 6.7 Hz, C***H***$_3$) ppm. ^{13}C{^{1}H} NMR (125 MHz, $CDCl_3$) δ_C = 170.8 (***C***O), 165.2 (***C***O), 163.6 (***C***O), 162.9 (***C***O), 151.6, 147.6, 145.8, 143.3, 142.3, 141.4, 141.0, 139.4, 137.7, 131.4, 130.7, 130.2, 129.0, 128.1, 125.2, 81.1, 59.1, 57.3, 56.6, 51.7, 50.9, 47.2, 31.8, 29.5, 29.3, 28.1, 22.6, 21.4, 14.1 ppm. LRMS (AP$^+$) found *m/z* 958.62, calculated 958.67 for [M+H]$^+$; found 980.59, calculated 980.66 for [M+Na]$^+$. HRMS (ES$^+$) found *m/z* 980.6558, calculated *m/z* 980.6565 for $[C_{55}H_{87}N_7O_7Na]^+$. UV-Vis (CH_3CN): λ_{max}/nm (ε/M^{-1} cm^{-1}) = 263 (78900). IR (solid/cm^{-1}): *v* 2972, 2924, 2853 (C-H), 1726, 1647 (C=O), 1458 (C=C), 1366 (C-N), 1229, 1219, 1150 (C-O), 849 (C=C), 762, 698 (C-H).

Synthesis of 2,2',2''-(10-(2-(dodecyl((3-phenylquinoxalin-2-yl)methyl)amino)-2-oxoethyl)-1,4,7,10-tetraazacyclododecane-1,4,7-triyl)triacetic acid DO3AQuinC_{12}

Deprotected as for **DO3ANaphC_{12}** using TFA (approx. 6 mL) and triester (0.98 g, 0.94 mmol) in DCM (7 mL) to give the title compound as a dark brown solid. Yield: 0.73 g, 0.72 mmol, 76%. ^{1}H NMR (400 MHz, CD_3CN): δ_H = 8.05-7.98 (2H, br. m, H_{phenyl}), 7.80-7.74 (2H, br. m, $H_{quinox.}$), 7.64-7.60 (2H, br. m, $H_{quinox.}$), 7.54-7.49 (3H, br. m, H_{phenyl}), 4.22-2.61 (28H, br. m, NC***H***$_2$), 1.29-1.04 (20H, br. m, -(C***H***$_2$)$_{10}$-), 0.81 (3H, t, $^3J_{HH}$ = 3.3 Hz, C***H***$_3$) ppm. ^{13}C{^{1}H} NMR (175 MHz, CD_3CN) δ_C = 161.2 (***C***O), 160.9 (***C***O), 160.6 (***C***O), 160.4 (***C***O), 155.0, 142.4, 142.2, 141.5, 138.5, 131.5, 130.7, 130.3, 129.9, 129.8, 120.6, 56.0, 54.5, 52.0, 49.7, 43.8, 32.6, 30.3, 30.0, 27.6, 23.3, 14.3 ppm. HRMS (ES$^+$) found *m/z* 790.4849, calculated 790.4862 for $[C_{43}H_{64}N_7O_7]^+$. UV-Vis (CH_3CN): λ_{max}/nm (ε/M^{-1} cm^{-1}) = 318 (4200), 254 sh. (7400), 233 (15500). IR (solid/cm^{-1}): *v* 3088 br., 2926, 2855 (C-H), 1722, 1653 (C=O), 1458, 1387, 1352 (C-N), 1180, 1128 (C-O), 796, 719 (C-H).

5.5.3 Complexes

The lanthanide complexes of each ligand described above were achieved *via* addition of 1 equivalent of the corresponding $Ln(OTf)_3$ salt to the ligand in MeOH. The reaction was stirred at 50°C for 24 hours before being dried *in vacuo* to give the corresponding complexes as brown or black solids. Yields: 18 – 88 %

[Eu(DO3ANaphC$_{12}$)]

LRMS (ES^+) found *m/z* 860.37, calculated 860.35 for $[M-H]^+$, found *m/z* 884.34, calculated 884.34 for $[M+Na]^+$. HRMS (ES^+) found *m/z* 884.3440, calculated 884.3445 for $[EuC_{39}H_{58}N_5O_7Na]^+$. UV-Vis ($CH_3CN$): λ_{max}/nm ($\varepsilon/M^{-1}\ cm^{-1}$) = 285 (2600), 273 (3100), 266 (3100), 215 (24200). IR (solid/cm^{-1}): *v* 2980, 2916, 2849 (C-H), 1739, 1620, 1591 (C=O), 1464 (C=C), 1377 (C-N), 1271, 1223, 1159, 1080, 1026 (C-O), 635, 515 (C-H).

[Gd(DO3ANaphC$_{12}$)]

LRMS (ES^+) found *m/z* 867.37, calculated 867.37 for $[M+H]^+$. HRMS (ES^+) found *m/z* 867.3657, calculated 867.3660 for $[GdC_{39}H_{59}N_5O_7]^+$; found *m/z* 889.3483, calculated 889.3472 for $[GdC_{39}H_{58}N_5O_7Na]^+$. UV-Vis ($CH_3CN$): λ_{max}/nm ($\varepsilon/M^{-1}\ cm^{-1}$) = 273 (5700), 263 (6100), 253 (5400), 215 (31500). IR (solid/cm^{-1}): *v* 2980, 2926, 2855 (C-H), 1738, 1591 (C=O), 1379 (C=C), 1244 (C-N), 1223, 1153, 1084, 1028 (C-O), 637, 517 (C-H).

[Yb(DO3ANaphC$_{12}$)]

LRMS (ES^+) found *m/z* 883.39, calculated 883.38 $[M+H]^+$. HRMS (ES^+) found *m/z* 883.3803, calculated 883.3804 for $[YbC_{39}H_{59}N_5O_7]^+$. UV-Vis (CH_3CN): λ_{max}/nm ($\varepsilon/M^{-1}\ cm^{-1}$) = 285 (3000), 273 (4600), 262 (4600), 215 (29100). IR (solid/cm^{-1}): *v* 3375 br., 2980 (C-H), 1744, 1655, 1622 (C=O), 1221, 1177, 1024 (C-O), 621, 575, 517 (C-H).

[Tb(DO3ANaphC$_{12}$)]

LRMS (ES^+) found *m/z* 868.47, calculated 868.37 for $[M+H]^+$. HRMS (ES^+) found *m/z* 868.3654, calculated 868.3653 for $[TbC_{39}H_{59}N_5O_7]^+$. UV-Vis (CH_3CN): λ_{max}/nm ($\varepsilon/M^{-1}\ cm^{-1}$) = 284 (4200), 272 (6800), 262 (7400), 215 (37800). IR (solid/cm^{-1}): *v* 2980, 2923, 2857 (C-H), 1732, 1591 (C=O), 1456 (C=C), 1398 (C-N), 1221, 1159, 1084, 1026 (C-O), 637, 515 (C-H).

[Nd(DO3ANaphC$_{12}$)]

LRMS (ES$^+$) found *m/z* 853.36, calculated 853.36 for [M+3H]$^+$. HRMS (ES$^+$) found *m/z* 853.3518, calculated 853.3515 for [NdC$_{39}$H$_{59}$N$_5$O$_7$]$^+$. UV-Vis (CH$_3$CN): λ_{max}/nm (ε/M^{-1} cm^{-1}) = 284 (2800), 273 (5000), 262 (6000), 215 (20600). IR (solid/cm^{-1}): *v* 2980, 2923, 2857 (C-H), 1732, 1591 (C=O), 1456 (C=C), 1398 (C-N), 1221, 1159, 1084, 1026 (C-O), 634, 513 (C-H).

[Gd(DO3AAnthC$_{12}$)]

LRMS (ES$^+$) found *m/z* 727.31, calculated 727.30 for [M-AnthMe+2H]$^+$. HRMS (ES$^+$) found *m/z* 741.3173, calculated *m/z* 741.3173 for [GdC$_{29}$H$_{53}$N$_5$O$_7$]$^+$ ([M-C$_{14}$H$_{12}$]$^+$). UV-Vis (CH$_3$CN): λ_{max}/nm (ε/M^{-1} cm^{-1}) = 392 sh. (3800), 253 (17400). IR (solid/cm^{-1}): *v* 3420 br., 2963, 2926 (C-H), 1734, 1636 (C=O), 1256, 1163, 1086, 1024 (C-O), 795, 637 (C-H).

[Yb(DO3AAnthC$_{12}$)]

LRMS (ES$^+$) found *m/z* 791.59, calculated 791.48 for [M-Yb+MeOH-2H]$^+$.UV-Vis (CH$_3$CN): λ_{max}/nm (ε/M^{-1} cm^{-1}) = 265 sh. (13100), 247 (21500). IR (solid/cm^{-1}): *v* 3418 br., 2963, 2926 (C-H), 1734, 1636 (C=O), 1256, 1163, 1086, 1024 (C-O), 795, 637 (C-H).

[Eu(DO3AQuinC$_{12}$)]

LRMS (ES$^+$) found *m/z* 940.45, calculated 940.38 for [M+H]$^+$. HRMS (ES$^+$) found *m/z* 940.3845, calculated 940.3844 for [EuC$_{43}$H$_{61}$N$_7$O$_7$]$^+$. UV-Vis (CH$_3$CN): λ_{max}/nm (ε/M^{-1} cm^{-1}) = 318 (3500), 233 (12600). IR (solid/cm^{-1}): *v* 2980, 2928 (C-H), 1730, 1581 (C=O), 1456, 1395 (C-N), 1285, 1219, 1153, 1084, 1026 (C-O), 635, 515 (C-H).

[Gd(DO3AQuinC$_{12}$)]

LRMS (ES$^+$) found *m/z* 945.39, calculated 945.40 for [M+H]$^+$. HRMS (ES$^+$) found m/z 967.3693, calculated 967.3695 for [GdC$_{43}$H$_{60}$N$_7$O$_7$Na]$^+$. UV-Vis (CH$_3$CN): λ_{max}/nm (ε/M^{-1} cm^{-1}) = 318 (2300), 257 sh. (6200), 235 (9100). IR (solid/cm^{-1}): *v* 3431 br., 2926, 2855 (C-H), 1734, 1589 (C=O), 1445, 1410 (C-N), 1223, 1161, 1082, 1026 (C-O), 635, 515 (C-H).

[Tb(DO3AQuinC$_{12}$)]

LRMS (ES$^+$) found *m/z* 946.39, calculated 946.39 for [M+H]$^+$. HRMS (ES$^+$) found *m/z* 946.3872, calculated 946.3871 for [TbC$_{43}$H$_{61}$N$_7$O$_7$]$^+$. UV-Vis (CH$_3$CN): λ_{max}/nm (ε/M^{-1} cm^{-1}) = 318 (2300), 258 sh. (6000), 234 (12600). IR (solid/cm^{-1}): *v* 3412 br., 2980, 2928 (C-H), 1738, 1591 (C=O), 1456, 1396 (C-N), 1221, 1161, 1084, 1026 (C-O), 634, 513 (C-H).

[Yb(DO3AQuinC_{12})]

LRMS (ES^+) found *m/z* 961.40, calculated 961.40 for $[M+H]^+$. HRMS (ES^+) found *m/z* 983.3832, calculated 983.3827 for $[YbC_{43}H_{60}N_7O_7Na]^+$. UV-Vis ($CH_3CN$): λ_{max}/nm ($\varepsilon/M^{-1}\ cm^{-1}$) = 317 (3000), 256 sh. (7700), 235 (11100). IR (solid/cm^{-1}): *v* 3420 br., 2924, 2855 (C-H), 1732, 1593 (C=O), 1445, 1416 (C-N), 1223, 1163, 1084, 1026 (C-O), 635, 515 (C-H).

[Nd(DO3AQuinC_{12})]

LRMS (ES^+) found *m/z* 953.35, calculated 953.37 for $[M+Na+2H]^+$. HRMS (ES^+) found *m/z* 931.3736, calculated 931.3735 for $[NdC_{43}H_{61}N_7O_7]^+$. UV-Vis (CH_3CN): λ_{max}/nm ($\varepsilon/M^{-1}\ cm^{-1}$) = 317 (4000), 233 (12600). IR (solid/cm^{-1}): *v* 3435 br., 2926, 2855 (C-H), 1734, 1589 (C=O), 1445, 1410 (C-N), 1223, 1161, 1082, 1026 (C-O), 635, 515 (C-H).

5.6 Appendix

Parameters for crystal structure of *N,N*-bis(naphthalen-1-ylmethyl)dodecan-1-amine (Figure 5.7)

Compound	*N,N*-bis(naphthalen-1-ylmethyl)dodecan-1-amine
Formula	$C_{34}H_{43}N$
$D_{calc.}$/ g cm^{-3}	1.128
μ/mm^{-1}	0.475
Formula Weight	465.69
Colour	colourless
Shape	block
Size/mm^3	0.290×0.150×0.050
T/K	100(2)
Crystal System	triclinic
Space Group	P-1
a/Å	9.02115(16)
b/Å	9.1545(3)
c/Å	17.1568(4)
α/°	83.153(2)
β/°	77.6933(17)
γ/°	85.009(2)
V/Å^3	1371.67(6)
Z	2
Z'	1
Wavelength/Å	1.54184
Radiation type	CuK$_\alpha$
Θ_{min}/°	2.650
Θ_{max}/°	68.229
Measured Refl.	22250
Independent Refl.	4958
Reflections Used	4699
R_{int}	0.0155
Parameters	317
Restraints	0
Largest Peak	0.297
Deepest Hole	-0.246
GooF	1.052
wR_2 (all data)	0.1334
wR_2	0.1317
R_1 (all data)	0.0452
R_1	0.0440

Experimental. Single colourless block-shaped crystals of (N,N-bis(naphthalen-1-ylmethyl)dodecan-1-amine) were obtained by recrystallisation from MeCN. A suitable crystal (0.290×0.150×0.050) mm^3 was selected and mounted on a MITIGEN holder in oil on a Rigaku 007HF equipped with Varimax confocal mirrors and an AFC11 goniometer and HG Saturn 944+ detector diffractometer. The crystal was kept at *T* = 100(2) K during data collection. Using **Olex2** (Dolomanov et al., 2009), the structure was solved with the **ShelXT** (Sheldrick, 2015) structure solution program, using the Intrinsic Phasing solution method. The model was refined with version 2014/7 of **ShelXL** (Sheldrick, 2015) using Least Squares minimisation. **Crystal Data.** $C_{34}H_{43}N$, M_r = 465.69, triclinic, P-1 (No. 2), a = 9.02115(16) Å, b = 9.1545(3) Å, c = 17.1568(4) Å, α = 83.153(2)°, β = 77.6933(17)°, γ = 85.009(2)°, V = 1371.67(6) Å^3, T = 100(2) K, Z = 2, Z' = 1, μ(CuK$_\alpha$) = 0.475, 22250 reflections measured, 4958 unique (R_{int} = 0.0155) which were used in all calculations. The final wR_2 was 0.1334 (all data) and R_1 was 0.0440 (I > 2(I)).

5.7 References

1. J. R. Lakowicz, *Principles of Fluorescence Spectroscopy*, Springer Science & Business Media, 2007.

2. M. Klessinger and J. Michl, *Excited States and Photochemistry of Organic Molecules*, VCH Publishers, Inc., New York, 1995.

3. A. Beeby, I. M. Clarkson, R. S. Dickins, S. Faulkner, D. Parker, L. Royle, A. S. de Sousa, J. A. G. Williams and M. Woods, *J. Chem. Soc., Perkin Trans. 2*, 1999, 493–504.

4. (a) J. L. Kropp and M. W. Windsor, *J. Chem. Phys.*, 1963, **39**, 2769–2770. (b) J. L. Kropp and M. W. Windsor, *J. Chem. Phys.*, 1965, **42**, 1599–1608.

5. W. D. Horrocks and D. R. Sudnick, *J. Am. Chem. Soc.*, 1979, **101**, 334–340.

6. W. D. Horrocks and D. R. Sudnick, *Acc. Chem. Res.*, 1981, **14**, 384–392.

7. S. Faulkner, A. Beeby, M.-C. Carrié, A. Dadabhoy, A. M. Kenwright and P. G. Sammes, *Inorg. Chem. Commun.*, 2001, **4**, 187–190.

8. S. I. Weissman, *J. Chem. Phys.*, 1942, **10**, 214–217.

9. A. N. Sevchenko and A. K. Trofimov, *J. Exptl. Theoret. Phys*., 1951, **21**, 220.

10. A. N. Sevchenko and A. G. Morachevsky, *Izvest. Akad. Nauk*, 1951, **15**, 628.

11. G. A. Crosby and M. Kasha, *Spectrochim. Acta*, 1958, **10**, 377–382.

12. A. Beeby, B. P. Burton-Pye, S. Faulkner, G. R. Motson, J. C. Jeffery, J. A. McCleverty and M. D. Ward, *J. Chem. Soc., Dalton Trans.*, 2002, **0**, 1923–1928.

13. M. G. B. Drew, *Coord. Chem. Rev.*, 1977, **24**, 179–275.

14. C. Benelli and D. Gatteschi, *Chem. Rev.*, 2002, **102**, 2369-2387.

15. (a) G. A. Molander, *Chem. Rev.*, 1992, **92**, 29-68 (b) M. Shibasaki and N. Yoshikawa, *Chem. Rev.*, 2002, **102**, 2187-2209

16. G. Marriott, M. Heidecker, E. P. Diamandis and Y. Yan-Marriott, *Biophys. J.*, 1994, **67**, 957–965.

17. A. A. Kaminskii, *Phys. Stat. Sol.*, 2003, **200**, 215-296.

18. I. Hemmilä and S. Webb, *Drug Discovery Today*, 1997, **2**, 373–381.

19. S. Petoud, S. M. Cohen, J.-C. G. Bünzli and K. N. Raymond, *J. Am. Chem. Soc.*, 2003, **125**, 13324–13325.

20. P. Gottlieb, E. Hazum, E. Tzehoval, M. Feldman, S. Segal and M. Fridkin, *Biochem. Biophys. Res. Commun.*, 1984, **119**, 203

21. S. Aime, M. Botta, D. Parker and J. A. G. Williams, *J. Chem. Soc., Dalton Trans.*, 1995, 2259–2266.

22. D. M. Gravett and J. E. Guillet, *J. Am. Chem. Soc.*, 1993, **115**, 5970–5974.

23. A. Ueno, *ACS Symp. Ser*., 1993, **538**, 74

24. (a) S. E, H. I and D. P, *Ann Biol Clin*, 1990, **48**, 567–571. (b) E. Lopez, C. Chypre, B. Alpha and G. Mathis, *Clin. Chem.*, 1993, **39**, 196–201. (c) G. Mathis, *Clin. Chem.*, 1995, **41**, 1391–1397.

25. A. J. Amoroso, I. A. Fallis and S. J. A. Pope, *Coord. Chem. Rev.*, 2017, **340**, 198–219.

26. E. Soini and H. Kojola, *Clin. Chem*., 1983, **29**, 65

27. I. Hemmilä, V.-M. Mukkala and S. Dakubu, *Anal. Biochem*., 1984, **137**, 375

28. E. F. Gudgin Dickson, A. Pollak and E. P. Diamandis, *J. Photochem. Photobiol.*, 1995, **27**, 3–19.

29. J. P. André, É. Tóth, H. Fischer, A. Seelig, H. R. Mäcke and A. E. Merbach, *Chem. Eur. J.*, 1999, **5**, 2977–2983.

30. R. Hovland, C. Gløgård, A. J. Aasen and J. Klaveness, *Org. Biomol. Chem.*, 2003, **1**, 644–647.

31. E. Kimura, H. Hashimoto, T.J. Koike, *J. Am. Chem. Soc.*, 1996, **118**, 10963-10970

32. W. C. Baker, M. J. Choi, D. C. Hill, J. L. Thompson and P. A. Petillo, *J. Org. Chem.*, 1999, **64**, 2683–2689.

33. G. W. Kabalka, M. A. Davis, T. H. Moss, E. Buonocore, K. Hubner, E. Holmberg, K. Maruyama and L. Huang, *Magn. Reson. Med.*, 1991, **19**, 406–415.

34. G. M. Nicolle, É. Tóth, K.-P. Eisenwiener, H. R. Mäcke and A. E. Merbach, *J. Biol. Inorg. Chem.*, 2002, **7**, 757–769.

35. A. Dadbhoy, S. Faulkner and P. G. Summers, *J. Chem. Soc. Perkin Trans. 2*, 2002, 348-357.

36. B. Jagadish, G. L. Brickert-Albrecht, G. S. Nichol, E. A. Mash and N. Raghunand, *Tet. Lett.*, 2011, **52**, 2058–2061.

37. E. E. Langdon-Jones, A. J. Hallett, J. D. Routledge, D. A. Crole, B. D. Ward, J. A. Platts, and S. J. A. Pope, *Inorg. Chem.*, 2013, **52**, 448–456.

38. G. A. Crosby, R. E. Whan and R. M. Alire, *J. Chem. Phys.*, 1961, **34**, 743–748.

39. O. J. Stacey, B. D. Ward, S. J. Coles, P. N. Horton and S. J. A. Pope, *Dalton Trans.*, 2016, **45**, 10297–10307.

40. E. V. Sayre and S. Freed, *J. Chem. Phys.*, 1956, **24**, 1213.

41. H. F. Geisler and K. H. Hellwege, *Z. Physik.*, 1953, **136**, 293.

42. G. H. Deike and H. M. Crosswhite, *J. Opt. Soc. Am.*, 1956, **46**, 885;

43. D. F. Evans, *J. Chem. Soc.*, 1957, 1351–1357.

44. D. Parker and J. A. G. Williams, *J. Chem. Soc., Dalton Trans.*, 1996, 3613–3628.

45. R. M. Supkowski and W. D. Horrocks, *Inorg. Chim. Acta*, 2002, **340**, 44–48.

46. P.C. Griffiths, I. A. Fallis, T. Chuenpratoon and R. Watanesk, *Adv. Colloid Interface Sci.*, 2006, 122, 107–117

47. M. M. McGoorty, R. S. Khnayzer and F. N. Castellano, *Chem. Commun.*, 2016, **52**, 7846–7849.

48. J. E. Jones and S. J. A. Pope, *Dalton Trans.*, 2009, **0**, 8421–8425.

49. M. Andrews, J. E. Jones, L. P. Harding and S. J. A. Pope, *Chem. Commun.*, 2010, **47**, 206–208.

Chapter Six

Summary and Future Work

6.1 Summary

This thesis presents the design, synthesis and characterisation of a range of amphiphilic ligand architectures for s-, d- and f-block metals. These surfactants and their metallosurfactants were found to form stable micellar systems either through self-assembly or *via* doping into a simpler carrier microemulsion. The various results obtained suggest that the surfactant ligands are capable of sequestering metal ions and localising them on the surface of micellar droplets within oil-in-water microemulsions.

Chapter One provides an introduction to surface active chemistry and the techniques used to characterise the systems produced in this thesis. The foundation of this thesis is the design of microemulsions for applications as LSC cocktails, therefore an overview of current industry standards is included.

Chapter Two describes the development of micellar systems based on 1-alkyl-3-methyl imidazolium salts which, in a 1:1 ratio with 1-butanol, were found to be capable of self-assembly and exhibited very high oil-loading capacities as well as acting as a carrier for more complex surfactants. Various alkyl chain lengths were investigated with the dodecyl analogue offering the greatest oil-solubilising capacity.

This chapter also reports the synthesis and characterisation of two novel macrocyclic ligand architectures designed to form a series of metallosurfactants capable of aggregation in aqueous media. Tensiometric studies proved these surfactants and metallosurfactants to be capable of self-aggregation in water to give stable micellar systems.

Despite the macrocyclic surfactants exhibiting microemulsion compatibility, the oil-loading of these systems was particularly low. Therefore the ligands were doped into the imidazolium/butanol system to give microemulsions with both high oil-loading capacities and metal-binding capabilities.

Chapter Three presents a series of novel acyclic amphiphilic ligands synthesised from ethylene diamine and diethylene triamine precursors. These ligands were functionalised with poly-alcohol arms to form surfactants capable of metal binding as alternatives to the macrocyclic architectures described in Chapter Two. Coordination of Ni(II) and Cu(II) provided an insight into their coordination geometries via photophysical studies. While all of the Ni(II) complexes showed octahedral (or near-octahedral) geometries the Cu(II) complexes were seen to be of octahedral geometry for the ethylene diamine-based ligands and square pyramidal geometry for the diethylene triamine-based ligands.

Tensiometric investigations of the free ligands and their Sr(II) and Y(III) metallosurfactants were used to understand their microemulsion compatibility. Changes in CMC values of the free ligands upon addition of metal salts was indicative of metal binding, however, competition studies were not sufficient to conclude which metal was preferentially bound.

Despite the formation of stable microemulsions, the oil-loading capacities of these systems were found to be particularly low. Doping of the acyclic ligand into the imidazolium/butanol system described in Chapter Two created a compromise between oil-loading capacity and metal –binding ability in stable microemulsion systems.

Chapter Four reports the synthesis and characterisation of three novel bipyridine-based ligands incorporating lipophilic alkyl chains. These ligands were successfully coordinated to iridium(III) as the ancillary ligands in six novel *bis*-cyclometallated complexes where the cyclometallating ligand could be deprotected to afford hydrophilicity, thus making amphiphilic complexes. These complexes exhibited good ^{3}MLCT emission and long phosphorescence lifetimes in line with previously reported analogues.

Despite ligand-deprotection affording water solubility the complexes were not soluble enough to form micelles on their own. Instead they were successfully doped into the imidazolium/butanol carrier system described previously. Combined tensiometric and photophysical studies found that aggregation of surfactants had a noted effect on the ratio of ligand-centred and ^{3}MLCT emission. These species were found to be dual emissive as free complexes in solution, with emission arising from both ligand-centred and metal-to-ligand charge transfer mechanisms, however, upon aggregation into micelles, either a quenching of the ligand-centred emission or an enhancement of the metal-to-ligand charge transfer rendered the complexes mono-emissive.

Chapter Five describes the synthesis and characterisation of three novel DO3A-based surfactant ligands incorporating pendent chromophores as antennae for near-IR sensitised emission from a range of Ln(II) ions. Luminescent lifetime studies determined that the ligands form 8-coordinate complexes with hydration states suggesting the presence of 0-1 inner sphere water molecules. Photophysical characterisation showed sensitised lanthanide emission in the visible and NIR regions for a number of complexes. Lack of sensitisation for some of the complexes was attributed to the large distance between the antenna and the metal ion caused by the presence of an amide linker group.

Combined tensiometric and photophysical studies proved the metallosurfactants to be capable of self-assembly into micelles in aqueous media and found aggregation to have a significant effect

on the local environment of the Ln(III) ions. Investigations into the photophysical properties of the Eu(III) complex showed subtle changes in the hyperfine structure of the emission spectra suggesting a consistent coordination structure but a change in the local metal environment below and above the CMC. It was also noted that the lifetime changed from mono- to bi-exponential upon micellisation, consistent with previous studies involving d-block metallosurfactants.

6.2 Future Work

There are many ways in which the work presented in this thesis could be expanded upon in order to gain a greater understanding of the micellar systems formulated and to optimise them for their respective applications.

In all of the cases where metallosurfactants were doped into the imidazolium/butanol system only very low loadings of approximately 2 wt% were formulated. It would be of great interest to examine the feasibility of increasing this loading and the effect it would have on the physical properties of the microemulsions and, in the cases of the Ln(III) and Ir(III) systems, the photophysical properties.

Although this thesis explores a number of different surfactants for various metals, determination of the selectivity of these ligands was beyond the scope of this work. Therefore, an ideal avenue for future study would be the additional functionalisation of the ligands in order to introduce selectivity for particular metals. An example of this would be to utilise the secondary amine site of the $N2O4mC_{12}$ ligand described in Chapter Two in order to add further metal-coordination sites to the ligand.

Scattering techniques such as Small Angle X-ray and Neutron Scattering could easily be applied to all of the micellar systems presented here. X-ray scattering has the ability to provide information on the localisation of metals within micellar systems while neutron scattering can be used to determine the size and shape of micelles. These techniques would be invaluable in gaining a full understanding of the micellar systems and the effects of altering various parameters.